Degradation of metoprolol by means of advanced oxidation processes

Rossmary Violette Romero Olarte

ENGINEERING AND ADVANCED TECHNOLOGIES

DEGRADATION OF METOPROLOL BY MEANS OF ADVANCED OXIDATION PROCESSES

Rossmary Violette Romero Olarte

Directed by:

Prof. Dr. Jaime Giménez Farreras

Prof. Dr. Pilar Marco Buj

Department of Chemical Engineering

University of Barcelona

Memoria para aspirar al grado de doctor por la Universidad de Barcelona presentada por Rossmary Violette Romero Olarte.

Rossmary Violette Romero Olarte

El Dr. Jaime Giménez Farreras y la Dra. Pilar Marco Buj, profesores del departamento de Ingeniería Química de la Universidad de Barcelona.

Certifican:

Que el presente trabajo de investigación titulado: "Degradation of Metoprolol by means of Advanced Oxidation Processes", constituye la memoria que presenta la Ingeniera Química Rossmary Violette Romero Olarte para aspirar al grado de Doctor por la Universidad de Barcelona y que ha realizado dentro del programa de Doctorado "Ingeniería y Tecnologías Avanzadas" en el período 2009-2015, en el Departamento de ingeniería Química de la Universidad de Barcelona bajo nuestra dirección.

Y para que así conste, firman el presente certificado en Barcelona, Febrero de 2015.

Dr. Jaime Giménez Farreras   Dra. Pilar Marco Buj

"Las nubes son los ríos

que regresan a las montañas,

pero llevando la sabiduría

del mar consigo"

Paulo Coelho.

To God, my family and my love.

Acknowledgments

Thanks God for giving me the opportunity to reach one of my goals.

I would like to thank specially the following persons for their dedication, prayers, and support:

In these first lines I want to thank to Dr. Jaime Giménez and Dr. Pilar Marco for given me their support in my entire thesis and for leaded me through the Advanced Oxidation Processes world. I also want to thank them for support me in the personal way to conclude this work.

Dr. Santiago Esplugas for given me the opportunity to belong to Advanced Oxidation Processes Engineering Group and for his help during all the time I have been developing this thesis.

Dr. Carmen Sans to give me the opportunity to join the research project funded by the European Union within FP7-PEOPLE Programme-2012-IRSES.

Dr. Sui Minghao and her research group for their warm welcome in the Tongji University, in Shanghai, for sharing their expertise and allowed to me to work with them.

I would also like to thank all the members and former members of the Advanced Oxidation Processes Engineering Group for their help, collaboration, and all colleagues and staff, from the Chemical Engineering Department. I want specially to thank Natalia who was sharing with me all this great experience and I wish all her dreams come true. I want also to thank a special people of my group: Oscar, Nardi, Renato, Fabiola, Ana, Antonella, Mireia and Angel. I hope the best for you guys.

I would also like to mention my gratitude to my love Manuel who always has been to my side helping me to achieve my goals and given me hope and love to complete my work, and he never let me down, particularly, when I felt that I was falling down, he was always by my side.

To all members of my family mainly to my mother, my father, my brothers, my sisters, my nephews, my cousin Maria B., my sister and brothers in law, for give me a hand no matter how far away we were and for all support that they have given to me in

all good and bad moments. To Orlando Caceres who always is going to be with us in our hearts.

Finally, to Pili, Manolo, Pilar, Paca and others, for always cheering me on whatever I planned to do, and for encouraging me to keep on moving always forward and specially because they have been my family in Spain.

ABSTRACT

Nowadays, there is worldwide concern about environmental problems such as water scarcity, droughts and water quality. The water pollution has been increasing along the time, being this big problem that threats the environment. In order to avoid this situation and increase the water quality, the treatment of different pollutants present in water plays an important role. In this way, the emerging pollutants imply a new challenge. Pharmaceuticals are considered as emerging pollutants and they present peculiar problems.

Pharmaceuticals in waters come from hospitals, pharmaceutical industry or from domestic waters, by rejected drugs not used or by human excretions, because they are partially metabolized by the body and excreted. In addition, the amount of these compounds is continuously increasing and they can be ecotoxicological important, because of their biological activity, causing potential environmental impact. Once in the sewage treatment plants, the complete removal of these pharmaceuticals cannot be assured by conventional water treatment methods because of the recalcitrant nature of many of these compounds. Thereby, it is necessary to use alternative treatments such as "Advanced Oxidation Processes" (AOPS) which are based on the production of very reactive species (especially hydroxyl radicals, HO·). The reactive species produced are able to degrade or transform chemical pollutants producing ultimately total mineralization.

For this study the emerging contaminant β-blocker Metoprolol has been selected due that it is a highly prescribed pharmaceutical to treat hypertension, tachycardia, and heart failure and it has been detected in waste water treatment plants influents, thus, in natural waters. Several studies, focused on the toxicological potential of Metoprolol, indicate its potential environmental relevance and its recalcitrant nature. To remove MET from water, different AOPs were used. The Total Organic Carbon (TOC) is monitored to observe the organic matter removal, HPLC is used to determine the concentration of this pharmaceutical along the experiments. The BOD_5 and COD are analyzed, and its ratio BOD_5/COD is used as a biodegradability index. Furthermore, toxicity bioassays were carried out with the marine bacterium vibrio fischeri.

MET removal was studied, in different reactors with natural and artificial light, by photolysis, UVC/H_2O_2, photocatalysis, Fenton, photo-Fenton, Bicarbonate-activated

hydrogen peroxide and Cobalt or iron/bicarbonate/hydrogen peroxide processes. After that, the different set-ups and technologies tested have been compared in order to establish the efficiency of the processes.

An actinometric method was used to measure the photon flow entering a photocatalytic reactor. In addition, it was studied the influence of suspended TiO_2 particles, inside the photoreactor, on the actinometry.

Photolysis experiments were carried out with 50 mg/L of initial MET in Milli-Q water, free pH, and 25 ± 5 ºC in solarbox (SB), Compound Parabolic Collector (CPC), Black light blue lamps (BLB) and $UVC_{254 nm}$ (UVC) reactors. The results show that after 240 minutes of irradiation MET removal was too low in all reactors except in reactor UVC where 93.5% of MET removal was achieved. However, photolysis did not promote relevant mineralization in all set-ups.

UVC/H_2O_2 experiments were carried out with 50 mg/L of initial MET in Milli-Q water, free pH, and 25 ºC in UVC reactor. Different hydrogen peroxide concentrations and pH solution were tested. An initial dose of 125 mg H_2O_2/L exhibited the best performance regarding to MET (98% in 7.5 minutes) and TOC degradations (70.7% in 230 minutes). Biodegradability was improved and the final toxicity decreases.

Photocatalysis experiments were carried out with 50 mg/L of initial MET in Milli-Q water, free pH, and 25 ± 5 ºC in solarbox (SB) and Compound Parabolic Collector (CPC). Different TiO_2 concentrations (0.05, 0.10 and 0.40 g /L) were studied in both reactors and the best concentration for MET and TOC removal was 0.4 g TiO_2/L. After 300 minutes of irradiation in SB, a complete MET removal and 45.7% of mineralization were observed. Photocatalytic experiments were also carried out varying the initial MET concentration (25, 50 and 100 mg/L), pH and the water matrix with 0.4 g TiO_2/L in SB. It is observed that at lower MET initial concentration there is higher MET and TOC removal. Complete MET elimination was achieved at pH 9 (240 min). Changing the water matrix to effluent from WWTP just 20.8 % of MET elimination was achieved. Additionally, 25 and 150 mg/L of H_2O_2 were added to 50 mg/L MET solution directly in the batch tank with catalyst. A complete depletion of MET is reached within 180 and 120 min by use of 25 and 150 mg/L of H_2O_2, respectively. Photocatalytic treatment in CPC reactor was also a good alternative in MET degradation (81.5% at 2.6 kJ/L for 0.4 g/L of TiO_2) and 29.2% of mineralization. In CPC reactor 70% (Q= 3.1 kJ/L) and 96%

(Q= 6.0 kJ/L) of MET removal is observed with 25 and 150 mg/L of H_2O_2, respectively, and 0.4 g/L of TiO_2. After 270 minutes the biodegradability increases and toxicity decreases.

From the intermediates identified using SB and CPC reactors, a possible MET fragmentation was proposed for photocatalysis/TiO_2 and UV-Vis/H_2O_2/TiO_2 processes, where, mainly oxidative attacks were detected and the binding of HO· radicals in the aromatic ring.

The dark-Fenton experiments were carried out with 50 mg/L of initial MET in Milli-Q water at pH 3 and 25ºC temperature in a reactor of 2 L. Two different amounts of Fe (II) (2.5 mg/L or 10 mg/L) and two different H_2O_2 concentrations (25 mg/L or 150 mg/L) were used. With the highest values of Fe (II) and H_2O_2, the highest MET and TOC conversions were reached (degradation: 67.0%, TOC: 8%, COD: 7.63%). To improve the Fenton process, the total Iron (II) concentration was divided in equal parts (5) and added at constant periods of time (12 minutes) during 1 hour. With the highest concentrations of iron and H_2O_2 the maximum MET conversion was 87.0% and mineralization 15.6%. From the intermediates identified a possible MET fragmentation was proposed.

Photo-Fenton experiments were carried out with 50 mg/L of initial MET in Milli-Q water, pH 3, and temperature of 14 or 25 ºC in BLB, SB, CPC and UVC reactors. Two different amounts of Fe (II) were used (2.5 mg/L or 10 mg/L) and two different H_2O_2 concentrations (25 mg/L or 150 mg/L). In all reactors with the highest iron and H_2O_2 concentrations, the best results in MET degradation were observed (BLB: 100% in 7 min; SB: 97.3% in 7 min; CPC: 98.3% in 3 min); however, in UVC the lowest iron and H_2O_2 concentrations were used and 97.0% of MET conversion was achieved in 20 min. Similar behavior was observed for TOC removal, biodegradability and toxicity.

From the intermediates identified, a possible MET fragmentation was proposed, where mainly oxidative attacks were detected.

The dark- Bicarbonate/hydrogen peroxide experiments were carried out with 5 mg/L of initial MET in drinking water, pH 6.2, and room temperature in a reactor of 0.5 L. The highest conversion of MET within 120 minutes was almost 20% when 600 mg/L of $NaHCO_3$ and 600 mg/L of H_2O_2 were used. This process does not show as a good alternative for MET degradation. To improve the process, Cobalt (II) as catalyzer was

added in the batch reactor. When 1 mg/L of cobalt were used an improvement of~1.6 times was observed. The highest MET conversion was reached when 600 mg/L of NaHCO$_3$, 2400 mg/L of H$_2$O$_2$ and 1 mg/L of cobalt were used (47.2%).

For the following series of experiments, cobalt was changed for iron as catalyst, the pH was 3.0 and the initial concentration of MET was 25 mg/L. Three different amounts of Fe (II) were used: 2.5 mg/L, 5.0 mg/L and 10 mg/L, and H$_2$O$_2$ concentration was constant (25 mg/L). When the process was carried out without HCO$_3^-$, lowest MET conversion was reached (25.5%). When HCO$_3^-$ was added, the process improves~1.3 times. The addition of TBA as scavenger showed a decrease of MET conversion in~3.5 times. To improve the process, the total Iron (II) concentration was divided in equal parts (5) and added at constant periods of time (12 minutes) during 1 hour. With the highest iron concentrations (10 mg/L) a complete MET conversion in 40 minutes was achieved.

The efficiency of different AOPs tested and reactors used was compared from the ratio between accumulated energy and MET eliminated. The efficiency is higher for UVC reactor (0.07 kJ/mg) than SB (0.25 kJ/mg), possibly due to the high MET absorbance centered on 221 and 273 nm.

Concerning the efficiency ratio for MET removal by photocatalysis, the energy is better used in CPC (0.065 kJ/mg) than in SB (0.275 kJ/mg). A possible explanation can be related to the fact that the CPC are able to concentrate on the receiver, practically, all the radiation arriving at the collectors.

Finally, the ratio energy/MET removal is compared in four different installations for photo-Fenton process: 0.04 kJ/mg in UVC, 0.05 kJ/mg in BLB, 0.26 kJ/mg in CPC and 0.30 kJ/mg in SB reactor. UVC and BLB reactor exhibit a much better performance than SB reactor and CPC reactor.

On the other hand, the irradiation in the photocatalytic reactor (SB) was measured by o-NB actinometry in two different ways, based on pH or o-NB concentration, giving photon flows of 2.81×10^{-6} Einstein/s and 2.68×10^{-6} Einstein/s, respectively. In addition, this work has demonstrated that the o-NB actinometry, followed by o-NB concentration consumption, could be used in the presence of the catalyst TiO$_2$.

Contents

Chapter I

Introduction

1 INTRODUCTION

1.1 Water and integrated water cycle

Water is life, it is essential for our planet and it is a precondition for human, animal and plant life. Water is an indispensable resource for the economy and essential for the maintenance of good environmental quality. In addition, water plays a fundamental role in the climate regulation cycle. Thus, it must be preserved, and it is necessary to ensure its effective protection (European Commission, 2000, 2014a).

Water is permanently renewed but it is also finite and cannot be made or replaced with other resources. Freshwater constitutes only about 2% of the water on the planet and competing demands may lead to an estimated 40% global water supply shortfall by 2030 (United Nations of Population Fund, 2011; Water Resources Group, 2014).

Water scarcity is a man-made phenomenon. It is a recurrent imbalance that arises from an overuse of water resources, caused by consumption being significantly higher than the natural renewable availability. High overuse tends to occur in regions heavily dependent on irrigated agriculture, and in areas undergoing rapid urbanization and industrial development. Additionally, water scarcity can be aggravated by water pollution and during drought (a rainfall deficit) episodes (Schmidt, Benítez, & Benítez, 2012).

Regarding to droughts, in 2012, a reduction in rainfall to below normal levels was recorded during the winter months, impacting the water resources of extended parts of southern and central Europe. Based on the Standard Precipitation Index for February 2012, France, Spain, Portugal and England experienced extreme and severe drought conditions, even more the northern part of the United Kingdom. In late August 2012 the Standard Precipitation Index shows a precipitation deficit in parts of Spain, Italy and the Balkans (European Environment Agency, 2012). Large parts of Africa, Asia and Europe, including the south east of Britain are categorized by the UN as facing water stress or scarcity (British Broadcasting Corporation (BBC) News, 2012) (see figure 1.1).
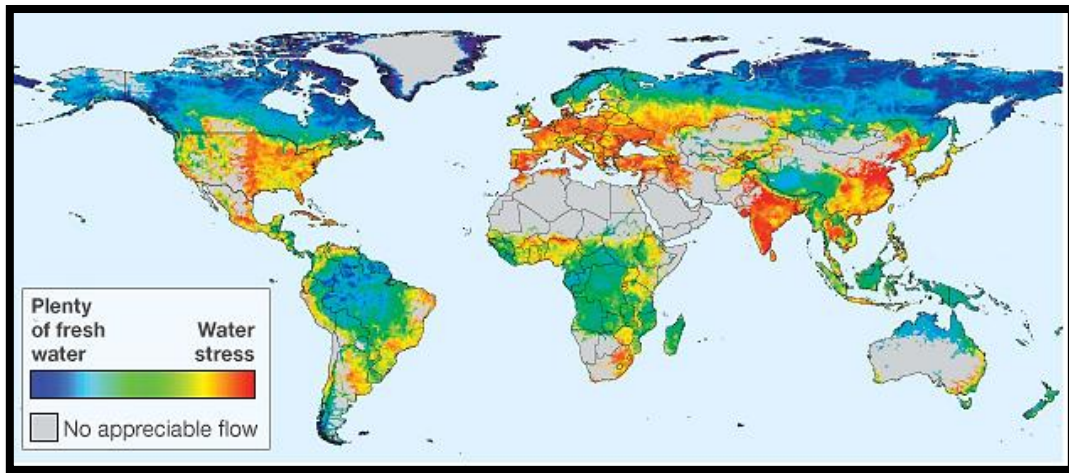
Figure 1.1. Overall picture of the state of the world's freshwater resources. Adapted from (British Broadcasting Corporation (BBC) News, 2012).

Water scarcity and the pollution found in it have prompted research directed at water reuse treatments in recent years to keep a natural balance regard to quantity and quality; thus, managing the water cycle in a sustainable way is the key to protect natural resources and human health (see figure 1.2).
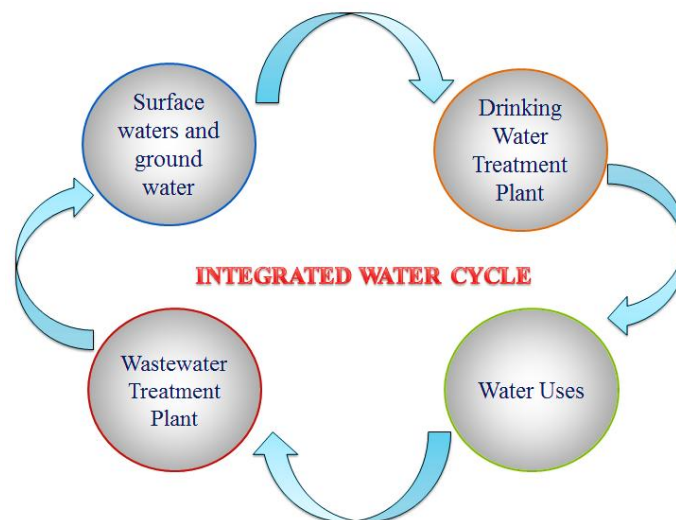
Figure 1.2- Integral Water Cycle. Adapted from (Junta de Andalucía, 2014).

1.2 Pharmaceutical compounds

Pharmaceuticals are used in large quantities in human and veterinary medicine (Wiegel et al., 2004). Among the pharmaceuticals β-blockers are very used and in this group there is a representative highly prescribed drug: the Metoprolol.

1.2.1 Emerging contaminants

Emerging contaminants can be broadly defined as a group of organic that were previously undetected or had not been considered as a risk (Polar, 2007) and which are not subject to restrictions of any kind, but may be candidates for future regulations, depending on the investigative results on the effects on human health, aquatic life forms and their presence in the environment (Malato, Maldonado, Fernández, Oller, & Polo, 2014; Petrovic, González, & Barceló, 2003).

A wide range of compounds are considered to be relevant emerging compounds, such as: detergents, personal care products (PPCPs), flame retardants, antiseptics, fragrances, industrial additives, steroids and hormones, pharmaceutical products and its metabolites, among others, and they are extensively consumed annually in the world (Benitez, Acero, Real, Roldan, & Casas, 2011; Nam, Jo, Yoon, & Zoh, 2014). They have been detected in ranges varying from (μg/L to ng/L) (Polar, 2007) in effluents of municipal wastewater treatment plants (Dougherty, Swarzenski, Dinicola, & Reinhard, 2010; Vulliet, Cren-Olivé, & Grenier-Loustalot, 2009), rivers, aquifers and even in drinking water (Cleuvers, 2003; Fatta, Achilleos, Nikolaou, & Meriç, 2007; Ioannou, Hapeshi, Vasquez, Mantzavinos, & Fatta-Kassinos, 2011; Kolpin et al., 2002; Muñoz, Gómez-Ramos, et al., 2009; Owen et al., 2007; Yu, Bouwer, & Coelhan, 2006).

In some cases, release of emerging contaminants to the environment has likely occurred for a long time, but may not have been recognized until new detection methods were developed. In other cases, synthesis of new chemicals or changes in use and disposal of existing chemicals can create new sources of emerging contaminants (U.S. Geological Survey (USGS), 2014).

Many of these emerging contaminants raise considerable toxicological and public concern (Ioannou et al., 2011; Rivas, Gimeno, Borralho, & Carbajo, 2010; Singh, Chaudhary, & Thakur, 2011) because, many of them are omnipresent and persistent, and these compounds have high biological activity, associated to persistent toxic

character, and such characteristics imply a potential impact on aquatic species even at low concentrations (Muñoz, Lopez-Doval, et al., 2009; Suárez, Carballa, Omil, & J.M. Lema, 2008).

1.2.2 Pharmaceutical Industry and pharmaceuticals in the water

Overall, the health care market is a growing market (see figure 1.3), many diseases are still untreatable, while increasing life expectancy and changing consumer interest, as well as the search for a higher quality of life, have increased the demand for health related services and products. Therefore, consumption of pharmaceuticals has increased over the last years not only in terms of expenditure, but also in terms of the volume or quantity of medicines consumed.
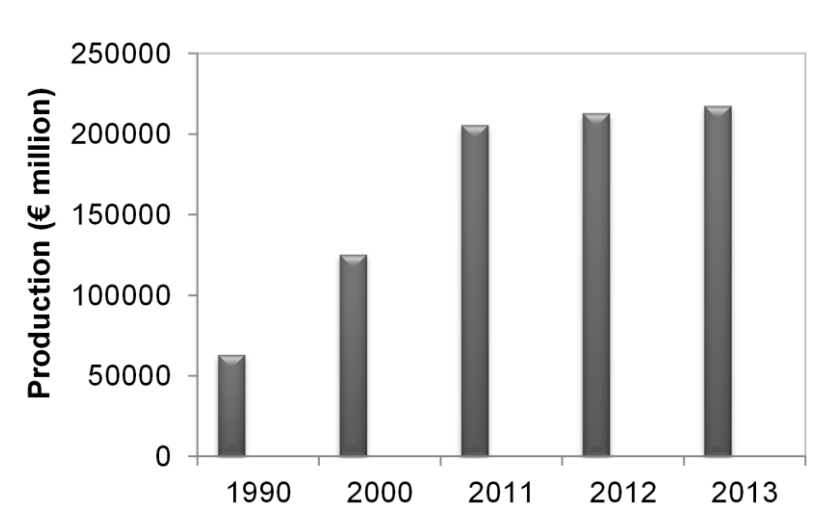
Figure 1.3- Total production of pharmaceutical industry EU. Ref: (European Federation of Pharmaceutical Industry and Associations. (EFPIA), 2014).

The number and concentrations of new and existing pharmaceuticals in the water environment are destined to increase further in the future as a result of increased consumption of pharmaceuticals as was mentioned before, becoming a growing environmental concern (Kolpin et al., 2002; Metcalfe, Miao, Koenig, & Struger, 2003; Muñoz, Lopez-Doval, et al., 2009). In figure 1.4 is presented the occurrence of pharmaceuticals distributed according to their highest concentration reported in each of the concentration ranges.
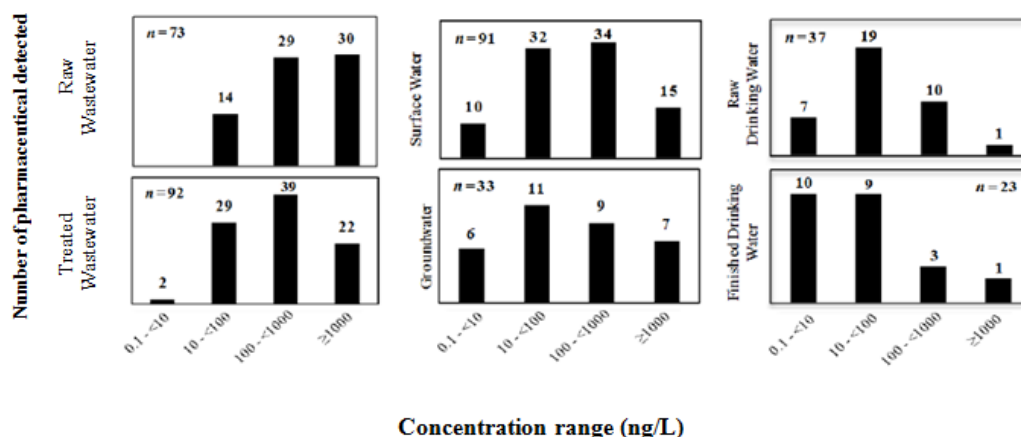
Figure 1.4- Number of pharmaceutical detected in various water matrices of the water environment in USA. Reference: (Randhir & Rolf, 2013).

1.2.2.1 Inputs of the pharmaceuticals to the environment and their environmental hazard risk

Pharmaceuticals enter the environment through emission from production sites (pharmaceutical industry), direct disposal of surplus drugs in households and hospitals, excretion across sewage systems (Carballa, Omil, & Lema, 2005; Gros, Petrovic, & Barceló, 2007; Heberer, 2002; Joss et al., 2005; Kolpin, Skopec, Meyer, Furlong, & Zaugg, 2004; Petrovic et al., 2009; J. L. Santos, Aparicio, & Alonso, 2007; Suárez et al., 2008; N. M. Vieno, Harkki, Tuhkanen, & Kronberg, 2007) after drug administration to humans (they are partially metabolized by the body and excreted completely unchanged or only slightly transformed) (Polar, 2007; L. Santos, Araujo, Fachini, Peña, & Deleure-Matos, C. Montenegro, 2010), and also from non-human uses, such as, wastewater from fish and other animal farms (Isarain-Chávez, Garrido, & Rodríguez, 2011; Jurado et al., 2012; Prieto-Rodríguez et al., 2013) such as livestock treatment, aquaculture and pet care (Thomas, Dye, Schlabach, & Langford, 2007). Figure 1.5 shows the inputs of pharmaceutical compounds and their metabolites to the aquatic environment.
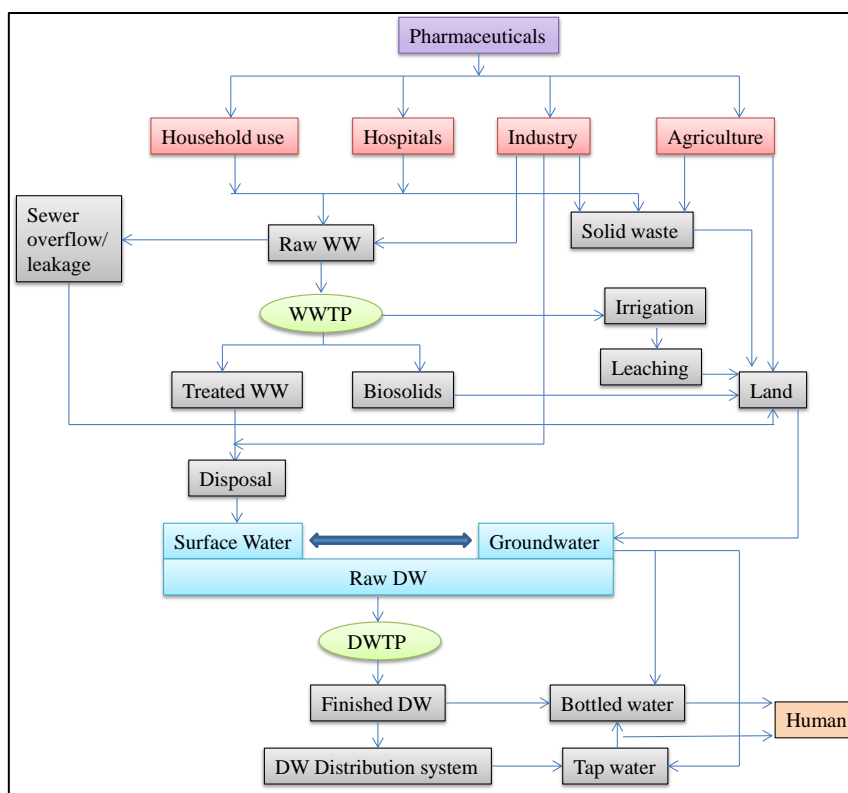
Figure 1.5- Inputs of pharmaceutical compounds and their metabolites to the aquatic environment. WWTP= wastewater treatment plant, WW=wastewater, DW= drinking water, DWTP= drinking water treatment plant. (Adapted from (Malato et al., 2014; Randhir & Rolf, 2013).

The present tendency to synthesize pharmaceuticals resistant to common biotransformation mechanisms, to extend their persistence in the organism, results in the obtaining of very stable molecules. This means, their resistance to chemical and biological degradation increases, with a consequent increased presence of these products in the environment, and especially in surface waters. Therefore, wastewater treatment plants (WWTP) effluent is widely regarded as an important pathway for human pharmaceutical compounds to enter the aquatic environment (Gros, Petrovic, & Barceló, 2006; Muñoz, Gómez-Ramos, et al., 2009; Yang et al., 2010).

A great diversity of trace pollutants can be found in treated effluents from urban waste-water treatment plants. The table 1.1 reviews the occurrence of pharmaceuticals (emerging pollutants) present in WWTP effluents around the world.

Table 1.1- Occurrence of emerging and priority pollutants in wastewater effluents. Ref. (Muñoz, Gómez-Ramos, et al., 2009)

Compound	Effluent concentration Medium-maximum (ng/L)	Country
PHARMACEUTICALS		
Analgesics/anti-inflamatories		
Diclofenac	680-5500	France, Greece, Italy, Sweden
	60-80	USA
Ibuprofen	50-320	USA
Naproxen	300-3200	USA
	1100-5200	France, Greece, Italy, Sweden
acetaminophen	10-19	South Korea
Ketoprofen	318-620	Croatia
N-acetyl-4-amino-antipiryne	2900-7000	Germany
(4-AAA) (Dipirone metabolite)	4440-4870	Germany
Salicilyc acid (aspirin metabolite)	3600-59600	Canada
Codeine	900-8100	Spain
Mefenamic acid	7-10	Croatia
Antibiotics		
Trimethoprim	550-1900	USA
	320-660	Germany
	58-188	South Korea
Ciprofloxacin	239-514	Italy
	170-860	USA
	120-400	Canada
Ofloxacin	652-1081	Italy
Erythromycin	89-353	Italy
	130-294	South Korea
	17-30	Croatia
Sulfamethoxazole	390-820	Croatia
	400-2000	Germany
	136-407	South Korea
β-blockers		
Metoprolol	730-2200	Germany
	60-160	USA
	80-390	France, Greece, Italy, Sweden
Propanolol	290-470	Croatia
	20-50	USA
Atenolol	400-1150	Croatia
Sotalol	185-210	Croatia
Lipid regulators		
Bezafibrate	10-10	Croatia
	2200-4600	Germany
	50-200	Canada
Gemfibrozil	120-320	Croatia
	920-5500	USA

Table 1.1 (Continued)		
Compound	**Effluent concentration Medium-maximum (ng/L)**	**Country**
Clofibric acid (metabolite)	28-30	Croatia
	360-1600	Germany
	30-80	Canada
Fenofibric acid (metabolite)	380-1200	Germany
Psychiatric drugs		
Diazepam	30-40	Germany
Fluoxetine	50-140	Canada
Carbamazepine	70-1200	France, Greece, Italy, Sweden
	110-2300	Canada
	2100-6300	Germany
Hormones		
Estrone	30-80	Spain
	42-48	Italy
Diethylstilbestrol		Spain
Estriol	16-25	South Korea
Anti-ulcer agent		
Ranitidine	135-200	Croatia
	298-610	Italy

Their persistence is of particular importance, because it increases the risk of long-term exposure which could be responsible for chronic toxicity and indirect effects in animals and plants (endocrine disruption, growth inhibition, disruption of microbial ecosystems, cytotoxicity, mutagenicity, teratogenicity, etc.). Sparking concerns about the impact drug traces could have not only on the environment (aquatic organisms) but also on human health.

In table 1.2, several pharmaceutical compounds and their environmental hazard risk assessment are indicated.

Table 1.2- Environmental hazard classifications and risk assessments of selected active pharmaceutical ingredients. Adapted from (Carlsson, Johansson, Alvan, Bergman, & Küler, 2006)

Compound	**Hazard classification**
Diclofenac	Dangerous for the environment
Ethinyloestradiol	Dangerous for the environment
Furosemid	Not dangerous for the environment
Hydrochlorothiazide	Not dangerous for the environment
Ibuprofen	Dangerous for the environment
Metoprolol	Dangerous for the environment
Norethisterone	Dangerous for the environment
Oestriol	Dangerous for the environment
Oxazepam	Dangerous for the environment
Salbutamol	Not dangerous for the environment

1.2.3 Beta blockers

Beta blockers are pharmaceuticals used to treat a variety of cardiovascular diseases, such as hypertension, coronary artery disease, and arrhythmias (Benner, Ternes, & Scholz, 2009; A. Ternes & Joss, 2006) by blocking the action of epinephrine and norepinephrine on the β-adrenergic receptors in the body, primarily in the heart.

Although, the basic chemical structures of β-blockers are quite similar, structural variations in the substituents of the aromatic ring lead to pharmacokinetic differences (Owen et al., 2007). As a result, the various β-blockers are metabolized to different extents in the human body (Escher, Bramaz, Richter, & Lienert, 2006; Lienert, Güdel, & Escher, 2007). Once consumed, beta blockers are excreted partly unchanged (Hernando, Gómez, Agüera, & Fernández-Alba, 2007; Maurer, Escher, Richle, Schaffner, & Alder, 2007). These pharmaceuticals are widely used around the Europe and have been detected in the order of ng L^{-1} to μg L^{-1} in the water (Andreozzi, Raffaele, & Nicklas, 2003; Gros et al., 2006; N. Vieno, Tuhkanen, & Kronberg, 2007), being emerging contaminants.

1.2.3.1 Metoprolol

Metoprolol (MET) is a selective beta blocker. It is a highly prescribed pharmaceutical to treat hypertension, tachycardia, and heart failure (Benitez, Real, Acero, & Roldan, 2009; Owen et al., 2007; Rivas et al., 2010; Scepanovic et al., 2012; Yang et al., 2010). Around 10% of the applied Metoprolol dose is excreted unchanged and, hence, it is present in wastewater treatment plant (WWTP) influents at concentrations of 0.6 to 2.0 μg/L (Bendz, Paxeus, Ginn, & Loge, 2005; Gros et al., 2006; Romero, Marco, Giménez, & Esplugas, 2013; Scepanovic et al., 2012; T. A. Ternes et al., 2003; N. M. Vieno et al., 2007; N. Vieno et al., 2007). Its presence has been also detected in rivers from Netherlands (25-100 ng/L) (Stolker et al., 2004), Poland (51-155 ng/L) (Kasprzyk-Hordern, Dinsdale, & Guwy, 2009), UK (7-11 ng/L) (Bendz et al., 2005), Sweden (60-70 ng/L) (Bendz et al., 2005), Germany (up to 1000 ng/L) (Wiegel et al., 2004) and united States (up to 1540 ng/L) (Cleuvers, 2003).

Several studies, focusing on the toxicological potential of Metoprolol, indicate its potential environmental relevance (Cleuvers, 2005; Dzialowski, Turner, & Brooks, 2006; Escher et al., 2006; Fraysse & Garric, 2005; Hernando, Mezcua, Fernandez-Alba,

& Barcelo, 2006; Owen et al., 2007). This might be even more of a concern if the concentrations of MET increase in the aquatic environment, due to its adverse effect on aquatic organisms, even at low concentration. Although in trace concentrations, this pharmaceutical is persistent against biological degradation and it retains its chemical structure long enough (Scepanovic et al., 2012).

Owing to its widespread occurrence and potential impact (Khetan & Collins, 2007; Moctezuma et al., 2013; Ratola, Cincinelli, Alves, & Katsoyiannis, 2012), MET must be removed from water before discharge or reuse. Several researches have demonstrated that MET shows slow direct photo-transformation and/or hydrolysis. (Liu, Cumming, & Sharpe, 2009; Piram, Salvador, Verne, Herbreteau, & Faure, 2008; Rivas et al., 2010; Romero et al., 2013; Scepanovic et al., 2012). The half-life of Metoprolol under sun light has been reported to be several hundreds of hours (Alder, Schaffner, Majewsky, Klasmeier, & Fenner, 2010; Liu & Williams, 2007; Rivas et al., 2010) due to its recalcitrant nature.

The achievement of effective technologies for elimination of Metoprolol from their original sources, such as hospital effluents (487 to 2232 ng/ L) (Thomas et al., 2007), domestic wastewaters (up to 2200 ng/L) (Owen et al., 2007) or pharmaceutical industry discharges, is an emerging research area in environmental field.

To emphasize the scope of this study, the efficiency of the works in removing Metoprolol present in effluents is a key factor. In this context, Advanced Oxidation Processes (AOPs) appear as a good alternative to upgrade existing treatments for its degradation due to their versatility and ability to increase biodegradability.

1.3   Legal framework

In many developed countries, there are legislations aimed to procure a sustainable use of water. On this base, Directive 2000/60/CE is one of the most important tools concerning the water quality conservation in Europe. Other regulations have been developed defining the emission levels and disposal of different pollutants. However, regulations about emission levels of emerging contaminants in water and persistent organic pollutants are not yet complete and they are being actualized and improved.

1.3.1   General legal framework of water

Directive 2000/60/CE

To protect our water resources and the water environment since 2000 the Water Framework Directive (WFD) has been in place as the main European legislation. It requires managing the water so that its quality and quantity does not affect the ecological services of any specific water body.

The purpose of this Directive is to establish a framework for the protection of inland surface waters, transitional waters, coastal waters and groundwater, which:

(a) Prevents further deterioration and protects and enhances the status of aquatic ecosystems.

(b) Promotes sustainable water use based on a long-term protection of available water resources.

(c) Aims at enhanced protection and improvement of the aquatic environment.

(d) Ensures the progressive reduction of pollution of groundwater and prevents its further pollution.

(e) Contributes to mitigating the effects of floods and droughts.

Member States shall identify the individual river basins lying within their national territory and, for the purposes of this Directive, shall assign them to individual river basin districts. Small river basins may be combined with larger river basins or joined with neighboring small basins to form individual river basin districts where appropriate. Member States shall ensure the establishment of a register or registers of all areas lying within each river basin district which have been designated as requiring special protection. The European Parliament and the Council shall adopt specific measures against pollution of water by individual pollutants or groups of pollutants presenting a significant risk to or via the aquatic environment, including such risks to waters used for the abstraction of drinking water (European Commission, 2000).

Other Directives at European level:

- Commission Directive 2009/90/EC, of 31 of July 2009, laying down, pursuant to Directive 2000/60/EC of the European Parliament and of the Council, technical

specifications for chemical analysis and monitoring of water status (European Commission, 2009a).

- Directive 2008/105/EC of the European Parliament and of the Council of 16 December 2008 on environmental quality standards in the field of water policy, amending and subsequently repealing Council Directives 82/176/EEC, 83/513/EEC, 84/156/EEC, 84/491/EEC, 86/280/EEC and amending Directive 2000/60/EC of the European Parliament and of the Council (European Commission, 2008).

Concerning to Spanish legislation, as basic texts related to water could be cite:

- Real Decreto Legislativo 1/2001, de 20 de Julio, por el que se aprueba el texto refundido de la ley de aguas (Spanish Goverment, 2001).

- Real Decreto Legislativo 606/2003, de 23 de Mayo, por el que se modifica el Real Decreto 849/1986, de 11 de abril, por el que se aprueba el Reglamento del Dominio Público Hidráulico, que desarrolla los Títulos preliminar, I, IV, V, VI y VIII de la Ley 29/1985, de 2 de Agosto, de aguas (Spanish Goverment, 2003).

- Real Decreto 60/2011, de 21 de Enero, sobre las normas de calidad ambiental en el ámbito de la política de aguas. Ministerio de Medio Ambiente y Medio Rural y Marino. Transpone: Directiva 2009/90/CE, de 31 de julio de 2009, Directiva 2008/105/CE, de 16 de diciembre, de conformidad con la Ley de Aguas, texto refundido aprobado por Real Decreto Legislativo 1/2001, de 20 de julio (Spanish Goverment, 2011).

- Real Decreto 670/2013, de 6 de Septiembre, por el que se modifica el Reglamento del Dominio Público Hidráulico aprobado por el Real Decreto 849/1986, de 11 de Abril, en materia de registro de aguas y criterios de valoración de daños al dominio público hidráulico (Spanish Goverment, 2013a).

1.3.2 Persistent organic pollutants and emerging contaminants regulations

In the EU, the commitments made under both the Stockholm Convention and the CLRTAP persistent organic pollutants (POPs) protocol are translated into directly applicable law by the POPs Regulation.

- Regulation (EC) No 850/2004 of the European Parliament and of the Council of 29 April 2004 on persistent organic pollutants and amending Directive 79/117/EEC (European Commission, 2004b).

Subsequent references: Amending: annexes IV y V, by regulation 1342/2014, of 17 of December (European Commission, 2014b), annex I, by regulation 519/2012, of 19 of June (European Commission, 2012), annexes I y III, by regulation 757/2010, of 24 of August (European Commission, 2010b), annexes IV y V, by regulation 304/2009, of 14 of April (European Commission, 2009b), annex V, by regulation 323/2007, of 26 of March (European Commission, 2007c), annex V by regulation 172/2007, of 16 of February (European Commission, 2007b). Replaced: annex IV and amending el V, by regulation 756/2010, of 24 of August (European Commission, 2010a), annex IV, by regulation 1195/2006, of 18 of July (European Commission, 2006b). Error correction: in DOUE number 204 of 4 of August 2007 (European Commission, 2007a), in DOUE L 229, of 29 of June 2004 (European Commission, 2004a). Conformity is issued: publishing the National Implementation Plan for the Stockholm Convention: Resolution of 10 of April 2013 (Spanish Goverment, 2013b). With the article 7.4, letter b), clause iii), publishing format for notification: Decision 2009/63, of 20 of November (European Union, 2009), on the common model for data presentation: Decision 2007/639, of 2 of October (European Union, 2007).

- 2006/507/EC: Council Decision of 14 October 2004 concerning the conclusion, on behalf of the European Community, of the Stockholm Convention on Persistent Organic Pollutants (European Commission, 2006a).

Regarding to emerging contaminants the NORMAN Project is based on (Brack, Dulio, & Slobodnik, 2012):

- A more rapid and wide-scope exchange of data and information on the occurrence and effects of emerging substances,
- Better data quality and comparability via validation and harmonisation of common measurement methods (chemical and biological) and monitoring tools.
- More transparent information.
- The establishment of an independent and competent forum for the technical/scientific debate on issues related to emerging substances.

Concerning to United States legislation:

Recommendations and regulations have been purposed for the Emerging Contaminants Environmental Council of the States -Cross Media Committee (ECOS-CMC) in cooperation with the U.S. Environmental Protection agency (EPA) Office in

order to prevent environmental contamination due to these chemicals (ECOS Green Report 2010; state experiences with emerging contaminants: recommendations for federal action (Environmental Council of the States, 2010). The Department of Defense has incorporated key elements in Directive 4715.18 of June 11, 2009 entitled "Emerging Contaminants" (Department of Defense, 2009).

1.4 Advanced Oxidation processes

Advanced Oxidation Processes (AOPs) are based on the production of very reactive species (especially hydroxyl radicals, HO·, whose standard redox potential is 2.8 V), generated in atmospheric or sub-supercritical conditions of temperature and pressure with or without catalyst and/or reactive energy (electrochemical, UV-Vis or ultrasounds). The reactive species produced are able to degrade or transform chemical pollutants producing ultimately total mineralization.

For the application of AOPs in wastewater treatment, the objectives can be either to (Malato et al., 2014):

1. Eliminate biorecalcitrant and toxic compounds.
2. Increase the biodegradability of wastewater before applying conventional biological process.
3. Reduce the level of toxicity in the effluent.
4. Disinfect the wastewater instead of applying traditional disinfection methods.

The complete mineralization is the main AOP´s goal and it could be represented as:

$$C_nH_mX_z + \left(n + \frac{m-z}{4}\right)O_2 + cat \rightarrow nCO_2 + \frac{m-z}{4}H_2O + zHX \qquad (1.1)$$
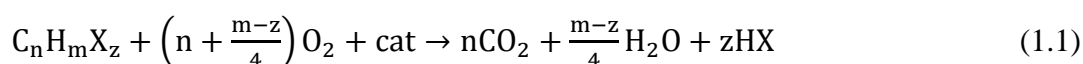
The catalyzer (cat) could be H_2O_2, O_3, Fe^{2+}, UV, semiconductor, energy, etc. It can be observed in the equation above that is possible to achieve the complete mineralization of the organic compounds up to CO_2 and water. In halogenated case it is going to produce the corresponding halide.

The Hydroxyl radical (HO·) is a short lived, extremely powerful oxidizing agent, capable to react with organic compounds mostly by hydrogen abstraction.

$$HO· + RH \rightarrow R· + H_2O \qquad (1.2)$$

This reaction generates organic radicals which by addition of molecular oxygen yield peroxide radicals. These intermediates initiate chain reactions of oxidative degradation, leading to carbon dioxide, water and inorganic salts (Legrini, Oliveros, & Braun, 1993).

$$R^{\cdot} + O_2 \rightarrow RO_2^{\cdot} \qquad (1.3)$$

Besides hydrogen abstraction, electron transfer to hydroxyl radical sis also possible (Legrini et al., 1993).

$$HO^{\cdot} + RX \rightarrow RX^{\cdot +} + HO^{-} \qquad (1.4)$$

Finally, electrophilic addition to double bound C=C constitutes the most common mechanisms of oxidative degradation of organics by $HO^{\cdot}$

$$HO\cdot + C=C \rightarrow HO\text{-}C\text{-}C\cdot \qquad (1.5)$$

The $HO\cdot$ radical presents characteristics that highlight its high oxidant power (see figure 1.6):

- It is highly reactive
- Acts non-selectively and therefore, is capable of attacking various functional groups
- It is easy to produce
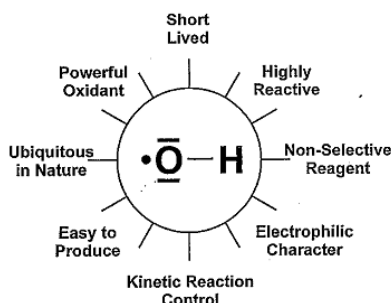- It has electrophilic character
- It has a very short lifetime

Figure 1.6- Hydroxyl radical characteristics

The standard redox potential equal to 2.8 V makes $HO\cdot$ a powerful oxidant, as it can be seen in the next table.

Table 1.3- Oxidation potentials of common substances and agents for pollution abatement. Adapted from (Legrini et al., 1993).

Species	Oxidation potential E^0 (V)
Fluorine (F)	3.03
Hydroxyl radical (HO·)	2.80
Ozone (O_3)	2.07
Hydrogen peroxide (H_2O_2)	1.78
Permanganate ($KMnO_4$)	1.68
Hypobromous acid (HOBr)	1.59
Chlorine dioxide (ClO_2)	1.57
Hypochlorous acid (HOCl)	1.49
Chlorine (Cl_2)	1.36
Bromine (Br_2)	1.09

Rate constants (k_{HO}, $r=k_{HO}$ [HO·] C) for most reactions involving hydroxyl radicals in aqueous solution are usually on the order of 10^6 to 10^9 M^{-1} s^{-1}. Their not-selective attack is a useful attribute for wastewater treatment. The versatility of AOPs is also enhanced by the fact that there are different ways of producing hydroxyl radicals, facilitating compliance with the specific treatment requirements.

Depending on the physicochemical process leading to the formation of radicals, AOPs can be divided into non-photochemical and photochemical processes (see table 1.4).

Table 1.4- Advanced Oxidation Processes. Adapted from (Litter & Quici, 2010).

Non-Photochemical Processes	Photochemical Processes	
	Type of Process	Irradiation Wavelength Range λ (nm)
Alkaline Ozonation (O_3/HO^-)	Water photolysis in vacuum ultraviolet (VUV)	<190
Ozonation with hydrogen peroxide (O_3/H_2O_2)	UV/hydrogen peroxide (UV/H_2O_2)	<280
Fenton and related processes (Fe^{2+}/H_2O_2)	UV/ozone (UV/O_3)	280-315
Electrochemical oxidation	Photo-Fenton and related processes	UV-Vis up to 450
γ -Radiolysis and electron-beam treatment	Heterogeneous photocatalysis (HP) using TiO_2	UV: up to 380-400
Non-thermal plasma (surface corona discharge)	Heterogeneous photocatalysis (HP) with hydrogen peroxide (TiO_2/H_2O_2)	UV: up to 380-400
Electrohydraulic discharge-ultrasound (US, cavitation)	Zerovalent iron plus UV light	UV range
Wet air oxidation	-	-
Supercritical water oxidation		
Zerovalent iron (ZVI)		
Ferrate		

1.4.1 Irradiation sources

a) *Artificial light (UV lamps) used in photochemical processes*

The lamp selection for a particular AOP application is governed by several factors among which, the most important are:

- Absorption spectrum of the pollutant (UV photolysis) or added oxidant. The lamp spectral emission domain should cover as much as possible the absorption spectrum of the reactant (depending on whether is required that photolysis occurs).
- Spectrum of the water background.
- Lamp power and radiant efficiency of the lamp. The photochemical degradation rate depends on the rate of photons emitted by the lamp.
- Lamp geometry. The shape and geometry of the lamp should be suitable to reactor design, such that a maximum reactor performance is achieved.
- Manufacturing and operation costs.

Monochromatic light sources:

Low-pressure Hg lamps: a low-pressure mercury lamp is a highly efficient UV light source of short wavelength, the main light emission (85-90%) is a 253.7 nm and about 7-10% at 184.9 nm.

Excimer lamps: emits vacuum ultraviolet (VUV) rays of wavelengths 180 nm or fewer.

Polychromatic light sources:

Medium-pressure Hg lamps: often named as UV-lamps, their spectral distribution of the radiations emit particularly strongly in the region between 200 to 400 nm.

Pulsed UV lamps: the light generated by pulsed UV lamps consists of a continuum broadband spectrum, especially rich in UV range below 400 nm, which is germicidal.

b) *Natural light (solar irradiation)*

The common drawback of AOPs is the high demand of electrical energy for devices and this makes such treatments economically disadvantageous (Malato et al., 2014).

The use of solar energy represents an ecological and economic source; especially when large-scale operations and long removal periods are needed.

The earth receives a power of 1.7 x 10^{14} kW from the sun, this means 1.5 x 10^{18} kWh per year (Singh et al., 2011). Solar radiation reaching the Earth's surface without being absorbed or deflected is called direct radiation. The radiation that reaches the earth's surface and is diverted is diffuse radiation and the sum of the diffuse and direct radiations is the global radiation. The following maps (figure 1.7) highlight the differences between direct and global irradiance where "global" includes diffuse light. Areas with a high proportion of diffuse light include Northern Europe, South-East China and the tropical belt around the equator.
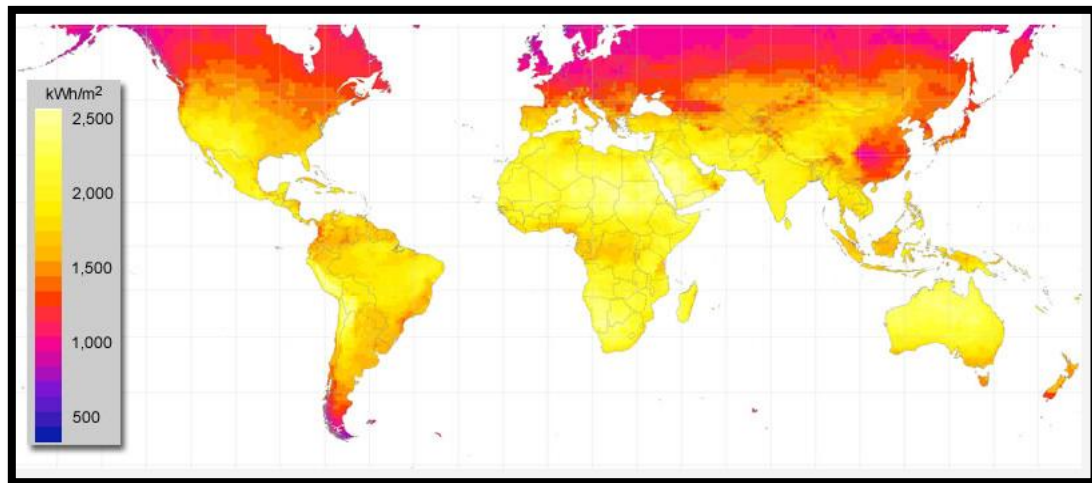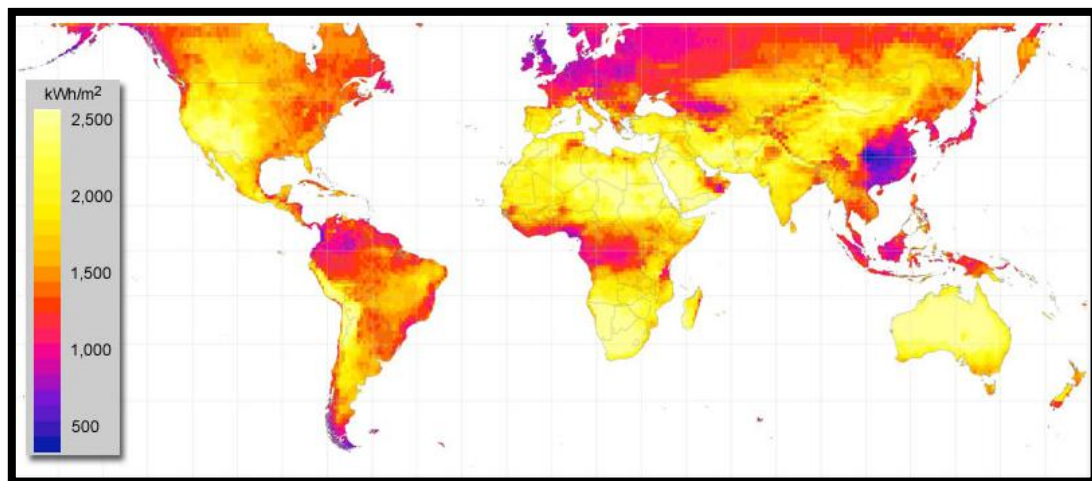
a-

b-

Figure 1.7- Annual solar beam radiation kWh/m^2.year from Meteonorm software. a- Global irradiance and b- direct irradiance. Source (Green Rhino Energy, 2014)

The solar spectrum is depicted in the figure 1.8, which shows the maximum peak near to 500 nm.
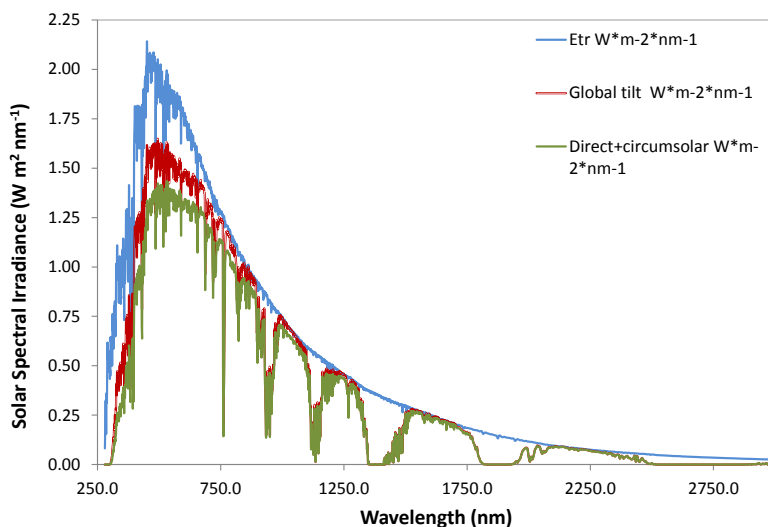
Figure 1.8- Solar spectrum. ETR = Extraterrestrial Radiation. Reference (American Society for Testing and Materials (ASTM), 2014)

Solar collector technology

Traditional solar collector classification considers only the thermal efficiency (non-concentrating or low-temperature, up to 150º C, medium concentrating or medium temperature, from 150º C to 400º C, and high concentrating or high temperature, over 400º C). However in photocatalysis applications the thermal factor is irrelevant whereas the amount of useful radiation collected (shorter than 385 nm in the case of the TiO_2) is very important (Blanco-Galvez & Malato-Rodríguez, 2003).

(a) One-sun (non-concentrating) collectors

These kinds of collectors do not have moving parts or solar tracking devices, they do not concentrate radiation and the optical efficiency is lower than for PTCs (Bahnemann, 2004; Bird, 1984; Blanco-Galvez, Fernández-Ibáñez, & Malato-Rodríguez, 2007; Blanco-Galvez & Malato-Rodríguez, 2003).

(b)Parabolic-trough concentrators (PTCs)

The initial solar photoreactor designs for photochemical applications were based on line-focus parabolic-trough concentrators (PTCs) considered medium concentrating collectors. There are two types: a) One-axis parabolic trough, b) Two-axis parabolic

trough. The basic components of a parabolic-trough collector are: the reflecting concentrator, the absorber tube (photoreactor) and the drive-tracking system (Blanco-Galvez & Malato-Rodríguez, 2003; Malato, Fernández-Ibáñez, Maldonado, Blanco, & Gernjak, 2009; Malato, Fernández-Ibáñez, Maldonado, Oller, & Polo-López, 2013).

(c) Compound Parabolic Concentrators (CPC)

CPC collectors are a very interesting cross between trough concentrators and one-sun systems and are one of the best options for solar photocatalytic applications. CPCs have been found to provide the best optics for low concentration systems were extensively employed (Blanco-Galvez & Malato-Rodríguez, 2003). They have high optical efficiency, since they make use of almost all the available radiation, and high quantum efficiency, as they do not receive a concentrated flow of photons (Malato et al., 2009, 2013).

Figure 1.9 describes the three solar reactors types described before.
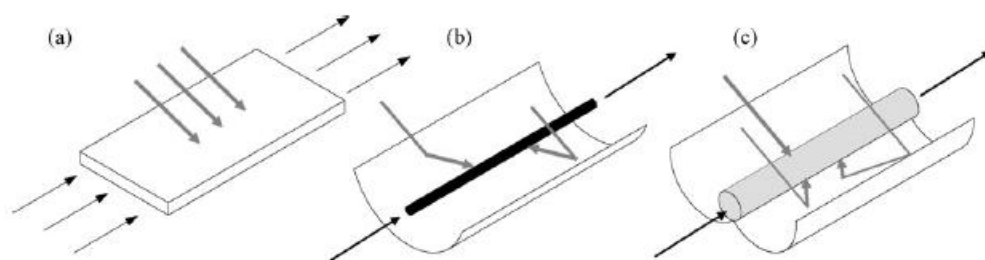
Figure 1.9- Solar water photocatalytic reactors: (a) non-concentrating (one-sun reactor), (b) concentrating (parabolic trough), and (c) compound parabolic collector. Source (Malato et al., 2009).

1.4.2 Photolysis

In UV direct photolysis, the contaminant to be destroyed must absorb the incident radiation and undergo degradation starting from its excited state. The typically low concentration of pollutants in the contaminated water and, in general, the low efficiency of photo-dissociation resulting from the light absorption event, limit the industrial applications of the UV photolysis process as compared to the hydroxyl radical- driven technologies, where the light absorption by the target pollutant is not absolutely required. However, there are many cases where the target pollutants are strong absorbers of the UV radiation, and therefore, their UV photolysis may become a significant component during the treatment by any AOP.

40

Indirect photolysis of organic pollutants is triggered by the photo-sensitisation processes from natural organic matter, or photolysis of water constituents. The long-lived (triplet) excited states of water organic constituents can induce chemical transformation of the organic pollutants either through direct energy transfer or by generating reactive species that further may react with pollutant. Among the most frequently encountered reactions in the aquatic environment involving short-lived reactive species, those involving HO· radicals seem to prevail.

Recently, studies on organic pollutant removal in the presence of real or simulated natural waters have been conducted to examine the interactions between organic pollutants and natural components in water under ultraviolet (UV) irradiation. Among the components that ubiquitously exist in natural waters, Fe (III) (0–0.94mg/L), NO_3 (0.186–20.026 mg/L) ions, and humic acid (HA) (0.3–30 mg/L) are reported to play important roles in the removal of organic pollutants under UV irradiation (Jong-Kwon, Yeomin, & Kyung-Duk, 2014).

The UV spectral range of interest for UV photolysis application in water is the UVC (200-280 nm), where both the pollutants and the water constituents (dissolved organic and inorganic compounds) absorb the radiation. The range between 280-315 nm is the UVB region and the range between 315-400nm is the UVA region. The vacuum UV (VUV) region within the 100-200 nm (Figure 1.10).
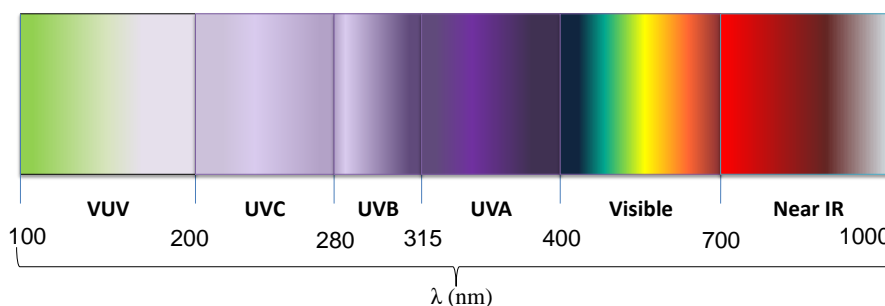

Figure 1.10- Spectrum of ultraviolet radiation

In the UV photolysis process, the electronically excited state RX* is generated.

$$RX + h\upsilon \rightarrow RX^* \quad\quad\quad\quad\quad (1.6)$$

It is highly energetic and can either deactivate to the ground state of the molecule through physical processes (such as fluorescence, phosphorescence, or non-radiative

deactivation) or undergo dark (thermal) chemical reactions. The most common chemical reactions pathways followed by the excited state are:

The homolytic bond scission is the predominant chemical pathway, and occurs in the solvent cage. Escaped from the solvent cage, the radicals undergo further oxidation/reduction reactions, depending on their structure (Parsons, 2004).

$$RX^* \rightarrow (R^\cdot ... X^\cdot)_{cage} \rightarrow R^\cdot + X^\cdot \tag{1.7}$$

Recombination of the primary radicals in the solvent cage leading to the parent molecule occurs with high probability, which explains the low quantum yields frequently observed with organic compounds in condensed media as compared to those in the gas phase.

$$(R^\cdot ... X^\cdot)_{cage} \rightarrow RX \tag{1.8}$$

In polar solvents, such as water, heterolytic bond scissions (intramolecular electron transfer).

$$RX^* \rightarrow (R^+ ... X^-)_{cage} \rightarrow R^+ + X^- \tag{1.9}$$

Energy and electron –transfer processes to oxygen are also possible, but require a relatively long-lived excited state, such as the triplet state. Very reactive species, such as di-oxygen radical anion (superoxide radical) and singlete oxygen are generated, along with the pollutant radical cation and the parent molecule in the ground state.

$$RX^* + O_2 \rightarrow RX^{+\cdot} + O_2^{-\cdot} \tag{1.10}$$

$$RX^* + {}^3O_2 \rightarrow RX^{+\cdot} + {}^1O_2^{-\cdot} \tag{1.11}$$

Proton and hydrogen atom transfers from the excited state to surrounding molecules are also possible, but with a much lower probability than all the reactions described before.

In the particular case of water photolysis in VUV region, the following reactions may occur (Kim & Tanaka, 2009; Parsons, 2004):

42

Electron generation in aqueous media:

$$H_2O + h\nu \rightarrow H^+ + HO\cdot + e^-_{aq} \tag{1.12}$$

- ▪ Fast generation of:

$$O_2 + H\cdot \rightarrow HO_2^{\cdot} \tag{1.13}$$

$$O_2 + e^-_{aq} \rightarrow O_2^{\cdot -} \tag{1.14}$$

1.4.3 UV/peroxide process

UV/ H_2O_2 processes generally involve generation of HO· radical through UV photolysis of H_2O_2. Thus, the organic compound is degraded by means of photon attack (direct UV photolysis) and hydroxyl radical reactions (Wols, Hofman-Caris, Harmsen, & Beerendonk, 2013). The most direct method for generation of hydroxyl radicals is through the cleavage of H_2O_2 with photons of high energy ($\lambda < 280$ nm), because the maximum absorbance of H_2O_2 occurs near 220 nm (Litter & Quici, 2010; Parsons, 2004). The reaction has a low quantum yield ($\varphi_{HO\cdot} = 0.5$) due to rapid recombination of the radicals in solution (Legrini et al., 1993; Litter & Quici, 2010; Parsons, 2004).

$$H_2O_2 + h\nu \rightarrow OH\cdot + OH\cdot \tag{1.15}$$

The sequence of reactions occurring during the H_2O_2/UV process used for the oxidation of organic compounds is described as follow (see figure 1.11):
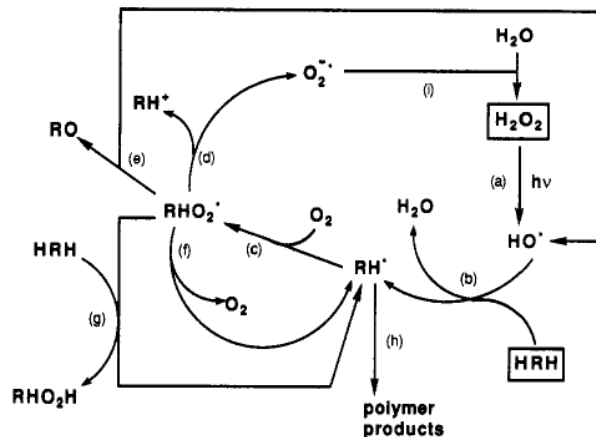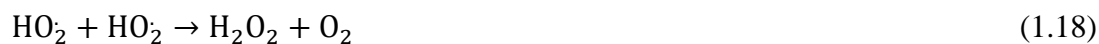

Figure 1.11- Reaction systems for the UV/H_2O_2 process. Source (Legrini et al., 1993)

43

Hydroxyl radicals generated by hydrogen peroxide photolysis (a) react with organic compounds (HRH) primarily by hydrogen abstraction to produce an organic radical (RH$^.$) (b). This radical reacts quickly with dissolved oxygen to yield an organic peroxyl radical (RHO$_2^.$) (c), initiating subsequent thermal oxidation reactions. Peyton (Peyton, 1990) proposed three different reaction paths to be followed by either peroxyl radicals or their tetraoxide dimers: (1) heterolysis and generation of organic cations as well as superoxide anion (d), (2) l,3- hydrogen shift and homolysis into hydroxyl radicals and carbonyl compounds (e), and (3) back reaction to RH$^.$ and O$_2$ (f).

Nevertheless, hydrogen abstraction by RHO$_2^.$ should not be discarded as a process of initiating a chain of thermal oxidation reactions (g). In aqueous systems, cations will further react by solvolysis, and superoxide anion will readily disproportionate to yield H$_2$O$_2$ (i). This is in contrast to the fate of superoxide anion in advanced oxidation processes utilizing ozone where it reacts primarily with ozone to produce hydroxyl radical. The latter figure reflects the importance of oxygen saturation in oxidative degradation processes. In cases of lack of oxygen, organic radicals will initiate polymerization of unsaturated organic substrate present in the reaction system or generated by dismutation (Legrini et al., 1993).

If low pressure lamps are used, a high concentration of H$_2$O$_2$ is needed to generate sufficient hydroxyl radicals because of low-absorption coefficient. However, high concentration of H$_2$O$_2$ scavenges the radicals, making the process less effective:

$$OH^. + H_2O_2 \rightarrow HO_2^. + H_2O \tag{1.16}$$

$$HO_2^. + H_2O_2 \rightarrow OH^. + H_2O + O_2 \tag{1.17}$$

$$HO_2^. + HO_2^. \rightarrow H_2O_2 + O_2 \tag{1.18}$$

$$HO_2^. + HO^. \rightarrow H_2O + O_2 \tag{1.19}$$

Hydroxyperoxyl radicals (HO$_2^.$) produced through the first reaction above, are much less reactive than HO$\cdot$ radicals (E^0=1.7 vs. 2.8 V) (Legrini et al., 1993; Litter & Quici, 2010).

To overcome the limitation of low absorptivity of H_2O_2 by the wavelength of 254 nm, it can be used a high intensity, medium pressure, broadband UV lamps (Parsons, 2004).

The use of hydrogen peroxide as an oxidant brings a number of advantages in comparison to other methods of chemical or photochemical water treatment:

- Commercial availability of the oxidant
- Thermal stability and storage on-site
- Infinite solubility in water
- Two hydroxyl radicals are formed for each molecule of H2O2 photolyzed
- Minimal capital investment
- Simple operation procedure

1.4.4 Photocatalysis

Photocatalysis may be defined as the "acceleration of a photoreaction by the presence of a catalyst". Heterogeneous processes employ semiconductor slurries for catalysis or supported catalyst, whereas homogeneous photochemistry is used in a single-phase system. In the last case, the interaction of a photon-absorbing species (transition metal complexes, organic dyes or metalloporphyrines), a substrate (e.g. the contaminant) and light can lead to a chemical modification of the substrate.

1.4.4.1 Heterogeneous photocatalysis

In the case of heterogeneous photocatalysis, when a catalyst being a semiconductor (for instance, TiO_2, ZnO, ZrO_2, CeO_2 or sulfides) is illuminated with photons whose energy is equal to or greater than their band-gap energy ($hv \geq E_g$), there is absorption of these photons and the generation of electron/hole (e^- and h^+) pairs, which dissociate into free photoelectrons in the conduction band and photoholes in the valence band. The excited electrons are transferred to the reducible specimen at the same time that the catalyst accepts electrons from the oxidizable specimen, which occupies the holes (see figure 1.12).
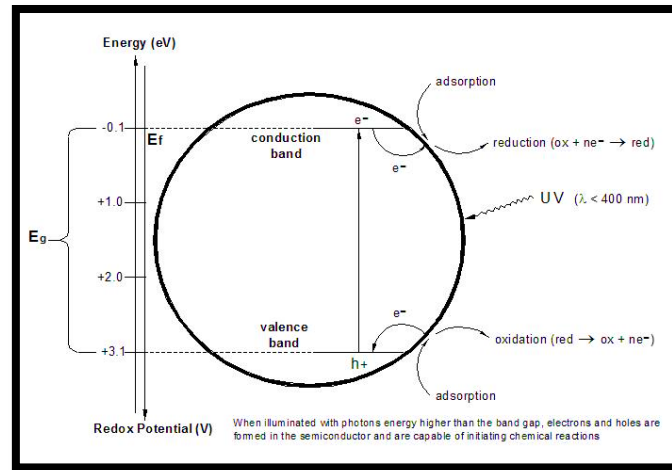
Figure 1.12- Simplified diagram of the heterogeneous photocatalytic processes occurring at illuminated TiO$_2$ particle. Source (Herrmann, 1999).

TiO$_2$ is so far the most useful semiconductor for photocatalytic purposes, owing to its exceptional optical and electronic properties, chemical stability, non-toxicity and low cost. The energy bandgaps of the photocatalytic forms of TiO$_2$, anatase and rutile, are 3.23 eV (corresponding to 384 nm) and 3.02 eV (corresponding to 411 nm). The most popular and photoactive commercial form of TiO$_2$ is produced by the German company Degussa (now Evonik) under the name P-25.

The figure 1.12 is completed by the following basic equations where e_{cb}^-, h_{vb}^+ and HO· are involved:

$$TiO_2 + hv \rightarrow e_{cb}^- + h_{vb}^+ \tag{1.20}$$

- Oxidation reactions:

  - electron transfer from adsorbed substrate RX

$$TiO_2(h_{vb}^+) + RX_{ad} \rightarrow TiO_2 + RX_{ad}^{\cdot+} \tag{1.21}$$

  - electron transfer from adsorbed solvent molecules (H$_2$O, HO$^-$)

$$TiO_2(h_{vb}^+) + (H_2O)_{ad} \rightarrow TiO_2 + HO_{ad}^{\cdot} + H^+ \tag{1.22}$$

$$TiO_2(h_{vb}^+) + HO_{ad}^- \rightarrow TiO_2 + HO_{ad}^{\cdot} \tag{1.23}$$

46
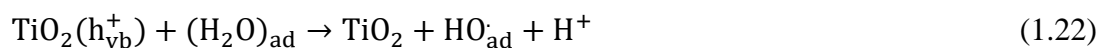
- The redox pathway is reached due to the excited electrons, once moved to the conduction band, are reducers able to be transferred to the acceptor specie adsorbed on the surface (normally O_2 to form $O_2 \cdot^-$)

$$TiO_2(e_{cb}^-) + O_2 \rightarrow TiO_2 + O_2^{\cdot-} \qquad (1.24)$$

- Addition of hydrogen peroxide (H_2O_2)

$$TiO_2(e_{cb}^-) + H_2O_2 \rightarrow TiO_2 + HO^- + HO \cdot \qquad (1.25)$$
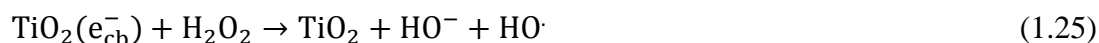
It has been shown that the addition of hydrogen peroxide considerable enhances the rate of the photodegradation, most probably via the latter reaction, or by surface-catalyzed dismutation of H_2O_2. Organic pollutants adsorbed onto the surface of the titanium dioxide particles will then be oxidized by HO· radicals.

1.4.5 Fenton

The conventional "dark" Fenton process involves the use of one or more oxidizing agents (usually hydrogen peroxide and/or oxygen) and a catalyst (a metal salt or oxide, usually iron). The reactions produce a range of free radicals, which can react with most organic compounds.

Fenton process brings a number of advantages:

- The key Fenton reagents, H_2O_2 and iron salts, are relatively inexpensive.
- Iron is highly abundant (and may be naturally occurring in the system being treated)
- Iron is non-toxic, however is important to know the limit allow in waters by the law.
- Hydrogen peroxide is relatively easy to transport and handle, as well as being environmentally benign in diluted form.

Fenton process (Fe (II)/H_2O_2/dark) involves the reaction between dissolved Fe (II) and H_2O_2 in acid aqueous solution leading to oxidation of Fe (II) to Fe (III) and the production of hydroxyl radicals (HO·) (W. Li, Nanaboina, Zhou, & Korshin, 2012; Litter & Quici, 2010; Parsons, 2004). The reaction is spontaneous and can occur without the influence of light:

$$Fe\ (II) + H_2O_2 \rightarrow Fe\ (III) + OH^\cdot + OH^- \qquad\qquad (1.26)$$
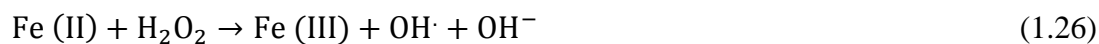
In the presence of H_2O_2 and at pH $\leq$ 3, the reaction system is autocatalytic, because Fe (III) reacts with H_2O_2 giving Fe (II), which can be generated at a slow rate (K=-0.001-0.02 $M^{-1}s^{-1}$) (Litter & Quici, 2010) through the next reaction (Bautista, Mohedano, Casaa, Zazo, & Rodriguez, 2008; Burbano, Dionysiou, & Suidan, 2008):

$$Fe\ (III) + H_2O_2 \rightarrow Fe(II) + HO_2^\cdot + H^+ \qquad\qquad (1.27)$$

Several reactions can then take place between the species in reaction:

$$Fe\ (II) + OH^\cdot \rightarrow OH^- + Fe(III) \qquad\qquad (1.28)$$

$$H_2O_2 + OH^\cdot \rightarrow HO_2^\cdot + H_2O \qquad\qquad (1.29)$$

$$Fe\ (II) + HO_2^\cdot + H^+ \rightarrow Fe(III) + H_2O_2 \qquad\qquad (1.30)$$

$$Fe\ (III) + HO_2^\cdot \rightarrow Fe(II) + O_2 + H^+ \qquad\qquad (1.31)$$

These reactions show that iron acts as catalyst. However, since the reduction of Fe (III) is generally much slower than the oxidation of Fe (II) (Litter & Quici, 2010; Malato et al., 2009; Parsons, 2004), iron exists mainly in the Fe (III) form in the systems (A. De León et al., 2014; Guz, Olivelli, Torres, Curutchet, & Candal, 2014).

The Fenton process (in its unmodified form) is more efficient around pH 2.8 (Parsons, 2004; Trapido, Kulik, Goi, Veressinina, & Munter, 2009). Hence the process is inefficient in the pH range of most natural waters (pH 5-9), particularly due to the precipitation of ferric hydroxides or oxyhydroxide occurring at pH>3-4 (depending on the iron concentration).

It has been found that addition of certain organic ligands that can complex Fe (III) enables the process to be carried out at higher pH.

1.4.6   Photo-Fenton process

Photo-Fenton or photo-assisted Fenton (Fe (II)/H_2O_2/light) process involves irradiation with sunlight or an artificial light source, which increases the rate of

contaminant degradation by stimulating the reduction of Fe (III) to Fe (II). When irradiated with light (ultraviolet and some visible light), Fe (III) can catalyze the formation of hydroxyl radicals (A. De León et al., 2014; Guz et al., 2014; Parsons, 2004). This process is characterized by photo-reduction of ferric to ferrous ions that is promoted concomitantly with the generation of additional HO·.

Photo-Fenton process stars with the classical Fenton's reagent

$$Fe\ (II) + H_2O_2 \rightarrow Fe(III) + HO· + HO^- \tag{1.32}$$

When the system is irradiated with UV or visible light, the photoassisted Fenton's process produces ferric ions as a by-product of the reaction between Fe (II) and H_2O_2 and then is photochemically transformed back into ferrous ions (Carra, Malato, Jiménez, Maldonado, & Sanchéz, 2014; A. De León et al., 2014; Guz et al., 2014; R. F. P. Nogueira, Trovó, da Silva, Villa, & de Oliveira, 2007; Parsons, 2004).

$$Fe\ (III) +\ H_2O_2 + h\nu \rightarrow Fe(II) + HO· + H^+ \tag{1.33}$$
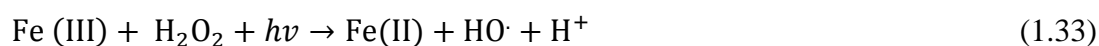
The HO· production is determined by the availability of light of suitable wavelength and H_2O_2 (A. De León et al., 2014; Guz et al., 2014; Parsons, 2004).

Photo-Fenton can use sunlight (Carra et al., 2014; Litter & Quici, 2010) instead of UV light with a minor decrease in the rate of degradation; this is very important factor, since the cost of the treatments will be lowered if sunlight is used.

1.4.7 Bicarbonate-activated hydrogen peroxide (BAP) method

Bicarbonate-activated hydrogen peroxide (BAP) is a method for activating hydrogen peroxide by using bicarbonate ion.

Bicarbonate (HCO_3^-), a relative nontoxic anion, is one of the most abundant anions in natural water. It is also an efficient activator for H_2O_2 to generate active oxidant species such as peroxymonocarbonate (HCO_4^-) formed by a labile pre-equilibrium reaction. This simple and green system has been successfully used for many oxidation reactions (Fakhraian & Valizadeh, 2010; Xu, Li, Xiong, & Yin, 2011).

$$HCO_3^- + H_2O_2 \leftrightarrow HCO_4^- + H_2O \tag{1.34}$$

In addition, HCO_3^- is an important complexing ligand for some metal ions, leading to significant changes in their redox potentials.

The conditions of the BAP system are mild with pH around neutral or weakly alkaline rather than the strongly alkaline conditions often employed for peroxide bleaching. The components of the system are inexpensive and environmentally friendly.

1.4.8   Cobalt (II)/Bicarbonate/Hydrogen Peroxide System

Adding trace redox metal ions, such as cobalt, to the bicarbonate/H_2O_2 system (Co (II) ions alone do not efficiently generate HO· radicals from H_2O_2) would greatly accelerate its degradation rate (X. Li et al., 2012; Xu, Li, Ye, Yin, & Zeng, 2011). The drawback is that these redox metal ions are actually toxic in flash water and need to be strictly regulated to the parts per million (ppm) levels.

Chapter II

Objectives

2   OBJECTIVES

2.1   General Objective

The main objective of this work is to study the efficiency of several Advanced Oxidation Processes (AOPs) to degrade Metoprolol (MET) present in waters, in different experimental conditions.

The AOPs to be tested: photolysis, UVC/H_2O_2, photocatalysis, Fenton, photo-Fenton, bicarbonate/H_2O_2 with and without catalyst.

2.2   Specific goals

2.2.1   Photolysis

- Study MET and TOC degradations by photolysis using artificial and natural light.
- Investigate the influence of the photoreactor material in photolysis process.

2.2.2   UVC/H_2O_2

- Asses MET and TOC removals by UVC with H_2O_2 at different pH and H_2O_2 concentration.

2.2.3   Photocatalysis

- Asses the treatment of MET by photocatalysis with TiO_2, using two different irradiation sources: artificial light and natural light.
- Study MET and TOC removals, biodegradability and toxicity varying the experimental conditions: pH, catalyst concentration, initial MET concentration, addition of oxidant agents (UV-Vis/H_2O_2/TiO_2, UV-Vis/H_2O_2) and water matrix (Mili Q water and water from effluent of a WWTP).

2.2.4   Fenton

- Study the treatment of MET removal by dark Fenton and the effect of different Fe (II) and hydrogen peroxide concentrations and the ways for the catalyst addition.

2.2.5 Photo-Fenton

- Asses the MET and TOC removals by photo-Fenton, using four different irradiation sources.
- Study the effect of different experimental conditions: Fe (II) and hydrogen peroxide concentrations, temperature and addition ways of the catalyst.

2.2.6 Catalyst/bicarbonate/H_2O_2

- Study the MET removal by Bicarbonate-activated hydrogen peroxide (BAP) method in drinking water and the effect of different experimental conditions: pH, HCO_3^-, hydrogen peroxide concentrations, addition of Co (II) or Fe (II) as catalyst and dosing ways of the catalyst.

2.2.7 Comparison of different set-ups and processes

- Compare three processes (photocatalysis, photo-Fenton and UVC/H_2O_2) and determine the performance in MET and TOC removal.
- Compare photocatalysis process using two different irradiation sources (artificial light and sunlight) and determine the efficiency (energy/MET removed).
- Compare photo-Fenton process carried out in four different devices, determining the energetic efficiency (energy/MET removed) of the processes.
- Compare all the techniques used under the best conditions tested and determine which process offers the best energetic efficiency.
- Propose possible degradation pathways for the different AOPs tested and compare these pathways.

2.2.8 Study of irradiation for photocatalytic reactors

- Use of a simple actinometric method which measures the irradiation entering into the photocatalytic system when there is a catalyst in suspension in the media.

Chapter III

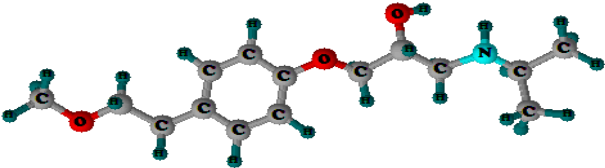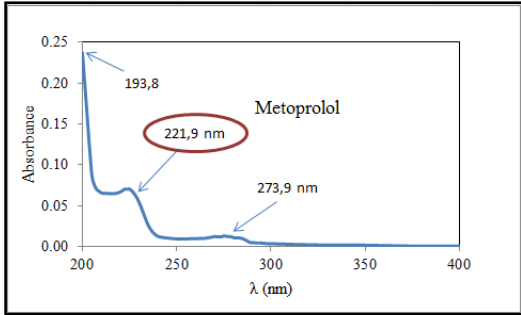# Materials, analytical methods and procedures

3   MATERIALS, ANALYTICAL METHODS AND PROCEDURES

3.1   Chemicals and reagents

Metoprolol

Metoprolol (MET) was purchased from Sigma-Aldrich (Spain) and Aladin Chemistry Co. Ltd (China) as Metoprolol Tartrate Salt CAS No: 56392-17-7 (purity >99%)

Table 3.1- Chemical properties of MET

Dissociation constant (pKa)	9.2-9.6
Character	hydrophilic
Molecular Weight (g/mol)	267.364
Formula	$C_{15}H_{25}NO_3$
Molecular structure	
UV –visible spectra	

Other chemicals and reagents

Table 3.2- Chemical properties of the all other reactive used in this work.

Name	CAS No.	Formula	Supplied by	Purity (%)	Used for/in
Titanium dioxide Degussa P-25	13463-67-7	TiO_2	Sigma-Aldrich	anastase~70 and rutile ~30	Photocatalysis process
Hydrogen peroxide	7722-84-1	H_2O_2	Merck and Sinopharm Chemical Reagent Co. Ltd	30	All processes
Iron (II) sulfate heptahydrate	7782-63-0	$FeSO_4.7H_2O$	Panreac and Sinopharm Chemical Reagent Co. Ltd.	99	Fenton and photo-Fenton and Fe/bicarbonate/H_2O_2 processes
Cobalt (II) acetate tetrahydrate	6147-53-1	$(CH_3COO)_2Co\ 4H_2O$	Sinopharm Chemical Reagent Co. Ltd.	98	Cobalt-bicarbonate-hydrogen peroxide process.
Sodium hydrogen carbonate	144-55-8	$NaHCO_3$	Sinopharm Chemical Reagent Co. Ltd.	99.7	Cobalt-bicarbonate-hydrogen peroxide and bicarbonate-hydrogen systems
Acetonitrile	75-05-8	C_2H_3N	Fischer Chemical	98	as mobile phase for HPLC analysis
Orthophosphoric acid	7664-38-2	H_3PO_4	Panreac	85	water pH adjustment for HPLC analysis
Sodium bisulfite	7631-90-5	$NaHSO_3$	Panreac	40	To quench TOC samples containing H_2O_2, to avoid further reactions.
Methanol	67-56-1	CH_3OH	Panreac	98	To quench HPLC samples containing H_2O_2 to avoid further reactions.
Liver bovine catalase	9001-05-2	$H_2O_2:H_2O_2$ oxidoreductase	Sigma-Aldrich	-	To quench COD samples containing H_2O_2 to avoid further reactions.
Sulfuric acid	7664-93-998	H_2SO_4	Panreac	98	pH adjustment (~2.8) in Fenton, photo-Fenton and Fe/bicarbonate/H_2O_2 reactions.
o-Nitrobenzaldehyde	552-89-6.	$C_7N_5NO_3$	Panreac	98	Actinometry process
Ethanol	64-17-5	C_2H_6O	Panreac	96	Actinometry process
Formic acid	64-18-6	CH_2O_2	Probus S.A	85	Actinometry process as scavenger.
Tert-butyl alcohol	75-65-0	$C_4H_{10}O$	Probus S.A	99	Actinometry process and Iron/bicarbonate system as scavenger.
Benzoquinone	106-51-4	$C_6H_4O_2$	Merck	98	Actinometry process as scavenger.
Sodium hydroxide	1310-73-2	$NaOH$	Panreac	98	Actinometry process

3.2 Techniques and analytical instruments

High Performance Liquid Chromatograph

MET concentrations were monitored by High Performance Liquid Chromatograph (HPLC) from Waters using a SEA18 (250 x 4.6 mm i.d.; 5µm particle size) Teknokroma column, and a Waters 996 photodiode array detector. The mobile phase was composed by water (pH 3) and acetonitrile (80:20), injected with a flow-rate of 0.85 mL/min. MET concentration was followed at UV maximum absorbance (221.9 nm).

Figure 3.1- HPLC (University of Barcelona)

Ultra Performance Liquid Chromatography

Ultra Performance Liquid Chromatography (UPLC) H class. UPLC was used to follow MET concentration in bicarbonate/H_2O_2 and Co (II)/ bicarbonate/H_2O_2 systems.

It has a BEH C18 column (1.7 µm, 2.1x 50 mm). The mobile phases used to detect MET were composed of water (pH 3) and acetonitrile (80:20), injected with a flow-rate of 0.4 mL/min and detected at its maximum UV absorbance of 221.9 nm.

Figure 3.2- UPLC (Tongji University)

HPLC-DAD-ESI-TOF (+) 175V Isocratic

To identify the intermediates LC/MSD-TOF (Agilent Technologies) was used with Electrospray (ion spray) ESI MS technique, lecture positive ion. SEA18 (250 x 4.6 mm i.d.; 5µm particle size) Teknokroma column. The mobile phase was composed by water (pH 3) and acetonitrile (80:20), injected with a flow-rate of 0.85 mL/min.

Total Organic Carbon

In this study, Total Organic Carbon (TOC) was measured with a Shimadzu TOC-V CNS instrument, with Auto sampler ASI-V and a measure unit of total nitrogen TMN-1.

Figure 3.3- Auto-sampler ASI-V (University of Barcelona)

Chemical Oxygen Demand

For the Chemical Oxygen Demand (COD) analysis, the Standard Methods (5220D: Closed Reflux, Colorimetric Method) procedure was followed by use of a spectrophotometer (Hach Lange DR 2500) at 420 nm, employing pyrex-glass vials after 2h of extreme catalytic oxidation conditions at 150ºC.

Figure 3.4- Analytical instruments for COD measurements.

Biochemical oxygen demand

Biochemical oxygen demand is determined by incubating a sealed sample of water for five days (BOD_5) and measuring the loss of oxygen from the beginning to the end of the test.

BOD_5 was determined according to Standard Method 5210 by respirometric process using OxiTop equipment during five days under constant stirring and controlled temperature (20ºC $\pm$ 1 ºC). The microorganism-seed (lyophilized capsules 5466-00, Cole-Parmer) were aerated during 2h before inoculation.

Figure 3.5- Oxitop equipment (University of Barcelona)

Aromaticity and Specific Ultraviolet Absorbance

Aromatic organics can be detected using the UV 254 nm wavelength because of the strong absorption properties that these double bond organics have at that wavelength. Ultraviolet absorbance (UVA) procedure requires that the sample be passed through a 0.45-µm filter and transferred to a quartz cell. It is then placed in a spectrophotometer and reported in cm^{-1}. The spectrophotometer used was in this work was Perkin Elmer UV/VIS Lambda 20.

Specific Ultraviolet Absorbance (SUVA) is defined as the UV absorbance of a water sample at a given wavelength normalized for dissolved organic carbon (DOC) concentration. The SUVA calculation requires both the DOC and UVA measurement. The SUVA is calculated by dividing the UV absorbance of the sample (in cm^{-1}) by the DOC of the sample (in mg/L) and then multiplying by 100 cm/M. SUVA is reported in units of L/mg-M.

Figure 3.6- Spectrophotometer Perkin Elmer UV/VIS Lambda 20 (University of Barcelona)

Hydrogen Peroxide consumption

Hydrogen peroxide (H_2O_2) determination was followed in TiO_2/H_2O_2, Fenton, photo-Fenton, UV/H_2O_2, and bicarbonate/H_2O_2 with and without catalyst processes, through metavanadate spectrophotometric procedure (R. F. Nogueira, Oliveora, & Paterlini, 2005) in order to know H_2O_2 consumption during photodegradation reactions.

The procedure is based on the reaction of H_2O_2 with ammonium metavanadate in acidic medium, which results in the formation of a red-orange color peroxovanadium cation, with maximum absorbance at 450 nm. The spectrophotometer used was Hach Lange DR 3900.

$$VO_3^- + 4H^+ + H_2O_2 \rightarrow VO_2^{3+} + 3H_2O \qquad\qquad (3.1)$$

Dissolved Iron measurement

Iron (Fe (II)) determination was assessed by colorimetric o-Phenanthroline method (International Organization for Standardization, 1988). Ferrous iron (Fe (II)) forms a red coloured complex with 1.10-phenantroline. The absorption of this complex measured at 510 nm, by spectrophotometer Hach Lange DR 3900, is proportional to ferrous iron concentration. Total iron can be measured after ferric iron (Fe (III)) reduction with ascorbic acid to ferrous iron (Fe (II)). Consequently, ferric iron concentration (Fe (III)) can be calculated as the difference between total iron and ferrous iron.

pH measurement

The pH determination was followed by pH meter VWR Symphony SB90M5.

Figure 3.7- pH meter VWR Symphony SB90M5 and analytical instruments.

Radiation measure

In order to measure the irradiance to which the processes are carried out, using natural or artificial irradiation, instrumental methods such as radiometry or spectroradiometry are used or actinometric measurements are made during photostability testing.

Solar irradiation

The solar irradiation was determinated by a spectroradiometer Bentham DMc300 with double monochromatic measuring between 290 and 1100 nm for photocatalysis process. The data were integrated from 290 to 315 nm for UVB and 315 to 400 nm for UVA. For photo-Fenton process the irradiation was measured by data logging radiometer PMA2100.

The amount of solar accumulated energy (Q (kJ/L)) was calculated according (De la Cruz, Dantas, Giménez, & Esplugas, 2013; Malato et al., 2009; Mendez-Arriaga, Maldonado, Giménez, Esplugas, & Malato, 2009; Singh et al., 2011):

$$Q = \sum_{i=0}^{n}(FA\Delta t_i)/V \tag{3.2}$$

Where A (m^2) is the mirror´s area of capture-reflection of solar irradiation, F is the average of the incident solar UV energy flux measured by radiometer (W/m^2) for Δt (s), time between two sampling periods (i) and V is the volume of the treated solution.

63

Actinometric measures

Is necessary to know the intensity of the laboratory light source, or natural irradiation at least over a specific wavelength range. Actinometries are well known processes based on the reaction of a determined compound, as a result of a photon absorption in a specified wavelengths range, the actinometric reaction rate is related to photons absorption. The extent of the reaction as a function of time can be measured with common analytical techniques, and the resulting rate of reactant loss can be converted into light intensity (De La Cruz et al., 2013).

An established chemical actinometer should meet the following requirements (Blanco-Galvez & Malato-Rodríguez, 2003; Kuhn, Braslavsky, & Schmidt, 2004):

- The photochemical system should be simple and well-studied. The photoreaction must be reproducible under well-defined and easily controllable experimental conditions.

- The chemical actinometer is unaffected by its photoproducts

- The chemical components should be thermally stable to exclude complications due to dark reactions.

- The analytical methods should be simple.

- The system should display large sensitivity.

- The handling of the photochemical system and the evaluation of the number of photons absorbed should be simple and straightforward.

- The actinometric material should be easy to synthesize and purify. Preferably, it should be commercially available. Disposal of the waste should be straightforward.

- Some commonly used actinometries have been carried out to quantify the radiation entering into the system (Kuhn et al., 2004).

The accumulated energy (Q (kJ/L)) was calculated according:

$$Q = \sum_{i=0}^{n}(I\Delta t_i)/V \qquad\qquad (3.3)$$

Where I is the incident photon flow (kJ/s) assessed by actinometry, Δt_i is the time (s) and V is the volume of the treated solution.

The photon flow entering solarbox and black light blue lamps reactors was measured by actinometry based on o-Nitrobenzaldehyde (o-NB) reaction. This actinometry has been selected, because actinometer absorbs in the range from 290 to 400 nm. It also entails a safe experimental procedure and easy to perform. Another advantage is that the o-NB actinometry can be used with common UV lamps and also in solar photoreactors.

o-NB actinometry was carried out adapting the method proposed by Willet and Hites (Willett & Hites, 2000). Thus, the incident photon flow obtained was 2.68 µEinstein/s for solarbox (De La Cruz et al., 2013).

For black light blue lamps reactor, the incident photon flow obtained was 6.0 µEinstein/s.

The light inside the photoreactor UVC was assessed by actinometric experiments (Kuhn et al., 2004) and the obtained value was 1.70 µEinstein/s at 254 nm.

Toxicity test (Vibrio Fischeri)

Toxicity of treated samples is assessed by measuring the inhibitory effect on the light emission of *vibrio fischeri* determined after 15 minutes in order to identify the EC_{50} (International Organization for Standardization, 2007).

According to AFNOR T90-301 standard, the results are expressed in "Equitox", whereas the number of Equitox content per cubic meter of water is equal to the inverse of EC_{50} expressed in percent.

$$Equitox/m^3 = \left(\frac{1}{EC_{50}}\right) * 100 \tag{3.4}$$

Biodegradability

The measurement of biodegradability was done based on BOD_5/COD ratio (values between 0 to 1), being 1 the ideal condition where total oxygen present is biologically up taken.

As known (Metcalf & Eddy, 1991), a municipal wastewater can be considered biodegradable when the BOD_5/COD ratio is higher than 0.4. However González and co-workers (González, Sans, Esplugas, & Malato, 2009) consider that a BOD_5/COD ratio higher than 0.25 is adequate for a biological treatment.

__Average Oxidation State__

AOS was calculated using equation 3.5:

$$AOS = 4\,[(TOC - COD)]/TOC \tag{3.5}$$

Where TOC and COD are reported in mol/L of carbon and oxygen, respectively (Stumm & Morgan, 1996). AOS takes values between +4 for CO_2, the most oxidized state of C and -4 for CH_4, the most reduced state of C (Sarria et al., 2002).

The AOS varies as function of the treatment time and it indicates the degree of oxidation of the different organic compounds present in the water.

3.3   Experimental devices

__Solarbox (SB)__

The photolysis, photo-Fenton and photocatalytic experiments were carried out in a solar simulator device solarbox (SB), from CO.FO.ME.GRA (220V 50 Hz), with Xenon lamp (Phillips 1kW) as irradiation source, with a photon flux 2.68 µEinstein/s (290-400 nm). The Duran tubular photoreactor (0.084 L, 24cm length x 2.11cm Ø) was placed at the bottom of the solarbox in the axis of a parabolic mirror made of aluminum reflective material. A filter cutting off wavelengths under 280 nm was placed between the lamp and the reactor when was necessary.

The solution to be treated was pumped to solarbox by peristaltic pump (Ecoline VC-280 II, Ismatec) from a stirred double jacket reservoir batch tank (total volume 1L) with a flow of 0.71 L/min. The reservoir was connected to an ultra-thermostatic bath (HaaKe K10) to assure constant temperature during the processes and all connections employed were made of Teflon to avoid losses by adsorption. Figure 3.8 shows SB and experimental device.
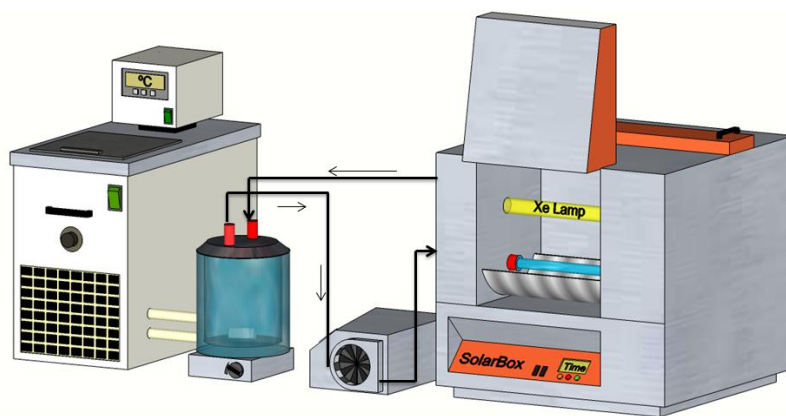
Figure 3.8- Solarbox device

The next table shows the most important technical characteristic of this installation.

Table 3.3- Technical characteristics of the solarbox

REACTOR: SOLARBOX (SB)	
Collector geometry	one -axis parabolic collector (PC)
Collector material	Al-reflective mirrors
Mirror´s area (m^2)	0.0151
Light source	Xe-OP (philips) 1000 W lamp
Photoreactor number	1
Photon flux	2.68 µEinstein/s (290-400 nm)
Glass material	Duran
Total volume of photoreactor (L)	0.084
Total volume of suspension (L)	1
Volume irradiated (L)	0.084
Volume irr-Volume dark (%)	8.4
Temperature (ºC)	14-25
Stirring system	Magnetic
Volumetric flow rate (L/min)	0.71

Solar pilot plant reactor based on compound parabolic collectors (CPC):

The CPC consists in a module, 41° inclined and made of polished aluminum, with 6 parallel tubular quartz reactors (figure 3.9). The total mirror´s area for solar irradiation capture-reflection was 0.228 m^2. The aqueous suspension of MET with TiO$_2$ was pumped with a peristaltic pump with a flow equal to 2.6 l min^{-1}, from the stirred reservoir tank (10 L) to irradiated quartz tubes and continuously recirculated. Solar irradiation was measured by a spectroradiometer Bentham DMc300. CPC reflectors are usually made of polished aluminum (aluminum is the only metal surface that is highly reflective throughout the ultraviolet spectrum; 92.3% at 280 nm to 92.5% at 385 nm) and the structure can be a simple photoreactor support frame with connecting tubing (Malato et al., 2013). The solution was constantly mixed by RW 16 basic agitator IKA.
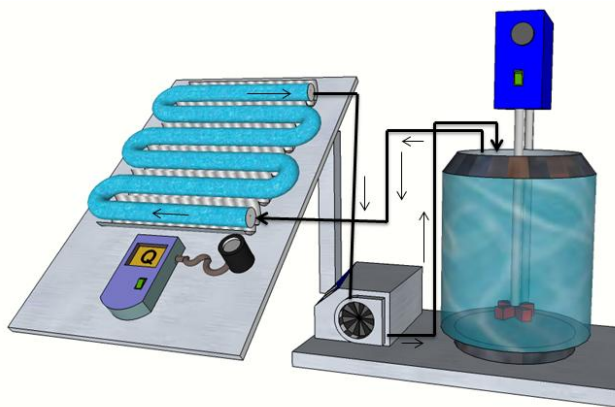
Figure 3.9- CPC device

The next table shows the most important technical parameters of CPC reactor.

Table 3.4- Technical characteristics of the pilot plant.

REACTOR: CPC	
Collector geometry	Compound Parabolic Collector (CPC)
Collector material	Al-reflective mirrors
Mirror´s area (m^2)	0.228
Light source	Solar light
Photoreactor number	6
Photon flux	Depending of day (290-400 nm)
Glass material	Quartz
Total volume of photoreactor (L)	0.95
Total volume of suspension (L)	10
Volume irradiated (L)	0.95
Volume irr-Volume dark (%-%)	9.5
Temperature (ºC)	30±5
Stirring system	Mechanic external
Volumetric flow rate (L/min)	2.6
Place localization (coordinates)	at sea level Barcelona
Inclination (º)	(Latitude 41º28´, Longitude 2º06´)

UVC reactor (UVC)

Consists in a thermostated Pyrex-jacketed 2 L vessel, equipped with three fluorescent low pressure mercury lamps (Phillips TUV 8W, G8T5), whose nominal power was 8W each one (figure 3.10). Lamps emitted monochromatic radiation between 200–280 nm, with a maximum at 254 nm. The intensity of the incident light inside the photoreactor was 1.70 µEinstein/s at 254 nm. The solution was fully mixed with a magnetic stirrer to ensure sufficient mixing. The reaction temperature was kept constant during all processes by thermostatic bath.
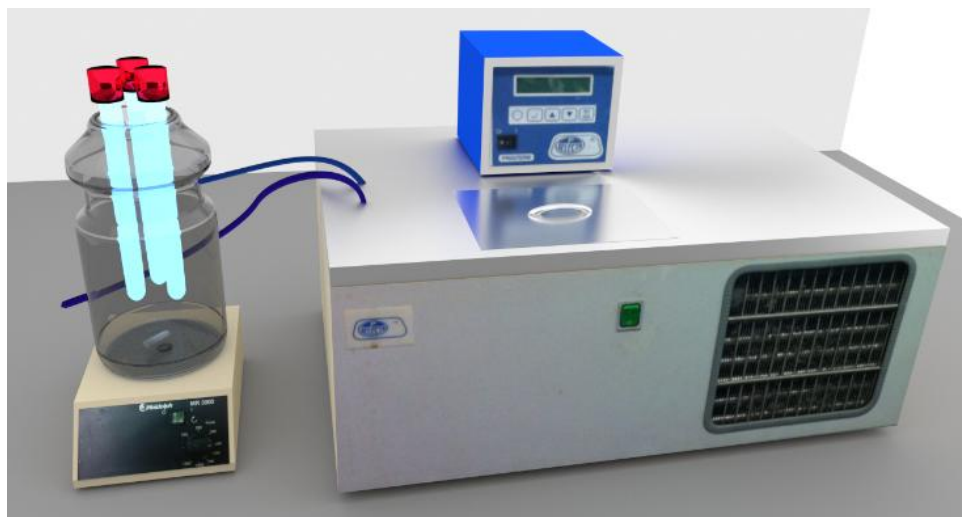
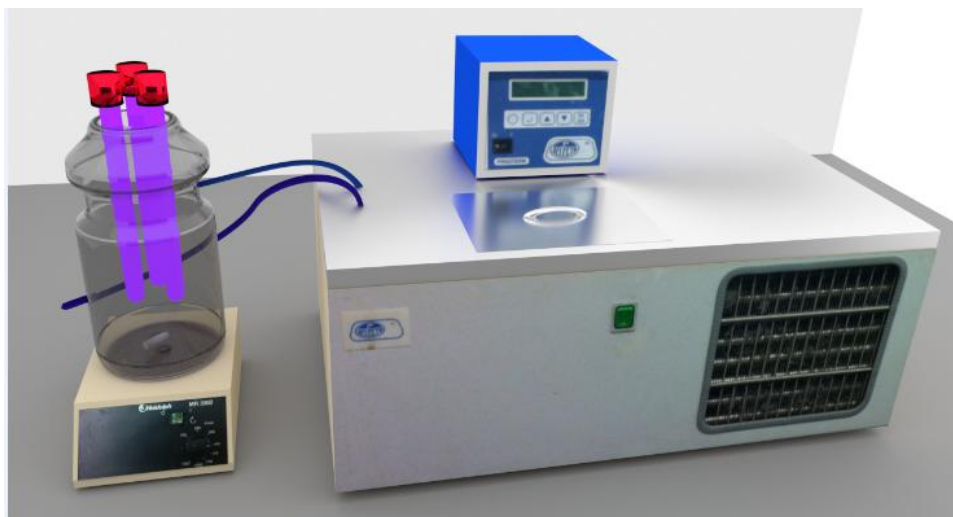Figure 3.10- UVC$_{254\ nm}$ reactor and experimental instruments

The next table shows the most important technical parameters of UVC reactor.

Table 3.5- Technical characteristics of the UV-C reactor

REACTOR: UVC	
Light source	Phillips TUV 8W, G8T5
lamps number	3
Photon flux	1.70 µEinstein/s (290-400 nm)
Glass material	Duran
Total volume of suspension (L)	2
Temperature (ºC)	25
Stirring system	Magnetic

Black light blue lamps (BLB)

Consists on a 2 L Pyrex-jacketed thermostatic vessel (inner diameter 11 cm, height 23 cm), equipped with three 8W BLB lamps (Philips TL 8W-08 FAM) placed in its centre (figure 3.11). Lamps emitted radiation between 350 and 400 nm, with a maximum at 365 nm. The radiation entering to the photoreactor was constant at 6.0 µEinstein/s in the 290-400 nm range. The reaction temperature was kept constant during all processes by thermostatic bath.

Figure 3.11- BLB reactor and experimental instruments

The next table shows the most important technical parameters of BLB reactor

Table 3.6- Technical characteristics of the BLB reactor.

REACTOR: BLB	
Light source	Philips TL 8W-08 FAM
lamps number	3
Photon flux	6.0 µEinstein/s (290-400 nm)
Glass material	Quartz
Total volume of suspension (L)	2
Temperature (ºC)	14-25
Stirring system	Magnetic

Fenton reactor

Consists on stirred 2 L Pyrex-jacketed thermostatic vessel (inner diameter 11 cm, height 23 cm) (figure 3.11), the temperature was kept constant at 25 ºC during all the reaction time. All Fenton processes were carried out under dark conditions (without lamps).

The next table shows the most important technical parameters of dark-Fenton reactor

Table 3.7- Technical characteristics of Fenton reactor.

REACTOR: Fenton	
Light source	-
Reactor material	Pyrex-jacketed vessel
Total volume of suspension (L)	2
Temperature (ºC)	25 ºC
Stirring system	Magnetic

Dark reactor for Bicarbonate/H$_2$O$_2$ experiments with and without catalyst

The reactor consists on stirred 500 mL dark Pyrex-jacketed vessel, the temperature room was kept constant at 25 ºC during all the reaction time. In this reactor were carried out all the series of experiments related to bicarbonate/hydrogen peroxide and catalyst/bicarbonate/hydrogen peroxide processes. These series were done under dark conditions. The dark reactor used in this section is the illustrated in figure 3.12.

Figure 3.12- Dark-Fenton reactor

The next table shows the most important technical parameters of dark-Fenton reactor

Table 3.8- Technical characteristics of dark reactor

REACTOR: Dark reactor for Bicarbonate/H$_2$O$_2$ with or without catalyst	
Light source	-
Reactor material	Pyrex vessel
Total volume of suspension (L)	0.5
Temperature (ºC)	Room temperature
Stirring system	Magnetic

Chapter IV

Results and

discussion

Table 4.1- General table (Photolysis process)

Exp Nº	[MET]$_0$ (mg/L)	pH$_0$	T (ºC)	Other	MET conversion (%)	TOC conversion (%)	Time (min)	wavelength range
				Photolysis (P)				
P-SB-1	50	6.2	25	quartz reactor/no filter	28.3	6.4	300	UV
P-SB-2	50	6.2	25	duran reactor/ filter	18.7	4.2	300	UV-B, UV-A
P-CPC-3	50	6.2	30 ± 5	Q=5.3 kJ/L	10.2	3.3	300	UV-B, UV-A
P-BLB-4	25	6.2	25		2.8	0	60	UV-A
P-BLB-5	50	6.2	25		3.0	2.1	240	UV-A
P-BLB-6	100	6.2	25		2.8	1.6	60	UV-A
P-UVC-7	50	3.0	25		93.8	3.3	240	UV-C
P-UVC-8	50	6.2	25		93.5	5.4	240	UV-C
P-UVC-9	50	9.0	25		97.3	7.5	240	UV-C

4   RESULTS AND DISCUSSION

4.1   Photolysis

Table 4.1 summarizes the results obtained by photolysis process carried out in different devices: SB, CPC, UVC and BLB reactors.

When studying a photocatalytic process, it is very important to be able to separate the influence of photolysis. For this purpose, a series of experiments were done with UV illumination, and without catalyst or oxidant agent to highlight the Metoprolol ability to absorb the radiation reaching the system.

Effect of the glass material photoreactor and filter in SB reactor

The effect of Duran and quartz glass material reactor was investigated under direct UV radiation in SB (P-SB-1and P-SB-2), taking into account that borosilicate glass has good transmissive properties in the range with a cut-off approximately 285 nm. Meanwhile quartz allows the pass of radiation with wavelengths higher than 200 nm (see figure 4.1).
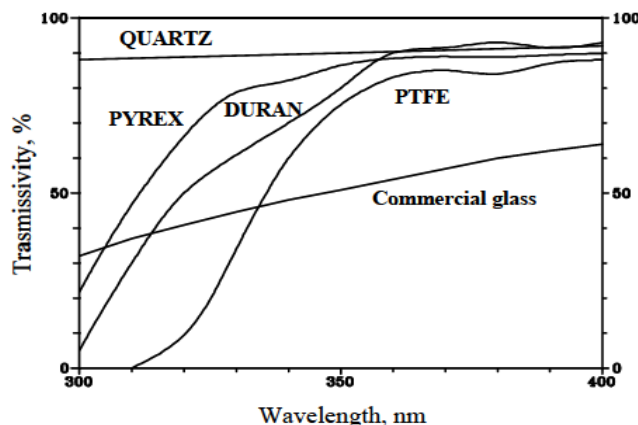
Figure 4.1 - Transmittance of different materials suitable for the manufacture of photoreactor tubes (Malato et al., 2013).

In this comparison it was observed that without filter cutting off wavelengths under 280 nm and quartz reactor (see figure 4.2), MET removal was 28.3% and mineralization was 6.4%. On the other hand, only 18.7% of MET in 300 minutes was eliminated and the TOC removal was 4.2% using Duran reactor.
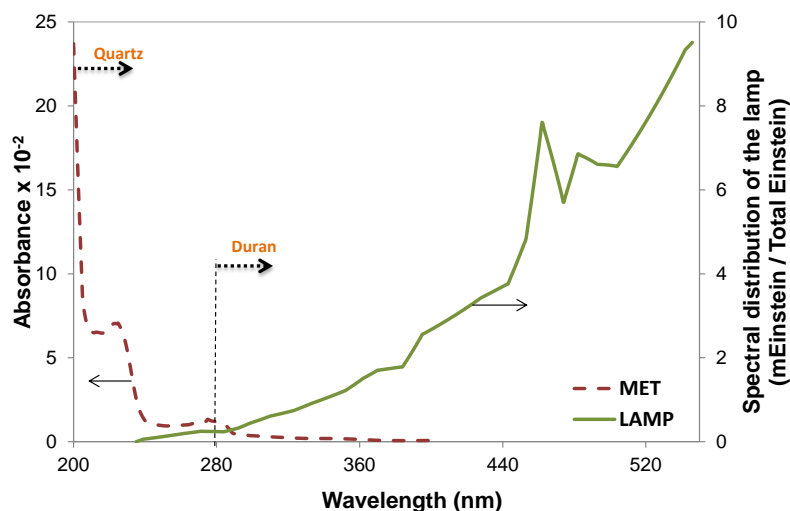
Figure 4.2- Absorbance spectrum of MET for aqueous solution (left axis) and lamp spectrum (right axis). Quartz and Duran transmittances.

Summing up, the maximum MET conversion reached by photolysis was lower than 30% after 300 minutes of irradiation when SB was used and quartz reactor without filter (< 280 nm), confirming that the direct photolysis is not fast enough to be considered as an adequate technology to remove the target compound and the mineralization obtained is too low.

Photolysis SB, CPC, UVC and BLB reactors

Photolysis experiments were carried out with 50 mg/L of initial MET in Milli-Q water, free pH, and 25 ± 5 ºC in all reactors (Exp. P-SB-2, P-CPC-3, P-BLB-5, and P-BLB-8).

The results observed during 240 minutes of irradiation (see figure 4.3) confirmed the low influence of photolysis on MET degradation in SB, CPC and BLB: 14.0%, 8.1%, and 3% respectively. However when UVC was used, MET solution has been degraded up to 93.5 %. This behavior can be explained because the MET absorption spectrum (peaks centered on 221 and 273 nm) correspond to UVC radiation.
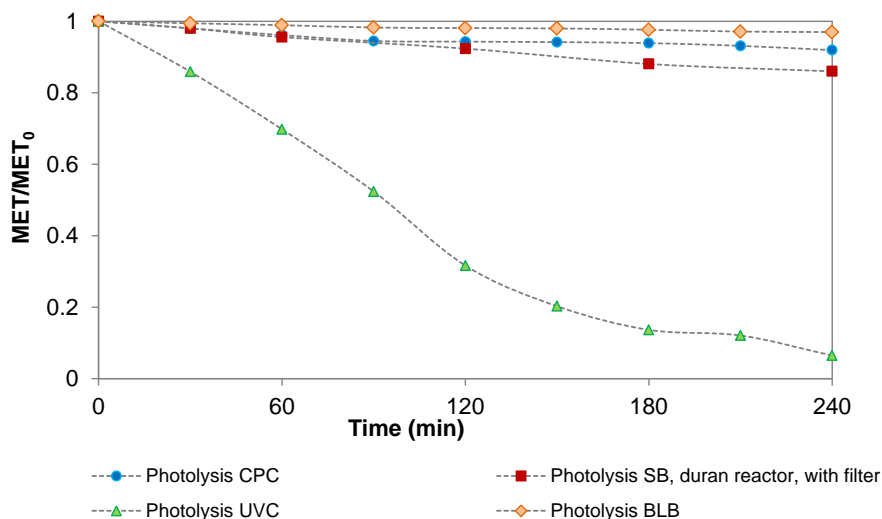
Figure 4.3- MET degradation by direct Photolysis using SB, CPC, BLB and UVC reactors, 50 mg MET/L, free pH and 25 ºC

Furthermore, photolysis did not promote relevant mineralization: the higher values reached were 2.5%, 2.7%, 2.1% and 5.4% in SB, CPC, BLB and UVC reactors respectively.

Going a step forward (Exp. P-BLB-4 and P-BLB-6), the influence of the initial MET concentration was studied. Thus, solution with 25 and 100 mg/L MET were degraded during 60 minutes under BLB radiation and the results show that MET conversion was still so low (~3%) and mineralization was negligible.

Additionally the photolysis was performed in the reactor $UVC_{254\,nm}$ at different pH (3, 6.2 and 9) (Exp. P-UVC-7, P-UVC-8 and P-UVC-9). The results obtained, within 240 minutes, showed a slight improvement when pH increases: 93.5%, 93.8% and 97.3% of MET elimination at pH 3, 6.2 and 9 respectively. TOC elimination was 3.3% at pH 3, 5.4% at pH 6.2 and 7.5% at pH 9.

Table 4.2- General table UVC/H_2O_2 process

UVC_{254}/H_2O_2 (UV-C)						
Exp Nº	pH_0	H_2O_2 (mg/L)	MET conversion (%)	Time (min)	TOC conversion (%)	Time (min)
UVC-1	3.0	25	98.1	30.0	11.3	160
UVC-2	3.0	50	98.6	20.0	32.3	240
UVC-3	3.0	75	98.1	16.0	44.0	300
UVC-4	3.0	100	100	15.0	52.1	285
UVC-5	3.0	125	98.7	12.0	62.0	200
UVC-6	6.5	25	100.0	25.0	11.3	105
UVC-7	6.5	50	95.3	11.0	30.8	280
UVC-8	6.5	75	96.8	9.0	52.3	330
UVC-9	6.5	100	100	15.0	58.1	300
UVC-10	6.5	125	97.8	7.5	70.7	230
UVC-11	9.0	25	98.0	30.0	17.4	160
UVC-12	9.0	50	98.5	20.0	33.7	240
UVC-13	9.0	75	96.8	12.5	53.2	320
UVC-14	9.0	100	100	7.5	56.5	260
UVC-15	9.0	125	97.8	10.0	70.0	230

4.2 UVC/H$_2$O$_2$ process

In table 4.2 there are described the UVC/H$_2$O$_2$ experiments carried out in UVC reactor. The main parameters, such as, initial MET concentration, initial solution pH, hydrogen peroxide concentration and the main results for every experiment are informed. The studies were carried out at 25 ºC and at three different pHs: 3, 6.2 (free pH) and 9. At each pH, H$_2$O$_2$ concentration was varied: 25, 50, 75, 100, 125 and 150 mg/L

Free pH

In this part several experiments using different initial H$_2$O$_2$ concentrations (from 25 to 125 mg/L) were performed in order to assess the performance of the UV/H$_2$O$_2$ process to degrade MET (Exp. UVC-6, UVC-7, UVC-8, UVC-9 and UVC-10).

As figure 4.4 shows, an initial dose of 125 mg H$_2$O$_2$/L exhibited the best performance about MET degradation. Almost 98% of MET removal was achieved in 7.5 minutes.

Under the operating conditions investigated, the scavenging effect of an excess of the promoter up to 125 mg/L of H$_2$O$_2$ was negligible in comparison to the increase in HO· production. In this process the elimination rate of MET can has as least two contributions: direct photolysis and hydroxyl-radical attack.
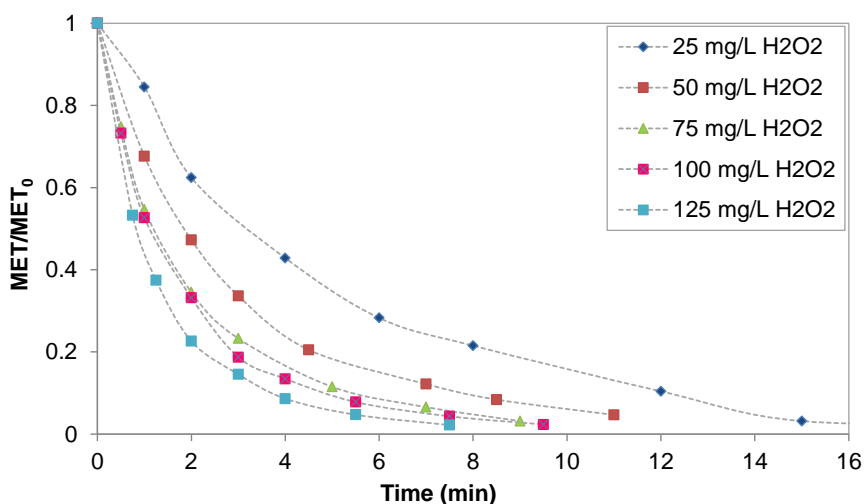
Figure 4.4- MET degradation profiles at several hydrogen peroxide concentrations using UVC reactor. [MET]$_0$=50 mg/L, Free pH and 25 ºC.

The performance of the hydrogen peroxide in MET elimination is compared on basis of the ratio MET removed /accumulated energy. The radiation entering in UVC reactor

was 8.01 J/s (254 nm). 90% of MET removal was chosen since MET removal rates became too slow near the total elimination (see figure 4.5).
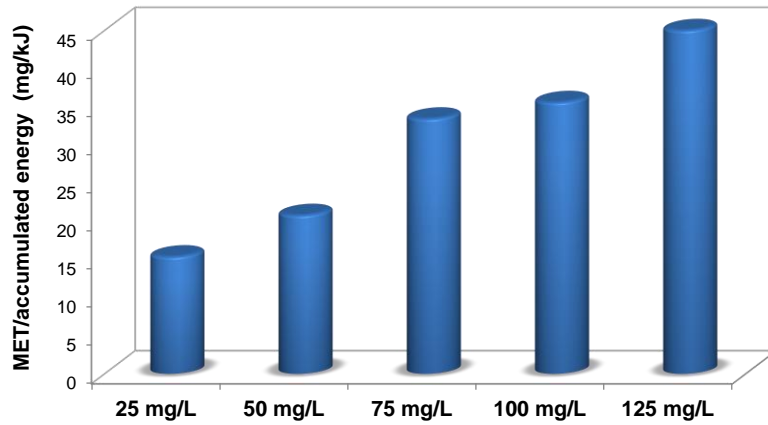
Figure 4.5- Efficiency ratio in MET removal per accumulated energy at several hydrogen peroxide concentrations. $[MET]_0$=50 mg/L, Free pH and 25 ºC.

Mineralization levels achieved with this system were very promising with the highest H_2O_2 concentrations used. 11.3%, 30.8%, 52.3%, 58.1% and 70.7% of TOC conversion was achieved with 25, 50, 75, 100, and 125mg/L of hydrogen peroxide, respectively (see figure 4.6).
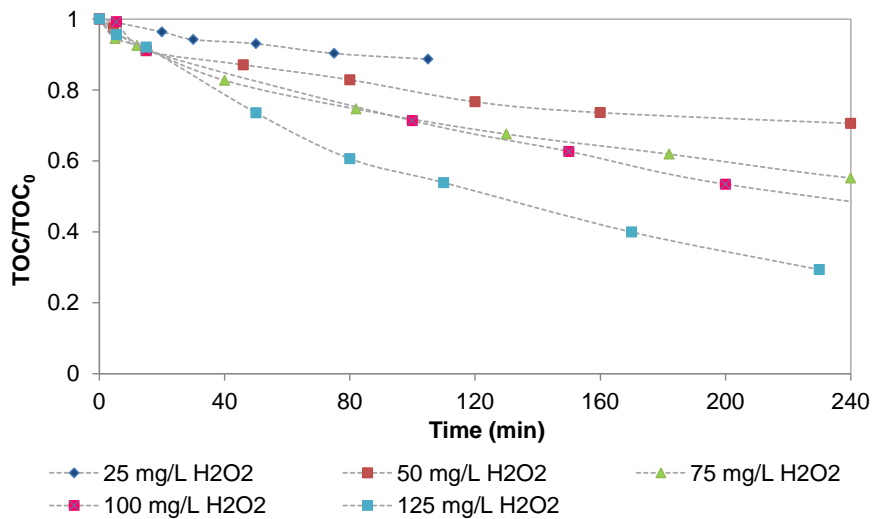
Figure 4.6- TOC degradation profiles at several hydrogen peroxide concentrations using UVC reactor. $[MET]_0$=50 mg/L, Free pH and 25 ºC.

84

pH influence

To observe the effect of the rate of photolysis of aqueous hydrogen peroxide under UVC lamp, all the hydrogen peroxide tested before (25, 50, 75, 100 and 125 mg/L) were also used at pH 3 and pH 9 (i.e 125 mg/L H_2O_2 figure 4.7).
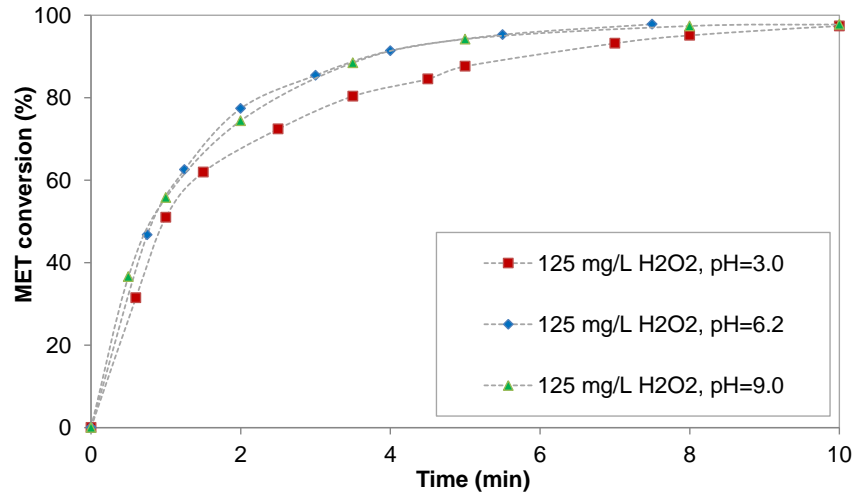
Figure 4.7- MET degradation rate obtained by use of 125 mg/L of hydrogen peroxide concentrations in UVC reactor at different pH. $[MET]_0$=50 mg/L, 25 ºC.

As it can be observed, MET degradation was rather lower when UVC/H_2O_2 process was carried out at pH acid, however not differences were noticed between MET degradation rate at pH 6.2 and 9. This behavior prevails in all hydrogen peroxide concentrations tested. With respect to mineralization, not improvements were detected at different pH (see figure 4.8).
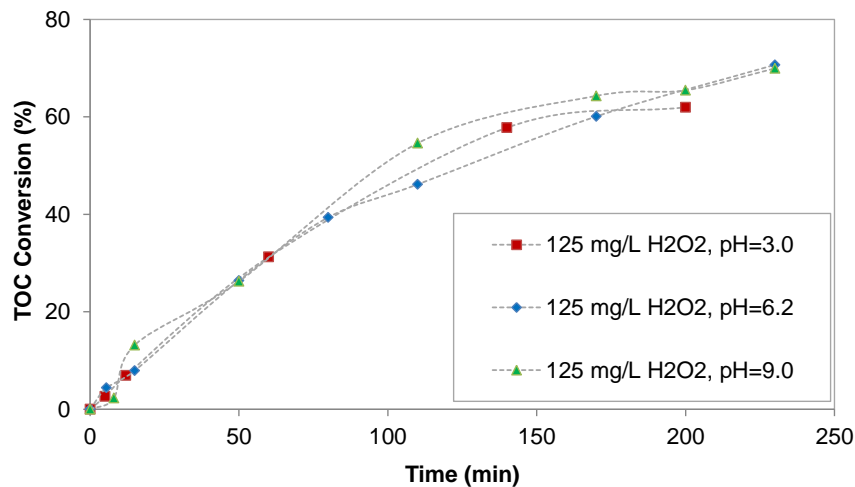
Figure 4.8- TOC degradation obtained by use of 125 mg/L of hydrogen peroxide concentrations in UVC reactor at different pH. $[MET]_0$=50 mg/L, 25 ºC.

This behavior likely can be explained because the pKa of the MET is around 9.2-9.6 and the pKa of H_2O_2 is 11.6, thus, using the initial MET solution at pH 9 is not enough high to assure higher MET degradation rate. MET reactivity towards the HO· radical could depend on its ionized form, which it is determined by the pH of the solution.

In any event, it is important to remark that a significant reduction of MET and TOC of the solution was achieved at the end of the treatment. For the same concentration of hydrogen peroxide, its consumption was almost the same at the different pH tested.

Chemical Oxygen Demand, biodegradability and Toxicity

Apropos of COD, using 125 of H_2O_2 at free pH is important to remark that a significant reduction of COD and TOC of the solution was achieved at the end of the treatment (see figure 4.9), and the same behavior can be observed at pH 9, because as higher hydrogen peroxide was used higher HO· radicals were formed then higher mineralization and oxidation were obtained.
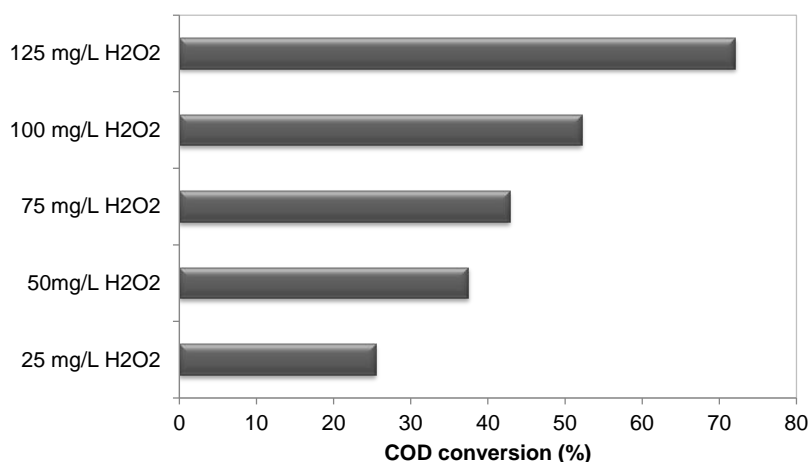
Figure 4.9- COD conversions at several hydrogen peroxide concentrations using UVC reactor. [MET]$_0$=50 mg/L, Free pH and 25 ºC.

Relating to biodegradability (BOD_5/COD), when the UVC/H_2O_2 was carried out with 100 and 125 mg/L of H_2O_2 at free pH, the treated solution can be considered suitable for a sequential biological treatment because their values were higher than 0.25. Figure 4.10 depicts the different biodegradability values reached at the end of every treatment.
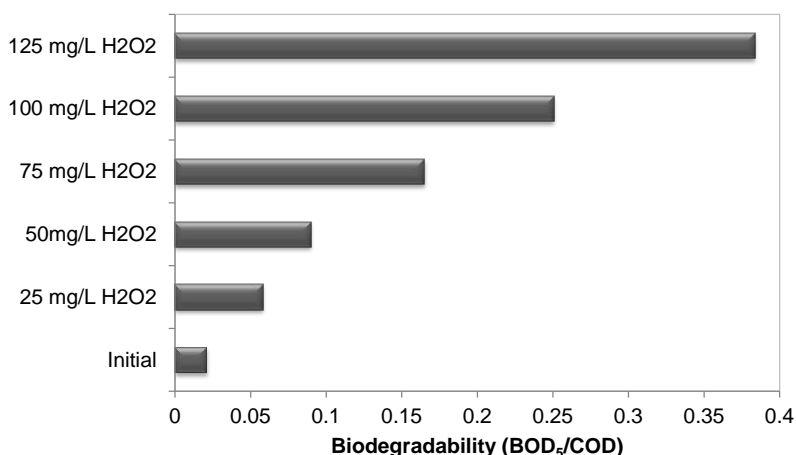
Figure 4.10- Biodegradability obtained by use of several hydrogen peroxide concentrations in UVC reactor. $[MET]_0 = 50$ mg/L, Free pH and 25 ºC.

AOS was calculated for 125 mg/L of H_2O_2 at free pH within 230 minutes of reaction. The value increased from the initial 0.73 to 0.85, also indicating that more biodegradable compounds were formed.

Two different hydrogen peroxide concentrations were selected at free pH, the lowest and the highest to analyze the toxicity by *Vibrio Fischeri* bio-assay in a final effluent after total hydrogen peroxide consumption (30 and 230 minutes 25 and 125 mg/L of H_2O_2 respectively).

The initial Equitox/m^3 value of the untreated solution was 6.2 and the final Equitox/m^3 was 0.56, for 25 mg/L of H_2O_2, and 0.42 for 125 mg/L of H_2O_2.

Intermediates

Intermediates identification was carried out in samples extracted at 6 minutes and 30 minutes of oxidation in UVC reactor when 25 mg/L of hydrogen peroxide were loaded at free pH (Table 4.3).

Table 4.3- Intermediates proposed structures for UVC/H_2O_2 process in MET degradation at 25 ºC and free pH. [MET]$_0$=50 mg/L; [H_2O_2]=25 mg/L. [1]Experiment at 6 minutes. [2]Experiment at 30 minutes.
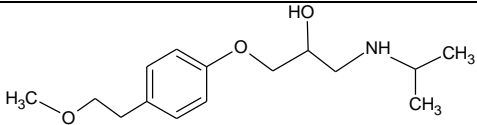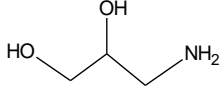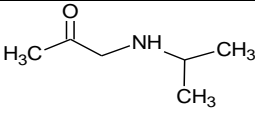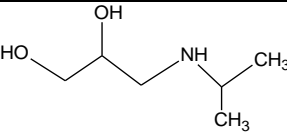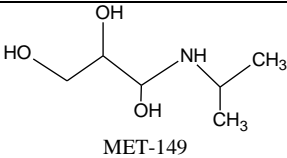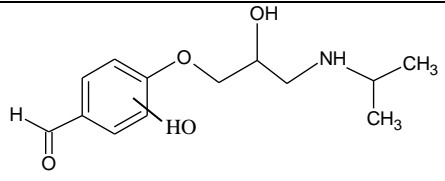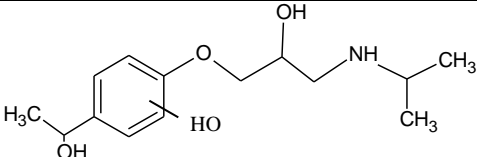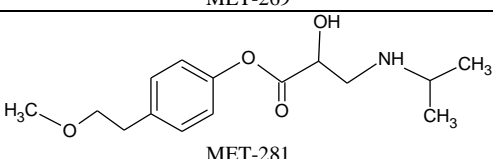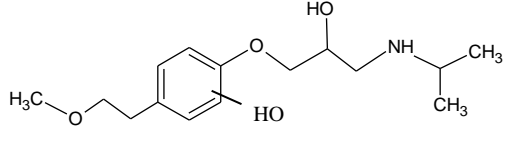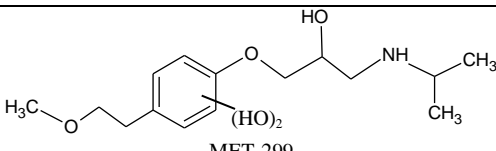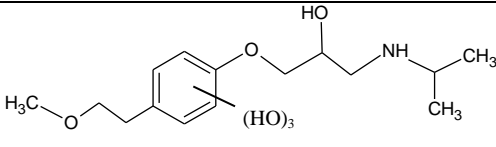
m /z (Da)	Elemental composition	Proposed structure (Label)	Photo-Fenton UVC reactor	
			1	2
267	$C_{15}H_{25}NO_3$	MET-267	x	x
91	$C_3H_9NO_2$	MET-91	x	x
115	$C_6H_{13}NO$	MET-115	x	x
133	$C_6H_{15}NO_2$	MET-133	x	x
149	$C_6H_{15}NO_3$	MET-149	x	-
253	$C_{13}H_{19}NO_4$	MET-253	x	-
269	$C_{14}H_{23}NO_4$	MET-269	x	-
281	$C_{15}H_{23}NO_4$	MET-281	-	x
283	$C_{15}H_{25}NO_4$	MET-283	x	x

Table 4.3 (Continued)				
m /z (Da)	Elemental composition	Proposed structure (Label)	Photo-Fenton UVC reactor	
			1	2
299	$C_{15}H_{25}NO_5$	MET-299	x	-
315	$C_{15}H_{25}NO_6$	MET-315	x	-
Other intermediates identifified (m/z)			163, 289, 301	163, 268, 280, 281, 289, 296.

MET was identified (*m/z*=267). After breaking the C–C bond in the aliphatic part of the MET molecule, amino-diol (MET-133) was identified. Different fragments of the ethanolamine side were also identified (MET-91 and MET-115), probably due to the loss of the hydroxyl group and the loss of isopropyl moiety. Three by-products corresponding to the binding of HO· radicals in the aromatic ring were detected mono-hydroxy (MET-283), di-hydroxy-(MET-299) and tri-hydroxy-(MET-315). MET-281 was identified as by-product of MET-267 oxidation. MET-149 was identified by the oxidation of MET-133. A simplified pathway of Metoprolol degradation by UVC/H_2O_2 process is proposed in Figure 4.11.
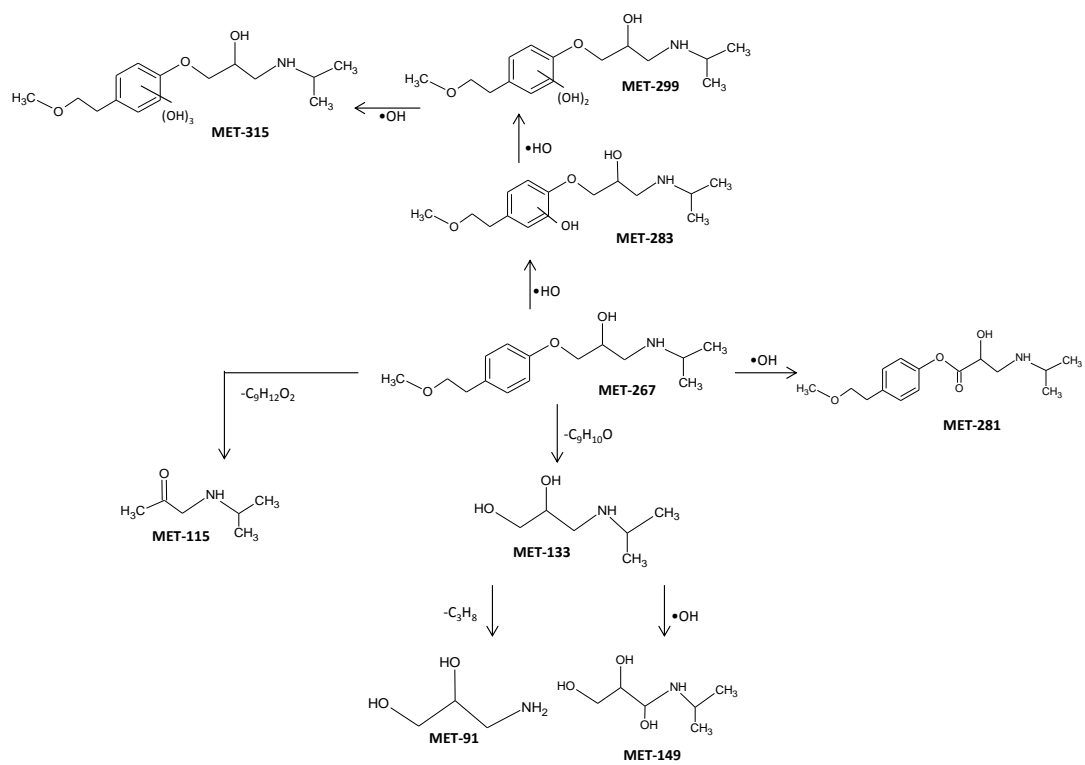
Figure 4.11- Possible pathways for MET degradation by UVC/H$_2$O$_2$ process.

Table 4.4- General table (Heterogeneous photocatalysis process)

Exp Nº	[MET]$_0$ (mg/L)	[TiO$_2$] (g/L)	pH$_0$	T (ºC)	H$_2$O$_2$ (mg/L)	Other	MET conversion (%)	Time (min)	TOC conversion (%)	Time (min)
HP-SB-1	50	0.05	6.2	25	0		87.1	360	24.6	360
HP-SB-2	50	0.1	6.2	25	0		95.8	360	39.9	360
HP-SB-3	50	0.4	6.2	25	0		100	300	53.0	360
HP-SB-4	25	0.4	6.2	25	0		100	180	67.9	300
HP-SB-5	100	0.4	6.2	25	0		91.9	360	39.1	360
HP-SB-6	50	0.4	3.0	25	0		91.0	300	29.7	300
HP-SB-7	50	0.4	9.0	25	0		100	240	61.8	300
HP-SB-8	50	0.4	6.2	25	0	real water	20.8	300	-	-
HP-SB-9	50	0.4	6.2	25	0	supplying air	100	300	61.5	360
HP-SB-10	50	0	6.2	25	25		29.2	300	3.8	300
HP-SB-11	50	0	6.2	25	150		55.0	300	9.9	300
HP-SB-12	50	0.4	6.2	25	25		100	180	57.4	300
HP-SB-13	50	0.4	6.2	25	150		100	120	63.5	300
HP-CPC-14	50	0.05	6.2	30 ± 5	0	Q= 5.94 kJ/L	68.1	330	20.8	330
HP-CPC-15	50	0.1	6.2	30 ± 5	0	Q= 3.77 kJ/L	73.1	300	22.1	300
HP-CPC-16	50	0.4	6.2	30 ± 5	0	Q= 2.64 kJ/L	81.5	270	29.2	270
HP-CPC-17	50	0	6.2	30 ± 5	25	Q= 7.95 kJ/L	13.8	300	11.2	300
HP-CPC-18	50	0	6.2	30 ± 5	150	Q= 7.95 kJ/L	57.9	300	16.9	300
HP-CPC-19	50	0.4	6.2	30 ± 5	25	Q= 3.1 kJ/L	69.9	90	18.0	90
HP-CPC-20	50	0.4	6.2	30 ± 5	150	Q= 6.0 kJ/L	95.6	180	38.3	180

The table heading "Heterogeneous Photocatalysis (HP)" spans across all columns.

4.3 Heterogeneous photocatalysis

The results obtained in the photocatalysis/TiO_2 process at 25 ± 5 ºC are summarized in table 4.4. Two different devices were used: SB and CPC reactors.

This section will be divided following the parameters studied:

- Influence of Catalyst concentration
- Influence of initial MET concentration
- pH influence
- Influence of water matrix and air supplied
- Influence of oxidant agents
- Absorbance and aromaticity
- BOD_5, COD and biodegradability
- Toxicity and intermediates

Preliminary studies were done in order to determine the influence of factors such as temperature and adsorption in the process.

4.3.1 Preliminary experiments

Thermo-degradation

Preliminary experiments were carried out to study the thermo-degradation of 50 mg/L MET, in 0.4 g TiO_2/L suspension, at 20, 25, 40, and 60ºC during a period of 30 minutes under dark conditions. The results obtained showed that, at 20 and 25ºC, there was not MET degradation. At 40 and 60ºC, degradation was 2.8 and 3% respectively. There was not mineralization in any case.

Adsorption on catalyst

Studies of MET adsorption on TiO_2 were carried out. Different MET concentrations (0, 6.2, 12.5, 25, 37.5, 50, 75 and 100 mg/L) were prepared with 0.4 g TiO_2/L, at the natural pH(~6.2), constant stirring and temperature ($25°C \pm 0.5$) under dark conditions.

After 1, 5 and 24 h of contact, MET concentration was evaluated. Adsorption of MET onto TiO_2 was negligible. However, because the adsorption capacity is also influenced by pH (Lee, Kwon, Thiruvenkatachari, & Moon, 2006), experiments were carried out

varying the pH of suspension (3 and 9.2). The results indicate that the amount adsorbed increases when pH does it.

For acid condition, adsorption was not significant. Nevertheless, in the case of pH 9.2 almost 14% of the initial substrate was adsorbed onto the catalyst.

The increase in the adsorption of Metoprolol when increasing pH can be elucidated by considering the pK_a of MET (~9.2-9.6) as well as the point of zero charge of TiO_2 (pH_{pzc} ~6.5). TiO_2 surface is positively charged in acid media (pH $\leq$ 6.5) whereas it is negatively charged under alkaline conditions (pH $\geq$ 6.5). Under free pH conditions, close to the point zero charge of TiO_2 (~6.5), MET is positively charged. A low adsorption was observed due to no electrostatic attraction between the surface charge and MET.

Thus, within the range 6.5<pH<9.2, the catalyst, with negative surface charge, attracts the dissociated MET cation and it can explain the 14% of MET adsorption at pH 9.

4.3.2 Heterogeneous photocatalysis

Influence of catalyst concentration

The effect of the TiO_2 concentration (0.05, 0.10 and 0.40 g /L) was studied for degradation of MET (50 mg/L) in SB and CPC reactors (Exp. HP-SB-1, HP-SB-2, HP-SB-3, HP-CPC-14, HP-CPC-15 and HP-CPC-16). Higher TiO_2 concentrations were also tested but TiO_2 settling in the reactor was observed. Therefore, those catalyst amounts were discarded.

Using SB, MET was degraded completely within 300 min irradiation using 0.4 g TiO_2/L. For concentrations of 0.05, and 0.1 g TiO_2/L after 300 min irradiation, MET conversion was 81.9% and 92.4% respectively (see figure 4.12).

Mineralization also increased with TiO_2 loading. Thus, 20.6, 34.6 and 45.7% of mineralization was obtained for 0.05, 0.1 and 0.4 g TiO_2/L, respectively, after 300 minutes of irradiation.
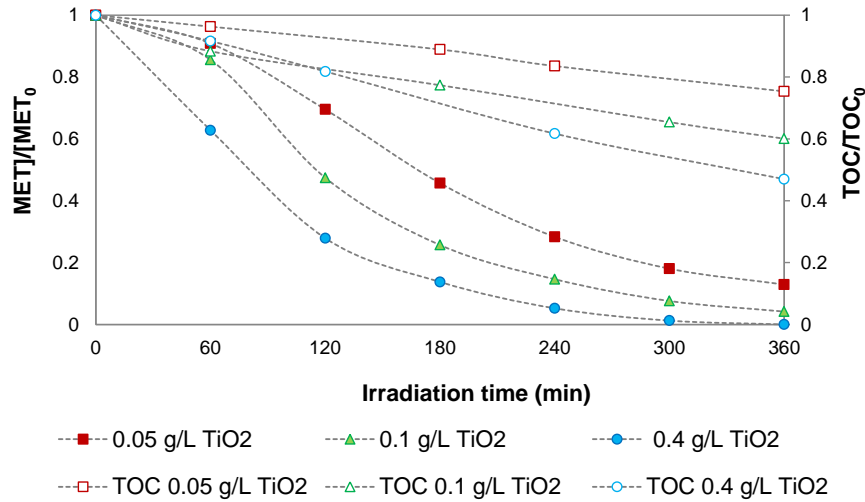
Figure 4.12- MET and TOC degradation using different catalyst loads in SB.

For CPC, Metoprolol and TOC degradation are going to be described in terms of accumulated energy due to there is not a constant irradiation along of the time. Thus, the use of the time, as the calculation unit, could give rise to misinterpretation of results, because the differences in the incident radiation in the reactor during an experiment are not taken into account (Malato et al., 2009).

At 2.5 kJ/L, MET was degraded 9.38%, 18.5 kJ/L and 65.9 % for 0.05, 0.1 and 0.4 g/L of TiO_2 respectively (see figure 4.13). MET and TOC removals increase when TiO_2 concentration does it. Thus, at 2.5 kJ/L 6.0%, 7.8% and 19.9% of mineralization was obtained for 0.05, 0.1 and 0.4 g TiO_2/L, respectively.
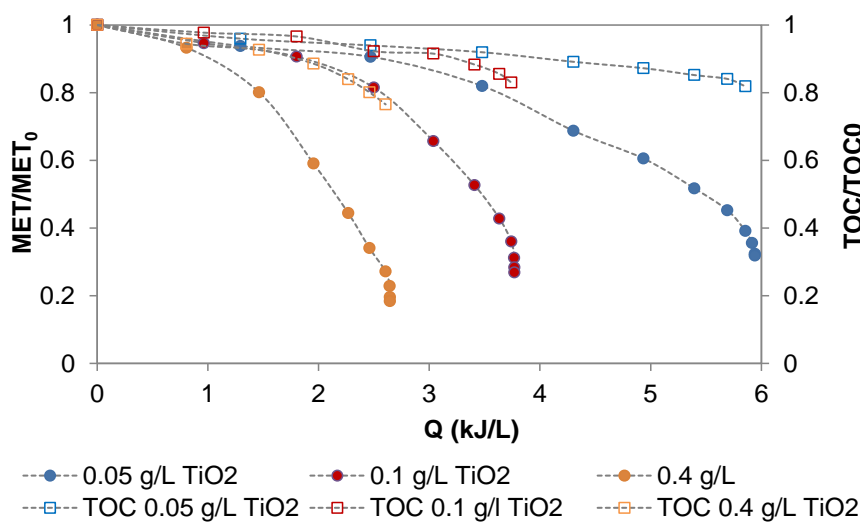
Figure 4.13- MET and TOC degradation using different catalyst loads in CPC.

For this study the best catalyst concentration was 0.4 g TiO_2/L, hence, this is the selected catalyst concentration used in heterogeneous photocatalysis.

Kinetic Study

Degradation results were fitted to apparent pseudo-first order kinetics. Some authors (Malato et al., 2009) established that photocatalysis experiments follow Langmuir-Hinshelwood model. However, if the adsorption of MET onto the surface of the photocatalyst is very low, the process can be described by first-order kinetics:

$$-\ln\left(\frac{c}{c_0}\right) = k_{ap} * t \qquad (4.1)$$

Where c_0 is the initial concentration at t=0 and k_{ap} is the apparent first-order kinetic constant.

k_{ap} values could be obtained from the slopes -ln (C/Co) vs. time. The data obtained for the experiments (HP-SB-1, HP-SB-2, HP-SB-3, HP-CPC-14, HP-CPC-15 and HP-CPC-16) are summarized in table 4.5.

Table 4.5- Apparent first-order rate constant for photocatalysis/TiO_2 using SB and CPC.

$[TiO_2]_0$ (g/L)	Exp.	SB k_{ap} (min^{-1})	Exp.	CPC k_{ap} (min^{-1})
0.05	HP-SB-1	6.1×10^{-3}	HP-CPC-14	3.9×10^{-3}
0.1	HP-SB-2	9.3×10^{-3}	HP-CPC-15	5.0×10^{-3}
0.4	HP-SB-3	1.2×10^{-2}	HP-CPC-16	7.1×10^{-3}

The results are consistent with the TiO_2 loading used in each experiment. When the initial concentration of TiO_2 catalyst increases, the kinetic constant also increases.

Influence of initial MET concentration

The initial substrate concentration has a relevant influence on the overall photocatalytic performance. Photocatalytic experiments were carried out varying the initial MET concentration (25, 50 and 100 mg/L) and using 0.4 g TiO_2/L (Exp. HP-SB-3, HP-SB-4, and HP-SB-5) in SB.

Figure 4.14 shows MET degradation as well as mineralization degree. It is observed that at lower MET initial concentration there is higher TOC removal (67.9%), and lower irradiation time is needed to reach full MET degradation.

Using 25 mg/L MET, a complete MET removal was achieved after 180 minutes of irradiation. For 50 and 100 mg/L more time of irradiation was necessary, achieving almost 100% of MET elimination after 300 minutes and 91.9% after 360 minutes respectively. When the initial concentration of reactant increases, the intermediates concentration also increases, leading to a slowdown in the disappearance of MET by the competition of intermediates. Moreover, there is the same TiO_2 concentration, the same HO· produced for higher reactant concentration. This relation can be appreciated if we compare mg of Met degraded/g of TiO_2 in 180 minutes, and the results obtained were 58.8, 104.1 and 159.8 mg MET/g TiO_2 for 25, 50 and 100 mg/L of initial MET.

Regarding to mineralization for 25, 50 and 100 mg MET/L the conversion was 67.9% (at 300 min.), 53% (at 360 min.) and 39.1% (at 360 min.) respectively.
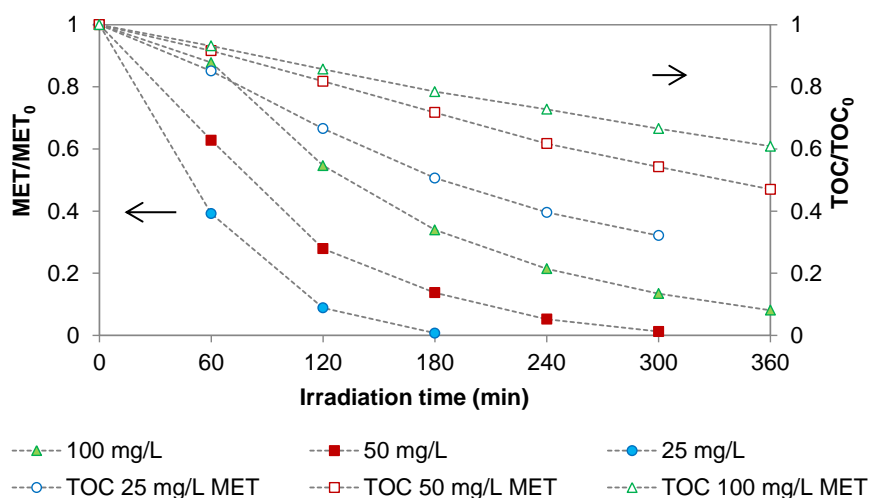
Figure 4.14- Effect of the initial MET concentration on MET degradation and mineralization in SB device and 0.4 g/LTiO$_2$.

Influence of initial pH

Photocatalytic degradation of 50 mg MET /L, with 0.4 g/L TiO_2 and constant temperature (25ºC), was carried out changing the initial pH (free pH, pH 3 and pH 9) in SB (Exp. HP-SB-3, HP-SB-6, and HP-SB-7).

A complete MET elimination was achieved at pH 9 (240 min) and pH 6.0 (300 min). When initial pH was adjusted at 3, the MET conversion obtained after 300 minutes of irradiation was 91%. The effect of pH on the conversion is a complex issue related to the ionization states of the catalyst surface and the substrate, as well as the rate of formation of radicals and other reactive species in the reaction mixture. These effects

can be assessed since the action of the holes is favoured at acidic conditions, while hydroxyl radicals become the dominant species at neutral and alkaline conditions. The higher MET degradation and the low MET adsorption on catalyst at a pH 9 suggest that the HO· attack in the bulk of solution can be responsible for the MET degradation.

The TOC evolution during the photocatalytic degradation of MET, at these different pH, are given in figure 4.15. The highest TOC conversion (62%) at 300 minutes of irradiation was obtained when pH solution was adjusted at 9. Meanwhile, when the experiment was adjusted at pH 3 the TOC conversion reached was ~2 times lower (30%) and when the system was not adjusted (free pH) TOC conversion was ~1.47 times lower (46%) than this one reached at pH 9.
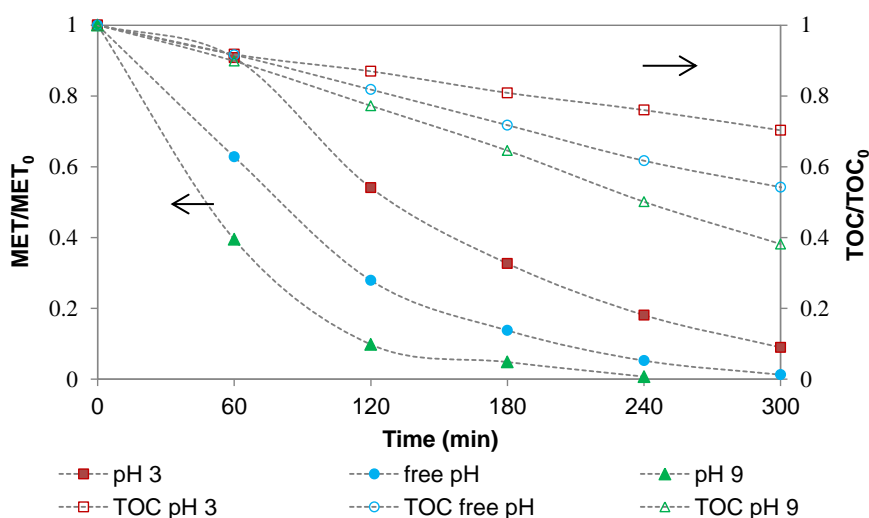
Figure 4.15- Effect of the initial pH solution in MET and TOC degradation using SB device and 0.4 g/LTiO$_2$.

Influence of water matrix and air supplied

In this part of the study, the attention was focused on the possible influence of different water matrixes (Milli Q water and water from effluent of a secondary biological reactor of WWTP) or direct air supplied into the SB reactor (Exp. HP-SB-3, HP-SB-8 and HP-SB-9).

Real water was collected from the WWTP located in Gavà (Catalonia-Spain) and its physicochemical characterization is described in table 4.6.

Table 4.6- Physicochemical characterization of filtered real water, from the secondary clarifier of a wastewater treatment plant (WWTP) (Gavá-Catalonia-Spain).

Parameter	Value
BOD_5 (mg/L)	9
COD (mg/L)	54.7
TOC (mg/L)	11.6
UV absorbance at 254 nm (cm^{-1})	0.29
Turbidity (NTU)	2.1
pH	7.9
Total suspended solids (mg/L)	3.60
Volatile suspended solids (mg/L)	3.00
Chloride (mg/L)	589
Nitrite (mg/L)	9.9
Nitrate (mg/L)	30.1
Sulfate (mg/L)	205
Phosphate (mg/L)	9.2
Potassium (mg/L)	45
Magnesium (mg/L)	45
Calcium (mg/L)	124
Ammonium (mg/L)	< 0.5
Alkalinity (mg HCO_3^-/L)	526.7

Within 300 min irradiation and using 0.4 g TiO_2/L, MET was degraded completely in Milli Q water and just 20.8 % of MET elimination was achieved when real water was used (see figure 4.16). Evidently, the real water matrix has a detrimental effect on conversion. Thus, after several hours of irradiation MET exhibits a low conversion due to the fact that reactive species produced by the photocatalysis process are partially consumed to attack the organic matter present in the real matrix water. On the other hand, the presence of other species such as inorganic ions can produce inactivation of the catalyst surface.
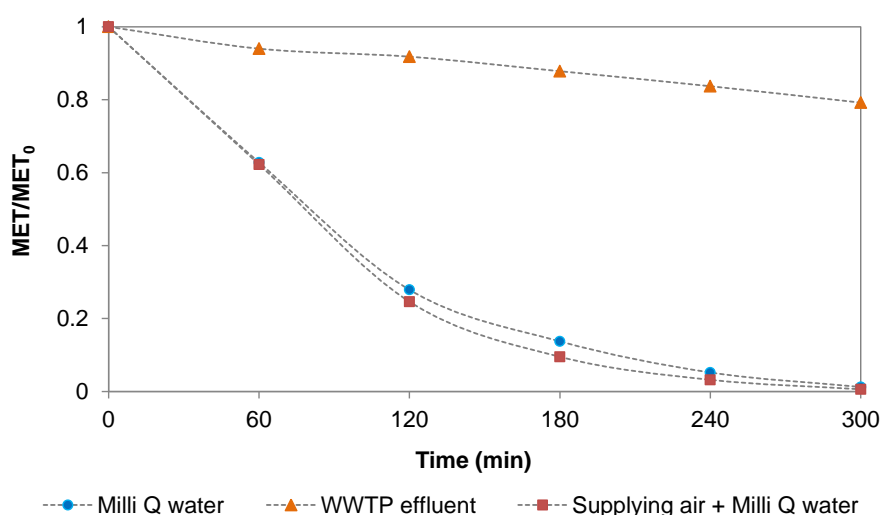

Figure 4.16- MET degradation, loading 0.4 g/L TiO_2, using two different water matrixes and supplying air into the reactor in SB

Otherwise, air was supplied into the reactor to see the possible effect in MET degradation, but there was not influence However, an improvement of 13.8% about

final TOC elimination was observed when air was supplied into the reactor (TOC conversion: 61.5% within 360 min). It is clear that the system has enough oxygen for MET degradation but there is not enough oxygen to degrade the intermediates, for this reason when air was supplied TOC conversion was higher.

Influence of oxidant agents

The effect of the oxidant agent as promoter (H_2O_2, 25 and 150 mg/L) was assessed.

Firstly, the influence of H_2O_2 alone was tested. Thus, 25 and 150 mg/L of H_2O_2 were added to 50 mg/L MET solution directly in the batch tank without catalyst (Exp. HP-SB-10, HP-SB-11, HP-CPC-17, and HP-CPC-18).

The H_2O_2 alone, under 300 minutes of irradiation (15.7 kJ/L) in SB, was able to degrade 29% and 55% of MET with 25 and 150 mg/L H_2O_2 respectively. However, only a slight TOC elimination was observed (approximately 4% and 10% removal for 25 and 150 mg/L of H_2O_2 respectively) mainly due to a remarkable hydroxylation step.

Experiments carried out in presence of 25 and 150mg H_2O_2/L in CPC showed a MET degradation of 14% and 57.9% respectively, after 300 minutes of irradiation (8.0 kJ/L of accumulated energy).

Degradation of MET by the sole presence of H_2O_2 under irradiation is attributed to the photochemical cleavage of H_2O_2 to yield HO· and/or other radical species by light absorption.

$$H_2O_2 + hv \rightarrow HOO\cdot + H\cdot \tag{4.2}$$
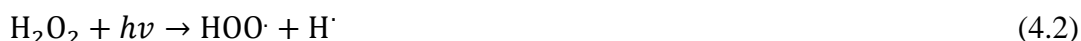
The maximum absorbance of H_2O_2 occurs nearly at 220 nm (Parsons, 2004), and the solar spectrum is not reach in this wavelength. This fact can explain that a high concentration of H_2O_2 is needed to generate sufficient hydroxyl radicals because of low-absorption coefficient.

In the second case, 0.4 g TiO_2/L were mixed with 50 mg/L of MET solution before addition of H_2O_2 (Exp. HP-SB-12, HP-SB-13, HP-CPC-19, HP-CPC-20).

The addition of H_2O_2 improve MET and TOC removal (see figures 4.17 and 4.18). In SB a complete depletion of MET is reached within 180 and 120 min by use of 25 and

150 mg/L of H_2O_2, while 300 min of reaction are needed for total elimination of MET when only TiO_2 was used. By sole presence of H_2O_2 the maximum MET conversion was 29.2% and 55.0% when 25 and 150 mg/L of H_2O_2 were used, respectively, after 300 minutes of irradiation.
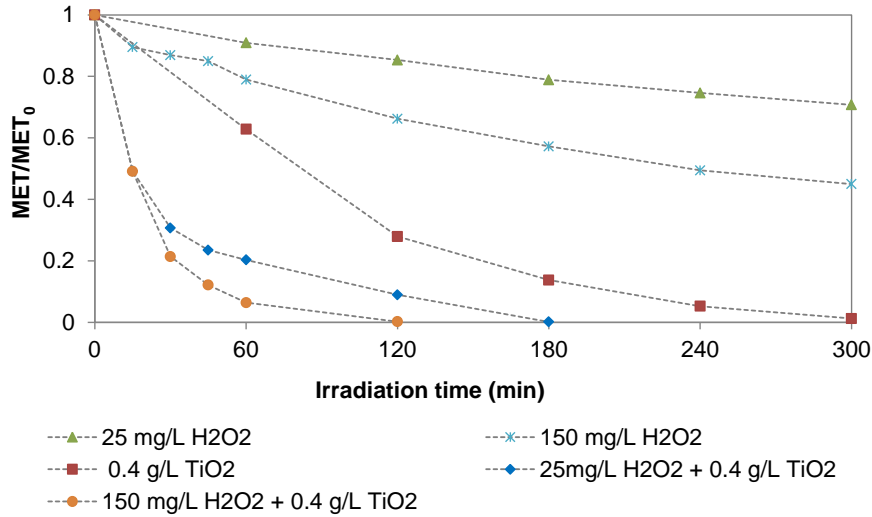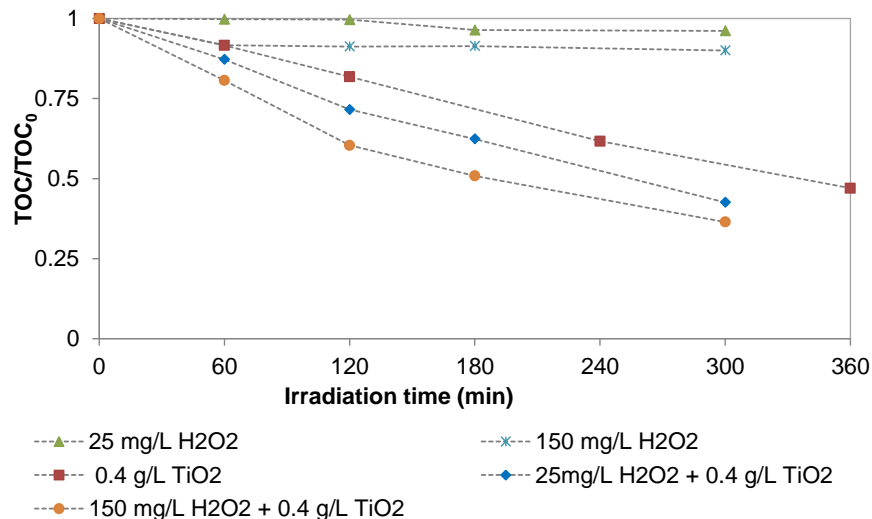

Figure 4.17- Effect of the H_2O_2 concentration on MET degradation in SB device. Initial MET concentration 50 mg/L, free pH and with or without 0.4 g/L of catalyst.

Concerning TOC conversion, when 25 and 150 mg/L of H_2O_2 with 0.4 g/L TiO_2 were used 57.4% and 63.5% within 300 minutes were achieved respectively. By the sole presence of hydrogen peroxide 3.83% and 9.95% of TOC conversion were obtained for 25 and 150 mg/L of H_2O_2, respectively within 300 minutes.

Figure 4.18- Effect of the H_2O_2 concentration on mineralization in SB device. Initial MET concentration 50 mg/L, free pH, with or without 0.4 g/L of catalyst.

In CPC reactor 70% (Q= 3.1 kJ/L) and 96% (Q= 6.0 kJ/L) of MET removal is observed with 25 and 150 mg/L of H_2O_2, respectively, and 0.4 g/L of TiO_2. By sole presence of hydrogen peroxide 13.8% and 57.3% of MET conversion was reached for 25 and 150 mg/L of H_2O_2, respectively (see figure 4.19).
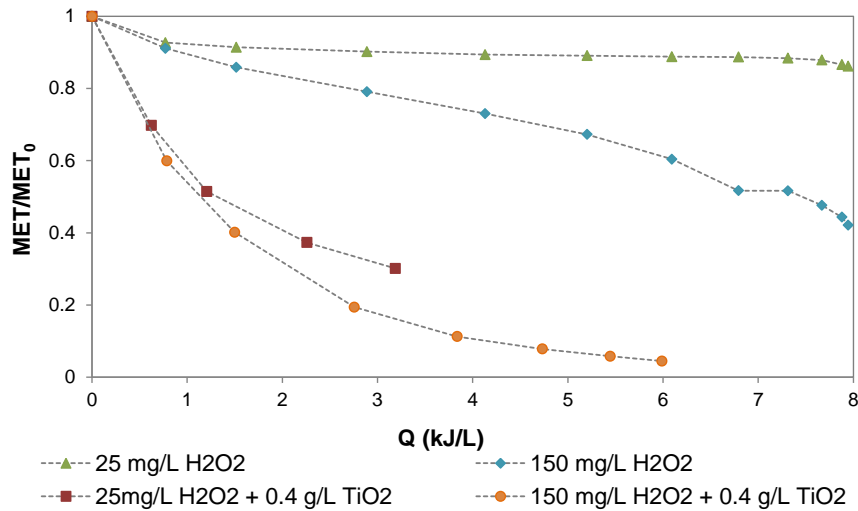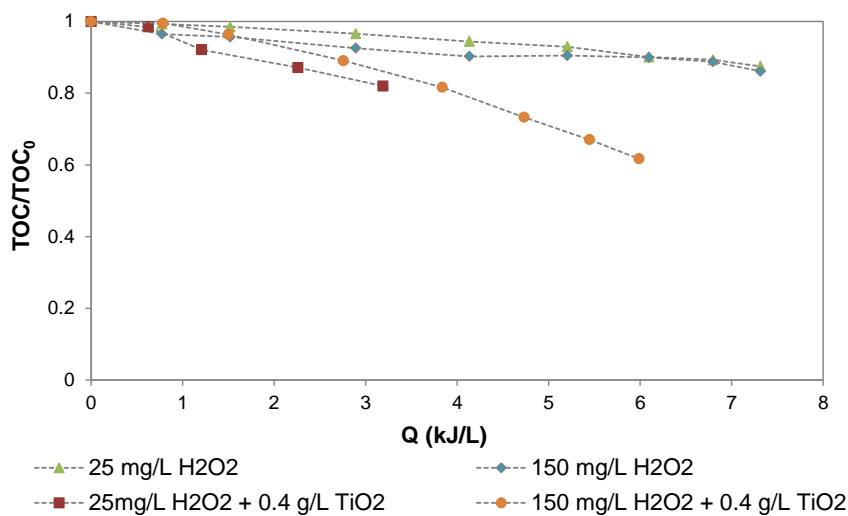

Figure 4.19- Effect of the H_2O_2 concentration on MET degradation in CPC reactor. Initial MET concentration 50 mg/L, free pH and with or without 0.4 g/L of catalyst.

Moreover, 38.3% of the initial organic carbon is mineralized, for 6.0 kJ/L of cumulated energy, in the presence of 150 mg/L of H_2O_2/0.4 g TiO_2/L. In the case of 25 mg/L of H_2O_2/0.4 g TiO_2/L the highest TOC conversion was 18% at 3.1 kJ/L of accumulated energy (see figure 4.20). Complete consumption of H_2O_2 was observed in both cases at the end of the experiments.

Figure 4.20- Effect of the H_2O_2 concentration on mineralization on CPC reactor. Initial MET concentration 50 mg/L, free pH and with or without 0.4 g/L of catalyst.

In this way, the addition of oxidizing species increases the efficiency of the photocatalytic process (Nosaka & Nosaka, 2013), maybe due to the H_2O_2 electron acceptor nature, which implies that it reacts with conduction band electrons (Eq 4.3) to generate hydroxyl radicals (Malato et al., 2009; Mendez-Arriaga et al., 2009).

$$H_2O_2 + e^- \rightarrow HO^{\cdot} + HO^- \tag{4.3}$$

In addition, because of disproportion over UV-irradiated TiO_2, H_2O_2 is an additional source of O_2 on the TiO_2 surface (Beat & Pichat, 1991).

It is not convenient to work with H_2O_2 concentrations above the optimum range because an inhibitory effect is produced by H_2O_2 excess, in which hydrogen peroxide captures hydroxyl radicals to form hydroperoxyl radicals. The hydroperoxyl radicals have a lower oxidation capability making the process less effective (Femia, Mariani, Cassano, Zalazar, & Tiscornia, 2014; Parsons, 2004).

Absorbance and aromaticity

For 50 mg/L of MET solution the initial UV absorbance at 254 nm was 0.062 cm^{-1} and after 360 minutes of irradiation was 0.040 cm^{-1} with SB and 0.143 cm^{-1} with CPC.

Aromaticity, represented by SUVA, shows a global increase.

While scanning it during the experiment in SB, it could be seen how it increased in the first hours (figure 4.21). Finally, there is a decrease of it at six hours of irradiation, where the value goes down, but still being higher than the initial one. In CPC the behaviour shows an increase during 300 minutes and after, between the period of 180 and 360, it is almost constant (figure 4.22). The increase on aromaticity could be explained likely, because there are more resonance forms when MET photo-degradation starts and at the end of treatment the by-products showed the still their presence in the solution.
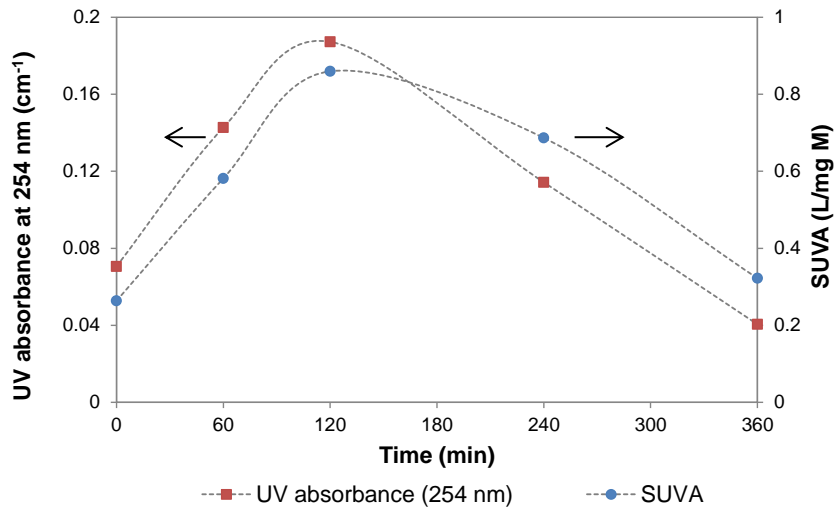
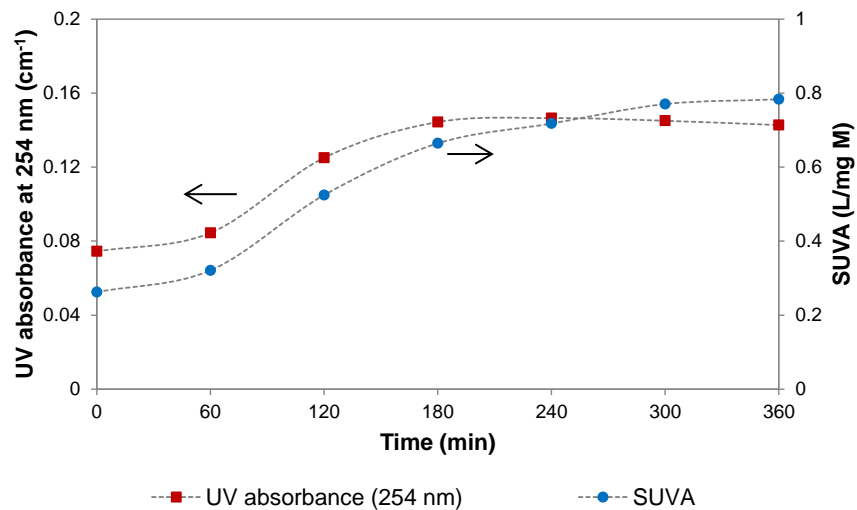Figure 4.21- Absorbance and SUVA for MET photocatalysis, using 0.4 g/L TiO_2 in SB.

Figure 4.22- Absorbance and SUVA for MET photocatalysis, loading 0.4 g/L TiO_2 in CPC reactor.

Biological Oxygen Demand, Chemical Oxygen Demand and Biodegradability

BOD_5 and COD for the photocatalytic treatment was measured at initial and final point in each experiment (see Table 4.7). It can be observed that the BOD_5 increases and COD decreases in all the cases throughout the experiment.

Biodegradability (BOD_5/COD ratio) enhancement was highest at the lowest initial MET concentration.

Table 4.7- BOD$_5$, COD and biodegradability for different initial MET concentrations and 0.4 g/L of TiO$_2$ using SB and CPC.

Device	MET (mg/L)	Initial BOD$_5$ (mg/L)	Final BOD$_5$ (mg/L)	Initial COD (mg/L)	Final COD (mg/L)	Initial Biodegradability BOD$_5$/COD	Final Biodegradability BOD$_5$/COD
SB	25	0.65	4.47	29.68	8.22	0.02	0.54 (300 min)
	50	1.35	6.35	65.3	15.61	0.02	0.41 (360 min)
	100	2.87	11.47	119.5	73.2	0.02	0.16 (420 min)
CPC	50	1.35	4.57	65.3	37.6	0.02	0.12 (270 min)

When 25 mg/L and 50 mg/L of initial MET concentrations were used in solarbox, biodegradability indicators reached for both treated solutions were higher than 0.4 (see section 3.2). This means that these treated solutions can be coupled to biological process after 300 min and 360 min respectively. In the case of 100 mg/L of initial MET concentration, the solution remains being considered not biodegradable at the end of the photocatalytic process, after 420 minutes, because biodegradability indicator for the treated solution was lower than 0.4.

For 50 mg/L of MET and 0.4 g/L of TiO$_2$, in CPC a slight increase from the initial BOD$_5$ 1.35 mg/L to 4.57 mg/L at 2.64 kJ/L (270 minutes) was observed while COD decreases from the initial COD 65.3 mg/L to 37.6 mg/L. Thus, after 270 minutes, the biodegradability indicator (BOD$_5$/COD) was 0.12. This value indicates that the solution remains being considered not biodegradable and cannot be submitted to a subsequent biological treatment.

Toxicity

To complement the information about the hazardousness of a treated effluent the toxicity assessment was also carried out (by *Vibrio fischeri*).

The initial solution of 50 mg MET /L has an Equitox/m^3 equal to 6.25 and after photocatalysis process the treated solution has an Equitox/m^3 equal to 0.72 and 0.57 using SB and CPC reactors respectively (see figure 4.23). Thus, the treatment is sufficient to produce effluent within safe toxicity limits.
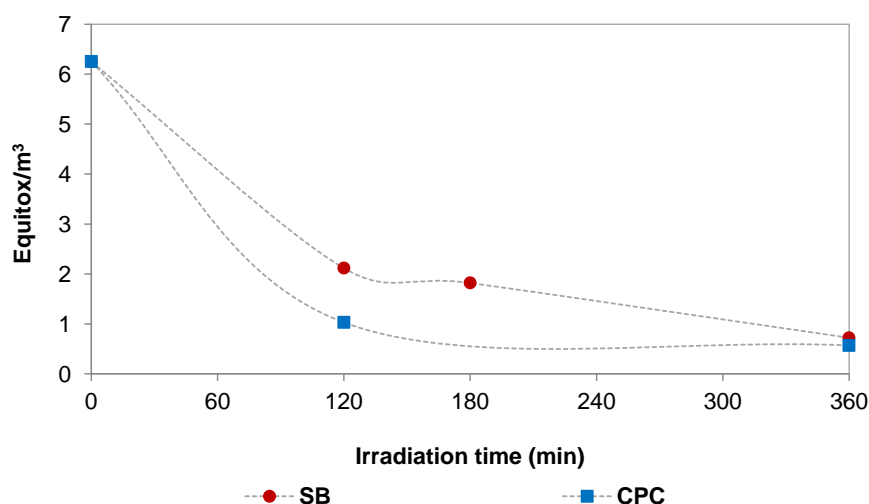
Figure 4.23- Toxicity for MET photocatalysis, using 0.4 g/L TiO_2 in SB and CPC.

Similar results were obtained when UV-Vis/H_2O_2/TiO_2 was used.

In the following table the values of toxicity for the different processes are summarized.

Table 4.8- Equitox for MET degradation under UV-Vis/TiO_2 and UV-Vis/H_2O_2/TiO_2, using 0.4 g TiO_2/L in SB and CPC reactors and two different hydrogen peroxide concentrations (25 mg/L and 150 mg/L).

Process (device)	Initial solution Equitox/m3	Treated solution Equitox/m3	Irradiation Time (min)
0.4 g/L TiO_2 (SB)	6.25	0.72	360
0.4 g/L TiO_2 (CPC)	6.25	0.57	270
0.4 g/L TiO_2, 25 mg/L H_2O_2 (SB)	6.25	0.67	300
0.4 g/L TiO_2, 25 mg/L H_2O_2 (CPC)	6.25	0.70	90
0.4 g/L TiO_2, 150 mg/L H_2O_2 (CPC)	6.25	0.53	180

Intermediates

In order to evaluate the oxidation of the Metoprolol and to obtain a better understanding of the reaction mechanisms involved, a by-products evaluation is needed. However, given the complex variety of the reaction products that could be generated in this process, an exhaustive identification and quantification of all the intermediate species is very difficult. For this reason, this study was focused on the major stable by-products of the reaction (Table 4.9).

Table 4.9- Intermediates identified by electrospray mass technique. Photocatalysis/TiO$_2$ degradation of MET in SB, UV-Vis/H$_2$O$_2$/TiO$_2$ processes in SB and CPC reactor. 50 mg/L of MET and 0.4 g/L of TiO$_2$. [1] 25 mg H$_2$O$_2$/L and [2] 150 mg H$_2$O$_2$/L.
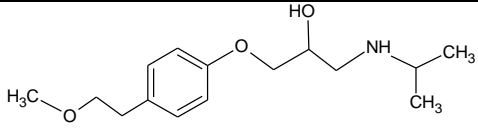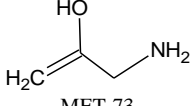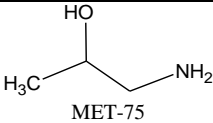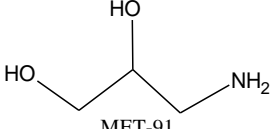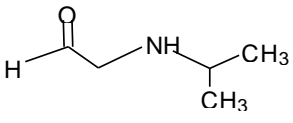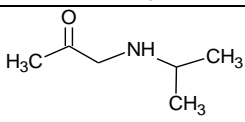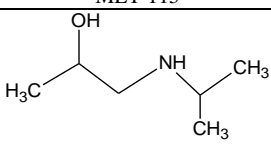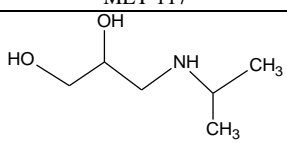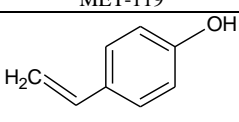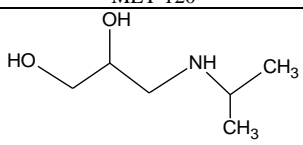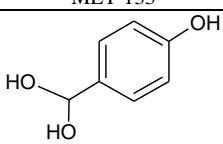
m/z	Molecular formule	Proposed structure	UV-VisTiO$_2$ SB	UV-Vis/H$_2$O$_2$/TiO$_2$		
				SB[1]	CPC[1]	CPC[2]
267	C$_{15}$H$_{25}$NO$_3$	MET-267	X	X	X	X
73	C$_4$H$_{11}$N	MET-73	X	-	-	-
75	C$_3$H$_9$NO	MET-75	X	-	-	-
91	C$_3$H$_9$NO$_2$	MET-91	X	-	-	-
101	C$_5$H$_{11}$NO	MET-101	X	-	-	-
115	C$_6$H$_{13}$NO	MET-115	X	X	-	-
117	C$_6$H$_{15}$NO	MET-117	X	X	-	X
119	C$_5$H$_{13}$NO$_2$	MET-119	X	-	-	-
120	C$_8$H$_8$O	MET-120	-	X	X	-
133	C$_6$H$_{15}$NO$_2$	MET-133	X	X	X	X
140	C$_7$H$_8$O$_3$	MET-140	-	X	-	-
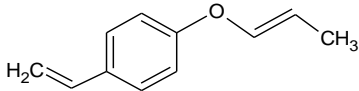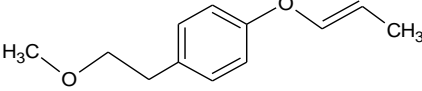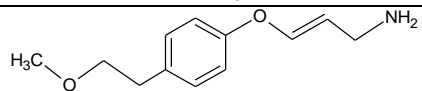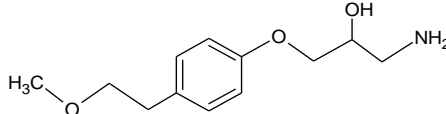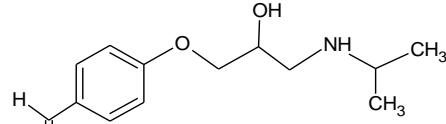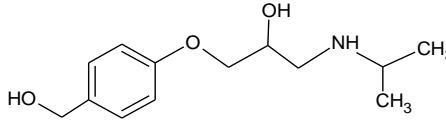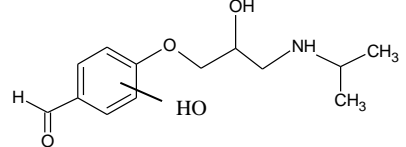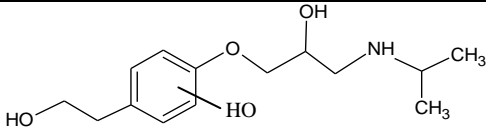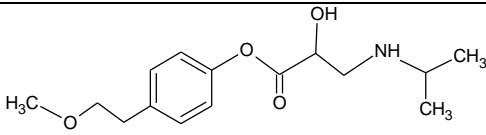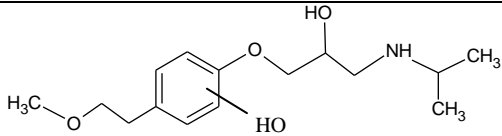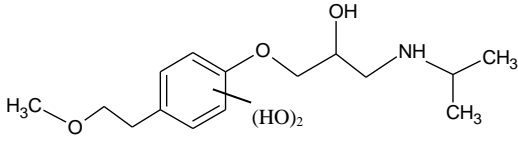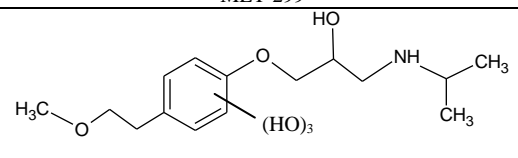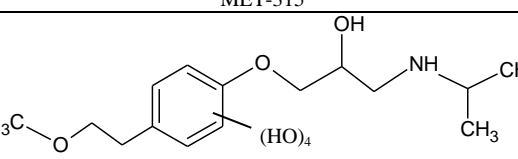
			UV-VisTiO₂ SB	UV-Vis/H₂O₂/TiO₂		
m/z	Molecular formule	Proposed structure		SB[1]	CPC[1]	CPC[2]
160	$C_{11}H_{12}O$	MET-160	X	-	-	-
192	$C_{12}H_{16}O_2$	MET-192	X	-	-	-
207	$C_{12}H_{17}NO_2$	MET-207	X	-	-	-
225	$C_{12}H_{19}NO_3$	MET-225	X	-	-	-
237	$C_{13}H_{19}NO_3$	MET-237	X	-	-	-
239	$C_{13}H_{21}NO_3$	MET-239	X	-	X	-
253	$C_{13}H_{19}NO_4$	MET-253	-	-	X	X
269	$C_{14}H_{23}NO_4$	MET-269	-	-	X	-
281	$C_{15}H_{23}NO_4$	MET-281	-	-	X	X
283	$C_{15}H_{25}NO_4$	MET-283	X	-	X	X

Table 4.9 (Continued)

108

m/z	Molecular formule	Proposed structure	UV-VisTiO$_2$ SB	UV-Vis/H$_2$O$_2$/TiO$_2$		
				SB[1]	CPC[1]	CPC[2]
299	C$_{15}$H$_{25}$NO$_5$	MET-299	X	-	-	-
315	C$_{15}$H$_{25}$NO$_6$	MET-315	X	-	X	X
331	C$_{15}$H$_{25}$NO$_7$	MET-331	X	-	-	-

Table 4.9 (Continued)

Metoprolol has a molecular weight $m/z = 267$. Three intermediates corresponding to the binding of HO· radicals in the aromatic ring were detected di-(MET-299), tri-(MET-315), and tetrahydroxy (MET-331), respectively. After breaking the C– C bond in the aliphatic part of the MET molecule, amino-diol (MET-133) was identified as one of the dominant intermediates with $m/z = 133$. Different fragments of the ethanolamine side were also identified (MET-73, MET-75, MET-91, MET-101, MET-115, MET-117), probably due to the loss of the hydroxyl group and the loss of isopropyl moiety. MET-239 can be formed probably by reactions which involve attack on the ether side chain followed by its elimination. On the other hand, the oxidation of alcohols to aldehydes can explain the formation of MET-237. The hydrogen abstraction and the water elimination of MET-237 probably generate a carbonyl, followed by an intermolecular electron transfer; thus, a double bond is generated and MET-219 is formed. Oxidative attack on the dimethyl-amine moiety results in a MET-225. Following this, the hydrogen abstraction and elimination of water of MET-225 generate a carbonyl which followed by intermolecular electron transference, generates a double bond and forms MET-207. Moreover MET-207 can generate MET-192 corresponding to a loss of ammonia after the hydrogen abstraction. The intermediate MET-160 could be formed by the loss of methanol combined with the attack of HO· on the C atom next to the ether oxygen in the aliphatic part of MET-192. It can be observed that the cleavage of MET molecule leads to smaller fragments producing more biodegradable compounds at the

end of the processes. A simplified fragmentation pathway of Metoprolol degradation by photocatalysis/TiO$_2$ and UV-Vis/H$_2$O$_2$/TiO$_2$ processes is proposed in figures 4.24 and 4.25. The two different degradation mechanisms have been proposed because different intermediates were found in each process.
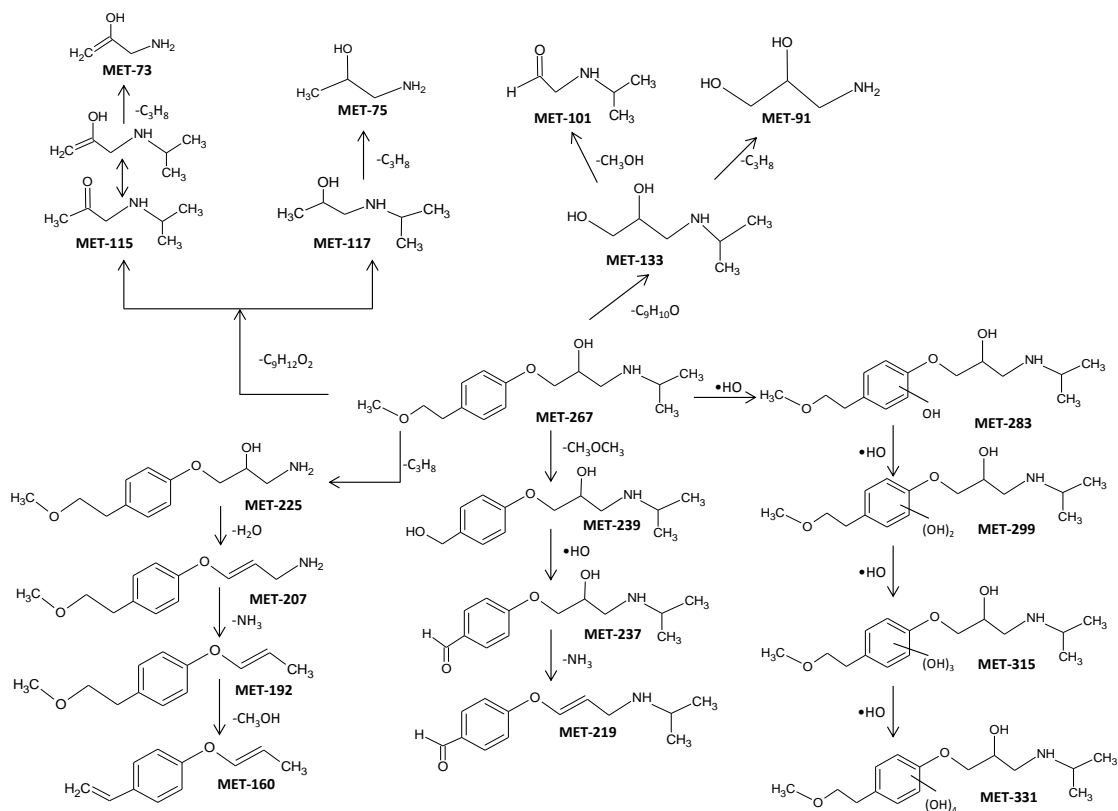
Figure 4.24- Possible pathways for MET degradation by photocatalysis/TiO$_2$ process.
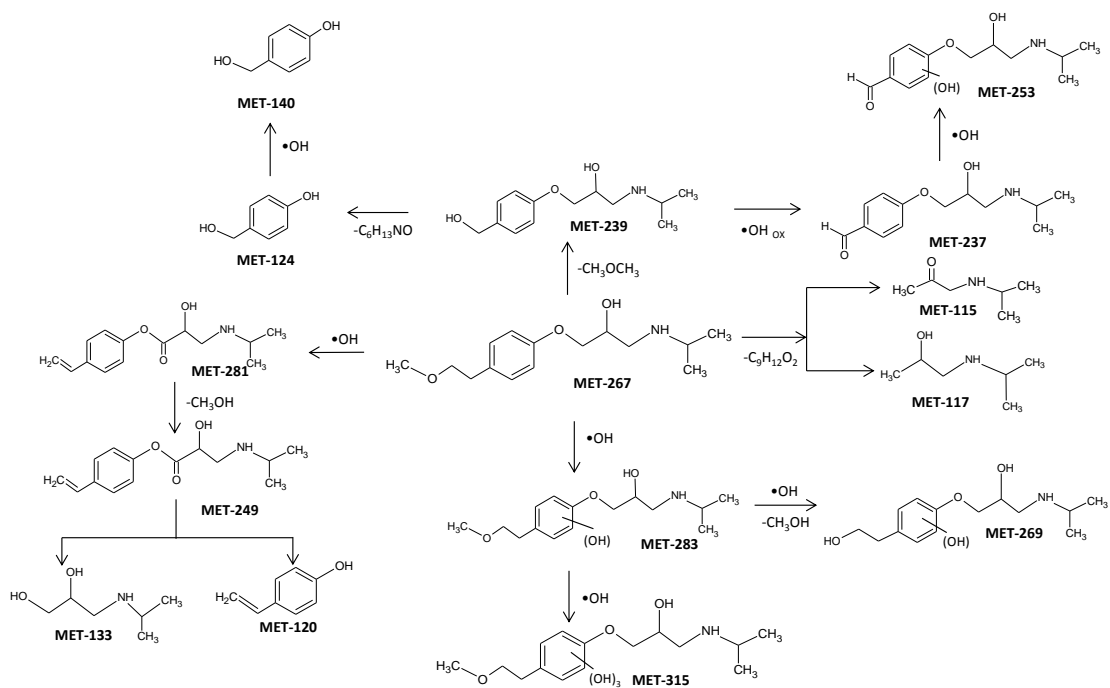
Figure 4.25- Proposed MET degradation pathways for UV-Vis/H_2O_2/TiO_2 process.

Table 4.10- General table (Fenton process)

Exp Nº	[MET]$_0$ (mg/L)	[Fe^{2+}] (mg/L)	H$_2$O$_2$ (mg/L)	MET conversion (%)	TOC conversion (%)	Time (min)	Other
F-1	50	2.5	25	23.2	4.0	60	Fe one addition
F-2	50	10	150	67.0	8.0	60	Fe one addition
F-3	50	2.5	25	29.0	4.7	60	Fe by steps (0.5 mg/L x 5 times)
F-4	50	2.5	150	34.7	5.9	60	Fe by steps (0.5 mg/L x 5 times)
F-5	50	10	25	77.4	10.5	60	Fe by steps (2 mg/L x 5 times)
F-6	50	10	150	87.0	15.6	60	Fe by steps (2 mg/L x 5 times)
F-7	25	10	25	100	-	40	Fe by steps
F-8	25	10	25	19.4	-	60	Fe by steps/TBA scavenger
F-9	25	10	25	17.2	-	60	Fe one addition/TBA scavenger

4.4 Dark-Fenton Process

Table 4.10 describes the results obtained for dark-Fenton process carried out in dark and temperature room conditions.

The pH of the initial MET solution was first adjusted to 3 with H_2SO_4 to avoid iron precipitation (at least under low to moderate iron concentration below approx. 1 mM) (Malato et al., 2009). Then, the required amounts of Fe (II) and H_2O_2 were added to the solution to initiate the oxidation. The reagents were mixed by a magnetic stirrer to ensure complete homogeneity. After 60 minutes, Fenton oxidation was stopped. The treated solution was filtered through a 0.45 mm filter for all analysis except iron measure.

Two different amounts of Fe (II) were used: 2.5 mg/L or 10 mg/L and two different H_2O_2 concentrations: 25 mg/L or 150 mg/L.

These Fe (II) and H_2O_2 concentrations can be broadly found in literature and they were also selected based on the previous group experience. Further, the maximum 10 mg/L of Fe (II) was selected due to the positive effect of the cation on the reaction kinetics. In addition, it is the limit value allowed in discharge of municipal water according to Spanish regulations (Catalunya, 2004).

Preliminary experiments

In order to establish the possible interactions between Iron (II)/MET and hydrogen peroxide/MET, preliminary experiments were carried out. All experiments were done in a reactor of 500 mL in dark conditions and 25ºC.

Firstly, 50 mg/L MET in solution were mixed with 25 mg/L H_2O_2 in the reactor. After 300 minutes of reaction, not MET and TOC degradation was observed.

In a second place, 50 mg/L MET in solution were mixed with 2.5 mg/L Fe (II), without H_2O_2. Within 24 hours of reaction, not MET degradation was observed, TOC removal was negligible and Iron (II) was held constant. So that, no complexes are formed between Iron (II) and MET by themselves.

In the last place, 50 mg/L MET in solution were mixed with 2.5 mg/L Fe (II), without H_2O_2 but Iron (II) additions were done successive and continuously (0.5 mg/L Fe (II) were added every 12 minutes during 1 hour). Not MET and TOC elimination were observed.

These results showed that independently of the iron addition ways, there is not any interaction between MET and iron (II) to produce complexes.

Influence of ways to add iron

a. *Fenton assessment with one Iron (II) addition*

When 2.5 mg/L of Fe (II) and 25 mg/L of H_2O_2 were used (esp. F-1), MET degradation was 23.2%. Increasing Fe (II) up to 10 mg/L and H_2O_2 up to 150 mg/L (exp. F-2), higher MET conversion was reached up to 67.0%. Apropos of mineralization the results are rather low for both experiments. TOC conversions were 4% and 8% for exp. F-1and F-2 respectively.

The efficiency of the process improves with increasing Iron (II) and H_2O_2 concentrations. However, MET oxidation increases sharply during the initial 2 min of reaction and then it goes slower reaching a plateau (see Figure 4.26). A likely explanation is that ferric ions (Fe (III)) would prevail in the aqueous medium as a by-product of the oxidation reaction between Fe (II) and H_2O_2, reducing the effectiveness

of the process (the reduction of ferric iron is the rate limiting step in Fenton process) (Gónzalez-Alvarez, 2009; Malato et al., 2009; Spuhler, Rengifo, & Pulgarín, 2010).
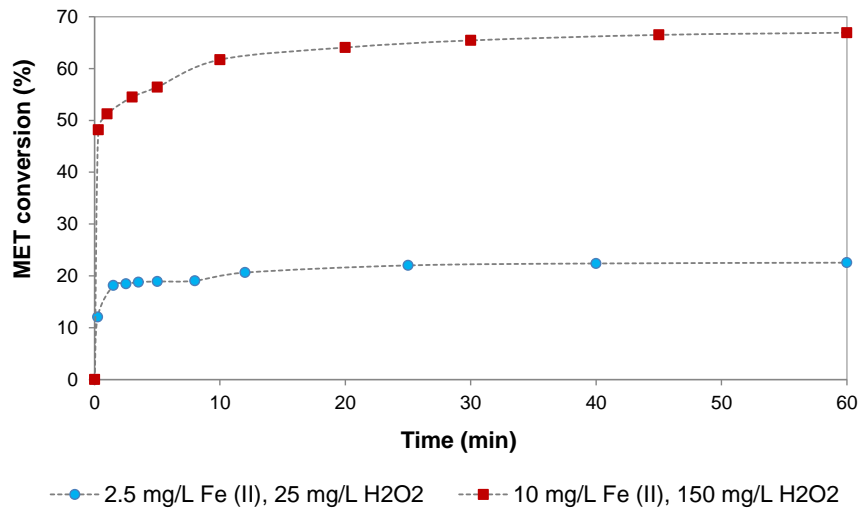
Figure 4.26- Removal of 50 mg/L of MET solution, using 2.5 mg/L Fe (II) and 25 mg/L H_2O_2 or 10 mg/L Fe (II) and 150 mg/L H_2O_2, by Fenton Process and adding the total Fe (II) at the beginning of the experiment.

b. *Fenton assessment with Iron (II) addition by steps*

In order to improve the process, the additions of Iron (II) were done in successive steps (iron was not totally added at the beginning of the experiment). The total Iron (II) concentration was divided in equal parts (5) and added at constant periods of time (12 minutes) during 1 hour.

The experiments were carried out, using two different Iron (II) concentrations and two different H_2O_2 concentrations (Exp. F-3, F-4, F-5 and F-6).

MET removal reached was 29.0%, 34.7%, 77.4% and 87.0% respectively for experiments F-3, F-4, F-5 and F-6 (see figure 4.27).

For a constant Fe (II) concentration as higher hydrogen peroxide concentration was added higher MET conversion was achieved.

117
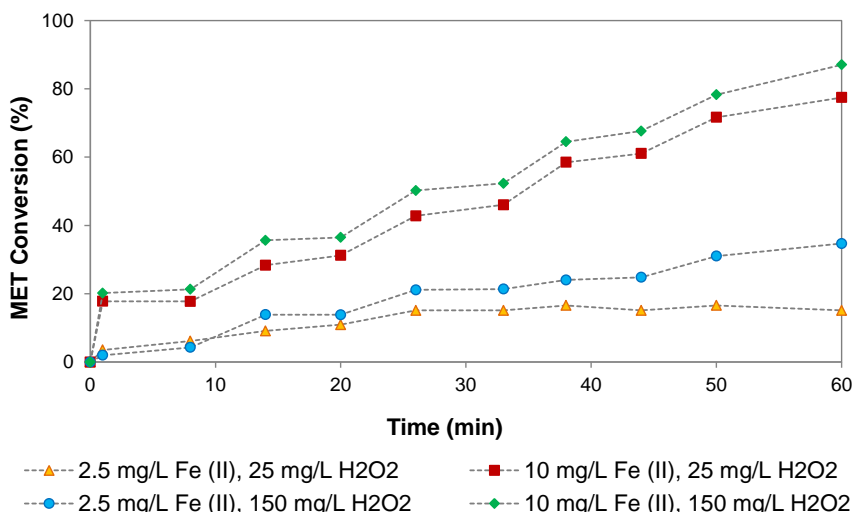
Figure 4.27- Degradation of 50 mg/L of MET solution by Fenton Process, adding Fe (II) by steps.

For the same H_2O_2 concentration, it can be observed, in all the series, the higher concentration of Fe (II) leads to a higher degradation rate. Thus, for 25 mg/L H_2O_2, when 10 mg/L Fe^{2+} were used, 77.4 % of MET was removed in 60 minutes whereas 29% of MET was degraded when 2.5 mg/L Fe (II) were added.

Similar behaviour was observed for TOC removal and the mineralization is much faster when 10 mg/L Fe (II) were used (see figure 4.28). TOC removal was a function of Fe (II) and initial H_2O_2 concentrations, being 4.7%, 5.9%, 10.5% and 15.6% for experiments (F-3, F-4, F-5 and F-6), respectively.
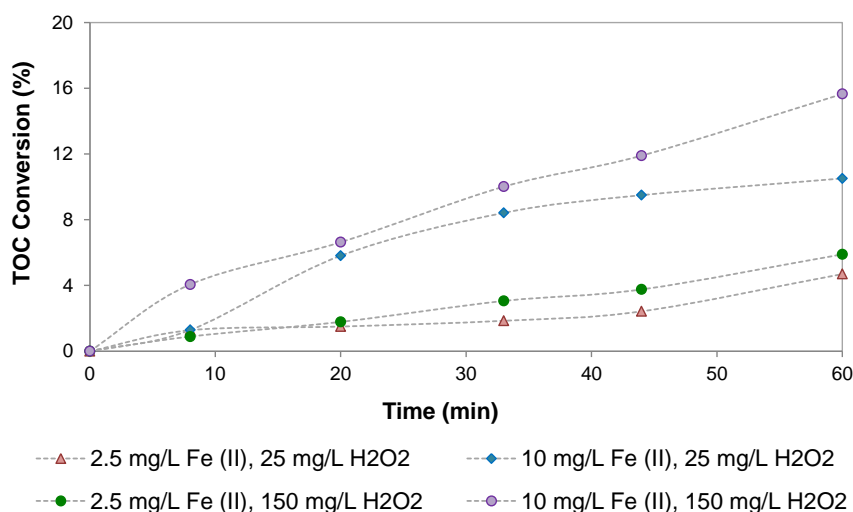
Figure 4.28- Mineralization by Fenton Process, adding Fe (II) by steps. $[MET]_0$=50 mg/L.

Chemical Oxygen Demand and Toxicity

With the highest values of catalyst and promoter (10 mg/L of iron (II) and 150 mg/L of hydrogen peroxide), the maximum COD conversion was 7.63% after 60 minutes of irradiation when iron was added at the beginning. The Average Oxidation state (AOS) was calculates with Eq. 3.5 and obviously, the result obtained was almost the same of the untreated solution (0.8) due to the low removal of COD and TOC reached.

Toxicity was measured in the MET solution treated by Fenton in the best conditions (10 mg/L of iron (II) and 150 mg/L of hydrogen peroxide). After 60 minutes of treatment the treated solution could be considered non-toxic because the final Equitox/m^3 was 0.93

When 10 mg/L of iron were added by steps and 150 mg/L of hydrogen peroxide were used, a low conversion of COD was achieved, only 14.8% after 60 minutes of reaction. This result show a very low contaminant oxidation along the process and this result is also in accordance with the low TOC degradation (15.6%). The toxicity expressed as Equitox/m^3 shows an improvement after the period of treatment (60 minutes), achieving an effluent that can be consider non-toxic for subsequent biological treatment. The final value of Equitox/m^3 was 0.90.

Intermediates

This study was focused on the identified major stable by-products, formed during 100 minutes of Fenton treatment of MET, when 10 mg/L of iron were added totally at the beginning of the experiment and mixed with 150 mg/L of hydrogen peroxide (Exp. F-2 in table 4.11). The by-products were identified by HPLC/MS in positive electrospray model.

Table 4.11- Intermediates proposed structures for Fenton process in MET degradation within 100 minutes, loading the total Iron concentration at the beginning of the experiment. [Fe (II)]$_0$=10 mg/L; [H$_2$O$_2$]=150 mg/L.
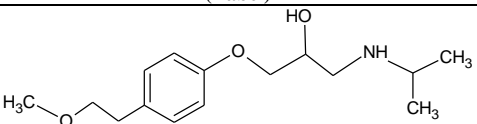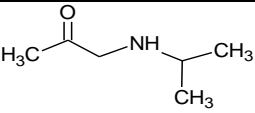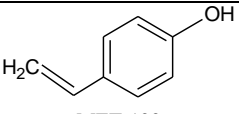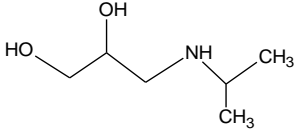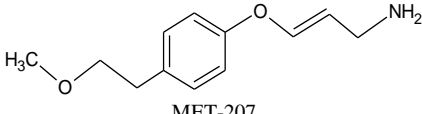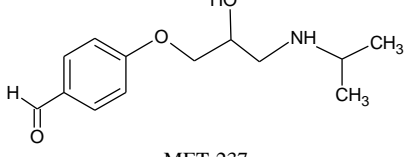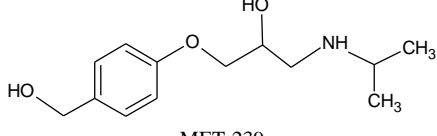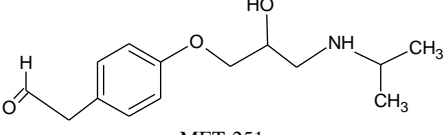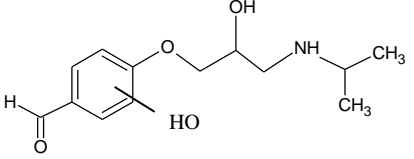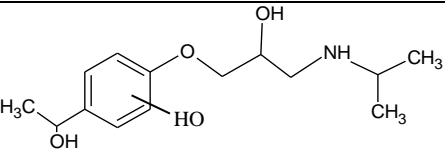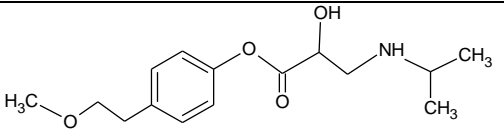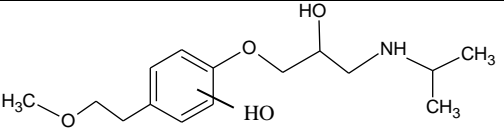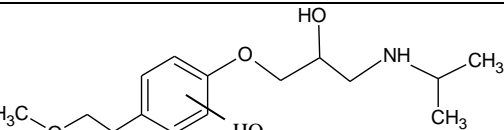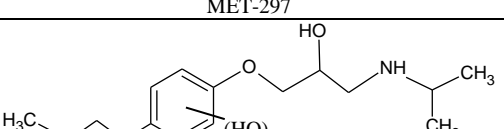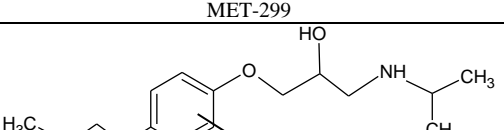
m /z (Da)	Elemental composition	Proposed structure (Label)
267	C$_{15}$H$_{25}$NO$_3$	MET-267
115	C$_6$H$_{13}$NO	MET-115
120	C$_8$H$_8$O	MET-120
133	C$_6$H$_{15}$NO$_2$	MET-133
207	C$_{12}$H$_{17}$NO$_2$	MET-207
237	C$_{13}$H$_{19}$NO$_3$	MET-237
239	C$_{13}$H$_{21}$NO$_3$	MET-239
251	C$_{14}$H$_{21}$NO$_3$	MET-251
253	C$_{13}$H$_{19}$NO$_4$	MET-253
269	C$_{14}$H$_{23}$NO$_4$	MET-269

Table 4.11 (Continued)		
m /z (Da)	Elemental composition	Proposed structure (Label)
281	$C_{15}H_{23}NO_4$	MET-281
283	$C_{15}H_{25}NO_4$	MET-283
297	$C_{15}H_{23}NO_5$	MET-297
299	$C_{15}H_{25}NO_5$	MET-299
315	$C_{15}H_{25}NO_6$	MET-315
Other intermediates identified (m/z) 163, 265, 289.		

Metoprolol was identified in with m/z=267. MET-239 can be formed probably by reactions which involve attack on the ether side chain followed by elimination. On the other hand, the oxidation of alcohols to aldehydes can be explained by the formation of MET-237. The binding of HO· radicals in the aromatic ring MET-237 generates the formation of MET-253. The hydrogen abstraction and elimination of water generates a possible by-product to produce by loss of isopropyl moiety MET-207. Binding of HO· radical in the aromatic ring was detected in MET-283, MET-299 and MET-315 (mono, bi and tri hydroxylation, respectively); MET-283 is also oxidized to MET-297. By oxidation of MET-267 is produced MET-281which after its breaking produces MET-133 (aminodiol) and MET-120. MET-267 by abstraction of dimethyl ether produce MET-239 which is oxidized progressively forming MET-237 and MET-253. A simplified pathway of Metoprolol degradation by Fenton process is proposed in figure 4.29.
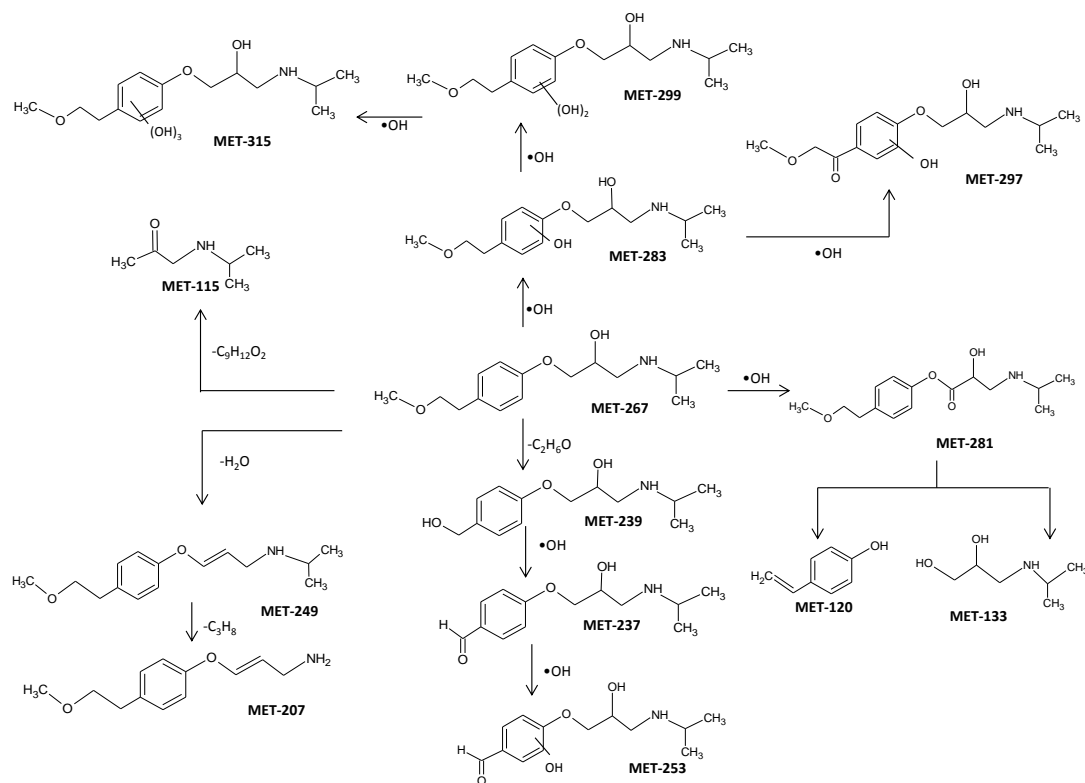
Figure 4.29- Proposed MET degradation pathways for dark-Fenton process.

Effect of scavengers

In order to understand better the mechanism of the process, 25 mg/L of MET were mixed with 10 mg/L of iron (II) added five times every 12 minutes and 25 mg/L of hydrogen peroxide and a complete MET degradation was reached within 40 minutes. After, 500 mg/L of Ter-butil-alcohol (TBA) were added into the reactor with 25 mg/L of MET at the beginning of the reaction (Exp. F-8 and F-9). When the Iron (II) was added by steps 19.4 % of MET was removed and 17.2% when the total Fe (II) was added at the beginning of the experiment. TBA functions as HO· scavenger, hence it can be clearly appreciated (see figure 4.30) that HO· are mainly responsible of MET degradation, because the reaction rate decreases when scavenger was added.
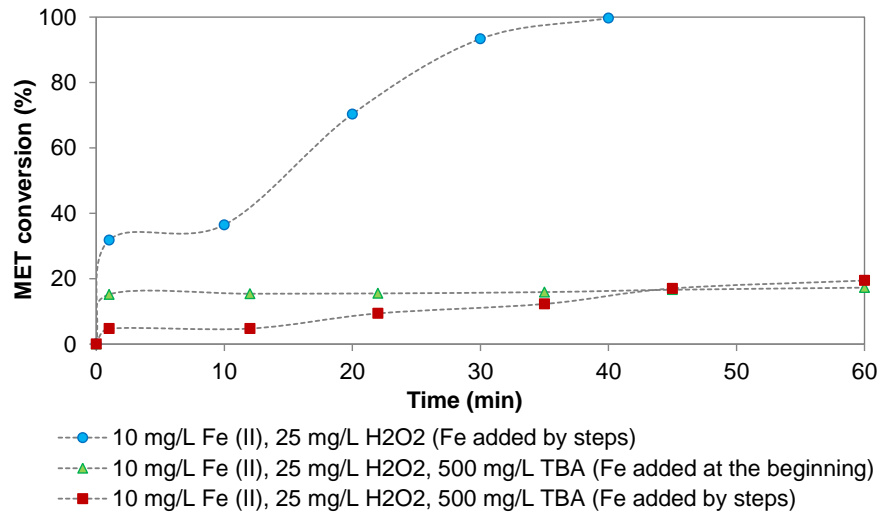
Figure 4.30- Effect of TBA scavenger in MET elimination in Fenton process.

Table 4.12- General table of photo-Fenton process.

Exp Nº	[MET]$_0$ (mg/L)	[Fe^{2+}] (mg/L)	H$_2$O$_2$ (mg/L)	T (ºC)	MET conversion (%)	Time (min)	TOC conversion (%)	Time (min)	Other
Photo-Fenton (PF)									
PF-BLB-1	50	2.5	25	25	97.2	100	16.4	100	Fe one addition
PF-BLB-2	50	2.5	150	25	88.1	15	82.3	285	Fe one addition
PF-BLB-3	50	10	25	25	97.5	20	19.9	20	Fe one addition
PF-BLB-4	50	10	150	25	100	7	81.2	90	Fe one addition
PF-BLB-5	50	2.5	25	14	97.7	230	12.3	230	Fe one addition
PF-BLB-6	50	2.5	150	14	89.7	30	82.5	510	Fe one addition
PF-BLB-7	50	10	25	14	96.5	40	14.6	40	Fe one addition
PF-BLB-8	50	10	150	14	100	10	73	185	Fe one addition
PF-BLB-9	50	2.5	25	25	81.0	60	8.5	60	Fe by steps
PF-BLB-10	50	2.5	150	25	90.5	60	17.3	60	Fe by steps
PF-BLB-11	50	10	25	25	98.0	50	27.1	60	Fe by steps
PF-BLB-12	50	10	150	25	100	33	61.5	60	Fe by steps
PF-SB-13	50	2.5	25	25	88.6	60	35.1	290	Fe one addition
PF-SB-14	50	2.5	150	25	91.5	30	73.3	340	Fe one addition
PF-SB-15	50	10	25	25	90.2	10	28.9	60	Fe one addition
PF-SB-16	50	10	150	25	97.3	7	78.8	120	Fe one addition
PF-SB-17	50	2.5	25	14	81.8	60	34.1	300	Fe one addition
PF-CPC-18	50	2.5	25	30 ± 5	95.7	60	32.0	240	Fe one addition
PF-CPC-19	50	2.5	150	30 ± 5	89.8	30	72.0	300	Fe one addition
PF-CPC-20	50	10	25	30 ± 5	94.0	1	47.0	80	Fe one addition
PF-CPC-21	50	10	150	30 ± 5	96.4	1	83.7	150	Fe one addition
PF-UVC-22	50	2.5	25	25	97.0	20	17.6	60	Fe one addition/pH 2.8

4.5   Photo-Fenton Process

Table 4.12 shows the main results obtained in the (PF) treatment of MET.

Photo-Fenton (PF) experiments were carried out with 50 mg/L of initial MET in Milli Q water, with iron (II) as catalyst and H_2O_2 as promoter. pH 3 was adjusted with H_2SO_4 to avoid iron precipitation, as indicated in the case of dark Fenton (section 4.4), in all experiments a complete homogeneity was ensures by magnetic stirring. Different irradiation sources were used: BLB, SB, CPC and UVC reactors. The treated solution was filtered through a 0.45 mm filter for all analyses except iron measure.

As commented in dark Fenton (section 4.4) and for the same reasons two different amounts of Fe (II) were used: 2.5 mg/L and 10 mg/L and two different H_2O_2 concentrations: 25 mg/L and 150 mg/L.

4.5.1 Photo-Fenton in BLB reactor

In this part of the study Photo-Fenton process was considered as complete when all H_2O_2 was consumed. Two temperature conditions were chosen (14ºC and 25ºC) based on the common values found for wastewater streams in the area of study at different seasons. In the current study MET and TOC degradations were faster in the experiments at 25ºC (figure 4.31). Increasing temperature leads to faster kinetics of the process (Gernjak, Fuerhacker, Fernández-Ibañez, Blanco, & Malato, 2006; Göb et al., 2001; Malato et al., 2009; Sawage, Lehnard, Lübber, & Bahnemann, 2001). Using the highest concentrations of Fe (II) and H_2O_2 a complete MET degradation is reached, for both temperatures (Exp. PF-BLB-4 and PF-BLB-8). For a constant Fe (II) concentration as higher hydrogen peroxide concentration was added higher the MET conversion. For a constant H_2O_2 concentration as higher iron (II) concentration was loaded higher the MET conversion.
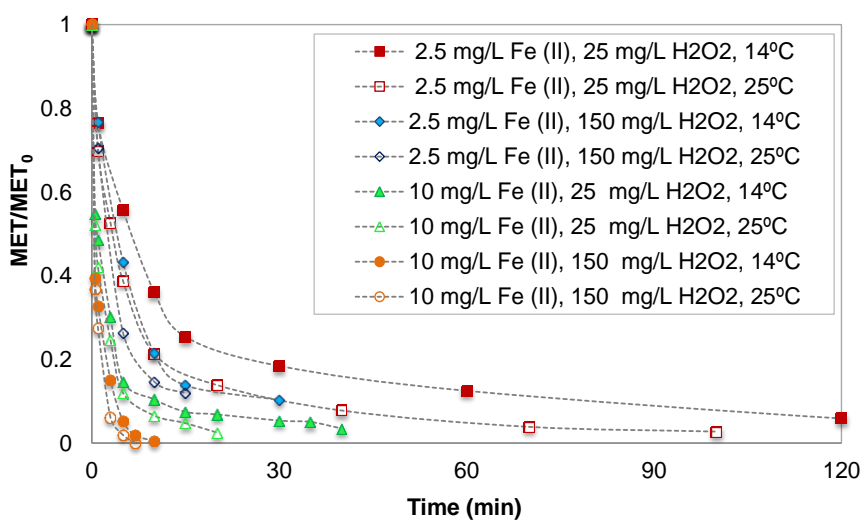
Figure 4.31- MET degradation profiles for the different initial Fe (II) and H_2O_2 concentrations and temperatures assayed. $[MET]_0$=50 mg/L.

Concerning the TOC conversions obtained, at 25 ºC were 16.4% (100 min.), 82.3% (285 min), 19.9% (20 min) and 81.2% (90 min.), for experiments PF-BLB-1, PF-BLB-2, PF-BLB-3 and PF-BLB-4, respectively. At 14ºC the TOC conversions obtained were: 12.3% (230 min.), 82.5% (510 min), 14.6% (40 min), and 73.0% (185 min.) for experiments PF-BLB-5, PF-BLB-6, PF-BLB-7 and PF-BLB-8, respectively (see table 4.13).

Table 4.13- TOC degradation for photo-Fenton process in BLB reactor at 14 and 25 ºC.

Iron (II) (mg/L)	H₂O₂ (mg/L)	TOC at 25ºC (mg/L)	Time (min)	TOC at 14ºC (mg/L)	Time (min)
2.5	25	16.4	100	12.3	230
2.5	150	82.3	285	82.5	510
10	25	19.9	20	14.6	40
10	150	81.2	90	73.0	185

In order to see the effect of the way of dosing iron in PF process, experiments were carried out using the same Fe (II) and H_2O_2 concentrations, at 25 ºC, but the total iron was added in 5 parts every 12 minutes (Exp.PF-BLB-9, PF-BLB-10, PF-BLB-11 and PF-BLB-12).

After one hour of experimental time, MET elimination reached was 81.0%, 90.5%, 98% for experiments PF-BLB-9, PF-BLB-10, PF-BLB-11, respectively, and a complete MET elimination was obtained after 33 minutes for experiment PF-BLB-12 (figure 4.32).
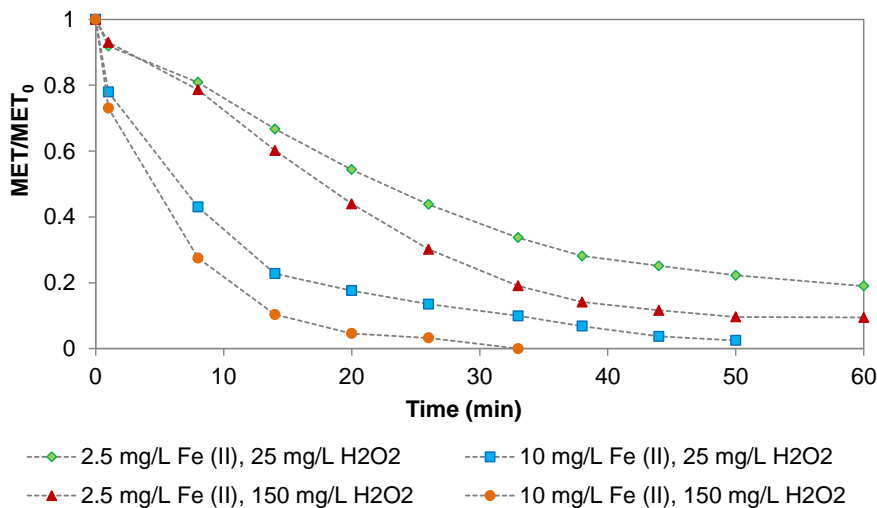
Figure 4.32- MET degradation profiles for the different initial H_2O_2 and Fe^{2+} concentrations used in photo-Fenton process at 25ºC and iron added by steps.

Within 60 minutes, the highest TOC conversion obtained was: 8.5%, 17.3%, 27.1% and 61.5% for experiments PF-BLB-9, PF-BLB-10, PF-BLB-11 and PF-BLB-12, respectively (figure 4.33).
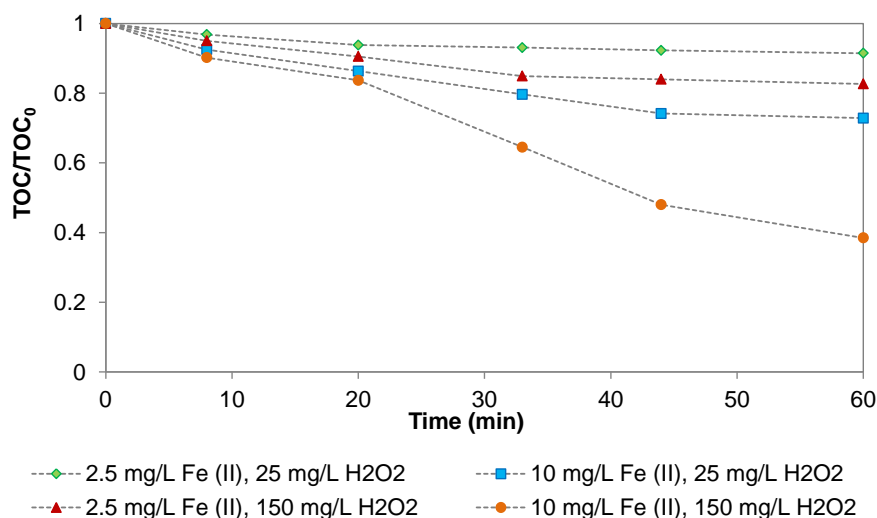
Figure 4.33- TOC degradation profiles for the different initial H_2O_2 and Fe^{2+} concentrations used at 25ºC, iron added by steps.

With respect to MET and TOC degradation, under all the different conditions tested, the best results obtained were using concentrations of 10 mg/L Fe (II) and 150 mg/L H_2O_2.

Comparing the ways to add the iron it could be observed that the process efficiency in MET and TOC degradation was better when the iron was added totally once at the beginning of the experiment in all series.

Chemical Oxygen Demand and Biodegradability

Regarding to COD, at 25ºC, the highest COD removal was reached in PF-BLB-2 and PF-BLB-4 experiments and there was almost the same COD removal (88.7% and 85.6%) but the time needed for PF-BLB-2 was 3.2 times higher than the time required in PF-BLB-4. In this way the optimum removal obtained was using PF-BLB-4 (table 4.14).

In experiments PF-BLB-2 and PF-BLB-4, the treated solution can be joined to biological treatment, because, at the end of irradiation time, biodegradability indicator was higher than 0.4 (see section 3.2).

With respect to COD, at 14ºC, the removal in PF-BLB-6 and PF-BLB-8 experiments was almost the same (92.1% and 89.4%) but the time needed for PF-BLB-6 was 2.8 folds higher than the time required in PF-BLB-8. In this way the optimum removal obtained was using PF-BLB-8 (table 4.14).

Table 4.14- COD removal and biodegradability for different photo-Fenton conditions in BLB reactor.

	Experiment	Time (min)	COD removal (%)	Biodegradability
25 ºC	2.5 mg Fe/L, 25 mg H_2O_2/L	100	21.5	0.15
	2.5 mg Fe/L, 150 mg H_2O_2/L	285	88.7	0.68
	10 mg Fe/L, 25 mg H_2O_2/L	20	24.6	0.12
	10 mg Fe/L, 150 mg H_2O_2/L	90	85.6	0.53
14ºC	2.5 mg Fe/L, 25 mg H_2O_2/L	230	42.3	0.19
	2.5 mg Fe/L, 150 mg H_2O_2/L	510	92.1	0.7
	10 mg Fe/L, 25 mg H_2O_2/L	40	23.5	0.15
	10 mg Fe/L, 150 mg H_2O_2/L	185	89.4	0.54

Relating to biodegradability, after experiments PF-BLB-6 and PF-BLB-8, the solution can be joined to biological treatment, because, the biodegradability was higher than 0.4 (see section 3.2).

Working at 25 ºC and dosing iron by steps COD and AOS were assessed for 10 mg/L of Fe (II) and 150 mg/L of H_2O_2.

After 60 minutes of treatment 78.6 % of COD conversion was reached and AOS increases from 0.77 to 2.2. The formation of more oxidized intermediates is an indirect indication of the ability of the treatment to improve MET biodegradability.

Factorial design 2x2

A factorial design 2x2 (O. G. León & Montero, 2001) was used to study the interaction between two factors (iron and hydrogen peroxide concentrations) in MET treatment by photo-Fenton (figure 4.34).

Observing the lines obtained in figure 4.34, it could be appreciated that there is not interaction between the factors because the lines are practically parallels.

It could be also observed that the slopes are higher when iron concentration appears as factor studied (a-, c- and e-), showing its higher influence. In addition, the slopes of the lines have the same sign (positive), meaning that, when iron concentration increases, MET degradation also does it.

The effect of the H_2O_2 as variable (b-, d- and f-) could be appreciated in the slopes of the lines and the effect of the iron as variable is showed in the distance between the lines. When H_2O_2 concentration increases, MET degradation also does it.

a-

b-

c-

d-

e-

f-
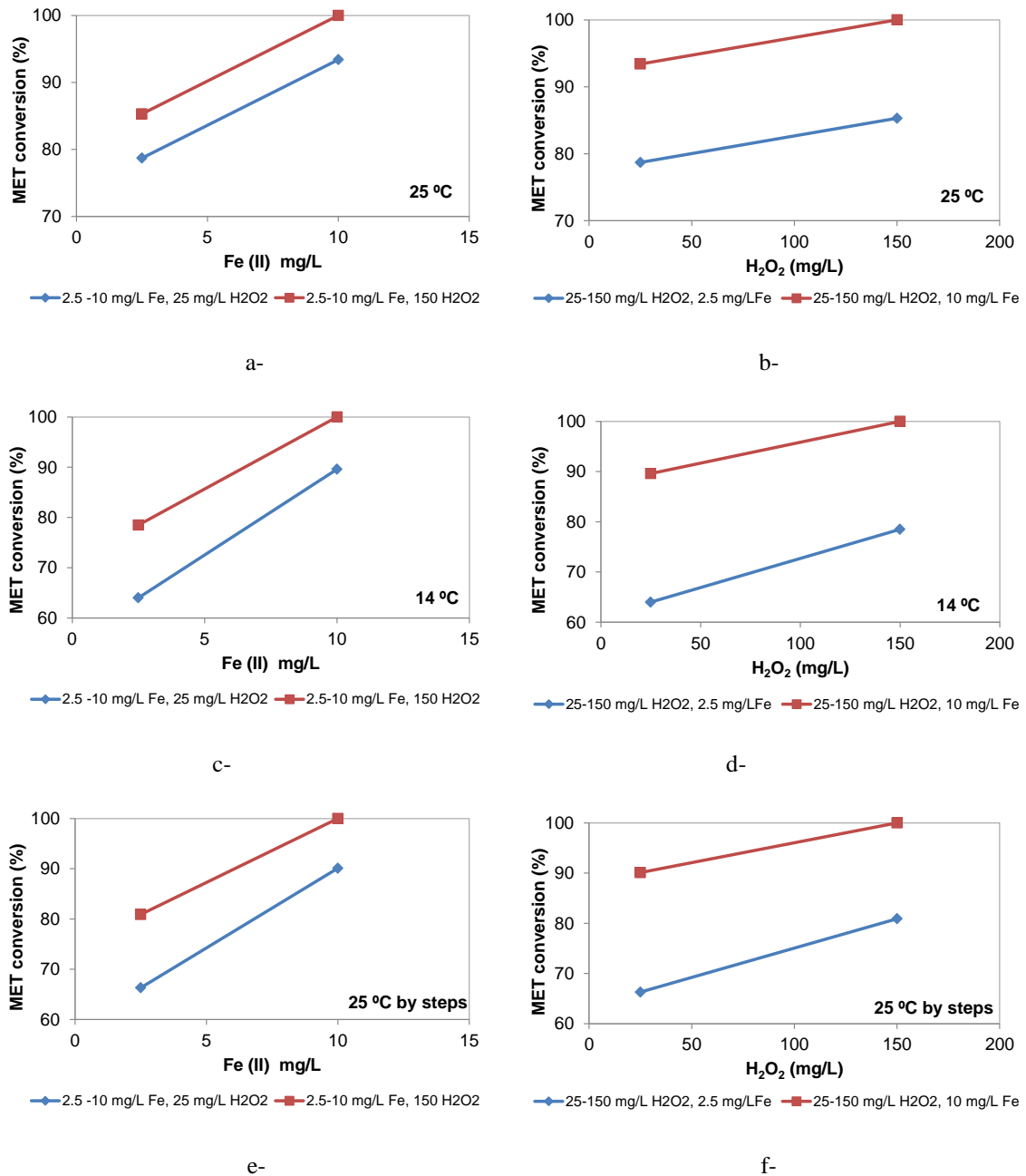
Figure 4.34- Representation of the possible factor interactions in photo-Fenton process. MET degradation at 10 minutes for 14 and 25°C adding total iron in the beginning and 33 minutes for 25°C, adding iron by steps.

Summing up: Among the different conditions tested in BLB reactor, the best way to reach the highest MET and TOC conversions in the shorter time by photo-Fenton is adding the total iron amount in one addition at the beginning of the treatment (time 0) and 25 °C.

132

4.5.2   Photo-Fenton in SB reactor

Preliminary experiments

Some preliminary assays were done in SB to investigate possible MET degradation not referable to photo-Fenton process. Thus, MET degradation by hydrogen peroxide in the dark does not show significant oxidation. Also, photolysis with H_2O_2 (150 and 25 mg/L) was investigated and transformation resulted more significant. MET removal achieved was 32.5% and 14.6%, after 120 min, for 150 mg/L H_2O_2 and 25 mg/L H_2O_2 respectively. However, mineralization was negligible. Finally, dark Fenton process was performed (150 mg/L H_2O_2 and 10 mg/L Fe^{2+}), after 10 min MET was degraded 62.8% but the mineralization obtained was too low (~10%).

Photo-Fenton

Photo-Fenton process was considered as complete when all H_2O_2 was consumed (Exp. PF-SB-13, PF-SB-14, PF-SB-15, PF-SB-16 and PF-SB-17).

This part of the study has been carried out at 25 ºC for all series and it has also done at 14 ºC for the lowest catalyst and promoter concentration (due that with these concentrations were obtained the lowest reaction rate and the effect of the temperature could be better appreciated) and in both cases the total iron was added at the beginning of the experiment.

Working at 25 ºC, MET degradation was 88.6 % (60 min.), 91.5% (30 min.), 90.2% (10 min.) and 97.3% (7 min.) for experiments PF-SB-13, PF-SB-14, PF-SB-15 and PF-SB-16, respectively. Working with 14 ºC, the maximum MET conversion was 81.8 % within 60 minutes (PF-SB-17) (see Figure 4.35). As it can be observed when increases catalyst and promoter concentrations higher reaction rate.
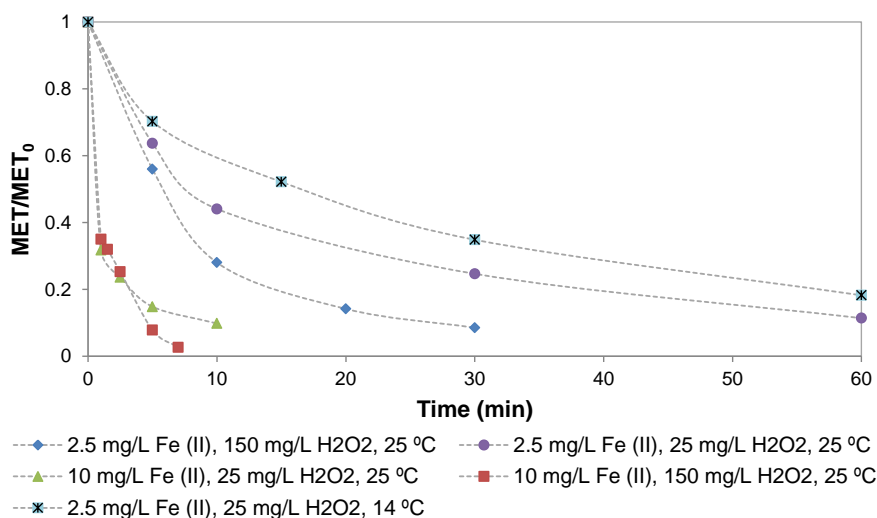
Figure 4.35- MET degradation for the different initial H_2O_2 and Fe^{2+} concentrations used at 14 ºC and 25 ºC.

Concerning TOC degradation the maximum values were 35.1 % (290 min.), 73.3% (340 min.), 28.9 % (60 min.) and 78.8 % (120 min.) for experiments PF-SB-13, PF-SB-14, PF-SB-15 and PF-SB-16, respectively, (figure 4.36) at 25 ºC and 34.1% (300 min.) at 14 ºC.
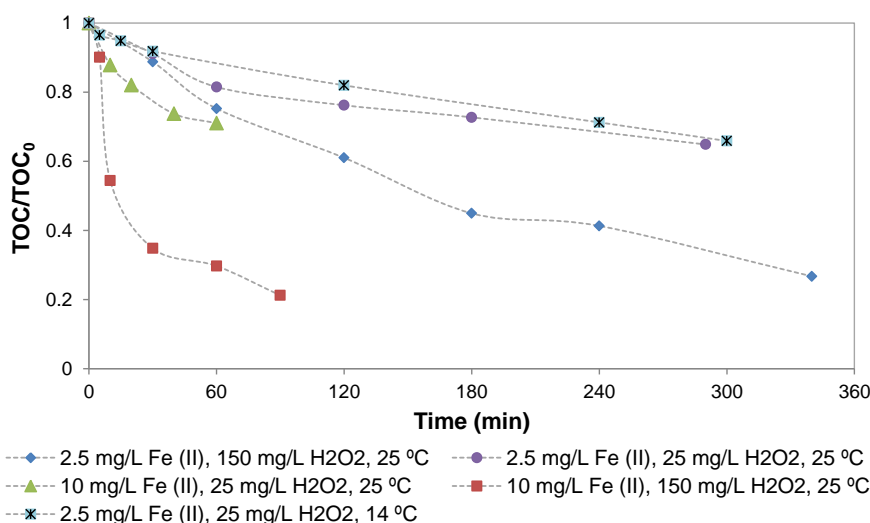
Figure 4.36- Mineralization profiles for the different initial H_2O_2 and Fe^{2+} concentrations used at 14 ºC and 25 ºC.

MET and TOC degradations were faster in the experiments at 25ºC but the differences were not really very important because, the difference of the temperatures is not higher enough.

4.5.3 Photo-Fenton in CPC reactor

In this section the Metoprolol and TOC degradation are going to be described in terms of accumulated energy per volume of treated solution (kJ/L) for the same reason explained in section 4.3.2.

In CPC reactor working at 30 ($\pm$ 5 ºC), MET elimination achieved at 5.45 kJ/L of accumulated energy was 79%, 90%, 95% for experiments PF-CPC-18, PF-CPC-19, PF-CPC-20, respectively, and 98.3% for experiment PF-CPC-21 at 0.67 kJ/L (figure 4.37).
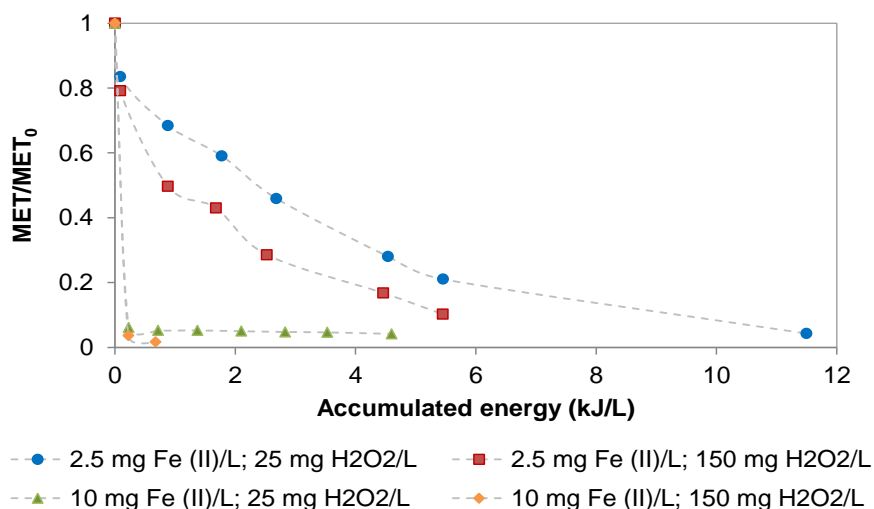
Figure 4.37- MET degradation for the different initial H_2O_2 and Fe^{2+} concentrations used at 30 $\pm$ 5 ºC. Photo-Fenton process, loading the total iron at the beginning of the experiment in CPC.

Moreover, 32% (43.5 kJ/L), 71.8% (40.3 kJ/L), 47% (15.22 kJ/L) and 83.7% (33.9 kJ/L) of TOC removal was achieved, for experiments PF-CPC-18, PF-CPC-19, PF-CPC-20 and PF-CPC-21, respectively (figure 4.38).

Complete consumption of H_2O_2 was observed in all cases at the end of the experiments.
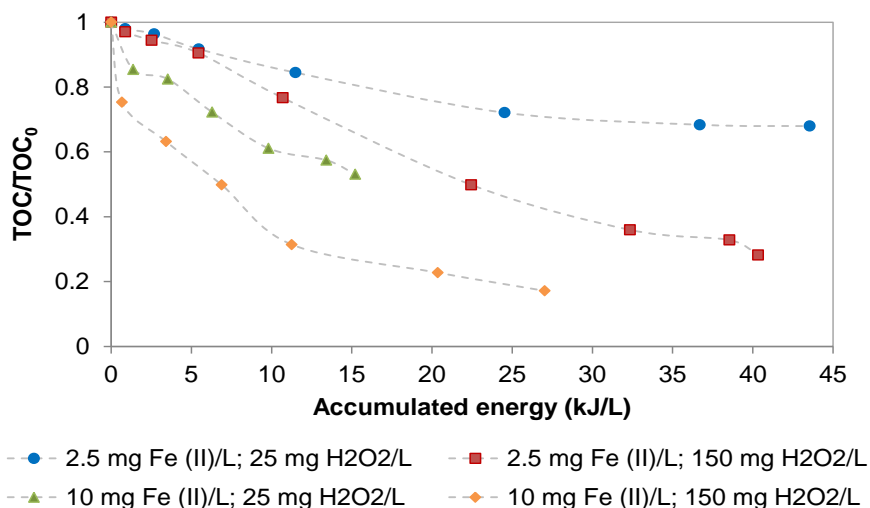
Figure 4.38- TOC degradation for the different initial H_2O_2 and Fe^{2+} concentrations used at 30 ± 5 ºC. Photo-Fenton process, loading the total iron at the beginning of the experiment in CPC.

For constant iron concentration, the increase of hydrogen peroxide concentration leads a higher MET and TOC removals. Moreover, for constant hydrogen peroxide concentration, the increase of iron leads a higher MET and TOC conversion due to the higher production of HO· radicals in the media.

4.5.4 Photo-Fenton in UVC reactor

In an attempt to find a suitable oxidation system capable of removing a significant fraction of the organic carbon content the photo-Fenton system was studied by UVC radiation. This process is characterized by a continuous regeneration of the Fe (II) species. Thus, three simultaneous actions can be contemplated, direct photolysis, hydrogen peroxide photolysis and Fenton's reagent.

This part of the study has been carried out at 25 ºC, pH 3, H_2O_2 concentration 25 mg/L and iron (II) concentration 2.5 mg/L (Exp. PF-UVC-22). The total iron was added at the beginning of the experiment and the treatment was carried out up to all hydrogen peroxide was consumed.

In figure 4.39 it can be seen that a complete MET elimination was reached in 20 minutes of treatment. However, mineralization was rather low and after 60 minutes of treatment 17.6% of TOC was degraded.
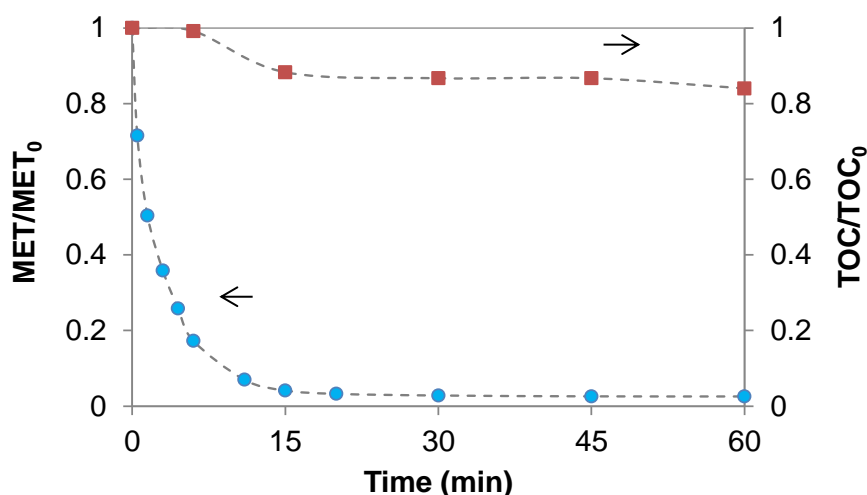
Figure 4.39- MET degradation and mineralization profiles in UVC reactor by photo-Fenton process. $[MET]_0$=50 mg/L; $[Fe (II)]_0$=2.5 mg/L and $[H_2O_2]_0$=25 mg/L.

Toxicity

The toxicity was assessed for Exp. PF-BLB-1, PF-BLB-12, PF-SB-13, PF-CPC-18 and PF-UVC-22. At the end of the processes the toxicity decreases from 6.25 to 0.56, 0.5, 0.51, 0.59 and 0.43 Equitox/m^3, respectively. The toxicity of the treated sample shows that the oxidation of MET promoted the overall toxicity reduction of the sample to non- toxic effluents for the environment. Table 4.15 summarizes the toxicity obtained for the experiments described before.

Table 4.15- Toxicity for photo-Fenton process in different devices

Device	MET (mg/L)	Fe (II) (mg/L)	H_2O_2 (mg/L)	T (ºC)	Initial toxicity (Equitox/m^3)	Final toxicity (Equitox/m^3)	Other
BLB	50	2.5	25	25		0.56	Fe one addition
BLB	50	10	150	25		0.50	Fe by steps
SB	50	2.5	25	25	6.25	0.51	Fe one addition
CPC	50	2.5	25	30 ± 5		0.59	Fe one addition
UVC	50	2.5	25	25		0.43	Fe one addition

Intermediates

The major by-products produced from photo-Fenton treatment of 50 mg/L of MET solution were identified and summarized in (table 4.16).

Table 4.16- Intermediates proposed structures for photo-Fenton process in MET degradation $[Fe(II)]_0$=2.5 mg/L; $[H_2O_2]$=25 mg/L. [1]25 ºC experiment at 100 minutes in BLB . [2]14 ºC experiment at 230 minutes in BLB, [3]adding the iron (II) by steps experiment at 10 minutes in BLB, [4] 25ºC experiment at 80 minutes in SB, [5]25ºC experiment at 60 minutes in UVC and [6]25ºC experiment at 240 minutes in CPC.
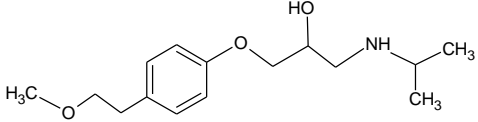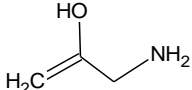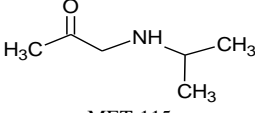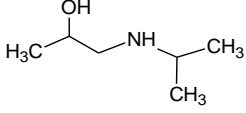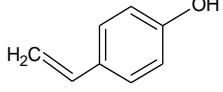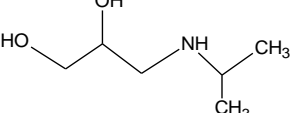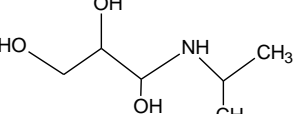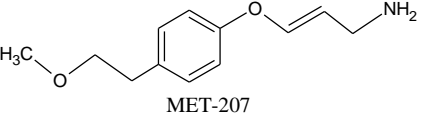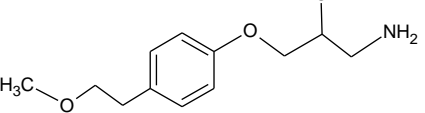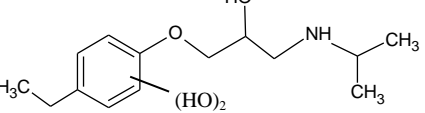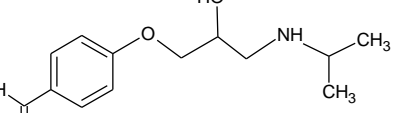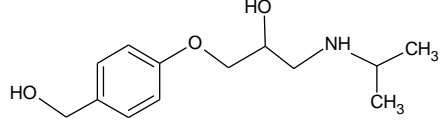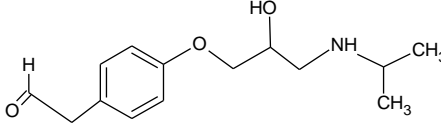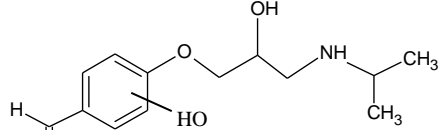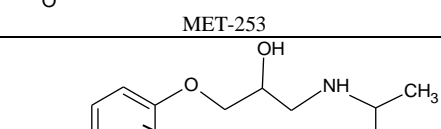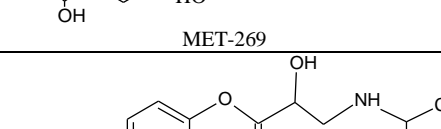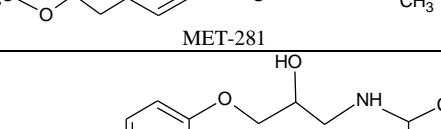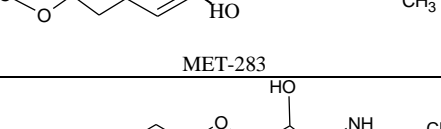
Element. Compos.	Proposed structure (Label)	PF BLB			PF SB	PF UVC	PF CPC
		1	2	3	4	5	6
$C_{15}H_{25}NO_3$	MET-267	x	x	x	x	x	x
$C_4H_{11}N$	MET-73	-	-	x	-	-	-
$C_6H_{13}NO$	MET-115	x	x	x	-	x	x
$C_6H_{15}NO$	MET-117	-	x	-	-	-	-
C_8H_8O	MET-120	-	x	x	-	x	x
$C_6H_{15}NO_2$	MET-133	x	x	x	x	x	x
$C_6H_{15}NO_3$	MET-149	-	-	-	x	x	x
$C_{12}H_{17}NO_2$	MET-207	-	-	x	x	x	x
$C_{12}H_{19}NO_3$	MET-225	-	x	x	-	-	x
$C_{10}H_{17}NO_5$	MET-231	-	-	-	x	-	-
$C_{13}H_{19}NO_3$	MET-237	x	-	x	x	x	x

	Table 4.16 (continued)						
$C_{13}H_{21}NO_3$	MET-239	-	X	X	X	X	X
$C_{14}H_{21}NO_3$	MET-251	-	-	X	-	-	-
$C_{13}H_{19}NO_4$	MET-253	X	X	X	X	-	X
$C_{14}H_{23}NO_4$	MET-269	-	X	X	-	-	-
$C_{15}H_{23}NO_4$	MET-281	X	-	-	X	X	X
$C_{15}H_{25}NO_4$	MET-283	X	X	X	X	-	-
$C_{15}H_{23}NO_5$	MET-297	X	-	X	-	-	-
Other intermediates		163	136, 189, 173, 78, 82	163, 187, 209, 268, 289, 295, 305	163, 179	103, 158, 163, 224, 229, 234, 247, 259, 275.	89, 97, 131, 172, 218, 199, 259, 278, 165.

Metoprolol was identified in all processes with $m/z=267$. MET-120, MET-133, MET-149, MET-207, MET-225, MET-237, MET-239, MET-253, MET-283 and MET-297, have been detected in processes described and explained before (sections 4.2 and 4.3), thus, a simplified pathway of Metoprolol degradation by photo-Fenton process is proposed in figure 4.40.
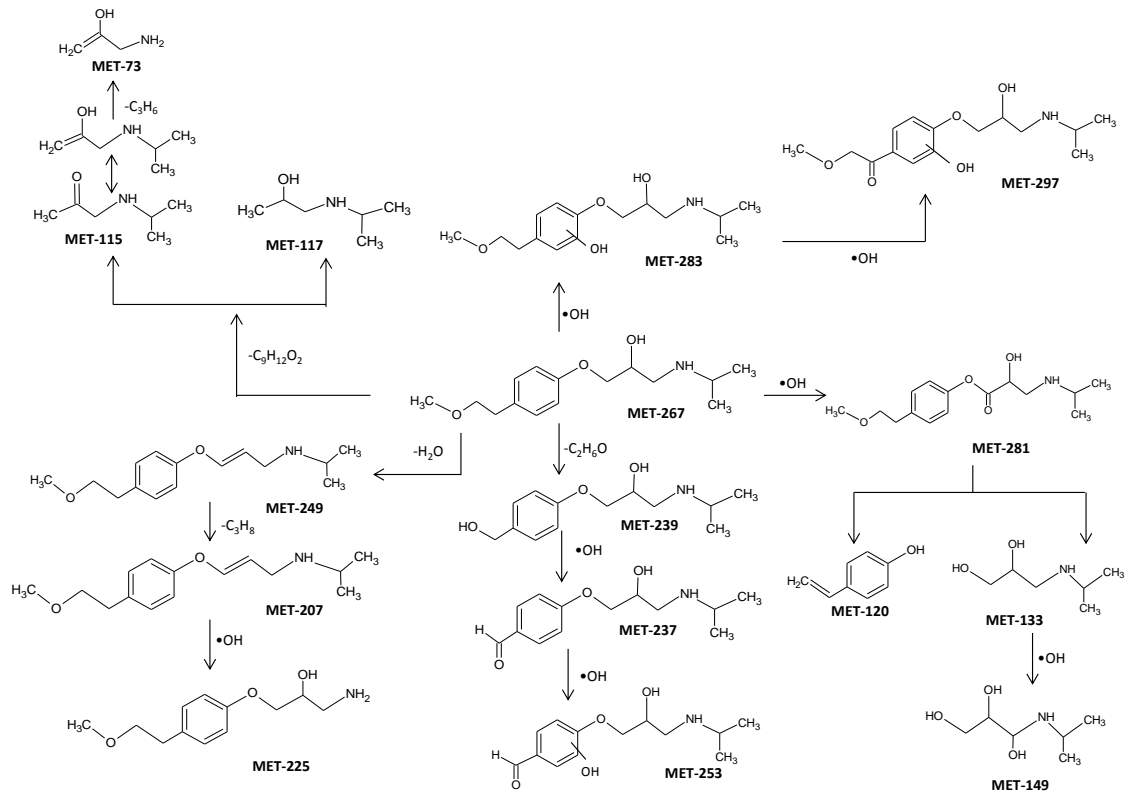
Figure 4.40- Proposed MET degradation pathways by photo-Fenton process.

Table 4.17- General table Bicarbonate-activated hydrogen peroxide method

Bicarbonate/Hydrogen peroxide							
Exp Nº	$[MET]_0$ (mg/L)	$NaHCO_3$ (mg/L)	$[H_2O_2]$ (mg/L)	pH	order of addition	MET conversion (%)	H_2O_2 consumption (%)
BAP-1	5	600	300	6.2	1	15.3	120	43.0
BAP-2	5	600	300	6.2	2	16.5	120	66.0
BAP-3	5	600	300	9.2	1	7.5	120	25.5
BAP-4	5	600	300	9.2	2	10.0	120	41.7
BAP-5	5	600	600	6.2	1	19.5	120	52.0
BAP-6	5	1200	600	6.2	1	16.3	120	18.0

4.6   Bicarbonate/hydrogen peroxide process

Table 4.17 describes the results obtained in applying Bicarbonate-activated hydrogen peroxide (BAP) method in dark conditions, room temperature and pH 6.2 or 9.2. The reactants addition was made in two ways:

Addition order (1): (MET/ HCO_3^-) + H_2O_2

Addition order (2): (HCO_3^-/ H_2O_2) + MET

As it can be observed in figure 4.41, the highest conversion of MET within 120 minutes was almost 20% when 600 mg/L of $NaHCO_3$ and 600 mg/L of H_2O_2 were used to degrade 5 mg/L of MET at free pH and following the addition way (1) (Exp. BAP-5). For the experiments (BAP-1, BAP-3 and BAP-4) the highest MET conversion was 15.3%, 7.5% and 10% respectively.

In the same experiments it can be observed that, when pH increases MET conversion decreases. Moreover, the reactants addition order has not shown a remarkable effect in MET conversion.
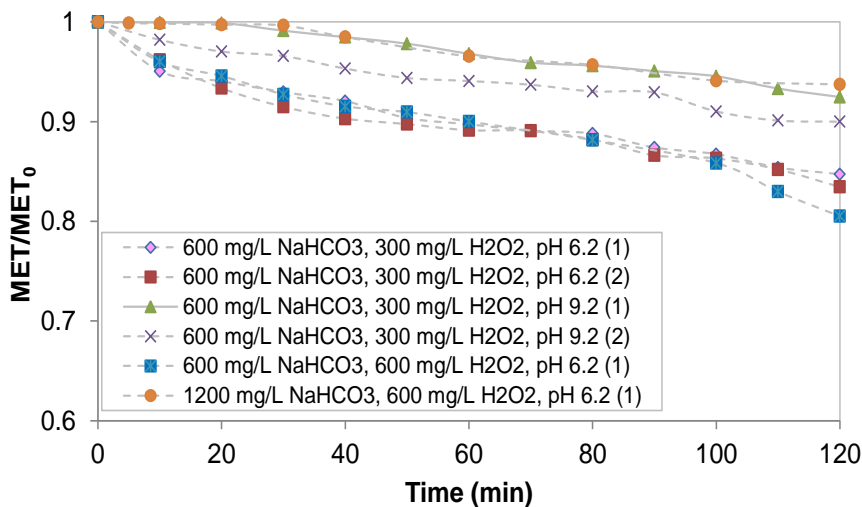
Figure 4.41- MET degradation by Bicarbonate/hydrogen peroxide process.

Relating to hydrogen peroxide consumption the highest conversion was 66% in 120 minutes of reaction, when free pH (6.2) was used and reactants addition order (2). It means, that the order (2) consumes higher hydrogen peroxide to obtain almost the same MET conversion, thus, this addition order is less effective. In general, it was observed that the hydrogen peroxide consumption is lower when the pH is basic and its consumption is higher when order (2) was used.

On the other hand, when hydrogen peroxide concentration was increased from 300 mg/L up to 600 mg/L (Exp. BAP-5) (see figure 4.42), MET degradation increases up to 20% and H_2O_2 consumption was 52%, this can be explained for a higher HCO_4^- ions production by eq.1.34.

Furthermore, increasing HCO_3^- concentration (Exp. BAP-6) from 600 mg/L to 1200 mg/L, MET degradation was 16%. It seems that, at higher HCO_3^- concentration, saturation kinetics was observed.
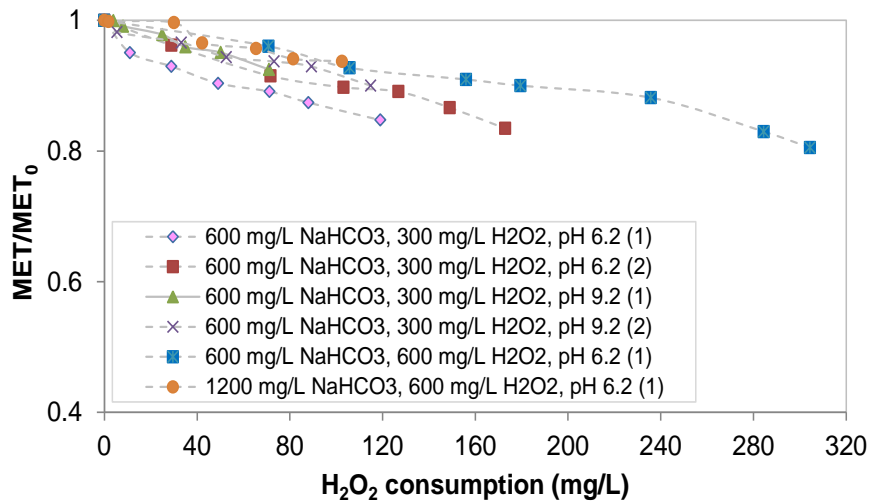
Figure 4.42- MET degradation by Bicarbonate/hydrogen peroxide process

Summarizing, this process does not show to be a good alternative for MET degradation.

Table 4.18- General table Catalyst/bicarbonate/hydrogen peroxide process

Catalyst/Bicarbonate/Hydrogen peroxide									
Exp Nº	Catalyst	$[MET]_0$ (mg/L)	$NaHCO_3$ (mg/L)	$[H_2O_2]$ (mg/L)	[Catalyst] (mg/L)	pH	MET conversion (%)	Time (min)	Other
BAP-Co-1	Cobalt (II)	5	600	200	1	6.2	16.0	120	-
BAP-Co-2	Cobalt (II)	5	600	600	1	6.2	32.0	120	-
BAP-Co-3	Cobalt (II)	5	600	600	5	6.2	26.0	120	-
BAP-Co-4	Cobalt (II)	5	600	600	10	6.2	22.5	120	-
BAP-Co-5	Cobalt (II)	5	600	1200	1	6.2	42.7	120	-
BAP-Co-6	Cobalt (II)	5	600	1200	10	6.2	27.1	120	-
BAP-Co-7	Cobalt (II)	5	600	2400	1	6.2	47.2	120	-
BAP-Co-8	Cobalt (II)	5	600	2400	10	6.2	37.0	120	-
BAP-Co-9	Cobalt (II)	5	1200	600	1	6.2	36.1	120	-
BAP-Co-10	Cobalt (II)	5	1200	600	5	6.2	32.2	120	-
BAP-Fe-11	Iron (II)	25	-	25	2.5	2.8	25.5	60	Fe one addition
BAP-Fe-12	Iron (II)	25	100	25	2.5	2.8	32.4	60	Fe one addition
BAP-Fe-13	Iron (II)	25	100	25	5	2.8	39.0	60	Fe one addition
BAP-Fe-14	Iron (II)	25	100	25	10	2.8	61.0	60	Fe one addition
BAP-Fe-15	Iron (II)	25	100	25	10	2.8	17.3	60	Fe one add/500 mg TBA/L
BAP-Fe-16	Iron (II)	25	100	25	2.5	2.8	53.5	60	iron 0.5x5
BAP-Fe-17	Iron (II)	25	100	25	5	2.8	88.0	60	iron 1x5
BAP-Fe-18	Iron (II)	25	100	25	10	2.8	100	40	iron 2x5 times
BAP-Fe-19	Iron (II)	25	100	25	10	2.8	21.0	60	iron 2x5 times/500 mg TBA/L

4.7   Catalyst/bicarbonate/hydrogen peroxide process

Table 4.18 shows the experiments of MET treatment carried out with Cobalt/bicarbonate/hydrogen peroxide in dark and room temperature. In these experiments the initial pH was 6.2 and the reactants addition MTS/ HCO_3^-/ Co (II) + H_2O_2. In all experiments the hydrogen peroxide was consumed. Cobalt oxide was selected as catalyst because it enhances the decomposition of hydrogen peroxide by the generation of hydroxyl radicals.

$$Co^{2+} + H_2O_2 \rightarrow Co^{3+} + HO^- + HO^{\cdot} \tag{4.4}$$

It also shows the results obtained in applying iron/bicarbonate/hydrogen peroxide process to MET treatment in dark and room temperature at pH 3.0.

In a preliminary study the system was proved without HCO_3^- and the results showed no MET degradation by Co (II) ions alone. Co (II) ions alone do not efficiently generate HO· radicals from H_2O_2.

However, the complex between HCO_3^- and Co (II) may form and serve as the catalyst to active H_2O_2 to HO· radicals in the Co (II)/HCO_3^-/system.

From the set of experiments described in figure 4.43, it can be observed that, increasing cobalt (II) concentration MET degradation decreases (Exp. BAP-Co-2 - BAP-Co-10) this behavior is due to the Co (II)/ HCO_3^- complex formed. At highest Co (II) concentrations, a possible complex formed could be [Co $(HCO_3)_2$], in which, the rates of HO· radicals production and MET degradation were expected to decrease, as there are no strongly binding equatorial positions available to bind the H_2O_2.

When hydrogen peroxide concentration increases MET conversion also increases (comparing BAP-Co-1, BAP-Co-5 and BAP-Co-7) because the highest rates of HO· production.
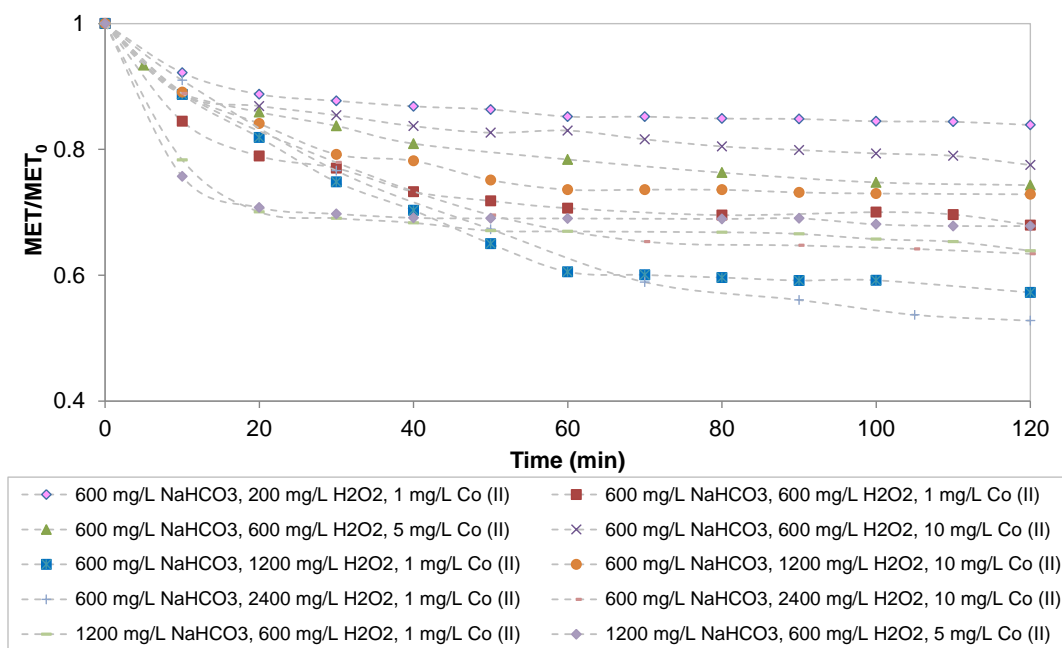
Figure 4.43- MET degradation by Cobalt-Bicarbonate/hydrogen peroxide process.

Comparing the experiments BAP-Co-2 and BAP-Co-9 and BAP-Co-3 - BAP-Co-10 it was observed that, increasing HCO_3^-, MET degradation also does it. This can be explained likely, because the complex formed can be [Co $(HCO_3)]^+$, which is relative more stable and can fast produce the active HO· radicals.

For the following series of experiments, cobalt was changed for iron as catalyst and the initial concentration of MET was 25 mg/L. Three different amounts of Fe (II) were used: 2.5 mg/L, 5.0 mg/L and 10 mg/L, and H_2O_2 concentration was constant (25 mg/L) (Exp. BAP-Fe-11 to BAP-Fe-19).

As it can be seen in figure 4.44, when the process was carried out without (HCO_3^-), lower MET conversion was reached (BAP-Fe-11), suggesting that, the complex between HCO_3^- and Fe (II) may form and serve as the catalyst to active H_2O_2 and produce HO· radicals (Exp. BAP-Fe-12, BAP-Fe-13 and BAP-Fe-14). This figure also shows the positive effect of the iron (II) concentration. However, MET oxidation increases sharply during the initial 1 min of reaction and then it goes slower reaching a plateau. A likely explanation is that higher ferric ions (Fe (III)) as a by-product of the oxidation reaction between Fe (II) and H_2O_2, which would prevail in the aqueous medium, reducing the effectiveness of the process.
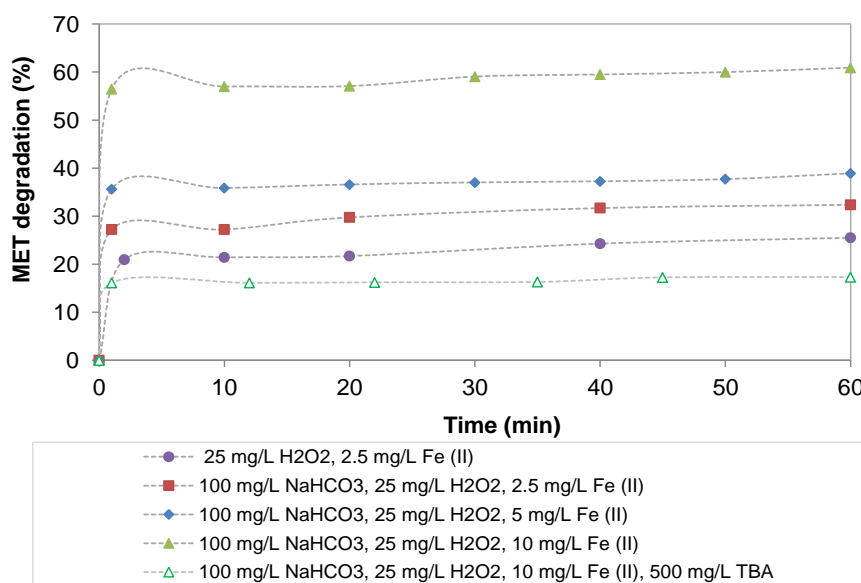
Figure 4.44 - Removal of 25 mg/L of MET solution, adding the total Fe (II) at the beginning of the experiment.

Furthermore, Experiment BAP-F-15 was carried out adding 500 mg/L of tert-butyl alcohol (TBA) in the beginning of the experiment, because, TBA reacts efficiently with hydroxyl radicals acting as an effective scavenger. The maximum MET conversion reached when TBA was used was 17.3%, indicating that this degradation is due to oxidizing species different to HO· radicals.

In the next experiments, the total Iron (II) concentration was divided in equal parts (5) and added at constant periods of time (12 minutes) during 1 hour (by steps). Figure 4.45

shows an enhancement of the process. MET removal reached was 53.5%, 88.0% and 100 % for experiments BAP-Fe-16, BAP-Fe-17 and BAP-Fe-18 respectively.
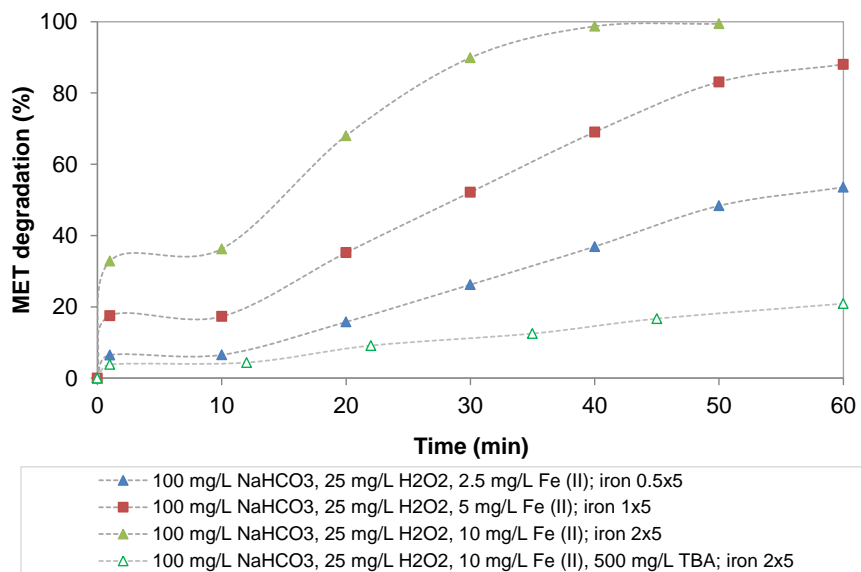
Figure 4.45- Removal of 25 mg/L of MET solution, adding the total Fe (II) by steps.

As commented before, 21.0% of MET conversion reached when TBA was added in the system (Exp. BAP-Fe-19) could be due to oxidizing species different to HO· radicals.

Chapter V

Set-up and processes comparison

5   SET-UP AND PROCESSES COMPARISON

This section has been focused on the comparison when different set-ups and processes are tested. The first comparison is about three different processes carried out in two different devices. The second comparison is for photocatalysis process but using two different devices. The third comparison is for photo-Fenton process using four different devices with different irradiation sources. The fourth comparison is about the different techniques used and their MET and TOC degradations under the best experimental conditions tested. Finally intermediates and degradation pathways for the different processes are compared.

5.1   UVC/H_2O_2, photo-Fenton and photocatalysis/TiO_2 processes

UVC/H_2O_2 (UVC reactor), photo-Fenton (SB) and photocatalysis/TiO_2 (SB) were compared evaluating the accumulated energy per MET removed.

The conditions selected were: in UVC/H_2O_2 (25 mg/L of H_2O_2), in photo-Fenton (2.5 mg/L of iron (II), 25 mg/L H_2O_2 and 25 ℃), in photocatalysis (0.4 g/L of TiO_2). In all cases the initial MET concentration was 50 mg/L. These conditions were selected basically because 25 mg/L was the common concentration of H_2O_2 in UVC and PF experiments and regarding to HP process catalyst concentration of 0.4 g/L was the used in all this study.

For comparison, the radiation entering the different reactors was measured by actinometric methods, taking into account the useful wavelengths involved in each photo-oxidation process and the emission spectrum of the radiation source. The radiation was 0.88 J/s (between 300 and 400 nm) in the case of photocatalysis with TiO_2, 3.59 J/s (between 300 and 500 nm) for the photo-Fenton experiments, and 8.01 J/s for the UVC lamp (254 nm).

The performance of the three set-ups in MET elimination is compared on basis of the ratio accumulated energy/ MET removed (table 5.1). 90% of MET removal was chosen as basis for calculations since MET removal rates became too slow near the total elimination.

153

Table 5.1- Energy that enters in each set-up used per removals of MET.

Chapter	Exp.	Process	Device	90% of MET removal (min)	Q (kJ/L) (300-500 nm) at 90% of MET removal	Energy/MET removed (kJ/mg)	Energy supplied to the lamp/MET removed (kJ/mg)
4.2	UVC-6	UVC/H_2O_2	UVC	13	3	0.07	0.2
4.3	HP-SB-3	Photocatalysis	SB	220	11.5	0.25	293.3
4.5	PF-SB-13	Photo-Fenton	SB	62	13.4	0.30	82.7

The ratio energy supplied to the lamp/MET removed was evaluated from equation 5.1.

$$\frac{P*t}{(C_0-C_f)*V_T}$$

5.1

Where, P is the power rating of the lamp, t is the time (s), C_0 is the initial MET concentration (mg/L), C_f is the final MET concentration (mg/L) and V_T is the total volume of the solution.

In order to reach the 90% of MET degradation it was observed that UVC process was the faster process and photocatalysis the slowest.

Concerning the ratio energy/MET removed, UV/H_2O_2 shows efficiency higher than the other two technologies. The high MET absorbance centered on 221 and 273 nm seems to be responsible for the good performance of UV/H_2O_2 process in MET elimination.

If we compare the energy supplied to the lamp, the consumption of energy in the SB is too high in comparison with the lamps used in UVC system. This behavior can be easily explained by considering that SB uses a lamp of 1000 W with a wide spectrum that means a great part of the energy supplied to the lamp is not used for photocatalysis. However, UVC lamps consume only 24 W and a great part of this energy is used in the process. In addition, in the photocatalysis process, the ratio is 3.5 times higher than photo-Fenton process due to the time that requires the process.

Figure 5.1 shows the MET and TOC elimination profiles in terms of time. The UVC/H_2O_2 system seems to be more optimized than photo-Fenton and photocatalysis in terms of time. This difference can be attributed to the high MET absorbance centered on 221 and 273 nm. However, it is important to remark that only 11% of TOC removal was

achieved by the UVC/H_2O_2 process while 28% was eliminated by the photo-Fenton system when the same amount of H_2O_2 has been consumed (90%).
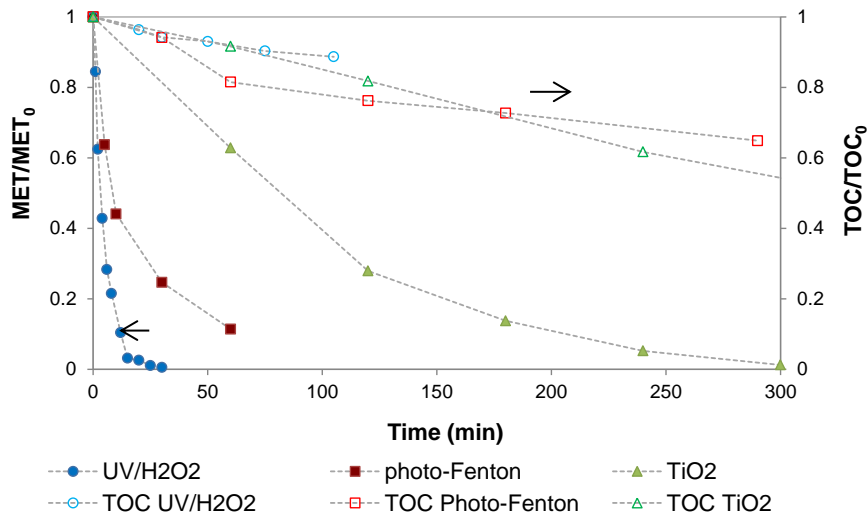
Figure 5.1- MET and TOC removal profiles for the different processes tested.

To complement the information the toxicity assessment was also carried out for all systems. The initial Equitox/m^3 value of the untreated solution was 6.2 and, after treatment, the Equitox/m^3 values were 0.72 (300 min), 0.56 (105 min) and 0.51(290 min) for photocatalysis, UV/H_2O_2 and photo-Fenton respectively.

5.2   Photocatalysis in a solarbox and CPC reactor

The results of MET removal at 240 minutes were compared for both devices and they are summarized in table 5.2. It could be appreciated that in both cases (laboratory and pilot plant) MET removal increases when TiO_2 concentration does it.

TOC was not completely removed even after several hours of irradiation in both devices. TOC conversion obtained at 240 min of experimental time, using 0.05, 0.1 and 0.4 g TiO_2/L for solarbox (12.6 kJ/L), was 16.4, 30.8, and 38.3 %, and in CPC it was 18.1 % (Q=5.85 kJ/L), 19.8 % (Q=3.77 kJ/L) and 28.1% (Q=2.64 kJ/L). Maximum TOC conversion reached for CPC was 29.2% (Q=2.64 kJ/L) after 270 minutes of irradiation, and 53.0% (Q=1.9 kJ/L) for solarbox system, after 360 minutes, using 0.4 g/L of catalyst.

Table 5.2 – Energetic efficiency as function of MET elimination and TiO_2 loaded, with 50 mg MET /L of initial concentration at 240 minutes.

Chapter	Exp.	Device	TiO_2 load (g/L)	MET (%) at 240 min	Q (kJ/L) (290-400 nm) at 240 min	Energy used for mg of MET removed (kJ/mg MET) at 240 min	Energy used by TiO_2 to remove 1 mg of MET (g TiO_2 kJ /mg MET) at 240 min	g TiO_2/mg MET
	HP-SB-1		0.05	71.7	12.6	0.358	0.018	0.001
4.3	HP-SB-2	SB	0.1	85.4	12.6	0.307	0.030	0.002
	HP-SB-3		0.4	94.8	12.6	0.275	0.110	0.009
	HP-CPC-14		0.05	60.8	5.9	0.205	0.010	0.002
4.3	HP-CPC-15	CPC	0.1	68.8	3.8	0.109	0.011	0.003
	HP-CPC-16		0.4	80.4	2.6	0.065	0.026	0.010

MET and TOC removals in terms of time seem to be more optimized in SB than in CPC. However, when the energy used is considered, CPCs seem to be more effective than SB. It could be possible that, in the solarbox, a part of radiation escapes from the reactor being not absorbed, while, CPCs concentrate on the receiver, practically, all the radiation arriving at the collectors.

In addition, the energy used for MET removed decreases as TiO_2 concentration increases in both devices. Other parameter which can be interesting is the amount of catalyst jointly the amount of energy needed to eliminate 1 mg of MET. This parameter increases when the catalyst concentration does it and is higher in SB.

5.3 Photo-Fenton process: in SB, BLB, CPC and UVC reactor

MET removal by photo-Fenton is compared in four different installations (CPC, SB, BLB and UVC).

Different experimental series were done, always working with the same initial amount of Fe (II) (2.5 mg/L), H_2O_2 (25 mg/L), MET (50 mg/L) and temperature (25 ºC) in all reactors. MET, TOC, and H_2O_2 were monitored along all the experiments.

Apart from the installation, the differences between the experiments were the type and amount of light irradiating the system and the reactor´s geometry. To allow a more accurate comparison, the ratio accumulated energy/MET removed and the ratio (calculated according equation 5.1) between energy (considering nominal power) supplied to irradiation sources and MET degradation are presented in table 5.3. Only radiation below 500 nm is taken into account. It refers to the part of the spectrum potentially useful for photo-Fenton.

Table 5.3- Energy in each set-up per removals of MET.

Chapter	Exp.	Process	Device	90% of MET removal (min)	Q (kJ/L) (300-500 nm) at 90% of MET removal	Energy/MET removed (kJ/mg)	Energy supplied to the lamps/MET removed (kJ/mg)
4.5	PF-BLB-1	Photo-Fenton	BLB	34	1.85	0.04	0.5
4.5	PF-UVC-22	Photo-Fenton	UVC	9	2.20	0.05	0.1
4.5	PF-SB-13	Photo-Fenton	SB	62	13.5	0.30	82.0
4.5	PF-CPC-18	Photo-Fenton	CPC	50	9.7	0.26	-

It could be appreciated how UVC and BLB reactor exhibit a much better performance than SB reactor and CPC reactor. In photo-Fenton process when UVC radiation was used, the complex $Fe\ (HO)^{2+}$, predominant in acid conditions, is formed and this complex absorbs in the range 180-410 nm, acting as supplementary source of OH· (Herney-Ramirez, Vicente, & Maderira, 2010; Pignatello, Liu, & Huston, 1999).

$$Fe^{2+} + H_2O_2 \Rightarrow Fe\ (HO)^{2+} + HO^{\cdot} \tag{5.2}$$

$$Fe\ (OH)^{2+} + hv \Rightarrow Fe^{2+} + HO^{\cdot} \tag{5.3}$$

Furthermore, in UVC system the influence of the photolysis should be considered. Concerning to H_2O_2 consumption it was observed that it was almost the same for BLB and UVC reactors.

On the other hand, the spectrum of the irradiation sources in SB and CPC reactor correspond to the solar one, rich in longer wavelengths and poor in UV. Actually, in the considered range (300-500 nm) only around 20% of emitted photons are in the 300-400 nm stretch. The rest of photons ($\approx$ 80%) are in the 400-500 nm part. Although light over 400 nm may be useful for photo-Fenton process, it is much less efficient and probably could be possible that not all the light in this range is absorbed by the system. It means that a part of the considered radiation is not being used, decreasing the overall yield of the process.

On the other hand, if only BLB and UVC are compared 18% of difference between them was observed. This can be attributed to the fact that, using the same volume and design of the reactor, the photo-Fenton process seems to work better with the wavelength of the BLB reactor (365 nm) than the UVC reactor (254 nm).

When the consumption of energy (energy supplied to the lamps) is compared, in the SB is too high in comparison with the lamps used in UVC and BLB systems. The irradiation source that performs the highest efficiency is the UVC reactor. The lowest efficiency was obtained by SB maybe due to the fact that the lamp needs a great power but it is not well used for the system, as commented in section 5.1.

The operational cost of the treatment of 50 mg/L of MET in each device by photo-Fenton process using 2.5 mg Fe (II)/L and 25 mg H_2O_2/L, has been evaluated (see table 5.4). For this simple economical study just variable costs have been considered, which are presented in Euro (€) per litre of treated water. The variable costs included: reactives consumption and electricity per operation. The costs per operation carried out in each device have been calculated considering 90% of MET removal. The electricity cost was considered as 0.13 €/kW-h, hydrogen peroxide (30%) price was 31 €/L, iron (II) sulfate heptahydrate price was 132.10 €/Kg. An increasing of 10% to the total power of the lamps was added to cover peripheral electrical equipment.

Table 5.4- Cost of treated water for photo-Fenton process using SB, BLB, UVC and CPC reactors.

Device	Total volume treated (L)	H_2O_2 (€/L)	Fe (II) (€/L)	Electricity of lamps (€/L)	Electricity of pumps (€/L)	Operational cost (€/L)
SB	1	0.01 (0.0026)	0.01 (0.0016)	0.15	0.01 (0.0003)	0.16
BLB	2	0.01 (0.0026)	0.01 (0.0016)	0.01 (0.0020)	-	0.01
UVC	2	0.01 (0.0026)	0.01 (0.0016)	0.01 (0.0005)	-	0.01
CPC	10	0.01 (0.0026)	0.01 (0.0016)	-	0.01 (0.0001)	0.01

The water treated in SB reactor seems to be more expensive than the other technologies and CPC seems to be the cheapest one, due there is not electrical cost by lamps. AOPs based on artificial light may be associated with increased operating cost related to energy consumption.

5.4   Comparison of different techniques used

In table 5.5 are showed the different process carried out under the best conditions tested.

Table 5.5- Summary of MET and TOC degradations and the operational conditions for the best conditions carried out in the different processes.

Chapter	Exp.	Process	Initial MET (mg/L)	Operational conditions	Time (min)	Radiation (kJ/L)	MET Conv. (%)	TOC Conv. (%)	kJ/mg MET
4.2	UVC-10	UVC	50	125 mg/L H_2O_2	7.5	1.8	97.8	4.5	0.038
4.3	HP-SB-3	HP SB	50	0.4 g/L TiO_2	300	15.8	100	45.2	0.330
4.3	HP-CPC-16	HP CPC	50	0.4 g/L TiO_2	270	2.6	81.5	29.2	0.065
4.4	F-2	Fenton	50	10 mg/L Fe, 150 mg/L H_2O_2, 1 add	60	-	67.0	8.0	-
4.4	F-6	Fenton	50	10 mg/L Fe, 150 mg/L H_2O_2, by steps	60	-	87.0	15.6	-
4.5	PF-BLB-4	PF BLB	50	10 mg/L Fe, 150 mg/L H_2O_2, 1 add, 25 ºC	7	0.4	100	22.3	0.008
4.5	PF-SB-16	PF SB	50	10 mg/L Fe, 150 mg/L H_2O_2	7	1.5	97.3	14.3	0.030
4.5	PF-CPC-21	PF CPC	50	10 mg/L Fe, 150 mg/L H_2O_2	3	0.7	98.3	15.3	0.014
4.5	PF-UVC-22	PF UVC	50	2.5 mg/L Fe, 25 mg/L H_2O_2	20	4.8	97.0	10.7	0.097
4.6	BAP-5	BAP	5	600 mg/L $NaHCO_3$, 600 mg/L H_2O_2, pH 6.2	120	-	19.5	-	-
4.7	BAP-Co-7	Co/HCO_3^-/H_2O_2	5	600 mg/L $NaHCO_3$, 2400 mg/L H_2O_2, 1 mg/L Co, pH 6.2	120	-	47.2	-	-
4.7	BAP-Fe-18	Fe/HCO_3^-/H_2O_2	25	100 mg/L $NaHCO_3$, 25 mg/L H_2O_2, 10 mg/L Fe, pH 2.8, by steps	40	-	100	-	-

This table shows the maximum MET conversion for the several processes tested and the TOC and time corresponding to this MET conversion.

Depending on the conditions of each process, the ratio accumulated energy/MET removed was calculated. Concerning to photocatalysis, it could be appreciated that using (0.4 g/L TiO_2), CPC shows a better energetic efficiency than SB. Regarding to photo-Fenton process, it was observed that using the highest catalyst and promoter concentrations (10 mg Fe (II)/L y 150 mg H_2O_2/L), BLB shows the highest energetic efficiency.

On the other hand, it can be seen that, when all MET degradation is reached, the highest mineralization is obtained by photocatalysis process, however more time is needed. Concerning to dark Fenton it can be esteemed that adding the iron by steps enhances the process.

5.5 Intermediates and degradation pathways for the different processes

In this part, MET and its main by-products detected (table 5.6) and a general MET degradation pathways in the different processes carried out have been proposed (figure 5.2).

Table 5.6- MET and its main intermediates detected by LC/MS analysis in UVC, HP, Fenton and PF processes.
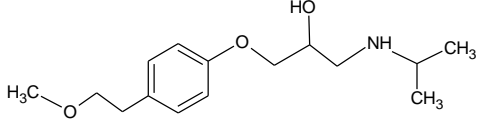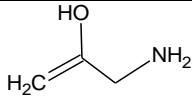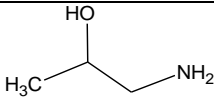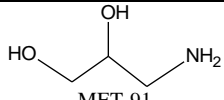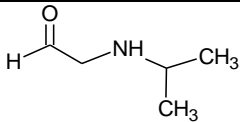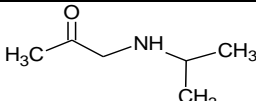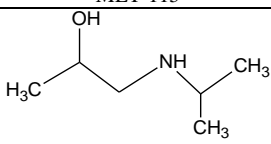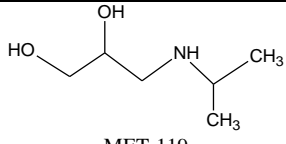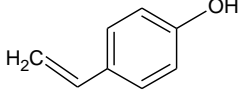
m/z (Da)	Elemental composition	Proposed structure (Label)	UVC	HP	Fenton	PF
267	$C_{15}H_{25}NO_3$	MET-267	X	X	X	X
73	$C_4H_{11}N$	MET-73	-	X	-	X
75	C_3H_9NO	MET-75	-	X	-	-
91	$C_3H_9NO_2$	MET-91	X	X	-	-
101	$C_5H_{11}NO$	MET-101	-	X	-	-
115	$C_6H_{13}NO$	MET-115	X	X	X	X
117	$C_6H_{15}NO$	MET-117	-	X	-	X
119	$C_5H_{13}NO_2$	MET-119	-	X	-	-
120	C_8H_8O	MET-120	-	-	X	X
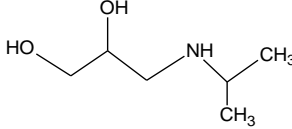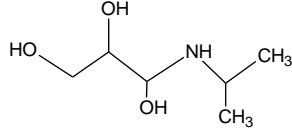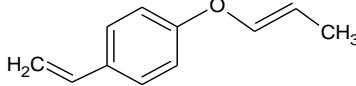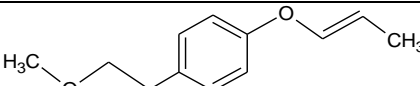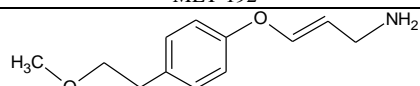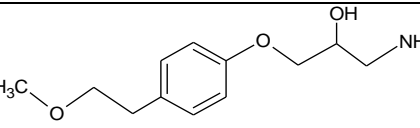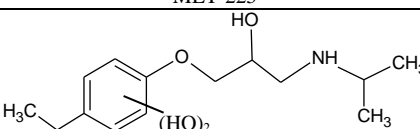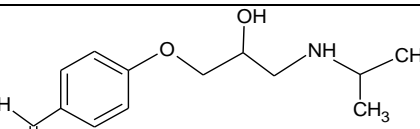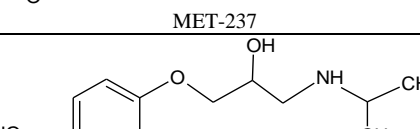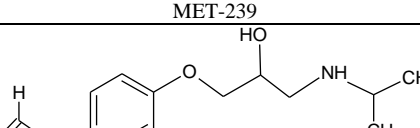
Table 5.6 (continued)						
133	$C_6H_{15}NO_2$	MET-133	X	X	X	X
49	$C_6H_{15}NO_3$	MET-149	X	-	-	X
160	$C_{11}H_{12}O$	MET-160	-	X	-	-
192	$C_{12}H_{16}O_2$	MET-192	-	X	-	-
207	$C_{12}H_{17}NO_2$	MET-207	-	X	X	X
225	$C_{12}H_{19}NO_3$	MET-225	-	X	-	X
231	$C_{10}H_{17}NO_5$	MET-231	-	-	-	X
237	$C_{13}H_{19}NO_3$	MET-237	-	X	X	X
239	$C_{13}H_{21}NO_3$	MET-239	-	X	X	X
251	$C_{14}H_{21}NO_3$	MET-251	-	-	X	X

161

Table 5.6 (continued)						
253	$C_{13}H_{19}NO_4$	MET-253	X	-	X	X
269	$C_{14}H_{23}NO_4$	MET-269	X	-	X	X
281	$C_{15}H_{23}NO_4$	MET-281	-	-	X	X
283	$C_{15}H_{25}NO_4$	MET-283	X	X	X	X
297	$C_{15}H_{23}NO_5$	MET-297	-	-	X	X
299	$C_{15}H_{25}NO_5$	MET-299	X	X	X	-
315	$C_{15}H_{25}NO_6$	MET-315	X	X	X	-
331	$C_{15}H_{25}NO_7$	MET-331	-	X	-	-

Figure 5.2- Proposed MET degradation pathways for UVC, HP, Fenton and PF processes.

Chapter VI
Study of irradiation for photocatalytic reactors

Table 6.1 General table of actinometry experiments.

Exp Nº	Reactor	$[o\text{-}NB]_0$ (M)	$[TiO_2]$ (g/L)	pH_0	T (ºC)	Other	Photonic flux (μEinstein/s)
						Actinometry (AC)	
AC-SB-1	Duran	0.1	-	12.8	25	0.0048 M NaOH	2.81
AC-SB-2	Duran	0.0025	0.4	7.3	25	-	2.68
AC-SB-3	Duran	0.0025	0.4	6.2	25	-	1.68
AC-SB-4	Duran	0.0025	0.4	5.1	25	60 mL/L TBA	1.90
AC-SB-5	Duran	0.0025	0.4	6.2	25	150 mL/L TBA	1.62
AC-SB-6	Duran	0.0025	0.4	3.5	25	1g/L formic acid	1.75
AC-SB-7	Duran	0.0025	0.4	2.9	25	2 g/L formic acid	1.67
AC-SB-8	Duran	0.0025	0.4	3.4	25	150 mL/L TBA+1 g/L formic acid	1.96
AC-SB-9	Duran	0.0025	0.4	6.0	25	0.027 g/L BQ	2.66
AC-SB-10	Duran	0.0025	0.4	6.2	25	Air	2.66

6   STUDY OF IRRADIATION FOR PHOTOCATALYTIC REACTORS

Table 6.1 shows the experiments carried out for the study of irradiation in photocatalytic reactors.

6.1   1 Introduction

Many actinometries have been developed (Kuhn et al., 2004) to measure photons absorption over different and specified wavelength ranges. In this study, o-nitrobenzaldehyde (o-NB) actinometry has been selected, primarily because of its accordance to the TiO_2 absorption wavelength range, giving photon absorption data in the range from 290 to 400 nm. It also entails a safe experimental procedure and easy to perform. Another advantage is that the o-NB actinometry may be used with common UV lamps and also in solar photoreactors. This is an actinometry which has been not deep studied yet.

The o-nitrobenzaldehyde (o-NB) actinometry is used to measure the photon flow entering the photocatalytic reactor in the solarbox. Two different proposed methods in bibliography are adapted and compared: by following pH or o-NB concentration. In addition, it was studied the influence of suspended TiO_2 particles, inside the photoreactor, on the o-NB actinometry. Particularly, the appearance of photocatalytic products was followed during actinometries with suspended TiO_2.

6.2   o-NB actinometry

The photo-degradation of o-NB has been reported by different authors (Bonetti, Vecli, & Viappiani, 1997; Choi & Terazima, 2003; George & Scaiano, 1980) and it is generally accepted that the photo-transformation of o-NB leads to o-nitrosobenzoic acid (o-HNB). The 2-NB photoreaction (figure 6.1) proceeds via an intramolecular rearrangement involving transfer of an $-NO_2$ oxygen atom to the aldehyde functionality yielding the nitrosobenzoic acid product.
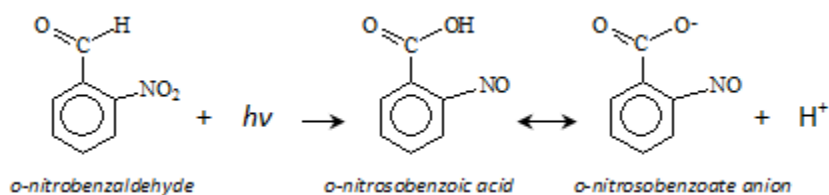
Fig. 6.1- Photochemical rearrangement of 2-NB to 2-nitrosobenzoic acid and dissociation of the product yielding H^+.

o-NB actinometry based on pH

o-NB actinometry was carried out by adapting the method described by (Allen, Allen, & Baertschi, 2000). The procedure used in this work involved the preparation of 1 L of a 0.1 M o-NB solution in NaOH 0.0048 M water/ethanol solution 50:50. This solution was irradiated and continuously recirculated in the tubular reactor described in SB. During the actinometric runs, the pH of the actinometric solution was monitored every minute or less at the reservoir tank and plotted as a function of illumination time. Time zero was established when turning the lamp on. When enough acid was formed, the added NaOH was neutralized and the pH dropped very fast (figure 6.2). Thus, the end point of the reaction was determined from the first derivative plot of the data (dpH/dt). At this point, the end time was established resulting to be 57 min.
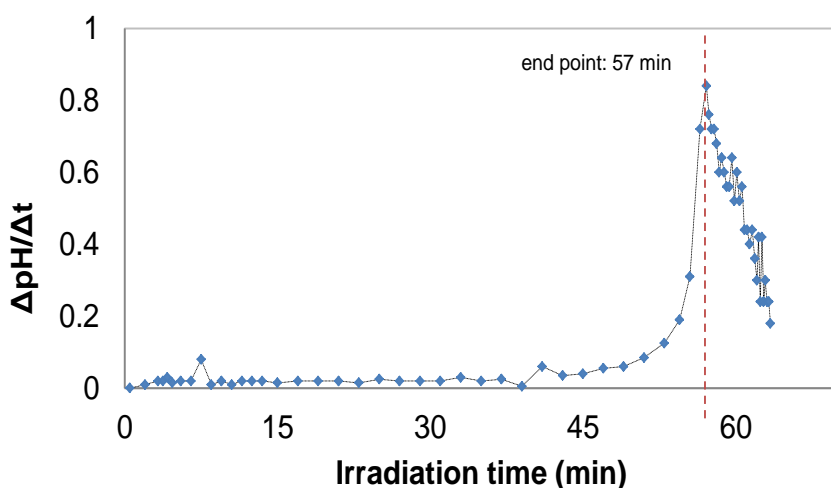
Figure 6.2- o-NB actinometry based on pH in SB.

At this time, the number of moles of $[H^+]$ formed was equivalent to the number of moles of o-HNB formed and to the number of moles of o-NB consumed. The o-NB actinometer has a quantum yield (Φ) of 0.5 in the 290–400 nm range. Thus, the photon

flow (I_0) was calculated by Eq. (6.1) (Willett & Hites, 2000), obtaining 2.81×10^{-6} Einstein/s.

$$I_0 = \frac{moles\ of\ o-NB\ consumed\ (mol\ L^{-1}s^{-1})}{\Phi(mol\ Einstein^{-1})} \tag{6.1}$$

Afterwards, the photon flow in Einstein/s was converted to W/m^2, for this conversion was obtained the wavelength average of the Xe lamp used and as result the value obtained was 369 nm (Eq. 6.2).

$$\frac{\sum_{290nm}^{400nm}(\lambda_{nm})(Irradiance_{Wm^{-2}})}{\sum_{290nm}^{400nm}Irradiance_{Wm^{-2}}} \tag{6.2}$$

The energy computed of a 369 nm photon was calculated by Planck's equation, giving 5.37×10^{-19} J/photon (3.24×10^5 J/Einstein). With the irradiated reactor's surface (151 cm^2), the incident light flux was calculated, giving 60.2 W/m^2 (Eq. 6.3),

$$E = h\nu = \frac{hc}{\lambda} = \frac{6.63 \cdot 10^{-34} J\ s^{-1} * 2.99 \cdot 10^8 m\ s^{-1}}{3.6887 \cdot 10^{-7} m} = 5.37 \cdot 10^{-19} \text{ J foton}^{-1} \tag{6.3}$$

Knowing the reactor´s surface irradiated (151 cm^2), the incident flux was calculated by eq. 6.4 obtaining a value of 60.2 W/m^2.

$$\frac{2.81 \cdot 10^{-6}\left(\text{Einstein s}^{-1}\right) \cdot 3.24 \cdot 10^5 (\text{J Einstein}^{-1})}{0.0151\ \text{m}^2} = 60.2 \text{ W m}^{-2} \tag{6.4}$$

Actinometry based on o-NB concentration

o-NB actinometry was also carried out adapting the method proposed by Willet and Hites (Willett & Hites, 2000). Thus, 1 L solution of o- NB 2.5×10^{-3}M was prepared using water/ethanol (50:50) as solvent. Solvent was changed from the originally proposed in order to exactly repeat the experimental conditions in previous section. That was possible since, in this type of actinometry, the quantum yield is independent of the organic solvent used (Galbavy, Ram, & Anastasio, 2010). In this set of experiments, samples were collected from the reservoir tank every 5 min after the lamp was turned

on. Samples were analyzed by HPLC to follow the o-NB concentration during the procedure. Then, o-NB concentration was plotted as a function of irradiation time. The curve was fitted to zero-order kinetics in the first 10 min (∼25% o-NB degradation). The incident photon flow was calculated through Eq. (6.5).

$$I_o = \frac{d\,[o-NB]}{dt}\left(\frac{1}{\Phi}\right)\left(\frac{1}{1-10^{-\varepsilon b[o-NB]_o}}\right) \qquad (6.5)$$

d[o-NB]/dt was approximated to the average zero-order kinetics constant (6.358×10^{-5} mol/Ls), Φ is the quantum yield (0.5 mol/Einstein (290–400 nm)), ε the molar absorptivity (128.6 L/mol.cm) and b the path length of the light (2.11 cm). ε was evaluated for the average wavelength of the lamp (369 nm). Thus, the incident photon flow obtained was 2.68×10^{-6} Einstein/s. The incident light flux in W/m^2 was also calculated, following the steps stated when pH was followed, resulting 57.7 W/m^2. It was observed a slight variation (5%) on the two actinometric methods.

6.3 Effect of TiO$_2$ on o-NB actinometry

Experiments were carried out in order to identify the influence of TiO$_2$ on the o-NB actinometry. Two purposes were chased during this type of actinometric experiment: (i) assessing the effect of TiO$_2$ particles on absorption and scattering phenomena, (ii) testing possible photocatalytic transformations of the o-NB. Therefore, the possibility of using this actinometric system with TiO$_2$ for modeling purposes could be established (Bayarri, Giménez, Curcó, & Esplugas, 2012). Due to the possibility that o-NB and its photoproducts can suffer photocatalysis when TiO$_2$ is present, the actinometries were always based on the o-NB concentration, and not on the pH.

To carry out the runs, 0.4 g/L of TiO$_2$ were added to the actinometric solution. Then, it was irradiated for 45 min and samples were collected periodically to follow the o-NB concentration and observe the chromatographic peaks formed during reactions. Representing o-NB concentration versus irradiation time (figure 6.3), the function was fitted to zero-order kinetics in the first 15 min (∼25% o-NB degradation). Following steps stated previously, the apparent photon flow obtained was 1.68×10^{-6} Einstein/s (36.1 W/m^2). Figure 6.3 shows that the o-NB reacts slower when TiO$_2$ is present in the media. It could be assumed that titania absorbs part of the incident light and besides scattering losses are taking place. The same could be proposed from the photon flows

data, this value went down from 2.68×10^{-6} to 1.68×10^{-6} Einstein/s when TiO$_2$ was added. The presence of the suspended catalyst seemed to produce a decrease of 38% in the apparent radiation absorbed by the o-NB. Next work presented was developed in order to assure that the observed difference on the photon flows was due to only TiO$_2$ absorption and lost scattering phenomena. Thus, possible parallel o-NB photocatalytic reactions were evaluated.
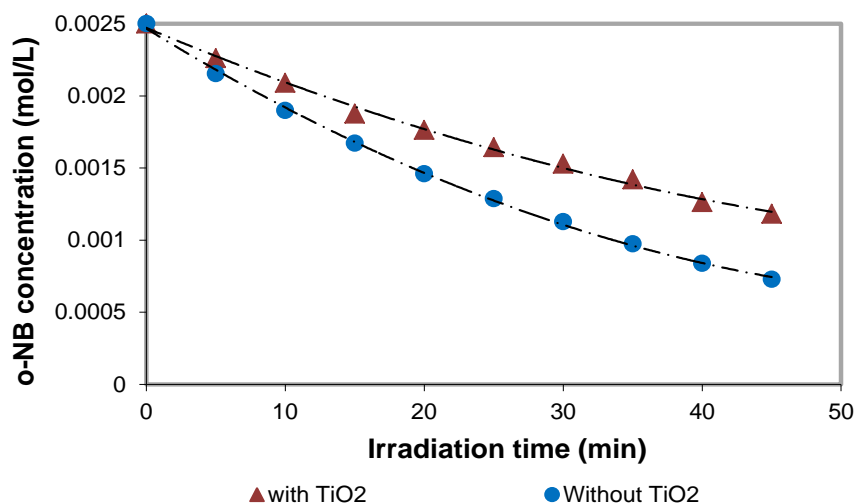
Figure 6.3- Variation of o-NB concentration during time.

Evaluation of possible o-NB photocatalytic reactions

To evaluate if o-NB was undergoing photocatalysis, HPLC chromatograms along the o-NB actinometry were studied, with and without TiO$_2$. Evaluating the HPLC chromatograms from the actinometry without TiO$_2$, it could be observed that o-NB (absorption bands centered ariund 220 and 260 nm) decreased when irradiation time increased (figure 6.4). To date, it has been generally accepted that the photo-transformation of o-NB gives o-HNB (Bonetti et al., 1997; Choi & Terazima, 2003; George & Scaiano, 1980; Heinz, Schmierer, Laimgruber, & Gilch, 2008).
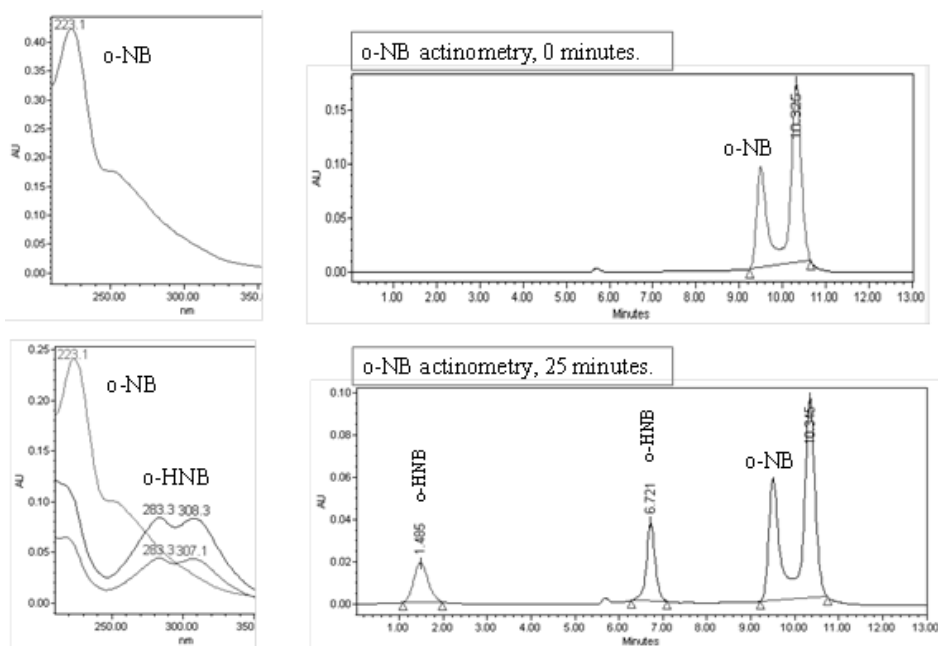
Figure 6.4- o-NB actinometry without TiO$_2$. Chromatograms at times 0 and 25 minutes. Peaks corresponding o-NB and o-HNB

Thus, as o-NB concentration decreased, new peaks appeared with absorption bands centered around 280 and 310 nm, which correspond to formation of the o-HNB photoproduct (Chen, Song, Yang, Yin, & Han, 2010). In addition, these peaks increased with time, confirming the formation of o-HNB due to o-NB photo-reaction. Observing the chromatograms of the actinometry employing 0.4 g/L of TiO$_2$ (figure 6.5), while o-NB was decreasing during irradiation, peaks corresponding to o-HNB became stronger with time; nevertheless this increase was much less noticeable than before. In this case, two new peaks came into view related to photocatalytic processes, with equal absorption bands centered around 217 and 326 nm, and became higher during irradiation competing with the formation of o-HNB peaks. It could be assumed that photocatalytic reactions were taking place. Next step in the research was to evaluate if this unknown photocatalytic product was related to the photocatalytic transformation of the actinometer.
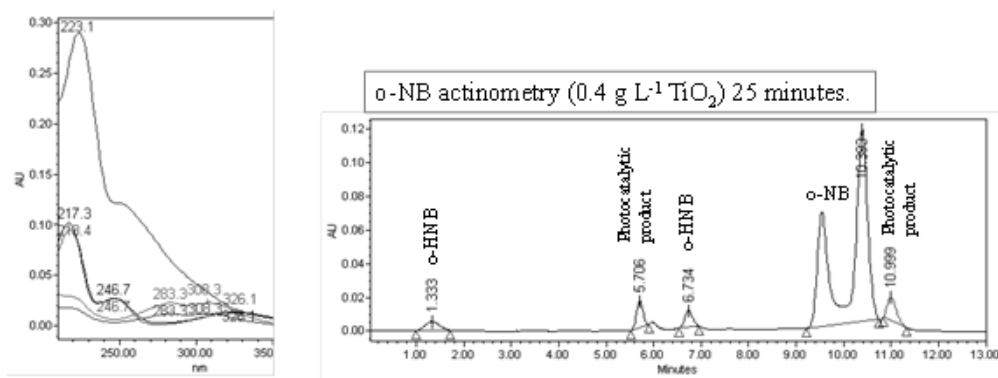
Figure 6.5- o-NB actinometry with 0.4 g L^{-1} of TiO$_2$. Chromatogram at 25 minutes.

Peaks of o-NB, o-HNB and a photocatalytic product

Evaluation of possible o-NB photocatalytic reactions – scavengers

To evaluate if o-NB was suffering photocatalysis when there was TiO$_2$ in the actinometric media, experiments employing different photocatalytic scavengers were carried out. The aim was to block likely pathways of the o-NB reacting with TiO$_2$ and consequently discern which reactions could be implicated. All the experiments were performed monitoring the o-NB concentration.

To recognize possible roles of the different reactive species involved in the o-NB reaction with TiO$_2$, diverse scavengers were employed. Experiments were carried out adding 0.4 g/L of TiO$_2$, to the 0.0025 M o-NB solution and a suitable scavenger dose. The studied scavengers and its corresponding doses were: oxygen (saturation with air), p-benzoquinone (BQ) (0.027 g/L corresponding to a molar relation of 1:10 for BQ/o-NB), tert-butyl alcohol (TBA) (60 and 150 mL/L) and formic acid (1 and 2 g/L, and 1 g/L combined with 150 mL/L of TBA). Oxygen is an electron scavenger used to inhibit recombination of the e$^-$/h$^+$ pair, promoting oxidative processes such as the formation of hydroxyl radicals (Ryu & Choi, 2004). To determine the O$_2$$^{\cdot-}$ participation in a photocatalytic reaction, benzoquinone (BQ) was used as a scavenger. TBA was used as HO· scavenger, and Formic acid (FA) was used as hole (h$^+$) scavenger during TiO$_2$ photocatalysis (Tan, Beydoun, & Amal, 2003; Zheng, Cai, & O´shea, 2010).

Figure 6.6 represents the o-NB degradation with irradiation time during actinometries employing different scavenger doses.
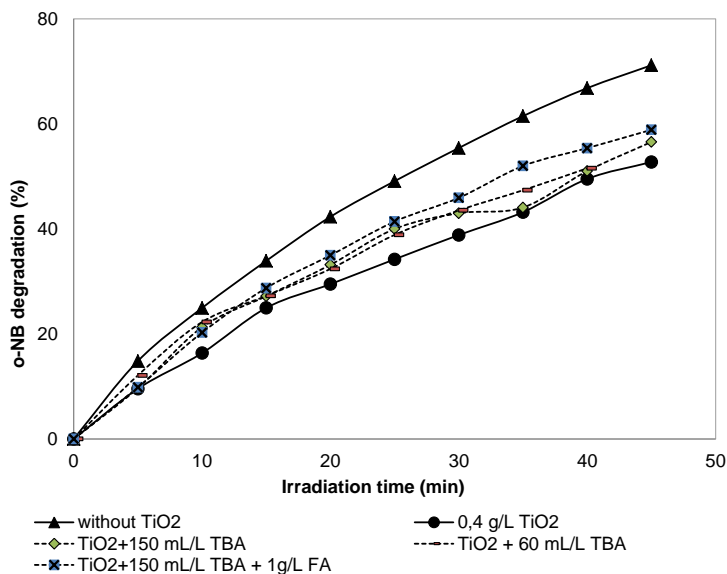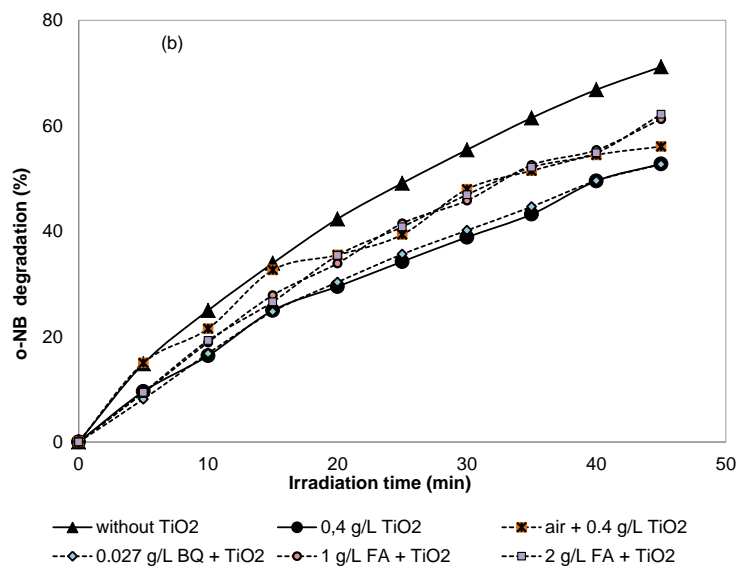
a-

b-

Figure 6.6- (a and b) o-NB actinometries employing different scavengers. Percentage of o-NB degradation versus time

Experiments with scavengers involved showed very similar trends. Slopes resulted to be close to the degradation profile of employing TiO_2 alone and even slightly higher degradation rates were observed. Somehow, scavengers contribute to o-NB consumption. The aim of this set of experiments was to discern if o-NB was undergoing photocatalysis besides photolysis. If o-NB had reacted by photocatalysis, the block of this reaction by any scavenger would have given a lower degradation rate, however this did not occur. Thus, from the results, we can assume that o-NB was not being consumed by photocatalytic reactions. To discern the appearance of unknown photocatalytic

176

products at the o-NB actinometry with suspended TiO_2, further experiments were carried out.

Thus, experiments were carried out to explain the appearance of photocatalytic products (peaks centered in 217 and 326 nm), which turned up only when there was TiO_2 involved. Following this purpose, 1 L of 0.025 M o-NB solution, without catalyst, was irradiated during 3 h to convert all the o-NB into o-HNB. Afterwards, 0.4 g/L of TiO_2 was added to the o-HNB solution and irradiated for one additional hour (figure 6.7).
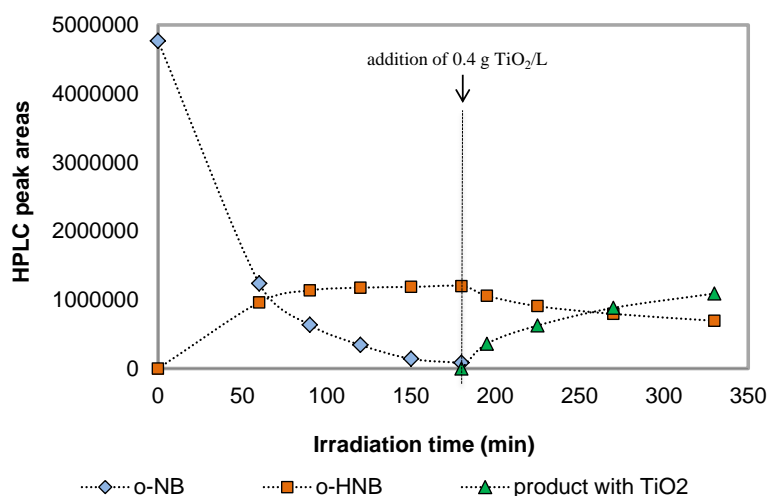
Figure 6.7- Three hours of basic o-NB actinometry, followed of 1 h of photocatalysis of o-HNB with 0.4 g/L of TiO_2. HPLC peak areas versus time.

It can be seen that, in the first 3 h of irradiation, o-NB was converted into o-HNB. At this point, when catalyst was added, the o-HNB concentration decreased with irradiation time. Meanwhile, the peaks related to the photocatalytic product constantly increased. Consequently, it could be assumed that the actinometric photoproduct, o-HNB, is the compound which underwent photocatalytic reactions when TiO_2 was added, and not the o-NB. This means that o-NB can be used as actinometer in the presence of TiO_2, since its decomposition is only due to the radiation absorption and not to photocatalysis.

Chapter VII

Conclusions and

Recommendations

7   CONCLUSIONS AND RECOMMENDATIONS

7.1   Conclusions

a. *General*

All the techniques used (photolysis, UVC/H_2O_2, photocatalysis, Fenton, Photo Fenton, Bicarbonate/H_2O_2, Co/bicarbonate/H_2O_2 and Fe/bicarbonate/H_2O_2) can be useful to degrade MET. Of course the rate and level of MET removal is different for each technique.

b. *Following up the global parameters*

MET elimination

- In SB, CPC and BLB reactors photolysis drives to a low MET degradation: 14.0%, 8.1%, and 3% respectively. However, when $UV_{254\ nm}$ was used, a high MET degradation by photolysis (93.5 % at 240 minutes) was observed.

- UVC/H_2O_2 was proved to be an effective technique to remove MET from waters in a short period of time, achieving 98.7% of degradation in 7.5 min with 125 mg H_2O_2/L.

- Photocatalysis was also effective in MET removal. Using 0.4 g/L of TiO_2, a complete MET degradation was reached after 300 minutes in SB, and 81.5% after 270 minutes in CPC.

- Fenton process removed 67% of MET using 10 mg/L of Fe (II) and 150 mg/L of H_2O_2 and adding the total iron at the beginning of the experiment. However, when iron (II) was added at constant periods of time, the efficiency of the process was enhanced up to 87% of MET degradation.

- Photo-Fenton process drives to the complete MET degradation in 7 minutes using BLB reactor, using the highest concentrations of Fe (II) (10 mg/L) and H_2O_2 (150 mg/L) at 25ºC. 97.3% in 7 minutes using SB and 98.3% within 3 minutes using CPC was obtained. A complete MET elimination was reached in 20 minutes of treatment with UVC reactor, for 2.5 mg/L of Fe and 25 mg/L of H_2O_2.

- Bicarbonate/hydrogen peroxide method (BAP) does not show to be a good alternative for MET degradation and maximum MET conversion reached was 20%.

The conversion improves to 47.2% of MET when Co was added and to complete MET removal when Fe was added.

Mineralization degree

- Photolysis did not promote relevant mineralization (SB: 2.5%, CPC: 2.7%, BLB: 2.1% and UVC: 5.4, within 240 minutes).
- UVC/H_2O_2 reached 70.7% of TOC conversion after 230 minutes.
- Photocatalysis achieved good levels of mineralization 53.0% in SB after 360 minutes and 29.2% in CPC after 270 minutes.
- In Fenton process mineralization was very poor 8% and 15.6% for 1 addition and by steps, respectively.
- In photo-Fenton using the highest concentrations of iron and H_2O_2, TOC removal was 81.2% (90 min), 78.8% (120 min), and 83.7% (150 min) for BLB, SB and CPC reactors respectively. For UVC reactor using the lowest concentrations of iron and H_2O_2, 17.6% of TOC was degraded after 60 minutes.

Biodegradability and Toxicity

- In UVC/H_2O_2 process after 230 minutes of irradiation, the MET solution was biodegradable (0.38) and toxicity was 0.42 Equitox/m^3, using 125 mg H_2O_2/L.
- In photocatalysis after 360 minutes, the solution can be considered biodegradable (0.41) for SB. However, after 270 minutes of treatment, the solution remains being considered not biodegradable (0.12) in CPC. The toxicity showed values of 0.72 and 0.57 Equitox/m^3 using SB and CPC reactors respectively.
- In Fenton with the highest values of catalyst and promoter and adding the total iron at the beginning, a low biodegradability was reached and after 60 minutes of treatment toxicity was 0.93 Equitox/m^3. When the iron was added by steps the toxicity value decreased up to 0.90 Equitox/m^3.
- In photo-Fenton process, using the highest concentrations of iron and H_2O_2, a high biodegradability (0.53) was reached in 185 minutes for BLB reactor. In photo-Fenton process all devices reached a final toxicity lower than 0.6 Equitox/m^3, using 2.5 mg/L of iron and 25 mg/L of H_2O_2.

c. *Influence of the particular conditions for each technique*

- UVC/H_2O_2.

    - As higher H_2O_2 concentration, higher MET and TOC removals were obtained, being 125 mg/L the best concentration for H_2O_2.

    - MET degradation was rather lower when UVC/H_2O_2 process was carried out at pH acid.

- Photocatalysis.

    - MET and TOC removals increase with TiO_2 concentration and the best value was 0.4 g/L of TiO_2.

    - As lower MET initial concentration, higher MET and TOC removals in shorter time (25 mg/L MET initial: 100% conversion in 180 minutes).

    - MET and TOC removals increase when pH increase.

    - The addition of H_2O_2 improves MET and TOC removal.

    - When MET was dissolved in real water (coming from WWTP), the degradation rate decreases due to the interference of the organic matter.

- Fenton.

    - As higher catalyst (Fe (II)) and promoter (H_2O_2) concentrations, higher MET and TOC removals. In addition, dosing the iron by steps enhances the process.

- Photo-Fenton.

    - MET and TOC removals are directly related to catalyst and promoter concentrations, and they increase with both.

    - The temperature influences the process and MET degradation increases when temperature does it.

- Bicarbonate/H_2O_2 process.

    - When H_2O_2 and HCO_3^- increase, MET degradation also does it.

    - Increasing cobalt (II) concentration MET degradation decreases.

    - Increasing Fe (II) concentration MET degradation increases. In addition, dosing the iron by steps enhances the process.

d. *Influence of the set-up and the process*

- UVC/H_2O_2, photo-Fenton and photocatalysis/TiO_2 processes achieved practically the total MET removal. Comparisons between the processes established that UVC/H_2O_2 shows the highest efficiency in the ratio accumulated energy/MET removed and the highest rate of MET elimination. If we compare the energy supplied to the lamp, things are different. Thus, to eliminate 1 mg of MET the consumption of the energy in the SB is too high in comparison with the lamps used in UVC system.

- Photocatalysis in a solarbox and CPC reactor promotes the MET and TOC degradation. Photocatalysis in a solarbox shows lower energetic efficiency than CPC.

- Photo-Fenton process exhibits a better performance in UVC and BLB reactors than SB and CPC reactors. From an economical point of view, SB reactor seems to be more expensive than the other technologies, being CPC the cheapest one per litre of treated water.

e. *Influence of irradiation in photocatalytic reactors*

- o-NB actinometry was carried out in two different ways, based on pH or o-NB concentration, giving photon flows of 2.81×10^{-6} Einstein/s and 2.68×10^{-6} Einstein/s, respectively, in SB.

- In addition, this work has demonstrated that the o-NB actinometry, followed by o-NB concentration consumption, could be used in the presence of the catalyst TiO_2. It was stated that o-NB suffers only photolysis and not photocatalysis, and it can be used to estimate the radiation entering the photoreactor when titania is present. It is the photolytic product (o-HNB) the compound which undergoes photocatalytic reactions when there is TiO_2 present.

7.2   Recommendations

- Based on current experience, it would be advisable to continue working on the degradation of Metoprolol by means of different Advanced Oxidation Processes using real waters and using very low initial MET concentrations.

- In order to complete the work in photocatalysis new catalysts can be investigated in order to compare and improve the performance of the process.

- It would be interesting to continue the work with Fenton and photo-Fenton at near neutral pH.

- It would be advisable to perform a comprehensive economic study of the different AOPs used. In this way, studies on the environmental impact of the different AOPs tested can also be interesting. In both cases, economic and environmental studies, comparison could be made related to the efficiency of the AOPs.

Chapter VIII

Bibliography

8 BIBLIOGRAPHY

Alder, A., Schaffner, C., Majewsky, M., Klasmeier, J., & Fenner, K. (2010). Fate of b-blocker human pharmaceuticals in surface water: Comparison of measured and simulated concentrations in the Glatt Valley Watershed, Switzerland. *Water Research*, *44*, 936–948.

Allen, J. M., Allen, S. K., & Baertschi, S. W. (2000). 2-Nitrobenzaldehyde: a convenient UV-A and UV-B chemical actinometer for drug photostability testing. *Journal of Pharmaceutical and Biomedical Analysis*, *24*, 167–178.

American Society for Testing and Materials (ASTM). (2014). Solar spectral irradiance. http://es.astm.org/

Andreozzi, R., Raffaele, M., & Nicklas, P. (2003). Pharmaceuticals in STP effluents and their solar photodegradation in aquatic environment. *Chemosphere*, *50*, 1319.

Bahnemann, D. (2004). Photocatalytic water treatment: solar energy applications. *Solar Energy*, *77*, 445–459.

Bautista, P., Mohedano, A. F., Casaa, J. A., Zazo, J. A., & Rodriguez, J. . (2008). An overwiev of the application of Fenton oxidation to industrial wastewaters treatment. *Journal of Chemical Technology and Biotechnology*, *83*, 1323–1338.

Bayarri, B., Giménez, J., Curcó, D., & Esplugas, S. (2012). Direct evaluation of the absorbed photon flow in a photocatalytic reactor by an actinometric method. *Chemical Engineering Journal*, *200-202*, 158–167.

Beat, J., & Pichat, P. (1991). Determination of the Actual Photocatalytic Rate of H_2O_2 Decomposition over Suspended TiO_2. Fitting to the Langmuir-Hinshelwood Form. *Langmuir*, *7*, 947–954.

Bendz, D., Paxeus, N. A., Ginn, T. R., & Loge, F. J. (2005). Occurrence and fate of pharmaceutically active compounds in the environment, a case study: Hoje River in Sweden. *Journal of Hazardous Materials*, *122*, 195–204.

Benitez, F. J., Acero, J. L., Real, F. J., Roldan, G., & Casas, F. (2011). Bromination of selected pharmaceuticals in water matrices. *Chemosphere*, *85*, 1430–1437.

Benitez, F. J., Real, F. J., Acero, J. L., & Roldan, G. (2009). Removal of selected pharmaceuticals in waters by photochemical processes. *Journal of Chemical Technology and Biotechnology*, *84*, 1186–1195.

Benner, J., Ternes, T. A., & Scholz, J. (2009). Ozonation of beta-blockers: kinetic studies, identification of oxidation products and pathways. *Environmental Science & Technology*, *42*, 10–18.

Bird, R. E. (1984). A simple, solar spectral model for direct-normal and diffuse horizontal irradiance. *Solar Energy*, *32*, 461–471.

Blanco-Galvez, J., Fernández-Ibáñez, P., & Malato-Rodríguez, S. (2007). Desinfection of water. Recent overview. *Journal of Solar Energy Engineering*, *129*(4).

Blanco-Galvez, J., & Malato-Rodríguez, S. (2003). Solar detoxification. *Unesco*.

Bonetti, G., Vecli, A., & Viappiani, C. (1997). Reaction volume of water formation detected by time-resolved photoacoustics: photoinduced proton transfer between o-nitrobenzaldehyde and hydroxyls in water. *Chemical Physics Letters*, *269*, 268–273.

Brack, W., Dulio, V., & Slobodnik, J. (2012). The NORMAN Network and its activities on emerging environmental substances with a focus on effect-directed analysis of complex environmental contamination. *Environmental Sciences Europe*, 24–29.

British Broadcasting Corporation (BBC) News. (2012). State of the world´s freshwater resources. http://www.bbc.com/news/science-environment-18353963

Burbano, A., Dionysiou, D. D., & Suidan, M. T. (2008). Effect of oxidant-to-substrate ratios on the degradation of MTBE with Fenton reagent. *Water Research*, *42*, 3225–3239.

Carballa, M., Omil, F., & Lema, J. M. (2005). Removal of cosmetic ingredients and pharmaceuticals in sewage primary treatment. *Water Research*, *39*, 4790–4796.

Carlsson, C., Johansson, A. K., Alvan, G., Bergman, K., & Küler, T. (2006). Are pharmaceuticals potent environmental pollutants?: Part I: Environmental risk assessments of selected active pharmaceutical ingredients. *Science of The Total Environment*, *364*, 67–87.

Carra, I., Malato, S., Jiménez, M., Maldonado, M. I., & Sanchéz, J. A. (2014). Microcontaminant removal by solar photo-Fenton at natural pH run with sequential and continuous iron additions. *Chemical Engineering Journal*, *235*, 132–140.

Catalunya. Reglament metropolità d'abocament d'aigües residuals CM 3/06/2004 BOP Núm. 142 14/06/2004 (2004).

Chen, S., Song, P., Yang, S. Q., Yin, H. M., & Han, K. L. (2010). Fluorescence and solvent-dependent phosphorescence studies of o-nitrobenzaldehyde: A combined experimental and theoretical investigation. *Physical Chemistry Chemical Physics*, *12*, 9067–9074.

Choi, J., & Terazima, M. (2003). Photochemical reaction of 2-nitrobenzaldehyde by monitoring the diffusion coefficient. *Journal of Physical Chemistry B*, *107*, 9552–9557.

Cleuvers, M. (2003). Aquatic ecotoxicity of pharmaceuticals including the assessment of combination effects. *Toxicology Letters*, *142*, 185–194.

Cleuvers, M. (2005). Initial risk assessment for three beta-blockers found in the aquatic environment. *Chemosphere*, *59*, 199–205.

De la Cruz, N., Dantas, R. F., Giménez, J., & Esplugas, S. (2013). Photolysis and TiO_2 photocatalysis of the pharmaceutical propranolol: Solar and artificial light. *Applied Catalysis B: Environmental*, *130-131*, 249–256.

De La Cruz, N., Romero, V., Dantas, R. F., Marco, P., Bayarri, B., Giménez, J., & Esplugas, S. (2013). o-Nitrobenzaldehyde actinometry in the presence of suspended TiO_2 for photocatalytic reactors. *Catalysis Today*, *209*, 209–214.

De León, A., Sergio, M., Bussi, J., Ortiz de la Plata, G., Cassano, A., & Alfano, O. (2014). Water decontamination by heterogeneous photo-Fenton processes over iron, iron minerals and iron-modified clays. In M. J. M., Litter, Marta I., Candal, Roberto J (Ed.), *Advanced Oxidation Technologies-Sustainable solutions for environmental treatments* (9th ed., pp. 197–216). London, UK.: Taylor & Francis Group.

Department of Defense. Emerging Contaminants, Pub. L. No. 4715.18 (2009). Department of Defense Instruction.

Dougherty, J. A., Swarzenski, P. W., Dinicola, R. S., & Reinhard, M. (2010). Occurrence of Herbicides and Pharmaceutical and Personal Care Products in Surface Water and Groundwater around Liberty Bay, Puget Sound, Washington. *Journal of Environmental Quality*, *39*, 1173–1180.

Dzialowski, E. M., Turner, P. K., & Brooks, B. W. (2006). Physiological and reproductive effects of beta adrenergic receptor antagonists in Daphnia magna. *Archives of Environment Contamination and Toxicology*, *50*, 503–510.

Environmental Council of the States. (2010). *State experiences with emerging contaminants: recommendations for federal action* (pp. 1–42). http://www.ecos.org/files/3959_file_January_2010_ECOS_Green_Report.pdf

Escher, B. I., Bramaz, N., Richter, M., & Lienert, J. (2006). Comparative ecotoxicological hazard assessment of beta blockers and their human metabolites using a mode-of-action-based test battery and a QSAR approach. *Environmental Science & Technology*, *40*, 7402–7408.

European Commission. Directive 2000/60/EC, Pub. L. No. DOUE, L 327 (2000). Diario Oficial de las Comunidades Europeas.

European Commission. Error correction Regulation (EC) 850/2004, Pub. L. No. DOUE, L 229 (2004). Diario oficial de la Unión europea.

European Commission. Regulation (EC) 850/2004, Pub. L. No. DOUE, L 158 (2004). Diario oficial de la Unión europea.

European Commission. 2006/507/EC, Pub. L. No. DOUE, L 209 (2006).

European Commission. Regulation (EC) 1195/2006, Pub. L. No. DOUE, L 217 (2006). Diario oficial de la Unión europea.

European Commission. Error correction Regulation (EC) 850/2004, Pub. L. No. DOUE, L 204 (2007). Diario oficial de la Unión europea.

European Commission. Regulation (EC) 172/2007, Pub. L. No. DOUE, L 55 (2007). Diario oficial de la Unión europea.

European Commission. Regulation (EC) 323/2007, Pub. L. No. DOUE, L 85 (2007). Diario oficial de la Unión europea.

European Commission. Directive 2008/105/EC, Pub. L. No. DOUE, L348 (2008). Diario oficial de la Unión europea.

European Commission. Directive 2009/90/EC, Pub. L. No. DOUE, L201 (2009). Diario oficial de la Unión europea.

European Commission. Regulation (EC) 304/2009, Pub. L. No. DOUE, L 96 (2009). Diario oficial de la Unión europea.

European Commission. Regulation (EU) 756/2010, Pub. L. No. DOUE, L 223 (2010). Diario oficial de la Unión europea.

European Commission. Regulation (EU) 757/2010, Pub. L. No. DOUE, L223 (2010). Diario oficial de la Unión europea.

European Commission. Regulation (EU) 519/2012, Pub. L. No. DOUE, L159 (2012). Diario oficial de la Unión europea.

European Commission. Regulation (EU) No 1342/2014, Pub. L. No. DOUE, L363 (2014). Diario oficial de la Unión europea.

European Commission. (2014a). Water. http://ec.europa.eu/environment/water/index_en.htm

European Environment Agency. (2012). *Water resources in Europe in the context of vulnerability* (pp. 1–96).

European Federation of Pharmaceutical Industry and Associations. (EFPIA). (2014). *The pharmaceutical industry in figures*. Retrieved from http://www.efpia.eu/uploads/Figures_2014_Final.pdf

European Union. Decisión 2007/639, Pub. L. No. DOUE, L 258 (2007). Diario oficial de la Unión europea.

European Union. Decisión 2009/63, Pub. L. No. DOUE, L 23 (2009).

Fakhraian, H., & Valizadeh, F. (2010). Activation of hydrogen peroxide via bicarbonate, sulfate, phosphate and urea in the oxidation of methyl phenyl sulfide. *Journal of Molecular Catalysis A: Chemical*, *333*, 69–72.

Fatta, D., Achilleos, A., Nikolaou, A., & Meriç, S. (2007). Analytical methods for tracing pharmaceutical residues in water and wastewater. *TrAC Trends in Analytical Chemistry*, *26*, 515–533.

Femia, J., Mariani, M., Cassano, A., Zalazar, C., & Tiscornia, I. (2014). Decontamination of commercial chlorpyrifos in water using the UV/H_2O_2 process. In M. J. M., Litter, Marta I., Candal, Roberto J (Ed.), *Advanced Oxidation Technologies- Sustainable solutions for environmental treatments* (9th ed., pp. 149–159). London, UK.: Taylor & Francis Group.

Fraysse, B., & Garric, J. (2005). Prediction and experimental validation of acute toxicity of beta blockers in Ceriodaphnia dubia. *Environmental Toxicology and Chemistry*, *24*, 2470–2476.

Galbavy, E. S., Ram, K., & Anastasio, C. (2010). 2-Nitrobenzaldehyde as a chemical actinometer for solution and ice photochemistry. *Journal of Photochemistry and Photobiology A: Chemistry*, *209*, 186–192.

George, M. V., & Scaiano, J. C. (1980). Photochemistry of o-nitrobenzaldehyde and related studies. *Journal of Physical Chemistry*, *84*, 492–495.

Gernjak, W., Fuerhacker, M., Fernández-Ibañez, P., Blanco, J., & Malato, S. (2006). Solar photo-Fenton treatment Process parameters and process control. *Applied Catalysis B: Environmental*, *64*, 121–130.

Göb, S., Oliveros, E., Bossmann, S. H., Braun, A. M., Nascimento, C. A. O., & Guardani, R. (2001). Optimal experimental design and artificial neural networks applied to the photochemically enhanced Fenton reaction. *Water Science & Technology*, *44*, 339–345.

González, O., Sans, C., Esplugas, S., & Malato, S. (2009). Application of solar advanced oxidation processes to the degradation of the antibiotic sulfamethoxazole. *Photochemistry & Photobiological Sciences*, *8*, 1032–1039.

Gónzalez-Alvarez, O. (2009). *Procesos fotoquímicos de oxidación para el tratamiento de sulfametoxazol en solución acuosa. integración con un reactor biológico SBBR*. University of Barcelona.

Green Rhino Energy. (2014). Annual Solar Irradiance, Intermittency and Annual Variations. http://www.greenrhinoenergy.com/solar/radiation/empiricalevidence.php

Gros, M., Petrovic, M., & Barceló, D. (2006). Development of a multi-residue analytical methodology based on liquid chromatography–tandem mass spectrometry (LC–MS/MS) for screening and trace level determination of pharmaceuticals in surface and wastewaters. *Talanta*, *70*, 678–690.

Gros, M., Petrovic, M., & Barceló, D. (2007). Wastewater treatment plants as a pathway for aquatic contamination by pharmaceuticals in the Ebro river basin (Northeast Spain). *Environmental Toxicology and Chemistry*, *26*, 1553–1562.

Guz, L. M., Olivelli, M., Torres, R. M., Curutchet, G., & Candal, R. J. (2014). Modified montmorillonite in photo-Fenton and adsorption process. In M. Litter, R.; Candal (Ed.), *Advanced Oxidation Technologies- Sustainable solutions for environmental treatments* (9th ed., pp. 217–234). London, UK.: Taylor & Francis Group.

Heberer, T. (2002). Occurrence, fate, and removal of pharmaceutical residues in the aquatic environment: a review of recent research data. *Toxicology Letters*, *131*, 5–17.

Heinz, B., Schmierer, T., Laimgruber, S., & Gilch, P. (2008). Excited state processes of nitrobenzaldehydes probed by ultrafast fluorescence and absorption spectroscopy. *Journal of Photochemistry and Photobiology A: Chemistry*, *199*, 274–281.

Hernando, M. D., Gómez, M. J., Agüera, A., & Fernández-Alba, A. (2007). LC-MS analysis of basic pharmaceuticals (beta-blockers and anti-ulcer agents) in wastewater and surface water. *Trends in Analytical Chemistry*, *26*, 581–594.

Hernando, M. D., Mezcua, M., Fernandez-Alba, A. R., & Barcelo, D. (2006). Environmental risk assessment of pharmaceutical residues in wastewater effluents, surface waters, and sediments. *Talanta*, *69*, 334–342.

Herney-Ramirez, J., Vicente, M. A., & Maderira, L. M. (2010). Heterogeneous photo-Fenton oxidation with pillared clay-based catalysts for wastewater treatment: A review. *Applied Catalysis B: Environmental*, *98*, 10–26.

Herrmann, J. M. (1999). Heterogeneous photocatalysis: fundamentals and applications to the removal of various types of aqueous pollutants. *Catalysis Today*, *52*, 115–129.

International Organization for Standardization. Determination of iron- Spectrometric method using 1,10-phenontraleine, Pub. L. No. ISO 6332 (1988).

International Organization for Standardization. determination of the inhibitory effect of water samples on the light emission of Vibrio fischeri (Luminescent bacteria test) – Part 3: method using freeze-dried bacteria, Pub. L. No. ISO 11348 (2007).

Ioannou, L. A., Hapeshi, E., Vasquez, M. I., Mantzavinos, D., & Fatta-Kassinos, D. (2011). Solar/TiO_2 photocatalytic decomposition of b-blockers atenolol and propranolol in water and wastewater. *Solar Energy*, *85*, 1915–1926.

Isarain-Chávez, E., Garrido, J. A., & Rodríguez, R. M. (2011). Mineralization of metoprolol by electro-Fenton and photoelectro-Fenton processes. *Journal of Physical Chemistry A*, *115*, 1234–1242.

Jong-Kwon, I., Yeomin, Y., & Kyung-Duk, Z. (2014). Optimization of naproxen and ibuprofen removal in photolysis using a Box–Behnken design: Effect of Fe(III), NO_3^-, and humic acid. *Journal of Environmental Science and Health, Part A: Toxic/Hazardous Substances and Environmental Engineering*, *49*, 422–433.

Joss, A., Keller, E., Alder, A. C., Göbel, A., McArdell, C. S., Ternes, T., & Siegrist, H. (2005). Removal of pharmaceuticals and fragrances in biological wastewater treatment. *Water Research*, *39*, 3139–3152.

Junta de Andalucía. (2014). Integral water cycle. http://www.juntadeandalucia.es/medioambiente/site/portalweb

Jurado, A., Vázquez-Suñé, E., Carrera, J., López de Alda, M., Pujades, E., & Barceló, D. (2012). Emerging organic contaminants in groundwater in Spain: a review of sources, recent occurrence and fate in a European context. *Science of the Total Environment*, *440*, 82–94.

Kasprzyk-Hordern, B., Dinsdale, R. M., & Guwy, A. J. (2009). Illicit drugs and pharmaceuticals in the environment-forensic applications of environmental data. Part 1: Estimation of the usage of drugs in local communities. *Environmental Pollution*, *157*, 1773–1786.

Khetan, S. K., & Collins, T. J. (2007). Human pharmaceuticals in the aquatic environment: A challenge to green chemistry. *Chemical Reviews*, *6*, 2319–2364.

Kim, I., & Tanaka, H. (2009). Photodegradation characteristics of PPCPs in water with UV treatment. *Environment International*, *35*(5), 793–802.

Kolpin, D., Furlong, W., Meyer, E., Thurman, M., Zaugg, E., Barber, S., & Herbert, T. (2002). Pharmaceuticals, hormones, and other organic wastewater contaminants in U.S. streams, 1999-2000: a national reconnaissance. *Environmental Science & Technology*, *36*, 1202–1211.

Kolpin, D., Skopec, M., Meyer, M. T., Furlong, E. T., & Zaugg, S. (2004). Urban contribution of pharmaceuticals and other organic wastewater contaminants to streams during differing flow conditions. *Science of The Total Environment*, *328*, 119–130.

Kuhn, H. J., Braslavsky, S. E., & Schmidt, R. (2004). Chemical actinometry (IUPAC Technical Report). *Pure and Applied Chemistry*, *76*, 2105–2146.

Lee, J., Kwon, T., Thiruvenkatachari, R., & Moon, I. (2006). Adsorption and photocatalytic degradation of bisphenol A using TiO$_2$ and its separation by submerged hollowfiber ultrafiltration membrane. *Journal of Environmental Sciences*, *18*, 193–200.

Legrini, O., Oliveros, E., & Braun, M. (1993). Photochemical processes for water treatment. *Chemical Reviews*, *93*, 671–698.

León, O. G., & Montero, I. (2001). Cómo explicar el concepto de interacción sin estadística: análisis gráfico de todos los casos posibles en un diseño 2 x 2. *Psicothema*, *13*, 159–165.

Li, W., Nanaboina, V., Zhou, Q., & Korshin, G. (2012). Effects of Fenton treatment on the properties of effluent organic matter and their relationships with the degradation of pharmaceuticals and personal care products. *Water Research*, *46*(2), 403–12.

Li, X., Xiong, Z., Ruan, X., Xia, D., Zeng, Q., & Xu, A. (2012). Kinetics and mechanism of organic pollutants degradation with cobalt–bicarbonate–hydrogen peroxide system: Investigation of the role of substrates. *Applied Catalysis A: General*, *411-412*, 24–30.

Lienert, J., Güdel, K., & Escher, B. I. (2007). Screening method for ecotoxicological hazard assessment of 42 pharmaceuticals considering human metabolism and excretory routes. *Environmental Science & Technology*, *41*, 4471–4478.

Litter, M., & Quici, N. (2010). Photochemical Advanced Oxidation Processes for Water and Wastewater Treatment. *Recent Patents on Engineering*, *4*, 217–241.

Liu, Q. T., Cumming, R. I., & Sharpe, A. D. (2009). Photo-induced environmental depletion processes of β-blockers in river waters. *Photochemical & Photobiological Sciences*, *8*, 768–777.

Liu, Q. T., & Williams, H. (2007). Kinetics and degradation products for direct photolysis of β-Blockers in water. *Environmental Science & Technology*, *41*, 803–810.

Malato, S., Fernández-Ibáñez, P., Maldonado, M. I., Blanco, J., & Gernjak, W. (2009). Decontamination and disinfection of water by solar photocatalysis: Recent overview and trends. *Catalysis Today*, *147*, 1–59.

Malato, S., Fernández-Ibáñez, P., Maldonado, M. I., Oller, I., & Polo-López, M. I. (2013). Solar photocatalytic pilot plants: Commercially available reactors. In P. Pichat (Ed.), *Photocatalysis and Water Purification* (pp. 377–406). Germany: Willey-VCH.

Malato, S., Maldonado, M. I., Fernández, P., Oller, I., & Polo, I. (2014). Decontamination of water by solar irradiation. In Litter, M.; Candal, R.; Meichtry J.M. (Ed.), *Advanced Oxidation Technologies-Sustainable solutions for environmental treatments* (9th ed., pp. 1–22). London, UK.: Taylor & Francis Group.

Maurer, M., Escher, B. I., Richle, P., Schaffner, C., & Alder, C. (2007). Elimination of beta-blockers in sewage treatment plants. *Water Research*, *41*, 1614–22.

Mendez-Arriaga, F., Maldonado, M. I., Giménez, J., Esplugas, S., & Malato, S. (2009). Abatement of ibuprofen by solar photocatalysis process: enhancement and scale up. *Catalysis Today*, *144*, 112–116.

Metcalf & Eddy. (1991). *Wastewater Engineering, Treatment, Disposal and Reuse* (3rd ed., p. 1334). New York, USA: McGraw-Hill, Inc.

Metcalfe, C. D., Miao, X. S., Koenig, B. G., & Struger, J. (2003). Distribution of acidic and neutral drugs in surface waters near sewage treatment plants in the lower great lakes, Canada. *Environmental Toxicology and Chemistry*, *22*, 2881–2889.

Moctezuma, E., Leyva, E., López, M., Pinedo, A., Zermeño, B., & Serrano, B. (2013). Photocatalytic degradation of Metoprolol Tartrate. *Top Catalysis*, *56*, 1875–1882.

Muñoz, I., Gómez-Ramos, M. J., Agüera, A., Fernández-Alba, A. R., García-Reyes, J. F., & Molina-Díaz, A. (2009). Chemical evaluation of contaminants in wastewater effluents and the environmental risk of reusing effluents in agriculture. *TrAC Trends in Analytical Chemistry*, *28*, 676–694.

Muñoz, I., Lopez-Doval, J. C., Ricart, M., Villagrasa, M., Brix, R., Geiszinger, A., Ginebreda, A., Guasch, H., López, M. J., Romaní, A. M., Sabater, S., & Barceló, D. (2009). Bridging levels of pharmaceuticals in river water with biological community structure in the Llobregat river basin (northeast Spain). *Environmental Toxicology and Chemistry*, *28*, 2706–2714.

Nam, S. W., Jo, B., Yoon, Y., & Zoh, K. D. (2014). Occurrence and removal of selected micropollutants in a water treatment plant. *Chemosphere*, *95*, 156–165.

Nogueira, R. F., Oliveora, M. C., & Paterlini, W. C. (2005). Simple and fast spectrophotometric determination of H_2O_2 in photo-Fenton reactions using metavanadate. *Talanta*, *66*, 86–91.

Nogueira, R. F. P., Trovó, A. G., da Silva, M. R. A., Villa, R. D., & de Oliveira, M. C. (2007). Fundamentos e aplicações ambientais dos processos Fenton e foto-Fenton. *Quimica Nova*, *30*, 400–408.

Nosaka, Y., & Nosaka, A. (2013). Identification and roles of the active species generated on various photocatalysts. In P. Pichat (Ed.), *Photocatalysis and Water Purification* (pp. 3–24). Germany: Willey-VCH.

Owen, S. F., Giltrow, E., Huggett, D., Hutchinson, T., Saye, J., Winter, M., & Sumpter, J. (2007). Comparative physiology, pharmacology and toxicology of beta-blockers: mammals versus fish. *Aquatic Toxicology*, *82*, 145–62.

Parsons, S. (2004). *Advanced Oxidation Processes for water and wastewater treatment*. London, UK. IWA Publishing.

Petrovic, M., González, S., & Barceló, D. (2003). Analysis and removal of emerging contaminants in wastewater and drinking water. *TrAC Trends in Analytical Chemistry*, *22*, 685–696.

Petrovic, M., Lopez de Alda, M. J., Diaz, S., Postigo, C., Radjenovic, J., Gros, M., & Barceló, D. (2009). Fate and removal of pharmaceuticals and illicit drugs in conventional and membrane bioreactor wastewater treatment plants and by riverbank filtration. *Philosophical Transactions of the Royal Society A*, *367*, 3979–4003.

Peyton, G. R. (1990). Oxidative treatment methods for removal of organic compounds from drinking water supplies. In K. P. Ram, Neil M.; Christman, Russell F.; Cantor (Ed.), *Significance and treatment of volatile organic compounds in water supplies* (pp. 313–362). United States of America: Lewis Publishers.

Pignatello, J. J., Liu, D., & Huston, P. (1999). Evidence for an additional oxidant in the photoassisted Fenton reaction. *Environmental Science Technology*, *33*, 1832–1839.

Piram, A., Salvador, A., Verne, C., Herbreteau, B., & Faure, R. (2008). Photolysis of β-blockers in environmental waters. *Chemosphere*, *73*, 1265–1271.

Polar, J. A. (2007). The fate of pharmaceuticals after wastewater treatment. *Florida Water Resources Journal*, 26–31.

Prieto-Rodríguez, L., Oller, I., Klamerth, N., Agüera, A., Rodríguez, E. M., & Malato, S. (2013). Application of solar AOPs and ozonation for elimination of micropollutants in municipal wastewater treatment plant effluents. *Water Research*, *47*, 1521–1528.

Randhir, P. D. ., & Rolf, U. H. (2013). Pharmaceuticals in the built and natural water environment of the United States. *Water*, *5*, 1346–1365.

Ratola, N., Cincinelli, A., Alves, A., & Katsoyiannis, A. (2012). Occurrence of organic microcontaminants in the wastewater treatment process. A mini review. *Journal of Hazardous Materials*, *239-240*, 1–18.

Rivas, F. J., Gimeno, O., Borralho, T., & Carbajo, M. (2010). UV-C radiation based methods for aqueous metoprolol elimination. *Journal of Hazardous Materials*, *179*, 357–362.

Romero, V., Marco, P., Giménez, J., & Esplugas, S. (2013). Adsorption and photocatalytic decomposition of the beta-blocker Metoprolol in aqueous titanium dioxide suspensions : kinetics , intermediates , and degradation pathways. *International Journal of Photoenergy*. doi:http://dx.doi.org/10.1155/2013/138918

Ryu, J., & Choi, W. (2004). Effects of TiO_2 surface modifications on photocatalytic oxidation of Arsenite: the role of superoxides. *Environmental Science & Technology*, *38*, 2928–2933.

Santos, J. L., Aparicio, I., & Alonso, E. (2007). Occurrence and risk assessment of pharmaceutically active compounds in wastewater treatment plants. A case study: Seville city (Spain). *Environment International*, *33*, 596–601.

Santos, L., Araujo, A., Fachini, A., Peña, A., & Deleure-Matos, C. Montenegro, M. (2010). Ecotoxicological aspects related to the presence of pharmaceuticals in the aquatic environment. *Journal of Hazardous Materials*, *175*, 45.

Sarria, V., Parra, S., Adler, N., Péringer, P., Benitez, N., & Pulgarin, C. (2002). Recent developments in the coupling of photoassisted and aerobic biological processes for the treatment of biorecalcitrant compounds. *Catalysis Today*, *76*, 301–315.

Sawage, G., Lehnard, A., Lübber, M., & Bahnemann, D. (2001). The Insulated Solar Fenton Hybrid Process: Fundamental Investigations. *Helvetica Chimica Acta*, *84*, 3742–3759.

Scepanovic, M., Abramovic, B., Golubovic, A., Kler, S., Grujic-Brojcin, M., Dohcevic-Mitrovic, Z., Babic, B., Matovic, B., & Popovic, Z. V. (2012). Photocatalytic degradation of metoprolol in water suspension of TiO_2 nanopowders prepared using sol–gel route. *Journal Sol-Gel Science &Technology*, *61*, 390–402.

Schmidt, G., Benítez, J., & Benítez, C. (2012). *Working definitions of water scarcity and drought* (pp. 1-11).

Singh, C., Chaudhary, R., & Thakur, R. S. (2011). Performance of advanced photocatalytic detoxification of municipal wastewater under solar radiation - A mini review. *International Journal of Energy and Environment*, *2*, 337–350.

Spanish Goverment. Real Decreto Legislativo 1/2001, Pub. L. No. BOE n° 176 (2001).

Spanish Goverment. Real Decreto 606/2003, Pub. L. No. BOE n° 135 (2003). Spain.

Spanish Goverment. Real Decreto 60/2011, Pub. L. No. BOE n° 19 (2011).

Spanish Goverment. Real Decreto 670/2013, Pub. L. No. BOE n° 227 (2013).

Spanish Goverment. Resolution 2013, Pub. L. No. BOE n° 103 (2013). Spain: Diario oficial del Estado.

Spuhler, D., Rengifo, J. A., & Pulgarín, C. (2010). The effect of Fe^{2+}, Fe^{3+}, H_2O_2 and the photo-Fenton reagent at near neutral pH on the solar disinfection (SODIS) at low temperatures of water containing Escherichia coli K12,. *Applied Catalysis B: Environmental*, *96*, 126–141.

Stolker, A. A. M., Niesing, W., Hogendoorn, E. A., Versteegh, J. F. M., Fuchs, R., & Brinkman, U. A. T. (2004). Liquid chromatography with triple-quadrupole or quadrupole-time of flight mass spectrometry for screening and confirmation of residues of pharmaceuticals in water. *Analytical and Bioanalytical Chemistry*, *378*, 955–963.

Stumm, W., & Morgan, J. J. (1996). *Aquatic Chemistry* (3rd. ed.). New York, USA: Wiley Interscience.

Suárez, S., Carballa, M., Omil, F., & J.M. Lema. (2008). How are pharmaceutical and personal care products (PPCPs) removed from urban wastewater. *Journal Reviews in Environmental Science & Biotechnology*, *7*, 125–138.

Tan, T. T. Y., Beydoun, D., & Amal, R. (2003). Photocatalytic reduction of Se(VI) in aqueous solutions in UV/TiO_2 system: importance of optimum ratio of reactants on TiO_2 surface. *Journal of Molecular Catalysis A: Chemical*, *202*, 73–85.

Ternes, A., & Joss, A. (2006). *Human pharmaceuticals, hormones and fragrances: the challenge of micropollutants in urban water management*. (T. A. T. and A. Joss, Ed.) (First edit., pp. 1–442). IWA Publishing.

Ternes, T. A., Stuber, J., Herrmann, N., McDowell, D., Ried, A., Kampmann, M., & Teiser, B. (2003). Ozonation: A tool for removal of pharmaceuticals, contrast media, and musk fragrances from wastewater. *Water Research*, *37*, 1976–1982.

Thomas, K. V., Dye, C., Schlabach, M., & Langford, K. H. (2007). Source to sink tracking of selected human pharmaceuticals from two Oslo city hospitals and a wastewater treatment works. *Journal of Environmental Monitoring*, *9*, 1410–1418.

Trapido, N., Kulik, N., Goi, A., Veressinina, Y., & Munter, R. (2009). Fenton treatment efficacy for the purification of different kinds of wastewater. *Water Science & Technology*, *60*, 1795–1801.

U.S. Geological Survey (USGS). (2014). Emerging contaminants in the environment. http://toxics.usgs.gov/regional/emc/index.html

United Nations of Population Fund. (2011). *People and possibilities in a world of 7 billion* (pp. 1–125).

Vieno, N. M., Harkki, H., Tuhkanen, T., & Kronberg, L. (2007). Occurrence of pharmaceuticals in river water and their elimination a pilot scale drinking water treatment plant. *Environmental Science & Technology*, *41*, 5077–5084.

Vieno, N., Tuhkanen, T., & Kronberg, L. (2007). Elimination of pharmaceuticals in sewage treatment plants in Finland. *Water Research*, *41*, 1001–12.

Vulliet, E., Cren-Olivé, C., & Grenier-Loustalot, M. F. (2009). Occurrence of pharmaceuticals and hormones in drinking water treated from surface waters. *Environmental Chemistry Letters*, *9*, 103–114.

Water Resources Group. (2014). Charting our water future a report of the 2030. http://www.mckinsey.com/client_service/sustainability/latest_thinking/charting_our_water_future

Wiegel, S., Aulinger, A., Brockmeyer, R., Harms, H., Löffler, J., Reincke, H., Schmidt, R., Stachel, W., Von-Tümpling, W., & Wanke, A. (2004). Pharmaceuticals in the river Elbe and its tributaries. *Chemosphere*, *57*, 107–126.

Willett, K. L., & Hites, R. A. (2000). Chemical actinometry: using o-Nitrobenzaldehyde to measure light intensity in photochemical experiments. *Journal of Chemical Education*, *77*, 900–902.

Wols, B. A., Hofman-Caris, C. H. M., Harmsen, D. J. H., & Beerendonk, E. F. (2013). Degradation of 40 selected pharmaceuticals by UV/H_2O_2. *Water Research*, *47*, 5876–5888.

Xu, A., Li, X., Xiong, H., & Yin, G. (2011). Efficient degradation of organic pollutants in aqueous solution with bicarbonate-activated hydrogen peroxide. *Chemosphere*, *82*, 1190–1195.

Xu, A., Li, X., Ye, S., Yin, G., & Zeng, Q. (2011). Catalyzed oxidative degradation of methylene blue by in situ generated cobalt (II)-bicarbonate complexes with hydrogen peroxide. *Applied Catalysis B: Environmental*, *102*, 37–43.

Yang, H., An, T., Li, G., Song, W., Cooper, W., Luo, H., & Guo, X. (2010). Photocatalytic degradation kinetics and mechanism of environmental pharmaceuticals in aqueous suspension of TiO_2 : A case of β-blockers. *Journal of Hazardous Materials*, *179*, 834–839.

Yu, J. T., Bouwer, E. J., & Coelhan, M. (2006). Occurrence and biodegradability studies of selected pharmaceuticals and personal care products in sewage effluent. *Agricultural Water Management*, *86*, 72–80.

Zheng, S., Cai, Y., & O´shea, K. E. (2010). TiO_2 photocatalytic degradation of phenylarsonic acid. *Journal of Photochemistry and Photobiology A: Chemistry*, *210*, 61–68.

Chapter IX
Contribution of this thesis to the science community

9   CONTRIBUTION OF THIS THESIS TO THE SCIENCE COMMUNITY

9.1   Communications to congresses

- V. Romero, O. González, S. Minghao, S. Esplugas. "Metoprolol removal by catalyst-bicarbonate-activated hydrogen peroxide in drinking water" The 13th Mediterranean Congress of Chemical Engineering (13MCCE), Barcelona, Spain, in the frame of the international fair of the Chemical Industry EXPOQUIMIA from 30 September to 3 October, 2014.

- V. Romero, E. Rodríguez, P. Marco, J. Giménez, S. Esplugas. "Effect of initial pH in the degradation of the emerging contaminant Metoprolol by means of UVC/H_2O_2" The 13th Mediterranean Congress of Chemical Engineering (13MCCE), Barcelona, Spain, in the frame of the international fair of the Chemical Industry EXPOQUIMIA from 30 September to 3 October, 2014.

- P. Marco, V. Romero, A. Solé, J. Giménez, S. Esplugas "Elimination of the emerging contaminant Metoprolol by photo-Fenton process with successive and continuous iron (II) additions" The 13th Mediterranean Congress of Chemical Engineering (13MCCE),Barcelona, Spain, in the frame of the international fair of the Chemical Industry EXPOQUIMIA from 30 September to 3 October, 2014.

- J. Giménez, V. Romero, P. Marco, S. Esplugas "Metoprolol abatement by means of Advanced Oxidation Processes" 8th European Meeting on Solar Chemistry and Photocatalysis: Environmental Applications – SPEA8 - Thessaloniki, Greece, on June 25-28, 2014.

- P. Marco, V. Romero, R.P. Cavalcante, B. Bayarri, J. Giménez, S. Esplugas "Degradación y mineralización del contaminante emergente Metoprolol por medio de diferentes Procesos de Oxidación Avanzada", XI Reunión de la Mesa Española de Tratamiento de Aguas, congreso nacional, organizado por Instituto del Agua y las Ciencias Ambientales de la Universidad de Alicante, Alicante, 18-20 of June 2014.

- S. Esplugas, V. Romero, O. Gonzalez, B. Bayarri, P. Marco, J. Giménez "Abatement of Metoprolol by photo-Fenton" 7th Congress of Environmental Applications of Advanced Oxidation Technologies (VII EPOA) and the 1st Iberoamerican Congress of Advanced Oxidation Technologies (I CIPOA), 15-18 of October 2013, Recife, Brazil

- J. Giménez, V. Romero, B. Bayarri, O. González, P. Marco, S. Esplugas. "Metoprolol Removal By Photo-Fenton: Convenience of artificial light or solar light", 3rd European conference on environmental applications of Advanced Oxidation Processes, Almería, Spain 27-30 2013. ISBN: 978-84-15487-99-9

- J. Giménez, V. Romero, M.A. Espuny, M. Hortós, B. Bayarri, O. González, P. Marco, S. Esplugas. "Performance of different Advanced Oxidation Technologies for the abatement of the beta-blocker Metoprolol", 3rd European conference on environmental applications of Advanced Oxidation Processes, Almería, Spain 27-30 2013. ISBN: 978-84-15487-99-9

- V. Romero, B. Bayarri, P. Marco, J. Giménez, S. Esplugas, "Kinetic of the photocatalytic removal of Metoprolol in TiO$_2$ suspensions with artificial light", 4th international conference on semiconductor photochemistry, SP4, Prague 23-27 of June 2013. ISBN: 978-80-7080-854-2

- N. De la Cruz, V. Romero, R. F. Dantas, P. Marco. J. Giménez y S. Esplugas, "Photocatalytic treatment of Metoprolol and Propranolol: comparison between laboratory and solar plant", 7th European Meeting on Solar Chemistry and Photocatalysis: Environmental Applications, SPEA7, Oporto, 17-20 of June 2012. ISBN: 978-989-97667-4-7

- N. De la Cruz, V. Romero, R. F. Dantas, J. Giménez y S. Esplugas, "o-nitrobenzaldehyde actinometry in the presence of suspended TiO$_2$ for photocatalytic reactors", 7th European Meeting on Solar Chemistry and Photocatalysis: Environmental Applications, SPEA7, Oporto, 17-20 of June 2012. ISBN: 978-989-97667-4-7

- V. Romero, N. De la Cruz, R. F. Dantas, P. Marco. J. Giménez y S. Esplugas, "Abatement of Metoprolol by heterogeneous photocatalysis process: artificial and solar radiation", 6th International Conference on Oxidation Technologies for Water and Wastewater Treatment, Goslar, 7-9 of May 2012.

- B. Bayarri, N. De la Cruz, V. Romero, R.F. Dantas, P. Marco, J. Giménez y S. Esplugas, "Eliminación de contaminantes emergentes mediante fotocatálisis solar: estudios de viabilidad y modelización". X Reunión de la Mesa Española de Tratamiento de aguas, Almería, 4-6 of October 2012. ISBN: 978-84-15487-33-33.

- N. De la Cruz, V. Romero, R. F. Dantas, J. Giménez y S. Esplugas, "Photolysis and TiO$_2$-photocatalysis of propranolol: solar and artificial light", 6th International

Conference on Oxidation Technologies for Water and Wastewater Treatment, Goslar, 7-9 of May, 2012.

- V. Romero, R. F. Dantas, P. Marco, J. Giménez y S. Esplugas, "Comparison between solar photocatalysis and simulated solar irradiation for the removal of Metoprolol in aqueous phase", IWA Specialist Conference - Water & Industry 2011 international conference, Valladolid, 1-4 of May 2011.

- V. Romero, R. F. Dantas, P. Marco, J. Giménez y S. Esplugas "Photocatalytic Metoprolol degradation process using simulated solar light" 12th Mediterranean Congress of Chemical Engineering , Barcelona, 15-18 of November, 2011. ISBN: 978-84-615-4777-7

- V. Romero, R. F. Dantas, P. Marco, J. Giménez y S. Esplugas "Photocatalytic Metoprolol degradation process using solar pilot plant reactor and TiO_2", 12th Mediterranean Congress of Chemical Engineering, Barcelona, 15-18 of November, 2011. ISBN: 978-84-615-4777-7

- N. De la Cruz, V. Romero, R. F. Dantas, P. Marco, J. Giménez y S. Esplugas, "Photocatalytic Treatment of Metoprolol and Propranolol", 6th European Meeting on Solar Chemistry & Photocatalysis: Environmental Applications, Prague, 13-16 of June 2010. ISBN: 978-80-7080-750-7

- Renato F. Dantas, Natalia de la Cruz, Ana Justo, Olga Callejo, Verónica Domínguez, Violette Romero, Javier Santiago, Pilar Marco, Santiago Esplugas "Application of Advanced Oxidation Processes for the treatment of micropollutants in wastewater" Simpòsium Internacional Qualitat Ambiental de les aigües litorals, Barcelona, 12 of November, 2010.

9.2 Publications

- Romero, V., González, O., Bayarri, B., Marco, P., Giménez, J., & Esplugas, S. Performance of different advanced oxidation technologies for the abatement of the beta-blocker Metoprolol. Catalysis Today, 240, 86-92 (2015).

- Romero, V., Méndez-Arriaga, F., Marco, P., Giménez, J., & Esplugas, S. Comparing the photocatalytic oxidation of Metoprolol in a solarbox and a solar pilot plant reactor. Chemical Engineering Journal, 254, 17-29 (2014).

- De la Cruz, N., Romero, V., Dantas, R. F., Marco, P., Bayarri, B., Giménez, J., & Esplugas, S. o-Nitrobenzaldehyde actinometry in the presence of suspended TiO_2 for photocatalytic reactors. Catalysis Today, 209, 209-214 (2013).

- Romero, V., Marco, P., Giménez, J., & Esplugas, S. (2013). Adsorption and Photocatalytic Decomposition of the-Blocker Metoprolol in Aqueous Titanium Dioxide Suspensions: Kinetics, Intermediates, and Degradation Pathways. International Journal of Photoenergy, (2013). http://dx.doi.org/10.1155/2013/138918.

- Romero, V., De la Cruz, N., Dantas, R. F., Marco, P., Giménez, J., & Esplugas, S. Photocatalytic treatment of Metoprolol and Propranolol. Catalysis Today, 161, 115-120 (2011).

Publications in progress:

- Romero, V., González, O., Bayarri, B., Marco, P., Giménez, J., & Esplugas, S. Photo-Fenton process comparison using different set-ups for the degradation of the emergent contaminant Metoprolol.

- Romero, V., Acevedo, S., Marco, P., Giménez, J., & Esplugas, S. Enhancement of Fenton and photo-Fenton processes at initial circumneutral pH for the degradation of Metoprolol.

Performance of different advanced oxidation technologies for the abatement of the beta-blocker metoprolol

V. Romero, O. González, B. Bayarri, P. Marco, J. Giménez*, S. Esplugas

Departamento de Ingeniería Química, Facultad de Química, Universidad de Barcelona, C/Martí i Franquès, 1, 08028 Barcelona, Spain

ABSTRACT

In this study UV/H_2O_2, photo-Fenton and photocatalysis (TiO$_2$) were used to degrade metoprolol tartrate salt (MET) in aqueous solution. This study investigates the variation of different parameters such as MET concentration, total organic carbon (TOC), chemical oxygen demand (COD) per accumulated energy (determined by actinometries), analyzing the performance of the different set-ups tested. First order apparent rate constants were calculated for the systems. Nearly total MET removal was achieved through the three technologies tested, the UV/H_2O_2 system being more efficient for MET degradation. On the other hand, the kinetic study indicated that TiO$_2$ photocatalysis seems to be one step ahead of the others when assessing the mineralization and the overall oxidation of the solution for a specific amount of accumulated energy (18 kJ/L). The acute toxicity measured by the inhibition percentage of bioluminescence from *Vibrio fischeri* indicates that all the processes tested promote the toxicity reduction for this target compound. The major reaction intermediates in the three processes were identified by ionization/mass spectrometry.

© 2014 Elsevier B.V. All rights reserved.

1. Introduction

Pharmaceutical and personal care products (PPCPs) are extensively consumed annually in the world [1]. As a result, these PPCPs may be found in waste effluents [2,3], in ranges varying from the value of an industrial discharge (10–100 mg/L) to the very small value founded in the aquatic environment (far less from 1 mg/L) [4]. These micropollutants are not completely eliminated by the conventional activated sludge treatment [5] and have been found at concentrations up to μg/L in the effluent of the municipal wastewater treatment plants (MWTP) [6,7]. This fact is in contrast to the Water Framework Directive which requires a 'good chemical and biological status' of all water bodies until 2015 [8]. Therefore, it is necessary to apply adequate technologies to definitively eliminate these contaminants from water. In this sense Advanced Oxidation Processes (AOPs) have been described as a useful tool for their completely degradation, increasing biodegradability and detoxifying effluents. A large number of studies have shown the potential for using single AOPs (UV radiation, ozone, photo-Fenton, photocatalysis, etc.) as well as different combinations of UV radiation and ozone with H_2O_2, TiO$_2$,

Fe(III), etc. [9]. All these processes are characterized by the production of hydroxyl radicals, which are extraordinarily reactive and present low selectivity, oxidizing most of the persistent pollutants in water.

Among these pharmaceuticals, β-blockers are frequently detected in the environment [10]. Metoprolol is one of the most commonly used β-blockers for the treatment of cardiovascular diseases [11]. According to the pharmacokinetics study [12], about 5% of metoprolol is excreted unchanged after oral administration and spilled into wastewaters. In addition, an important contribution to the occurrence of these drugs in the aquatic environment is the discharge of effluents from pharmaceutical industries, because discharge regulations are not focused on the concentration of these particular pollutants but on more general parameters such as COD or TOC [5]. In this framework, MET removal has been studied using many different AOPs, including UV/H_2O_2 [13], photocatalysis [14,15], photo and Fenton based technologies [9,13,16], in which the efficiency of MET degradation depends strongly on the particular technology and conditions used.

According to the state of the art, the objective of the present work was to compare H_2O_2/UV$_{254}$, TiO$_2$ photocatalysis and photo-Fenton, for the removal of MET. The efficiency of these three technologies in MET degradation was compared in terms of accumulated energy. Moreover, the pharmaceutical degradation kinetics at each process was modeled and compared.

2. Materials and experimental set-ups

2.1. Chemicals and reagents

Solutions of 50 mg/L of metoprolol tartrate salt (MET) (CAS: 56392-17-7, Sigma-Aldrich) were prepared using deionized water. TiO_2 Degussa P-25 was used as catalyst in heterogeneous photocatalysis. Acetonitrile (analytical reagent grade from Fischer Chemical) and orthophosporic acid (85% from Panreac Quimica) were used for HPLC analysis. H_2O_2 (30%, w/w, from Merck), $FeSO_4·7H_2O$ (Panreac PA), liver bovine catalase (Sigma-Aldrich), $NaHSO_3$ and MeOH (Panreac PAI) reagents were used without further purification.

2.2. Analysis

All samples were previously filtered with a polyethersulfone membrane (0.45 μm, Chmlab group) to remove the catalyst before analytical procedures. MET concentrations were monitored by HPLC Waters with a SEA18 column (5 μm, 25 × 0.46 cm, Teknokroma—Spain) and a Waters 996 photodiode array detector. The mobile phase was composed of water (pH 3 adjusted by orthophosporic acid) and acetonitrile (80:20), injected with a flow-rate of 0.85 mL/min and detected at its maximum UV absorbance of 221.9 nm. TOC was analyzed with a Shimadzu TOC-V CNS analyzer. To analyze COD, the Standard Methods (5220D) procedure was followed, using a spectrophotomer (Hach Lange DR 2500) at 420 nm. Biochemical oxygen demand (BOD_5) was determined according to Standard Methods (5210) by respirometric process using OxiTop equipment, during five days, under constant stirring and controlled temperature (20 °C ± 1 °C). H_2O_2 consumption was followed using the metavanadate spectrophotometric procedure [17]. H_2O_2 containing samples were quenched with sodium hydrogen sulfite, liver bovine catalase or the same volume of methanol to avoid further reactions depending on the analysis to be done. The ecotoxicity of the samples were measured by the acute toxicity using Microtox tests, where the inhibition of *Vibrio fischeri* bioluminescence at 15 min of incubation was determined. For the intermediates identification, samples were analyzed by the electrospray ionization/mass spectrometry using an electrospray (ion spray) ESI–MS, and a LCMSD–TOF (2006) mass spectrometer.

2.3. Solarbox: Artificial solar irradiation

Photocatalysis and photo-Fenton experiments were carried out in a solarbox (CO.FO.ME.GRA 220 V 50 Hz) with a Xenon lamp (Phillips XOP 1 kW), located at the top of the Solarbox [14,18]. The tubular photoreactor (24 cm length × 2.11 cm diameter) was placed at the bottom of the solarbox in the axis of a parabolic mirror. The radiation arriving at the photoreactor (2.68 μEinstein/s) was measured by *o*-Nitrobenzaldehyde (*o*-NB) actinometry 290–400 nm [19]. The procedure was as follows: batch tank (total volume 1 L) was fed with MET solution (50 mg/L) following the addition of TiO_2 (0.4 g/L) or Fe^{2+} (2.5, 10 mg/L) and/or H_2O_2 (25, 150 mg/L). In order to keep the solution at 25 °C or 14 °C, the jacket temperature of the stirred tank was controlled with an ultra-thermostat bath (Haake K10).

Samples were collected from the batch tank every 60 min during 360 min for the photocatalytic process. Photo-Fenton process was considered as complete when all H_2O_2 was consumed. Most experiments in solarbox were performed twice in order to ensure the system reproducibility and the error was calculated based on the standard deviations.

Radiation between 300 and 400 nm was considered for the TiO_2 experiments and between 300 and 500 nm for the photo-Fenton

technology since the photolysis of Fe(III) complexes with organic ligands is efficient up to 500 nm.

2.4. Double jacket reactor

All experiments for UV/H_2O_2 were performed in a thermostated Pyrex-jacketed 2 L vessel, equipped with three fluorescent low pressure mercury lamps (Phillips TUV 8 W, G8T5), emitting monochromatic radiation with a maximum at 254 nm. The light inside the photoreactor was assessed with actinometric experiments [20] and the obtained value was 1.70 μEinstein/s at 254 nm. The solution was fully stirred with a magnetic stirrer to ensure sufficient mixing. The reaction temperature was kept constant at 25 °C. UV/H_2O_2 experiments were considered finished once H_2O_2 reached a value of 10 mg/L due to the marked kinetic slowing down.

3. Results and discussion

3.1. Direct photolysis of MET

MET (initial concentration 50 mg/L) direct irradiation was carried out. MET removal achieved was 94%, using monochromatic radiation at 254 nm, and 18.0%, using solarbox, both after 300 min of irradiation. Moreover, mineralization accomplished resulted to be negligible for both processes (6% at 300 min). Experimental data were fitted to first order kinetics and the values obtained for the apparent rate constants were calculated from the slopes of the regression curves representing $-\ln(C/C_0)$ vs time. Thus, the apparent rate constants obtained were $0.00067\ min^{-1}$ ($R^2 = 0.994$) and $0.0101\ min^{-1}$ ($R^2 = 0.991$), for Xe and UV-C lamps, respectively. This behavior could be explained from MET absorption spectrum presented in Fig. 1, showing that MET has main UV absorption peaks centered on 221 and 273 nm. This means that UV-C spectrum covers much better than Xe lamp the zone where MET absorbs, and for this reason the photolysis of MET is faster with UV-C radiation.

3.2. Photocatalysis of MET

Four different catalyst loads were assessed for 0.05, 0.1, 0.4 and 0.5 g/L TiO_2 to choose the optimum catalyst concentration for further comparison with other processes.

Working with 0.5 g/L TiO_2, catalyst sedimentation at the bottom of the reactor was observed, therefore this catalyst concentration was not considered for the experiments. Figs. 2 and 3 show the effect of TiO_2 concentration on MET degradation and mineralization, and both improve when titania concentration increases.
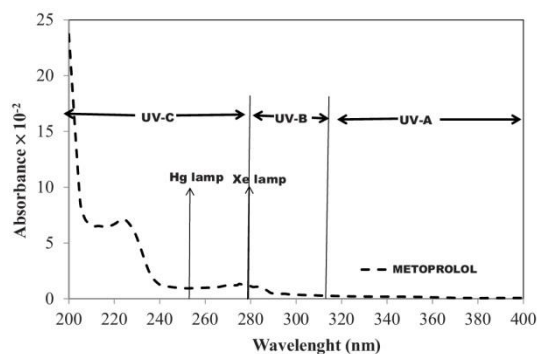

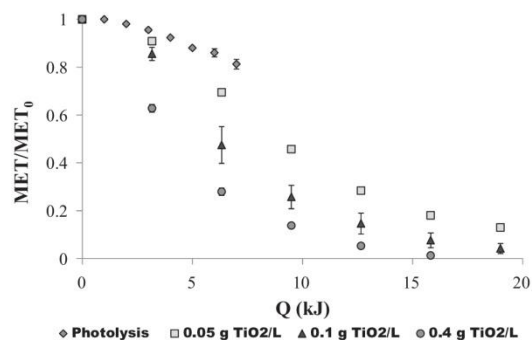
Fig. 1. MET absorption spectrum.

Fig. 2. MET degradation at different TiO$_2$ concentrations as function of accumulated energy.

The accumulated arriving energy necessary to achieve 90% of MET degradation was 22.0 kJ (after 418 min), 14.9 kJ (after 283 min) and 11.5 kJ (after 218 min) for 0.05, 0.1, and 0.4 g/L, respectively. Obviously, the energy needed decreases when TiO$_2$ concentration increases (1.9 times higher for 0.05 than for 0.4 g/L). These results can also be analyzed from the ratio MET degraded/accumulated energy. Following this criteria the results obtained are: 2.0 mg MET/kJ, 2.9 mg MET/kJ and 3.8 mg MET/kJ, for 0.05, 0.1 and 0.4 g/L TiO$_2$, respectively, obtaining the highest elimination rate using the highest catalyst concentration.

Mineralization was also evaluated using as a reference point the same accumulated energy (15.8 kJ). The conversion achieved was 20.5%, 34.6% and 45.6% for 0.05, 0.1 and 0.4 g/L TiO$_2$ respectively. Thus, the highest TiO$_2$ loading represents the best work conditions for TOC removal.

MET evolution was approached to first order kinetics. The kinetic apparent constants obtained were 0.0061 min^{-1} ($R^2 = 0.975$), 0.0093 min^{-1} ($R^2 = 0.987$) and 0.012 min^{-1} ($R^2 = 0.988$), for 0.05, 0.1 and 0.4 g/L TiO$_2$, respectively.

3.3. Photo-Fenton oxidation experiments

3.3.1. Preliminary experiments

As known, in photo-Fenton, H$_2$O$_2$ concentration is an important factor and an excess or absence of this reagent tends to reduce significantly the efficiency of the treatment.

Some preliminary assays were done to assure possible MET degradation not referable to photo-Fenton process. Thus, MET
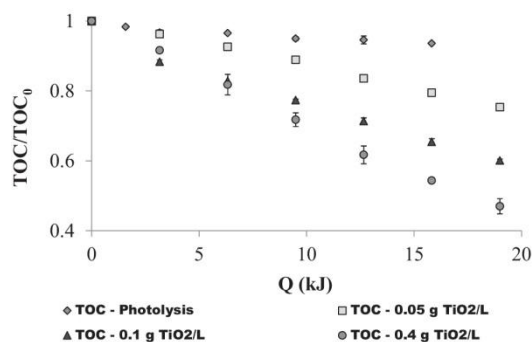

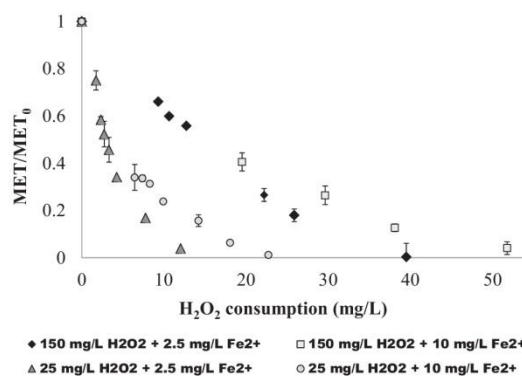**Fig. 3.** TOC profiles for the different TiO$_2$ concentrations assayed.

Fig. 4. MET degradation profiles for the different initial H$_2$O$_2$ and Fe^{2+} concentrations used.

degradation by hydrogen peroxide in the dark does not show significant oxidation. Also, photolysis with H$_2$O$_2$ (150 and 25 mg/L) was investigated and transformation resulted more significant. MET removal achieved was 32.5% and 14.6%, after 120 min, for 150 mg/L H$_2$O$_2$ and 25 mg/L H$_2$O$_2$, respectively. However, mineralization was negligible. Photolysis with iron (10 mg/L Fe^{2+}), in absence of hydrogen peroxide, drives to 90% of MET degradation, after 120 min, and 11.8% of mineralization. Finally, Fenton process was performed (150 mg/L H$_2$O$_2$ and 10 mg/L Fe^{2+}), after 10 min MET was degraded 62.8% but the mineralization obtained was too low ($\sim$10%).

3.3.2. Effect of hydrogen peroxide addition

Once all preliminary experiments were done and their impacts in MET degradation were measured, photo-Fenton experiments were carried out. The first variable studied was H$_2$O$_2$ initial concentration.

In Figs. 4 and 5, the hydrogen peroxide consumption effect on MET elimination and mineralization can be seen, suggesting a high efficiency of the photo-Fenton process when the lowest Fe^{2+} concentration was used. The faster MET removal was obtained using 2.5 mg/L Fe^{2+} and 25 mg/L H$_2$O$_2$.

This behavior is better explained according to the reactions that could take place in the solution, because high concentration of H$_2$O$_2$ scavenges the HO$^\bullet$ radicals, making the process less effective Eq. (1).

$$HO^\bullet + H_2O_2 \rightarrow HO_2^\bullet + H_2O \tag{1}$$

Moreover, an excess of H$_2$O$_2$ produces a higher concentration of ferric ions (Fe^{3+}) as a by-product of the oxidation reaction between
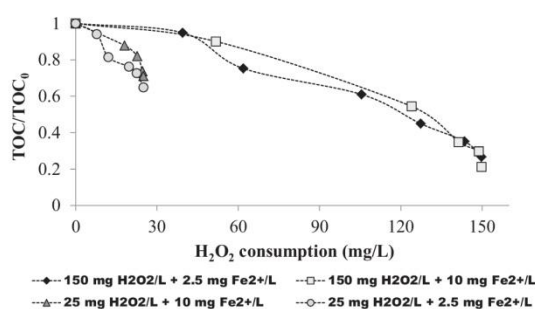

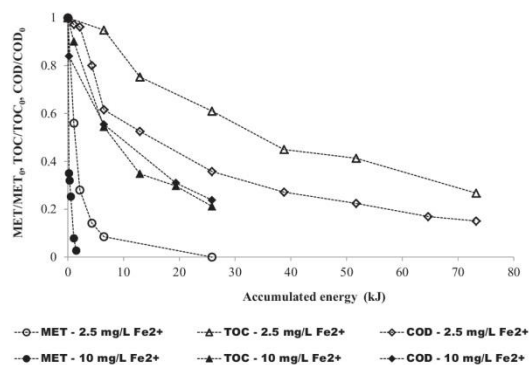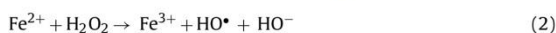**Fig. 5.** Mineralization profiles for the different initial H$_2$O$_2$ and Fe^{2+} concentrations.

Fig. 6. Photo-Fenton process: MET, TOC and COD degradation profiles for the different initial Fe^{2+} concentrations assayed. $[MET]_0 = 50$ mg/L, $[H_2O_2]_0 = 150$ mg/L.

Fe^{2+} and H_2O_2, which would prevail in the aqueous medium, reducing the effectiveness of the process Eq. (2).

$$Fe^{2+} + H_2O_2 \rightarrow Fe^{3+} + HO^\bullet + HO^- \qquad (2)$$

The explanation for this behavior is also complemented latterly when the effect of iron concentration is discussed (see Section 3.3.3).

3.3.3. Effect of iron concentration

Two different amounts of Fe^{2+} were used: 2.5 mg/L and 10 mg/L. As it can be broadly found in literature [21], in "normal" photo-Fenton applications (i.e., pH < 3, dissolved iron as catalyst), an increase in iron concentration always led to an increased reaction rate as well. This increase depends on the geometry of the reactor and the light pathway (it is important that all the reactor is "illuminated" so all the iron can be used) and on the competition for light between iron and the rest of substances present in the solution (normally photolysis reactions are less efficient than photo-Fenton reactions).

In Fig. 6, MET degradation as well as COD and TOC removal against time are depicted for Fe^{2+} concentrations of 2.5 and 10 mg/L. The initial H_2O_2 concentration was the same in both series, 150 mg/L. As it can be observed, in all the series, the higher concentration of Fe^{2+} leads to a higher degradation rate. When 10 mg/L Fe^{2+} were used, the 90% of MET was removed in 5 min whereas 30 min were necessary when 2.5 mg/L Fe^{2+} were added to the system. It means that increasing Fe^{2+} with a factor of 4, the degradation time was reduced by a factor of 6. The important increase in the degradation rate would point out also that probably no dark areas are present in this system even with the highest concentration of iron.

Similar behavior was observed for TOC removal and the mineralization is much faster when 10 mg/L Fe^{2+} were used. For the test conditions, the H_2O_2 was exhausted in 120 min whereas 340 min were needed in the experiments with 2.5 g/L Fe^{2+}. However, the final mineralization achieved was very similar for both amounts of Fe^{2+} used (78% and 71%, respectively). It is also noteworthy to mention the high final mineralization values obtained with this process.

Although not so remarkable, also COD removal was faster when 10 mg/L Fe^{2+} was used but again the final COD conversion obtained when all H_2O_2 was consumed was very close for both concentrations of iron used.

This fact is in agreement with Fig. 5 which shows that TOC was not a function of Fe^{2+} concentration but initial H_2O_2 concentration. Fig. 5 also shows how the system was more efficient for the lowest amount of H_2O_2 added, probably because less $OH^\bullet$ were lost due to
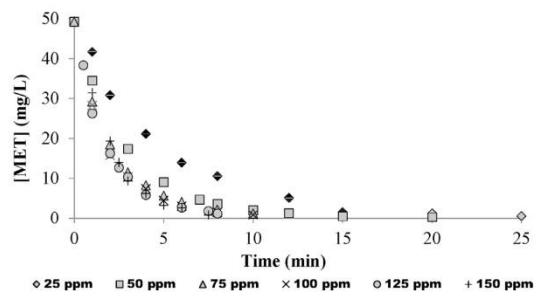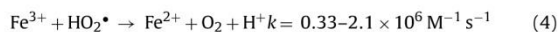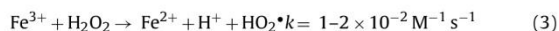

Fig. 7. MET degradation profiles for the different initial H_2O_2 concentrations tested.

recombination or direct reaction with peroxide. Actually, final conversions studied are mainly influenced by the amount of oxidant added to the system. The amount of Fe^{2+} only affects the speed to reach that point, i.e., the degradation rate, but not the extension of the degradation.

3.3.4. Effect of temperature

Two temperature conditions were chosen (14 °C and 25 °C) based on the common values found for wastewater streams in the area of study at different seasons. Increasing temperature leads to faster kinetics of the process [21]. In the current study also MET and TOC degradations were faster in the experiments at 25 °C but the differences were not really very important.

H_2O_2 consumption was higher at 25 °C. Actually, at 14 °C the system achieved a similar mineralization but consuming 25% less of H_2O_2. It means that the system was less efficient at the higher temperature. A possible explanation refers to the different influence that temperature presents over the several reactions taking place during the process. When increasing the temperature, some reactions which consume H_2O_2 but not produce $OH^\bullet$ are thermally favored, as for example the thermal reactions involved in the reduction of Fe^{3+} particularly Eqs. (3)–(5). Thus, the overall efficiency decreases.

$$Fe^{3+} + H_2O_2 \rightarrow Fe^{2+} + H^+ + HO_2^\bullet \, k = 1 - 2 \times 10^{-2} \, M^{-1} \, s^{-1} \qquad (3)$$

$$Fe^{3+} + HO_2^\bullet \rightarrow Fe^{2+} + O_2 + H^+ \, k = 0.33 - 2.1 \times 10^6 \, M^{-1} \, s^{-1} \qquad (4)$$

$$Fe^{3+} + O_2^{\bullet-} \rightarrow Fe^{2+} + O_2^\bullet \, k = 0.05 - 1.9 \times 10^9 \, M^{-1} \, s^{-1} \qquad (5)$$

On the other hand, in the photo reduction pathway, Fe^{3+} is reduced without consuming H_2O_2 and generates $HO^\bullet$.

$$Fe^{3+} + H_2O + h\nu \rightarrow Fe^{2+} + H^+ + HO^\bullet \qquad (6)$$
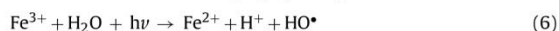
3.4. UV-C/H₂O₂ process

Several experiments using different initial H_2O_2 concentrations (from 25 to 150 mg/L) were performed in order to assess the performance of the UV/H_2O_2 process to degrade MET. For this purpose, MET concentration and several typical water quality parameters (TOC, COD, BOD_5 and UV_{254} absorbance) were monitored during the reactions. H_2O_2 concentration along the process was also followed.

As Fig. 7 shows, MET degradation rate increased with the initial H_2O_2 concentration used until a value of 75 mg H_2O_2/L. No significant improvements were observed for higher initial doses of oxidant. Therefore, an initial dose of 75 mg H_2O_2/L exhibited the best performance regarding the MET degradation.

Final TOC, COD and UV_{254} absorbance removals increased linearly with the initial H_2O_2 dose used as observed in Fig. 8. Maximum eliminations of TOC, COD and UV_{254} resulted in values of 56.1, 90.5 and 54.6%, respectively for the highest initial dose of H_2O_2.
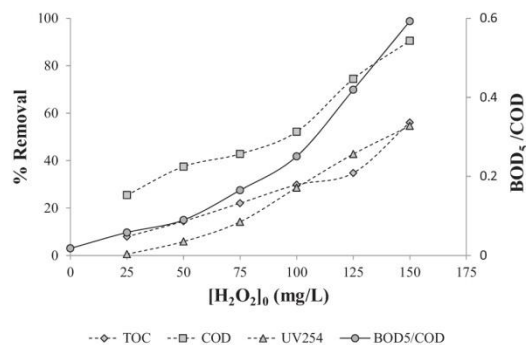
Fig. 8. Water quality parameters for the effluents obtained as function of the initial H_2O_2 used.

Regarding biodegradability, similar increasing trend was obtained. Acceptable BOD_5/COD values (0.25) in order to perform a subsequent biological treatment were already obtained for an H_2O_2 dose of 100 mg/L.

H_2O_2 consumption profiles denoted a significant competition of H_2O_2 and organic matter for UV light in the reaction system. Higher H_2O_2 initial doses (after 100 mg H_2O_2/L) allowed faster and higher mineralization of organic carbon which resulted in shorter times required for total consumption of H_2O_2.

3.5. Set-up comparison

For comparison, the radiation entering the different reactors was measured by actinometric methods, taking into account the useful wavelengths involved in each photo-oxidation process and the emission spectrum of the radiation source. The radiation was 0.88 J/s (between 300 and 400 nm) in the case of photocatalysis with TiO_2, 3.59 J/s (between 300 and 500 nm) for the photo-Fenton experiments, and 8.01 J/s for the UV-C lamp (254 nm).

The performance of the three set-ups in MET elimination is compared on basis of the ratio removed MET/accumulated energy. 90% of MET removal was chosen since MET removal rates became too slow near the total elimination. To complete the analysis, the TOC and COD removal per kJ of energy were also studied. In this case, 18 kJ/L was chosen as common criteria for the calculation of the ratios. Obtained values are shown in Fig. 9.

As it can be observed in Fig. 9, UV/H_2O_2 shows an efficiency ratio higher than the other two technologies in MET removal. In
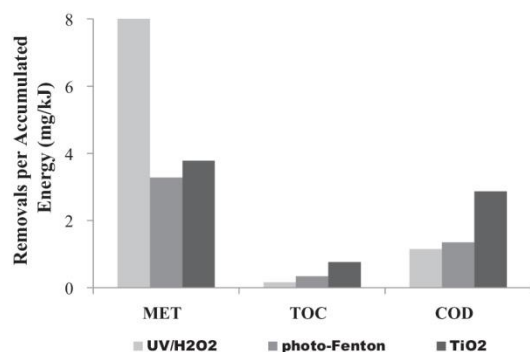

Fig. 9. Removals of MET, TOC and COD per accumulated energy in the three used set-ups.
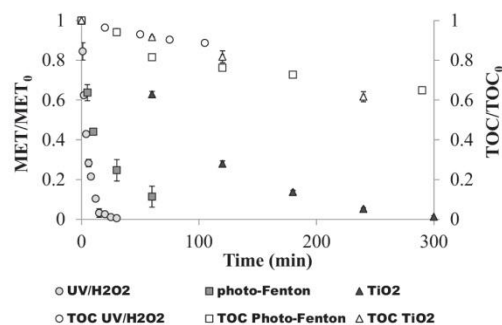

Fig. 10. MET and TOC removal profiles for the different processes tested.

addition, significant differences could be observed regarding the amounts of H_2O_2 consumed to achieve 90% of MET removal: 4.2 and 15.6 mg/L in UV/H_2O_2 and photo-Fenton, respectively. The high MET absorbance centered on 221 and 273 nm seems to be responsible for the good performance of UV/H_2O_2 process in MET elimination. Regarding the TOC elimination (see Fig. 10), the order in performance resulted curiously in the opposite than in MET degradation. TiO_2 photocatalysis also presented double efficiency ratio values for COD elimination compared to photo-Fenton and UV/H_2O_2 processes. In addition, UV/H_2O_2 and photo-Fenton reactions consumed 17.2 and 15.5 mg/L of H_2O_2, respectively when 18 kJ/L entered into the reaction systems.
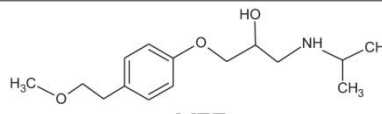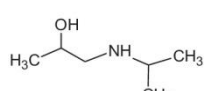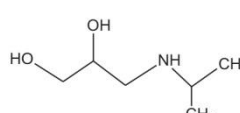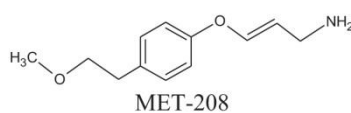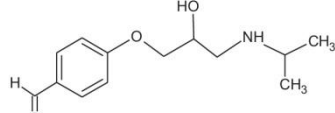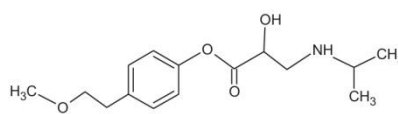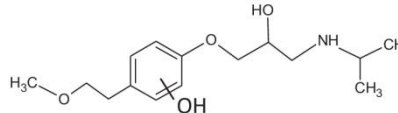
Fig. 10 shows the MET and TOC elimination profiles in terms of time. The UV/H_2O_2 system seems to be more optimized than the photo-Fenton one in terms of used radiation. The photo-Fenton system took almost double time (180 min) to consume 90% of the initial dosified H_2O_2. This difference between both technologies can be attributed to the effect of the direct photolysis of MET in UVC system. However, it is important to remark that only 11% of TOC removal was achieved by the UV/H_2O_2 process while 28% was eliminated by the photo-Fenton system when the same amount of H_2O_2 had been consumed (90%). The photo-Fenton set-up also achieved a reasonably rapid elimination of MET. On the other hand, the TiO_2 photocatalysis system exhibited much longer times to achieve the total MET elimination. However, similar to photo-Fenton, the TiO_2 system reached high eliminations of TOC in similar times.

To complement the information about the hazardousness of a treated solution, the toxicity assessment was also carried out for all systems. The toxicity of the treated sample shows that the oxidation of MET promoted the overall toxicity reduction of the sample since the beginning of the treatment. The initial equitox value of the untreated solution was ~6.2 and after to treat the solutions, the equitox values were 0.72, 0.56 and 0.51 for photocatalysis, UV/H_2O_2 and photo-Fenton, respectively.

Intermediates identification was carried out in samples taken in the middle and at the end of the experiments. Several ions masses were identified during MET degradation for all processes. The m/z (mass to charge ratio) are shown in Table 1.

According to the proposed structures, different degradation pathways could be deducted from the three processes tested. However, a predominant molecular weight $m/z = 268$ has been detected in common for the three cases (photocatalysis, UV/H_2O_2 and photo-Fenton), and it corresponds to metoprolol. The metoprolol molecule can be divided according to the detected structures as phenoxy group, ether side chain, and ethaloamine side chain. MET-134 is the aliphatic chain breakdown product of metoprolol. This amino-diol was identified as one of the dominant intermediates in photocatalysis, photo-Fenton and UV/H_2O_2 processes. MET-134 showed

Table 1
Metoprolol and its main intermediates detected by LC/MS analysis in photocatalysis, photo-Fenton and UV/H_2O_2 experiments.

m/z (Da)	Elemental composition	Proposed structure (Label)	Advanced oxidation processes (retention time, min)		
			Photocatalysis	Photo-Fenton	UV/H_2O_2
268	$C_{15}H_{25}NO_3$	MET	√ (3.24)	√ (5.87)	√ (5.993)
118	$C_6H_{15}NO$	MET-118	√ (3.24)	√ (3.17)	–
134	$C_6H_{15}NO_2$	MET-134	√ (2.59)	√ (2.40)	√ (2.30)
208	$C_{12}H_{17}NO_2$	MET-208	√ (3.24)	–	–
238	$C_{13}H_{19}NO_3$	MET-238	√ (4.71)	√ (3.41)	–
282	$C_{15}H_{24}NO_4$	MET-282	–	–	√ (5.993)
284	$C_{15}H_{26}NO_4$	MET-284	–	–	√ (4.68)

a prominent product at MET-118 in photocatalytic and photo-Fenton treatment, corresponding to the elimination of the hydroxyl group. The HO• attack to the ether oxygen and the oxidation of the hydroxyl group yields the MET-282 in UV/H_2O_2 process. In the case of photocatalytic treatment MET-208 is formed through the loss of water and isopropyl group from the ethanolamine chain reaction. Hydroxylated metoprolol with m/z 284 was detected, in considerable intensity, only in UV/H_2O_2 process as a result of the HO• attack on the C atoms of the aromatic ring. In photocatalytic treatment a new intermediate MET-238, has been formed by loss of the ether group, H-abstraction, possibly upon HO• radical attack on the alkyl group, and O-atom addition.

4. Conclusions

The three AOPs tested (UV/H_2O_2, photocatalysis with TiO_2 and photo-Fenton) achieved practically the total MET removal.

Comparisons between the processes established that UV/H_2O_2 shows the highest efficiency in the ratio removed MET/accumulated energy and the highest rate of MET elimination, probably because MET has main UV absorption peaks centered on 221 and 273 nm.

Concerning the TOC elimination, the order in performance resulted in the opposite than in MET degradation, and the highest efficient ratio TOC removal/accumulated energy was obtained

for the photocatalysis, the UV/H_2O_2 process being the worst in this case.

Similar behavior was observed in the COD removal, the higher efficiency in the ratio of COD removal/accumulated energy was also for photocatalytic process, and photo-Fenton and UV/H_2O_2 processes show very close results.

The ratios between the removal of pharmaceutical (or TOC or COD) and the energy used can be a good tool for the comparison of the efficiencies of different AOPs.

Regarding to toxicity and intermediates, all processes have promoted the overall toxicity reduction of MET solution and the three processes present different path ways for MET degradation, according to the intermediates detected.

Acknowledgments

References

[1] F.J. Benitez, J.L. Acero, F.J. Real, G. Roldan, F. Casas, Bromination of selected pharmaceuticals in water matrices, Chemosphere 85 (2011) 1430–1437.

[2] E. Vulliet, C. Cren-Olivé, M.-F. Grenier-Loustalot, Occurrence of pharmaceuticals and hormones in drinking water treated from surface waters, Environ. Chem. Lett. 9 (2009) 103–114.

[3] J.A. Dougherty, P.W. Swarzenski, R.S. Dinicola, M. Reinhard, Occurrence of herbicides and pharmaceutical and personal care products in surface water and groundwater around Liberty Bay, Puget Sound, Washington, J. Environ. Qual. 39 (2010) 1173.

[4] J.A. Polar, The fate of pharmaceuticals after wastewater treatment, Florida Water Resour. J. (2007) 26–31.

[5] M.J. Martín de Vidales, C. Sáez, P. Cañizares, M.A. Rodrigo, Metoprolol abatement from wastewaters by electrochemical oxidation with boron doped diamond anodes, J. Chem. Technol. Biotechnol. 87 (2012) 225–231.

[6] M.J.M. Bueno, M.J. Gomez, S. Herrera, M.D. Hernando, A. Agüera, A.R. Fernández-Alba, Occurrence and persistence of organic emerging contaminants and priority pollutants in five sewage treatment plants of Spain: two years pilot survey monitoring, Environ. Pollut. 164 (2012) 267–273.

[7] E. Gracia-Lor, J.V. Sancho, R. Serrano, F. Hernández, Occurrence and removal of pharmaceuticals in wastewater treatment plants at the Spanish Mediterranean area of Valencia, Chemosphere 87 (2012) 453–462.

[8] E.U., Directive 2000/60/EC of the European Parliament and of the Council of 23 October 2000 establishing a framework for community action in the field of water policy, in: Water Framework Directive, 2000.

[9] F.J. Benitez, J.L. Acero, F.J. Real, G. Roldan, F. Casas, Comparison of different chemical oxidation treatments for the removal of selected pharmaceuticals in water matrices, Chem. Eng. J. 168 (2011) 1149–1156.

[10] J. Corcoran, M.J. Winter, C.R. Tyler, Pharmaceuticals in the aquatic environment: a critical review of the evidence for health effects in fish, Crit. Rev. Toxicol. 40 (2010) 287–304.

[11] J. Huang, J. Sun, X. Zhou, T. You, Determination of atenolol and metoprolol by capillary electrophoresis with tris(2,2′-bipyridyl)-ruthenium(II) electrochemiluminescence detection, Anal. Sci. 23 (2007) 183–188.

[12] Medsafe, AFT-Metoprolol CR, 2013, http://www.medsafe.govt.nz/profs/datasheet/a/AFTMetoprololCRtab.pdf.

[13] F.J. Rivas, O. Gimeno, T. Borrallo, UV-C radiation based methods for aqueous metoprolol elimination, J. Hazard. Mater. 179 (2010) 357–362.

[14] V. Romero, N. De La Cruz, R.F. Dantas, P. Marco, J. Giménez, S. Esplugas, Photocatalytic treatment of metoprolol and propranolol, Catal. Today 161 (2011) 115–120.

[15] M. Šćepanović, B. Abramović, A. Golubović, S. Kler, M. Grujić-Brojčin, Z. Dohčević-Mitrović, et al., Photocatalytic degradation of metoprolol in water suspension of TiO_2 nanopowders prepared using sol–gel route, J. Sol-Gel Sci. Technol. 61 (2011) 390–402.

[16] L. Prieto-Rodríguez, I. Oller, N. Klamerth, A. Agüera, E.M. Rodríguez, S. Malato, Application of solar AOPs and ozonation for elimination of micropollutants in municipal wastewater treatment plant effluents, Water Res. 47 (2013) 1521–1528.

[17] R.F.P. Nogueira, M.C. Oliveira, W.C. Paterlini, Simple and fast spectrophotometric determination of H_2O_2 in photo-Fenton reactions using metavanadate, Talanta 66 (2005) 86–91.

[18] V. Romero, P. Marco, J. Giménez, S. Esplugas, Adsorption and photocatalytic decomposition of the β-blocker metoprolol in aqueous titanium dioxide suspensions: kinetics, intermediates and degradation pathways, Int. J. Photoenergy 2013 (2013), http://dx.doi.org/10.1155/2013/138918 (Article ID 138918, 10 pages).

[19] N. De la Cruz, V. Romero, R.F. Dantas, P. Marco, B. Bayarri, J. Giménez, S. Esplugas, o-Nitrobenzaldehyde actinometry in the presence of suspended TiO_2 for photocatalytic reactors, Catal. Today 209 (2013) 209–214.

[20] H.J. Kuhn, S.E. Braslavsky, R. Schmidt, Chemical actinometry (IUPAC technical report), Pure Appl. Chem. 76 (2004) 2105–2146.

[21] S. Malato, P. Fernández-Ibáñez, M.I. Maldonado, J. Blanco, W. Gernjak, Decontamination and disinfection of water by solar photocatalysis: recent overview and trends, Catal. Today 147 (2009) 1–59.

Comparing the photocatalytic oxidation of Metoprolol in a solarbox and a solar pilot plant reactor

CrossMark

Violette Romero [a,*], Fabiola Méndez-Arriaga [b], Pilar Marco [a], Jaime Giménez [a], Santiago Esplugas [a]

[a] *Department of Chemical Engineering, University of Barcelona, C/Martí i Franquès 1, 08028 Barcelona, Spain*
[b] *Engineering Institute, Universidad Nacional Autónoma de México, UNAM, Circuito Universitario, 04510 México City, Mexico*

HIGHLIGHTS

- We studied Metoprolol degradation by photolysis and photocatalysis processes.
- We studied Metoprolol degradation by UV–Vis/H_2O_2 and UV–Vis/H_2O_2/ TiO_2 processes.
- Two experimental devices were compared: solarbox (SB) and a solar pilot plant (CPC).
- Photocatalysis and UV–Vis/H_2O_2/TiO_2 appeared as useful for Metoprolol degradation.
- The required energy to remove 1 mg of MET decreases as TiO_2 concentration increases.

GRAPHICAL ABSTRACT
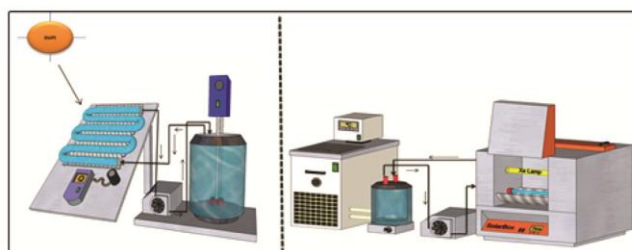
ABSTRACT

The aim of this work is to study and compare the removal of Metoprolol (MET) "1-(isopropylamino)-3-[p(β-methoxyethyl)phenoxy]-2-propanol" by photolysis, photocatalysis/TiO_2, UV–Vis/H_2O_2 and UV–Vis/H_2O_2/TiO_2 processes using two different experimental devices: solarbox (SB) with a Xe lamp and a solar pilot plant reactor with compound parabolic collectors (CPCs). Photolysis shows low MET removal (14% and 8%) with SB and CPCs respectively, and TOC almost negligible. Different TiO_2 concentrations (0.05, 0.1 and 0.4 g/L) were used in both devices and the best results were obtained for 0.4 g/L, after 360 min of irradiation (Q = 19 kJ/L) with complete MET elimination and 55% of TOC removal in SB. Tests done with real matrix water show a decrease in MET removal to 21% due the competition of the organic matter present for light and catalyst. The UV–Vis/H_2O_2/TiO_2 process represents an improvement with respect to the photocatalytic process (without H_2O_2) and times required to achieve the same MET o TOC removal are shortened in both devices, for instance, 120 min for total MET removal in SB. The best mg H_2O_2/mg MET ratio was 3. The MET photocatalysis (in solarbox) increases biodegradability and the treated solutions can be coupled to biological process after 360 min of irradiation and the solution treated in CPC reactor, after 270 min, remains not biodegradable. A pseudo-first order kinetics in photocatalytic processes were calculated in SB and CPC reactors. The toxicity, measured by *Vibrio Fischeri* method, decreases when MET is degraded by photocatalysis/TiO_2 and UV–Vis/H_2O_2/TiO_2 processes in both devices. The major reaction intermediates in UV–Vis/H_2O_2/TiO_2 process were identified by ionization/mass spectrometry and a MET photo-degradation pathway was proposed.

Finally, in photocatalysis (0.4 g/L TiO_2) the energy needed to degrade 1 mg of MET, at 240 min was evaluated, being 0.275 and 0.065 kJ/mg MET for SB and CPCs respectively.

© 2014 Elsevier B.V. All rights reserved.

* Corresponding author. Tel.: +34 680236937; fax: +34 934021291.
E-mail address: violette.romero@ub.edu (V. Romero).

1. Introduction

A wide range of human pharmaceuticals and personal care products (PPCPs), also called emerging contaminants, have recently received important attention as organic micro-pollutants in aquatic environments [1–3]. These compounds have high biological activity, associated to persistent toxic character. Such characteristics imply a potential impact on aquatic species even at low concentrations [3]. Several studies have demonstrated that removal of these pollutants in sewage treatment plants (STPs) is often incomplete and they are continuously released to freshwater systems [3–6]. PPCPs have been found in surface and drinking waters at ng/L to g/L concentrations [1,3,7–10].

Metoprolol (MET) is a selective β-blocker applied for therapies such as treatment of angina, heart failure, high blood pressure [6,8,11]. MET occurrence in the environment has been reported, highlighting its presence in rivers from Netherlands (25–100 ng/L) [12], Poland (51–155 ng/L) [13], UK (7–11 ng/L) [14], Sweden (60–70 ng/L) [14], Germany (exceeding 1000 ng/L) [15] and other places (1540 ng/L) [9].

The presence of this particular type of emerging pollutant has raised concern about its potential impact on environmental and public health, and consequently an increasing interest in reliable processes for pollutant removal. The achievement of effective technologies for elimination of pharmaceuticals from their original sources, such as hospital effluents (Metoprolol 487 and 2232 ng/L) [16], domestic wastewaters (Metoprolol 2200 ng/L) [8], pharmaceutical industry discharges (PPCPs 10–100 mg/L) [17], etc., is an emerging research area in environmental engineering [18]. In this context, the Advanced Oxidation Processes (AOPs) are promising solutions to upgrade existing treatments. As known, AOPs are based on the presence and reactivity of the hydroxyl radical (HO·), generated in atmospheric or sub-supercritical conditions of temperature and pressure with or without catalyst and/or reactive energy (electrochemical, UV–Vis or ultrasounds) [19]. The heterogeneous photocatalysis (HP) by using TiO_2 semiconductor, Fenton and Photo-Fenton reaction, UV–H_2O_2 processes and sonolysis are extensively used AOPs for water treatment.

MET contaminant has been removed by AOPs such monochromatic UV (254 nm) radiation [11], Fenton and photo-Fenton reagent as well as UVC/H_2O_2 process [20]. HP has begun to be studied in our earlier report where two β-blockers degradation was assessed, using TiO_2 in suspension and a Xe lamp [21]. Also HP has been reported [6,20] in combination with additional oxidants (H_2O_2) [20], but they used high-pressure mercury lamps and higher TiO_2 loadings [6] or UVC low pressure Hg lamp [20]. Abramovic and co-workers [22] have also studied HP at laboratory scale but using UV-C lamps and focused on photocatalytic transformation of MET as a function of the TiO_2 specimen. Other studies working with natural irradiation have also been carried out but applying electrochemical techniques [23].

However MET removal with natural solar irradiation at pilot plant scale and at low catalyst concentration has not yet been reported and it may be advantageous, from an economical point of view. Solar photochemical detoxification technologies have been developed in the domain of chemical water treatment as clean energy and have led to an improvement in oxidative degradation procedures for organic compounds dissolved in aqueous media. The solar reactor used in this work at pilot plant scale was based on the Compound parabolic collector (CPC) configuration capable to collect the direct and diffuse UV radiation [24]. In addition, simulated solar irradiation in a solarbox was employed at lab scale.

The aim of this work was to move a step further in the evaluation and comparison of the efficiency of HP treatment of MET by using two irradiation sources (natural and artificial), employing TiO_2 in suspension with and without an external oxidant agent H_2O_2. The evolution of MET, TOC, COD and BOD_5 was monitored in order to reach information on the treated final effluent. Because of analytical difficulties, we used mass concentrations of mg/L, which indeed corresponds to the concentration range of various pharmaceuticals in industrial waste waters.

2. Materials and methods

2.1. Chemicals and reagents

Metoprolol Tartrate Salt, CAS: 56392-17-7 (99% purity, Sigma–Aldrich) was dissolved in Milli Q water (50 mg/L). MET properties are summarized in Table 1. Heterogeneous photocatalysis was performed using TiO_2 Degussa P-25 (Frankfurt, Germany). Acetonitrile (analytical reagent grade purchased from Fischer Chemical) and orthophosporic acid (85% from Panreac Quimica) were used for HPLC analysis. H_2O_2 (30%, w/w, from Merck), $NaHSO_3$ (Panreac, 40%, w/w) and MeOH (Panreac PAI) reagents were used without further purification. Real water was collected from the secondary clarifier of a wastewater treatment plant (WWTP) located in Gavà-Viladecans (Catalonia-Spain) and its physicochemical characterization is described in Table 2.
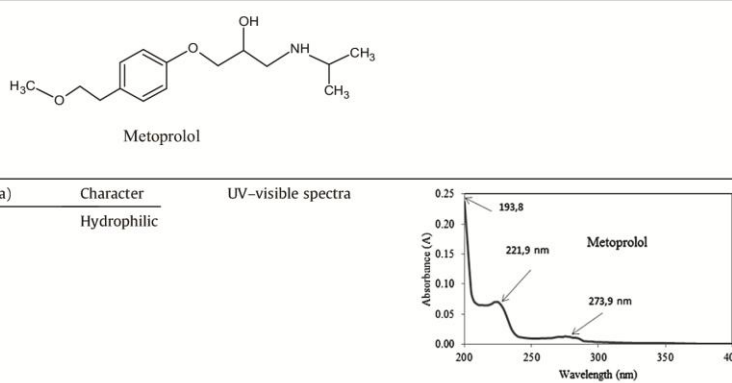
Table 1
Physicochemical properties of Metoprolol.

Metoprolol

Molecular weight	Dissociation constant (pKa)	Character	UV–visible spectra
267.36	9.2–9.6	Hydrophilic	

216

Table 2
Physicochemical characterization of filtered real water, from the secondary clarifier of a wastewater treatment plant (WWTP) (Catalonia-Spain).

Parameter	Value
BOD$_5$ (mg/L)	9
COD (mg/L)	54.7
TOC (mg/L)	11.6
UV absorbance at 254 nm (cm^{-1})	0.29
Turbidity (NTU)	2.1
pH	7.9
Total suspended solids (mg/L)	3.60
Volatile suspended solids (mg/L)	3.00
Chloride (mg/L)	589
Nitrite (mg/L)	9.9
Nitrate (mg/L)	30.1
Sulfate (mg/L)	205
Phosphate (mg/L)	9.2
Potassium (mg/L)	45
Magnesium (mg/L)	45
Calcium (mg/L)	124
Ammonium (mg/L)	<0.5
Alkalinity (mg HCO$_3$/L)	526.7

2.2. Techniques and analytical instruments

MET concentrations were monitored by HPLC from Waters using a SEA18 (250 × 4.6 mm i.d.; 5 μm particle size) Teknokroma column, and a Waters 996 photodiode array detector. The mobile phase was composed by water (pH 3) and acetonitrile (80:20), injected with a flow-rate of 0.85 mL/min. MET concentration was followed at UV maximum absorbance (221.9 nm). Total organic carbon (TOC) was measured with a Shimadzu TOC-V CNS instrument. For the chemical oxygen demand (COD) analysis, the Standard Methods (5220D) procedure was followed by use of a spectrophotomer (Hach Lange DR 2500) at 420 nm, employing Pyrex-glass vials, after 2 h of extreme catalytic oxidation conditions at 150 °C. Biochemical oxygen demand (BOD$_5$) was determined according to Standard Method 5210 by respirometric process using OxiTop equipment, during five days, under constant stirring and controlled temperature (20 °C ± 1 °C). The microorganism-seed (lyophilized capsules 5466-00, Cole-Parmer) were aerated during 2 h before inoculation. During the experiments H$_2$O$_2$ consumption was followed using metavanadate spectrophotometric procedure at 450 nm [25]. For the toxicity assessment, the bioassay Microtox was used, where the inhibition of *Vibrio fischeri* bioluminescence at 30 min of incubation was determined. In this

study the ecotoxicity is expressed as Equitox. For the intermediates identification, samples were analyzed by the electrospray ionization/mass spectrometry using an electrospray (ion spray) ESI–MS, and a LC/MSD-TOF (Agilent Technologies) mass spectrometer.

2.3. Experimental devices

2.3.1. Artificial solar irradiation: solarbox

Photocatalysis experiments were done in a solarbox (CO.FO.-ME.GRA 220 V 50 Hz, see Fig. 1) with a Xenon lamp (Phillips 1 kW), located at the top of the solarbox. The radiation entering the photoreactor (2.68 μEinstein/s) was measured by o-Nitrobenzaldehyde (o-NB) actinometry 290–400 nm [26]. The tubular photoreactor (24 cm length, 2.11 cm diameter) was placed at the bottom of the solarbox on the axis of a parabolic mirror made of aluminum reflective material inside of the chamber. A filter cutting off wavelengths under 280 nm was placed between the lamp and the reactor. Batch tank (total volume 1 L) was fed with MET solution (from 25 to 100 mg/L) following the addition of TiO$_2$ (from 0.05 to 0.4 g/L) and/or H$_2$O$_2$ (25 and 150 mg/L). Five minutes were sufficient to reach adsorption equilibrium, since the adsorption at free pH was negligible.

Samples were collected from the batch tank every 60 min during a total period of 300–360 min. All samples were filtered with a polyethersulfone membrane filter (0.45 μm, Chemlab) to remove the catalyst before analytical procedures. A preliminary sample was collected before irradiation to represent initial concentration at 0 min.

2.3.2. Solar irradiation: CPC reactor

Photocatalytic experiments were also carried out in a solar pilot plant (CPCs), at the University of Barcelona (latitude 41.4 N, longitude 2.1 W). The exposure time was approximately 5 h, from 13:00 to 18:00 h. The CPC consists in a module, 41° inclined and made of polished aluminum, with 6 parallel tubular quartz reactors. The total mirror's area for solar irradiation capture-reflection was 0.228 m^2 (see Fig. 2). The aqueous suspension (MET–TiO$_2$), with or without H$_2$O$_2$, was continuously pumped with a peristaltic pump from the stirred reservoir tank (10 L) to irradiated quartz tubes and continuously recirculated. The radiation arriving to CPC was determinated by a spectroradiometer Bentham DMc300 with double monochromatic measuring between 290 and 1100 nm. The data were integrated from 290 to 315 nm for UVB and 315 to 400 nm for UVA. Samples were collected from the reservoir tank every 30 min during a total period of 270–300 min. A
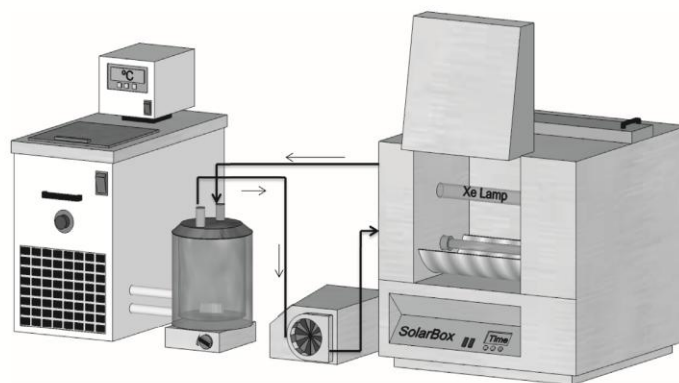

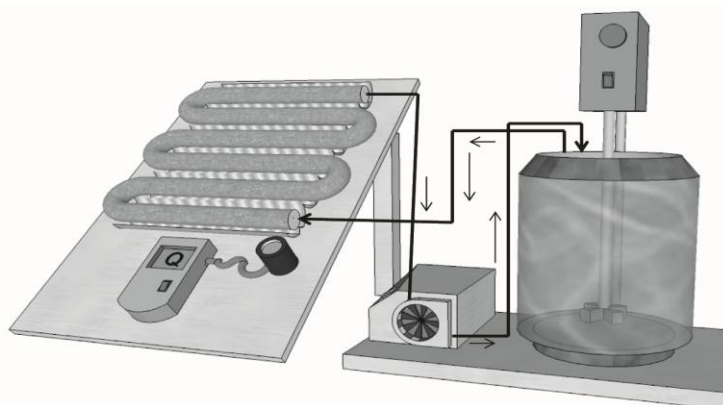**Fig. 1.** Solarbox and experimental instruments.

Fig. 2. CPC solar photoreactor.

Table 3
Technical characteristics of the solarbox and CPC photoreactors.

	Solarbox	CPC
Collector geometry	One-axis parabolic collector (PC)	Compound parabolic concentrator (CPC)
Collector material	Al-reflective mirrors	Al-reflective mirrors
Mirrós area (m²)	0.0151	0.228
Light source used	Xe-OP (Philips) 1000 W lamp	Solar light
Photoreactor number	1	6
Glass Material	Borosilicate Duran	Quartz
Total volume of photoreactor (L)	0.084	0.95
Total volume of suspension (L)	1	10
Virradiated (L)	0.084	0.95
Virr–Vdark (%–%)	8.4	9.5
Maximum temperature (°C)	25	25 ± 5
Stirring system	Magnetic	Mechanic external
Place localization (Coordinates)	University of Barcelona	At sea level Barcelona
Inclination (°)	0	(Latitude 41°28′, Longitude 2°06′)
Volumetric flow rate (L/min)	0.71	2.6

preliminary sample was collected before irradiation and represented initial time. TiO₂/H₂O₂ experiments were carried out till full peroxide consumption. Table 3 shows the most important technical parameters of solarbox and CPC reactors.

3. Results and discussion

3.1. Preliminary experiments: MET adsorption and photolysis

Preliminary experiments were carried out to study the termodegradation of 50 mg/L MET, in 0.4 g TiO₂/L suspension, at 20, 25, 40, and 60 °C, during 30 min at each temperature. The results showed that, at 20 and 25 °C, there was not MET degradation. At 40 and 60 °C, degradation was 2.8% and 3% respectively. There was not mineralization in any case.

Moreover, preliminary studies of MET adsorption on TiO₂ were carried out. Different MET concentrations (0, 12.5, 25, 50, 75 and 100 mg/L) were mixed with 0.4 g TiO₂/L, at natural pH (pH ≈ 6.0) and constant temperature (25 °C ± 0.5). After 1, 5 and 24 h of

contact, MET concentration was evaluated. Adsorption of MET onto TiO₂ was negligible. However, because the adsorption capacity is also influenced by pH, experiments were carried out varying the pH of suspension (3 and 9 with HCl and NaOH respectively). For acid condition, adsorption was not significant. In contrast in the case of pH 9 almost 14% of the initial substrate (50 mg/L) was adsorbed onto the catalyst. The last result is in agreement with the pK_a of MET (9.6, see Table 1) as well as the point of zero charge of TiO₂ (5.5–6.5). Thus, within the range 6.5 < pH < 9.6, the catalyst, with negative surface charge, attracts the dissociated MET cation and it can explain the 14% of MET adsorption at pH 9. The photocatalytic experiments were carried out at the free pH evolution in order to maintain operational conditions of common wastewater treatments.

On the other hand, photolysis experiments were carried out with 50 mg/L of initial MET in the solarbox and CPC reactor respectively without catalyst (25 ± 5 °C). The results observed during 240 min of irradiation confirmed the low influence of photolysis on MET degradation (14.0% and 8.1%, for solarbox and CPC respectively). Moreover, photolysis did not promote significant mineralization: the higher values reached were 5.4% and 2.7% in solarbox and CPC respectively.

3.2. Photocatalytic degradation at lab scale: solar simulator

The total accumulated energy Q (kJ/L) is calculated by:

$$Q = \sum_{i=0}^{n} \frac{I\Delta t_i}{V} \tag{1}$$

where I is the incident photon flow (kJ/s), Δt_i is the time between samples (s) and V is the volume of the treated solution.

3.2.1. Influence of initial MET concentration

The initial substrate concentration has a relevant influence on the overall photocatalytic performance. Photocatalytic experiments were carried out varying the initial MET concentration (25, 50 and 100 mg/L) using 0.4 g TiO₂/L and 1 L of total volume. Fig. 3(a and b) shows MET decay as well as mineralization degree. It is observed that at lower MET initial concentration there is higher TOC removal, and lower irradiation time is needed to reach full MET degradation. Degradation data were fitted to pseudo-first order kinetics and it was clearly appreciated that kinetic constant decreases when initial MET concentration increases, being the k values 2.7×10^{-2}, 1.2×10^{-2} and 7.3×10^{-3} min⁻¹ for 25, 50 and
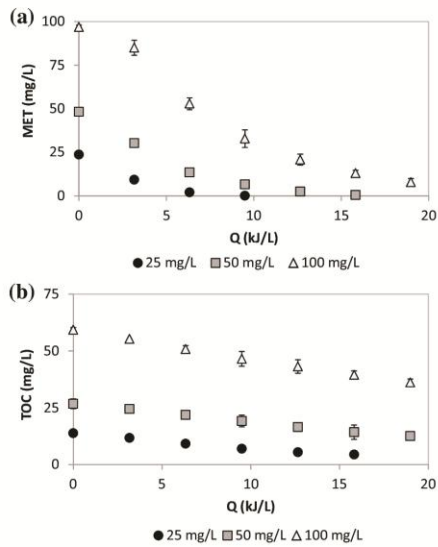
Fig. 3. Effect of the initial MET concentration on (a) MET degradation and (b) mineralization in solarbox device and 0.4 g/LTiO$_2$.

Fig. 4. Effect of the TiO$_2$ concentration on (a) MET degradation and (b) mineralization in solarbox device. Initial MET concentration 50 mg/L, free pH.

100 mg/L of MET respectively. When the initial concentration of reactant increases, the intermediates concentration also increases, leading to a slowdown in the disappearance of MET by the competition of intermediates.

The ratio removed MET/accumulated energy ((mg MET/L)/(kJ/L)) was calculated in order to compare the overall performance in MET elimination. At 9.5 kJ/L (180 min) the values obtained were 2.48, 4.38 and 6.73 mg MET/kJ, for 25, 50 and 100 mg/L of MET respectively. Thus, results show that for the same energy, a higher mass of pollutant is removed when the initial concentration is higher.

3.2.2. Influence of TiO$_2$ loading

The effect of the TiO$_2$ concentration (0.05, 0.10 and 0.40 g/L) was studied for degradation of MET (50 mg/L). Fig. 4 shows the behavior of the MET degradation and mineralization, in the solarbox, varying the catalyst loading.

Among the three concentrations of catalyst tested, when 0.4 g TiO$_2$/L was used, the best results could be observed. Higher TiO$_2$ concentrations were also tested but TiO$_2$ settling in the reactor was observed. Therefore, those catalyst amounts were discarded, because in our study the TiO$_2$ settling in the reactor could increases radiation scattering, decreasing the reaction rate.

MET was degraded completely within 300 min irradiation ($Q = 15.8$ kJ/L) using 0.4 g TiO$_2$/L in Mili Q water and 20.8% of conversion was achieved when real matrix water was used. Evidently, the real water matrix has a detrimental effect on conversion and this is believed to be due to the fact that the TOC of the real matrix water used represents approximately the 40% of the TOC corresponding to MET. Thus, after several hours of irradiation MET exhibits a low conversion due to the fact that reactive species produces by the photocatalytic process are partially consumed to attack the organic matter present in the real matrix water (see Table 2).

It is clear that the organic matter present in real matrix water when applying the photocatalytic process competes for the active species with MET and/or can absorber the photons and/or can produce screening effect of photons. On the other hand, the presence

of other species such as inorganic ions can produce inactivation of the catalyst surface. Thus, different species presents in the real water can be responsible for the low MET conversion.

For concentrations of 0.05, and 0.1 g TiO$_2$/L, after 300 min irradiation, MET conversion was 81.9% and 92.4% respectively. Fig. 5 shows MET conversion percentage reached at 300 min ($Q = 15.8$ kJ/L) for the different catalyst concentrations tested and its corresponding standard deviation.

In agreement with different authors the increase in the catalyst loading leads to higher MET degradation, however those studies have been done under different experimental conditions or/and using different β-blockers.
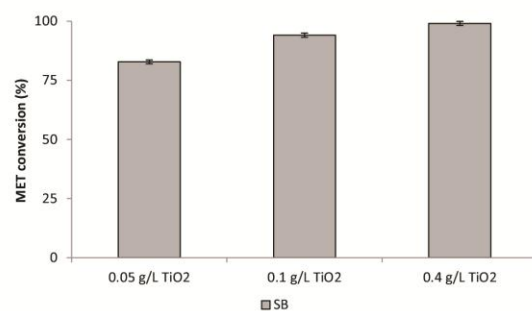
Fig. 5. MET conversion for different TiO$_2$ concentrations and its corresponding standard deviation in SB at 300 min of irradiation (Q:15.8 kJ).

Scepanovic and co-workers [27] used 34 mg/L of MET, 0.5–5.0 g/L of TiO$_2$ (prepared using sol–gel), UV radiation (CPC collector). They have reached a complete MET degradation after 60 min with an optimum catalyst concentration equal to 1 g/L TiO$_2$. Ioannou and co-workers [28] used 10 mg/L of Atenolol and Propranolol, 250 mg/L TiO$_2$ (Degussa P25) and Xe lamp. After 120 min of irradiation 58% and 64% of conversion were reached for Atenolol and Propranolol respectively. Rodriguez [29] studied as target compound 10 mg/L of Atenolol with TiO$_2$ concentrations between 0.05 and 0.2 g/L. De la Cruz [30] followed 50 mg/L of Propranolol degradation with TiO$_2$ (0.1, 0.2 and 0.4 g/L) using Xe lamp. This study after 240 min of irradiation reached 81.6%, 88% and 94.1% of Propranolol conversions. The values obtained in this study are so close to the results found in our study. Finally, Rivas [20] have used UVC radiation and 0.25–2.0 g/L TiO$_2$. The highest Met conversion obtained in their study was 10–20%, after 180 min of irradiation and they conclude that under UVC radiation increasing TiO$_2$ concentration did not affect the MET reaction rate.

MET mineralization varying catalyst concentration was also investigated and summarized in Fig. 4(b). TOC reduction was only 6.4% by photolysis. However, mineralization increased with TiO$_2$ loading. Thus, 20.6%, 34.6% and 45.2% of mineralization was obtained for 0.05, 0.1 and 0.4 g TiO$_2$/L, respectively, after 300 min of irradiation (Q = 15.8 kJ/L). Table 4 summarizes MET and TOC removal under several experimental conditions for solarbox and CPC reactors.

3.2.3. Influence of H$_2$O$_2$

The effect of H$_2$O$_2$ addition, as promoter, was evaluated without and with catalyst. In the first case, 25 and 150 mg/L of H$_2$O$_2$ were added to 50 mg/L MET solution directly in the batch tank. In the second case, 0.4 g TiO$_2$/L was mixed with the initial MET solution before addition of H$_2$O$_2$. Fig. 6 depicts (a) the MET conversion and (b) mineralization for experiments of photolysis, photocatalysis (0.4 g TiO$_2$/L) in Milli Q water or WWTP effluent, UV–Vis/H$_2$O$_2$ and UV–Vis/H$_2$O$_2$/TiO$_2$ cases.

The H$_2$O$_2$ alone, under 300 min of irradiation (Q = 15.8 kJ/L), was able to degrade 29% and 55% of MET with 25 and 150 mg/L H$_2$O$_2$ respectively. However only a slight TOC elimination was observed (approximately 4% and 10% removal in presence of 25 and 150 mg/L of H$_2$O$_2$ respectively) mainly due to a remarkable hydroxylation step.
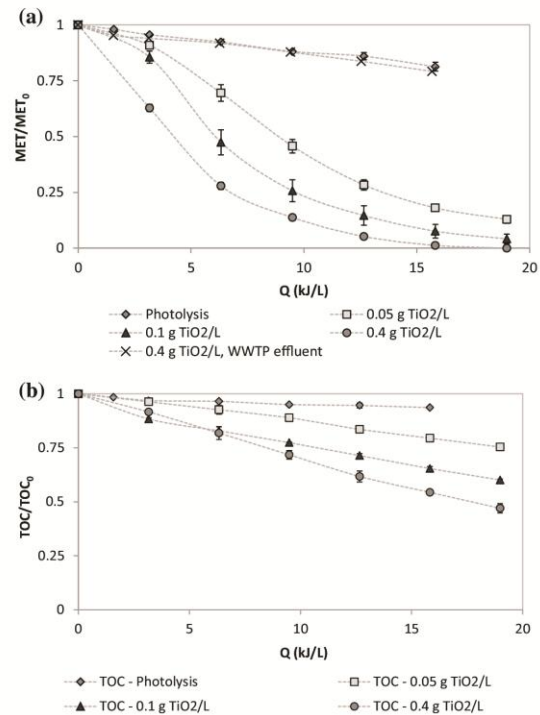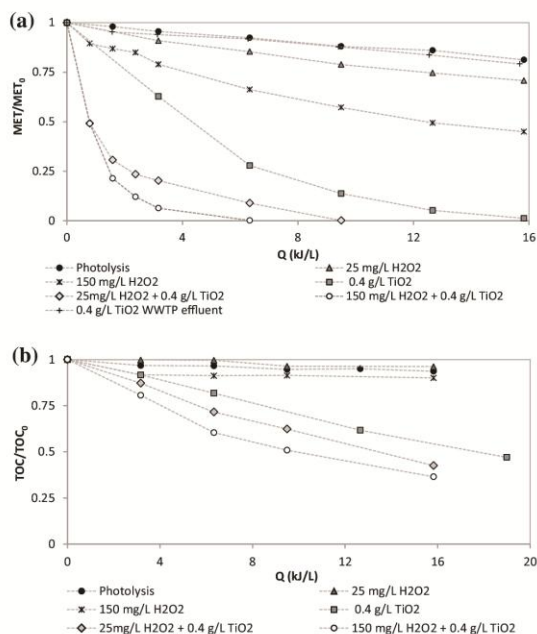

Fig. 6. Effect of the H$_2$O$_2$ concentration on (a) MET degradation and (b) mineralization in solarbox device. Initial MET concentration 50 mg/L, free pH.

In presence of TiO$_2$, the addition of H$_2$O$_2$ improves the degradation of MET and TOC removal: complete depletion of MET is reached within 180 (Q = 9.5 kJ/L) and 120 min (Q = 6.3 kJ/L) by use of 25 and 150 mg/L of H$_2$O$_2$, in contrast with the 300 min (Q = 15.8 kJ/L) needed for total elimination of MET by the sole presence of TiO$_2$. In this way, the addition of oxidizing species increases the efficiency of the photocatalytic process, because H$_2$O$_2$ acts as electron acceptor and reacts with electrons from the photoactivated surface of the catalyst, which constitutes an extra source of HO$\cdot$ [31]. In addition, because of disproportion over UV-irradiated TiO$_2$, H$_2$O$_2$ is an additional source of O$_2$ on the TiO$_2$ surface [32]. Additionally, pioneering studies showing the favorable effect of H$_2$O$_2$ in TiO$_2$/photocatalysis [33]. However, high concentration of H$_2$O$_2$ scavenges the hydroxyl radicals, making the process less effective [34].

The results obtained in this study are in agreement with those found by other authors, where, in presence of TiO$_2$, the addition of H$_2$O$_2$ improves the degradation of MET.

Ioannou and co-workers [28] used 10 mg/L of Atenolol and Propranolol, 250 mg/L TiO$_2$ and Xe lamp. After 120 min of irradiation 76% and 73% of conversion were reached for Atenolol and Propranolol respectively. In their study Atenolol degradation improved from 58% to 76% and Propranolol conversion from 64% to 73% when 1.4 mM of H$_2$O$_2$ was used. On the other hand, Rivas [20] also improves the results when TiO$_2$/H$_2$O$_2$ was used. After 180 min 5 × 10^{-3} M of H$_2$O$_2$ eliminates 5 × 10^4 of MET, compared to 10–20% of conversion achieved in the absence of promoters.

3.3. Photocatalytic degradation at pilot plant scale: CPC solar reactor

3.3.1. Influence of TiO$_2$ loading

The results obtained for 10 L of treated solution using CPC are summarized in Fig. 7 where is clearly appreciated a remarkable initial slow process of degradation in all of cases. After 240 min of

Table 4
Summary of MET and TOC removal at several experimental conditions.

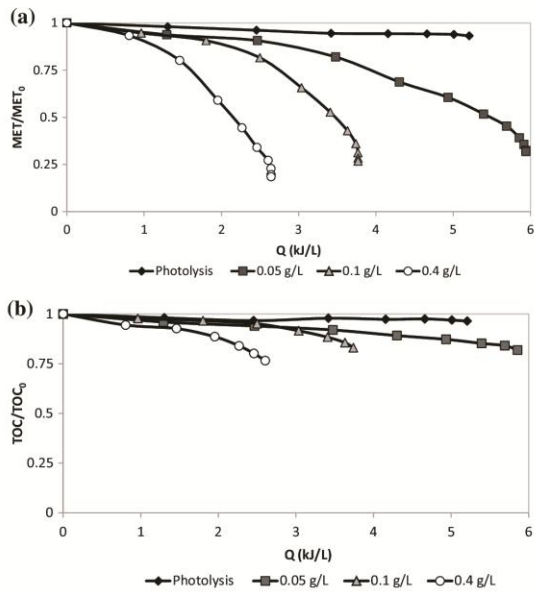| Device	MET (mg/L)	TiO$_2$ (g/L)	H$_2$O$_2$ (mg/L)	MET removal (at t min) (%)	TOC removal (at t min) (%)	Q Acc. energy (at t min) (kJ/L)
Solarbox	50	0	0	14.0 (240)	5.4 (240)	12.7 (240)
	25	0.40	0	100 (180)	49.0 (180)	9.5 (180)
	50	0.40	0	100 (300)	46.6 (300)	15.8 (300)
	100	0.40	0	86.6 (300)	33.4 (300)	15.8 (300)
	50	0.05	0	81.9 (300)	20.6 (300)	15.8 (300)
	50	0.10	0	92.4 (300)	34.6 (300)	15.8 (300)
	50	0.40	0	100 (300)	45.2 (300)	15.8 (300)
	50	0	25	29.2 (300)	3.8 (300)	15.8 (300)
	50	0	150	55.0 (300)	9.9 (300)	15.8 (300)
	50	0.40	25	100 (180)	37.6 (180)	9.5 (180)
	50	0.40	150	100 (120)	39.6 (120)	6.3 (120)
CPC	50	0	0	8.1 (240)	2.7 (240)	5.3 (240)
	50	0.05	0	60.8 (240)	18.1 (240)	5.9 (240)
	50	0.10	0	68.8 (240)	19.8 (240)	3.8 (240)
	50	0.40	0	80.4 (240)	28.1 (240)	2.6 (240)
	50	0	25	13.8 (300)	11.2 (300)	7.9 (300)
	50	0	150	57.9 (300)	16.9 (300)	7.9 (300)
	50	0.40	25	70.0 (90)	18.0 (90)	3.2 (90)
	50	0.40	150	95.6 (180)	38.3 (180)	6.0 (180)

Fig. 7. Effect of the TiO$_2$ concentration in CPC photoreactor on (a) MET degradation and (b) mineralization. Initial MET concentration 50 mg/L, free pH.

experimentation MET removal was 8.1% ($Q = 5.29$ kJ/L), 60.8% ($Q = 5.86$ kJ/L), 68.8% ($Q = 3.77$ kJ/L) and 80.4% ($Q = 2.64$ kJ/L) for 0, 0.05, 0.1 and 0.4 g TiO$_2$/L. The amount of solar accumulated energy Q in CPC is calculated according:

$$Q = \sum_{i=0}^{n} \frac{FA\Delta t_i}{V} \qquad (2)$$

where A (m^2) is the mirror's area of capture-reflection of solar irradiation, F is the average of the incident solar UV energy flux measured by radiometer (W/m^2) for Δt (s), time in the sampling periods i.

In Fig. 7(b) is shown the TOC removal. Mineralization levels in this system were not promising with only 2.7% ($Q = 5.29$ kJ/L), 18.1% ($Q = 5.86$ kJ/L), 19.8% ($Q = 3.77$ kJ/L) and 28.1% ($Q = 2.64$ kJ/L) of TOC conversion, for 0, 0.05, 0.1 and 0.4 g/L of catalyst respectively (see Table 4).

Fig. 8 depicts the irradiance data for photolysis and photocatalytic (0.05, 0.1 and 0.4 g TiO$_2$/L) experiments in CPC. It can be observed that the highest energy flux (W/m^2) for the experiments can be found at the beginning. The best combination to achieve the highest MET degradation is the highest daily irradiance and the
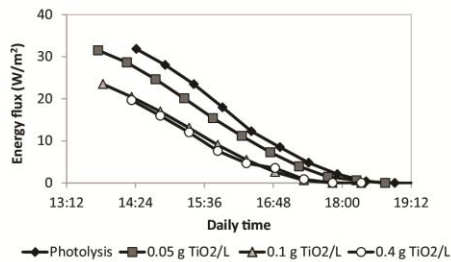

Fig. 8. Irradiance data for photocatalytic experiments in CPC at 290–400 nm.

best catalyst concentration tested, in this case, 0.4 g TiO$_2$/L. It is clear that at higher catalyst concentration lower energy is necessary to reach the best MET conversion.

3.3.2. Influence of H$_2$O$_2$ presence

Fig. 9 depicts (a) the MET conversion and (b) mineralization for experiments of solar photolysis, UV–Vis/H$_2$O$_2$ and UV–Vis/H$_2$O$_2$/TiO$_2$ in CPC reactor. As commented in Section 3.1 (see also Table 4), photolytic degradation with natural solar energy achieves very low values for MET depletion and TOC reduction. Experiments carried out in presence of H$_2$O$_2$ (25 mg/L), under irradiation, showed that, MET degradation is 1.2 times higher than the achieved by photolysis after 240 min of irradiation. However, to improve MET degradation, the concentration of H$_2$O$_2$ concentration has to be rather high to generate a sufficiently high level of HO· radicals in a solution [34].

If higher concentration of H$_2$O$_2$ is employed (150 mg/L), MET was depleted until 33%, for 5.3 kJ/L accumulated energy, or until 57.9% by extended irradiation time, till 8.0 kJ/L of accumulated energy. Degradation of MET by the sole presence of H$_2$O$_2$ under irradiation is attributed to the photochemical cleavage of H$_2$O$_2$ to yield HO· and/or other radical species by solar light absorption.

The maximum absorbance of H$_2$O$_2$ occurs at about 220 nm [34], and the solar spectrum is not reach in this wavelength. It means that the sole presence of H$_2$O$_2$ under irradiation presents low yield in formed hydroxyl radicals and, therefore, a high concentration of H$_2$O$_2$ is needed to generate sufficient hydroxyl radicals because of low-absorption coefficient.

However, the joint presence of UV and TiO$_2$ (UV–Vis/H$_2$O$_2$/TiO$_2$ process) improves MET degradation at low or high H$_2$O$_2$ concentra-
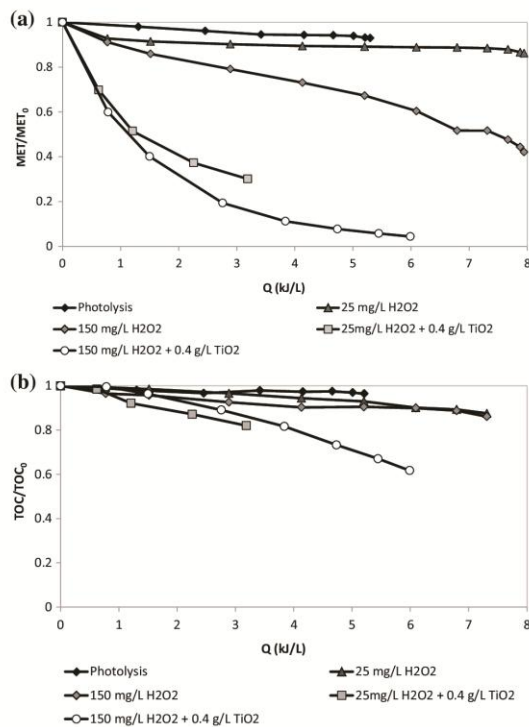

Fig. 9. Effect of the H$_2$O$_2$ concentration on (a) MET degradation and (b) mineralization in solar CPC. Initial MET concentration 50 mg/L, free pH.

Table 5
Summary of the energy consumed as function MET elimination and TiO_2 loaded, with 50 mg MET/L of initial concentration at 240 min.

Device	TiO_2 load (g/L)	MET (%) at 240 min	Q (kJ/L) (290–400 nm) at 240 min	Energy used for mg of MET removed (kJ/mg MET) at 240 min	Energy used by TiO_2 to remove 1 mg of MET (g TiO_2 kJ/mg MET) at 240 min	k_{ap} (min^{-1})	g TiO_2/mg MET
Solarbox	0.05	71.7	12.6	0.358	0.018	6.1×10^{-3}	0.001
	0.1	85.4	12.6	0.307	0.030	9.3×10^{-3}	0.002
	0.4	94.8	12.6	0.275	0.110	1.2×10^{-2}	0.009
CPC	0.05	60.8	5.9	0.205	0.010	3.9×10^{-3}	0.002
	0.1	68.8	3.8	0.109	0.011	5.0×10^{-3}	0.003
	0.4	80.4	2.6	0.065	0.026	7.1×10^{-3}	0.010

tion, because peroxide acts as additional source of hydroxyl radicals that combines with TiO_2, improving the overall efficiency [34].

Regarding to UV–Vis/H_2O_2/TiO_2 process, 70 and 86% of MET removal was observed with 25 and 150 mg/L of H_2O_2, respectively, and 0.4 g/L of TiO_2 for 3.1 kJ/L of accumulated energy. Moreover, 38.3% of the initial organic carbon is mineralized, for 6.0 kJ/L of cumulated energy, in the presence of 150 mg/L of H_2O_2. Complete consumption of H_2O_2 was observed in both cases.

3.4. Kinetics and comparison of devices

For 50 mg/L of MET and natural pH (6.0), MET concentration evolution was approached to first order kinetics and the first order rate constant (k_{ap}) values could be obtained from the slopes $-\ln$ (C/Co) vs. time, within the period of irradiation. These rate constants were calculated for both devices as 6.7×10^{-4}, 6.1×10^{-3}, 9.3×10^{-3} and 1.2×10^{-2} min^{-1}, using solarbox, and 3.2×10^{-4}, 3.9×10^{-3}, 5.0×10^{-3} and 7.1×10^{-3} min^{-1}, using CPC, for 0, 0.05, 0.1 and 0.4 g TiO_2/L respectively (see Table 5) and summarized in Fig. 10. The results are consistent with the TiO_2 loading used in each experiment, and using higher TiO_2 amount, higher kinetic constants were obtained. k_{ap} was also determinate for 50 mg/L of MET and 0.4 g TiO_2/L in the solarbox, but using water from a secondary treatment effluent from a WWTP and the value obtained was 7.1×10^{-4} min^{-1} which is quiet similar to the value obtained from photolysis with deionized water. Thus, using a real water matrix, MET degradation goes slower than using deionized water matrix due to the competition between the organic material and MET for the light. As a consequence, the maximum conversion of MET was 20.8%, after 300 min of irradiation ($Q = 15.8$ kJ/L). Talking in terms of ratio removed MET/energy entering into the system, 0.64 mg MET/kJ were calculated.
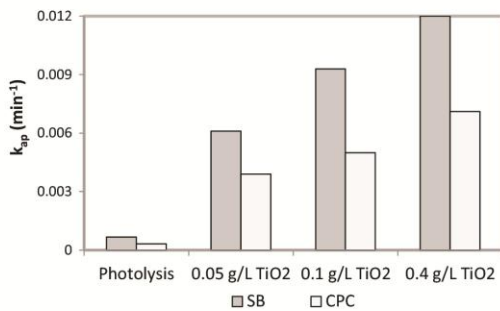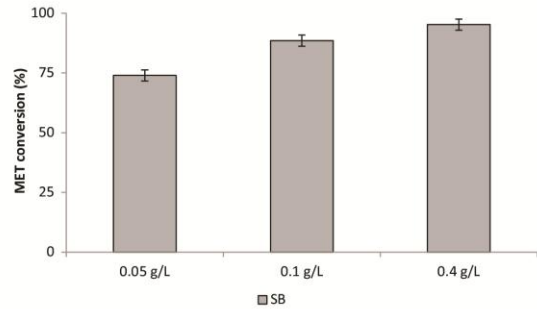
Fig. 11. MET conversion for different TiO_2 concentrations and its corresponding standard deviation in SB at 240 min of irradiation (Q:12.6 kJ).
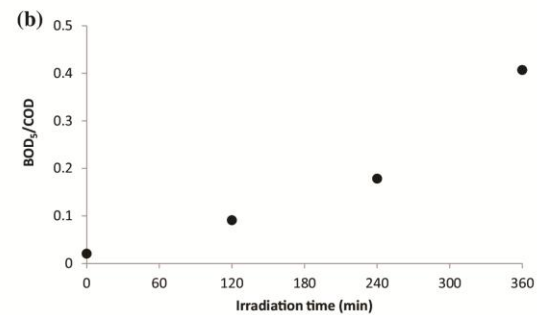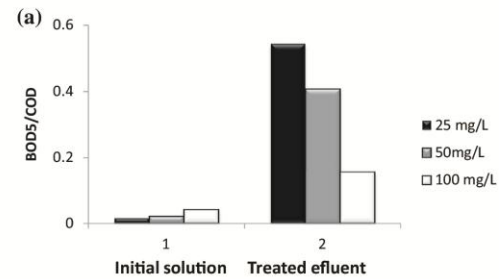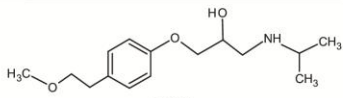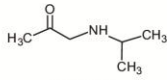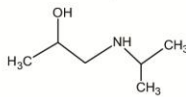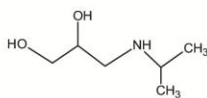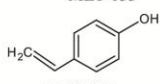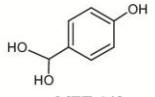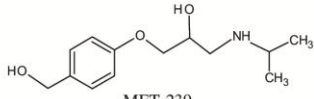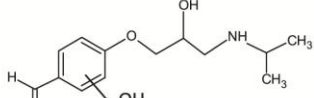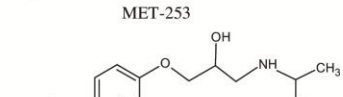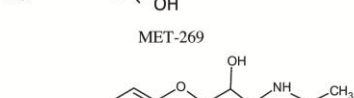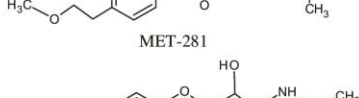
Fig. 12. BOD_5/COD evolution. (a) Effect of the initial MET concentration and (b) Evolution for initial MET concentration of 50 mg/L, 0.4 g/L of TiO_2 in SB.

Fig. 10. Kinetic constant (k_{ap}) values for SB and CPC reactors within the period of irradiation and different TiO_2 concentrations loaded. [MET]$_0$ = 50 mg/L, natural pH (6.0).
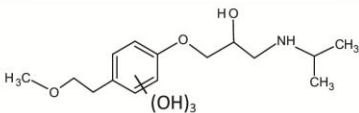
Furthermore the results of MET removal were compared for both devices, with deionized water media, and they are summarized in Table 5 for total accumulated energy at 240 min. In the solarbox,

Table 6
Intermediates identified by electrospray mass technique. UV–Vis/H_2O_2/TiO_2 processes in SB and CPC reactors. 50 mg/L of MET and 0.4 g/L of TiO_2.

m/z (Da)	Elemental composition	Proposed structure (Label)	UV–Vis/H_2O_2/TiO_2 (Retention time, min)		
			SB[a] (25 H_2O_2)	CPC[a] (25 H_2O_2)	CPC[b] (150 H_2O_2)
267	$C_{15}H_{25}NO_3$	MET	(6.07)	(3.29)	(6.04)
115	$C_6H_{13}NO$	MET-115	(2.36)	–	–
117	$C_6H_{15}NO$	MET-117	(3.21)	–	(3.195)
133	$C_6H_{15}NO_2$	MET-133	(2.36)	(2.38)	(2.30)
120	C_8H_8O	MET-120	(2.36)	(2.38)	–
140	$C_7H_8O_3$	MET-140	(3.21)	–	–
239	$C_{13}H_{21}NO_3$	MET-239	–	(2.82)	–
253	$C_{13}H_{19}NO_4$	MET-253	–	(3.03)	(3.00)
269	$C_{14}H_{23}NO_4$	MET-269	–	(2.95)	–
281	$C_{15}H_{23}NO_4$	MET-281	–	(3.29)	(5.66)
283	$C_{15}H_{25}NO_4$	MET-283	–	(4.69)	(4.72)

Table 6 (*continued*)

m/z (Da)	Elemental composition	Proposed structure (Label)	UV–Vis/H₂O₂/TiO₂ (Retention time, min)		
			SB[a] (25 H₂O₂)	CPC[a] (25 H₂O₂)	CPC[b] (150 H₂O₂)
315	$C_{15}H_{25}NO_6$	MET-315	–	(3.95)	(3.00)

[a] 25 mg H₂O₂/L.
[b] 150 mg H₂O₂/L.

with constant irradiation (12.6 kJ, in 290–400 nm, for 240 min of irradiation), 71.7%, 85.4%, and 94.8% of MET was removed with 0.05, 0.1 and 0.4 g TiO₂/L, respectively. Fig. 11, shows MET conversion at 12.6 kJ and its corresponding standard deviation.

In the pilot plant, working with 0.05, 0.1 and 0.4 g TiO₂/L, the MET removed was 60.8 (Q = 5.85 kJ/L), 68.8 (Q = 3.77 kJ/L) and 80.4% (Q = 2.64 kJ/L) respectively. It can be observed that using a laboratory lamp with a constant irradiation, MET was almost completely degraded with the highest TiO₂ concentration. In the pilot plant MET removal increases when TiO₂ concentration does it.

Table 5 shows the energy required to remove 1 mg of MET, after 240 min of irradiation, for different titania concentrations. From Table 5 results, it can be concluded that the required energy for MET removal decreases when titania concentration increases for both devices (solarbox and CPCs).

In addition, it can be observed that, at the same irradiation time and titania concentration, MET removal is higher in solarbox device and the required energy to remove 1 mg of MET is higher in SB than in CPC. A likely explanation for these results can be related to the fact that, in solarbox, TiO₂ absorbs radiation from 280 to 400 nm, approximately, and this not happens when solar radiation is used because there is not absorption in the 280–300 nm range. In this way, we observed that the required energy to remove 1 mg of MET is higher in SB than in CPC and this difference increases when catalyst concentration does it. Thus, the relations calculated (required energy in SB/required energy in CPC for 1 mg MET removal) are 1.74, 2.81 and 4.2 for 0.05, 0.1 and 0.4 g TiO₂/L respectively at 240 min. As it could be seen as higher TiO₂ concentration higher is the relation, so, it predicts that this behavior can be due to the difference in wavelength range where TiO₂ can absorb.

TOC was not completely removed even after several hours of irradiation in both devices. TOC conversion obtained at 240 min of experimental time, using 0.05, 0.1 and 0.4 g TiO₂/L for solarbox (12.6 kJ), was 16.4, 30.8, and 38.3%, and in CPC it was 18.1% (Q = 5.85 kJ/L), 19.8% (Q = 3.77 kJ/L) and 28.1% (Q = 2.64 kJ/L). Maximum TOC conversion reached for CPC was 29.2% (Q = 2.64 kJ/L) after 270 min of irradiation, and 53.0% (Q = 1.9 kJ/L) for solarbox system, after 360 min, using 0.4 g/L of catalyst.

3.5. Biodegradability, toxicity and intermediates

BOD₅ for the photocatalytic treatment was tested and assessed as BOD₅/COD ratio. Biodegradability enhancement was highest at the lowest initial MET concentration (see Fig. 12). In solarbox, 25 ppm MET shows a high biodegradability enhancement and, after 300 min of irradiation, BOD₅/COD increases from 0.01 to 0.54. In the case of 50 ppm initial MET, biodegradability was increased from 0.02 to 0.41 due to the increase of BOD₅ (1.35–6.35 mg/L) and the decrease of COD (65.3–15.6 mg/L), after 360 min of irradiation. With 100 ppm initial MET, BOD₅/COD increases from 0.04 to 0.16 in 420 min.

For 50 ppm MET in CPC, low biodegradability enhancement was observed from 0.02 to 0.12 after 270 min of irradiation, due to the slight increase in the BOD₅ (1.35–4.57 mg/L) and the low decrease of COD (67.1–39.2 mg/L).

As known [35], a municipal wastewater can be considered biodegradable when the BOD₅/COD ratio is higher than 0.4. However González and co-workers [36] consider that a BOD₅/COD ratio higher than 0.25 is sufficient for a biological treatment.

The biodegradability (BOD₅/COD) of the un-treated solutions was near zero, indicating that the target compound solutions are not biodegradable. Nevertheless, the continuous compound oxidation promoted by the reaction with hydroxyl radicals favored the formation of more biodegradable compounds. MET oxidation leaded to a gradual formation of more biodegradable compounds since the first minutes of reaction, achieving at the end of irradiation time a biodegradable treated solution. Thus, when 25 and 50 mg/L of initial MET concentrations were used in solarbox (Fig. 12), biodegradability indicators reached for both treated solutions were higher than 0.4. This means that these treated solutions can be coupled to biological process after 300 and 360 min respectively. In the case of 50 mg/L of initial MET concentration, using CPC reactor, the solution remains being considered not biodegradable at the end of the photocatalytic process, after 270 min, because biodegradability indicator for the treated solution was lower than 0.4. Therefore, this treated solution cannot be coupled to subsequent biological treatment.

During the photocatalytic process of MET photo-decomposition, several by-products are produced along the reaction time. To complete the UV–Vis/H₂O₂/TiO₂ process information, the intermediates formed in these reactions have been identified by electrospray mass technique (see Table 6).

In Table 6 there are described one process carried out in SB and two processes in CPC reactor. 50 mg/L of MET and 0.4 g/L of TiO₂ in all series were used. Different hydrogen peroxide concentrations were studied: 25 mg H₂O₂/L in SB; 25 mg H₂O₂/L and 150 mg H₂O₂/L in CPC.

Heterogeneous photocatalysis in solarbox has been studied in our earlier report [37] using 50 mg MET/L and 0.4 g TiO₂/L. The by-products were identified and a degradation pathway was proposed.

Comparing photocatalysis/TiO₂ by-products with the results obtained with UV–Vis/H₂O₂/TiO₂ process it can be deducted that a greater number of by-products were produced when the photocatalysis was carried out without H₂O₂. This is according with the higher photo-oxidation when UV–Vis/H₂O₂/TiO₂ was assessed. The intermediate with m/z = 133, amino-diol, was again identified in all series.

Moreover, when UV–Vis/H₂O₂/TiO₂ process was used a new by-products were found and reported for the first time (MET-140, MET-253, MET-269, MET-281 and MET-283), suggesting a new MET photo-degradation pathway (Fig. 13).
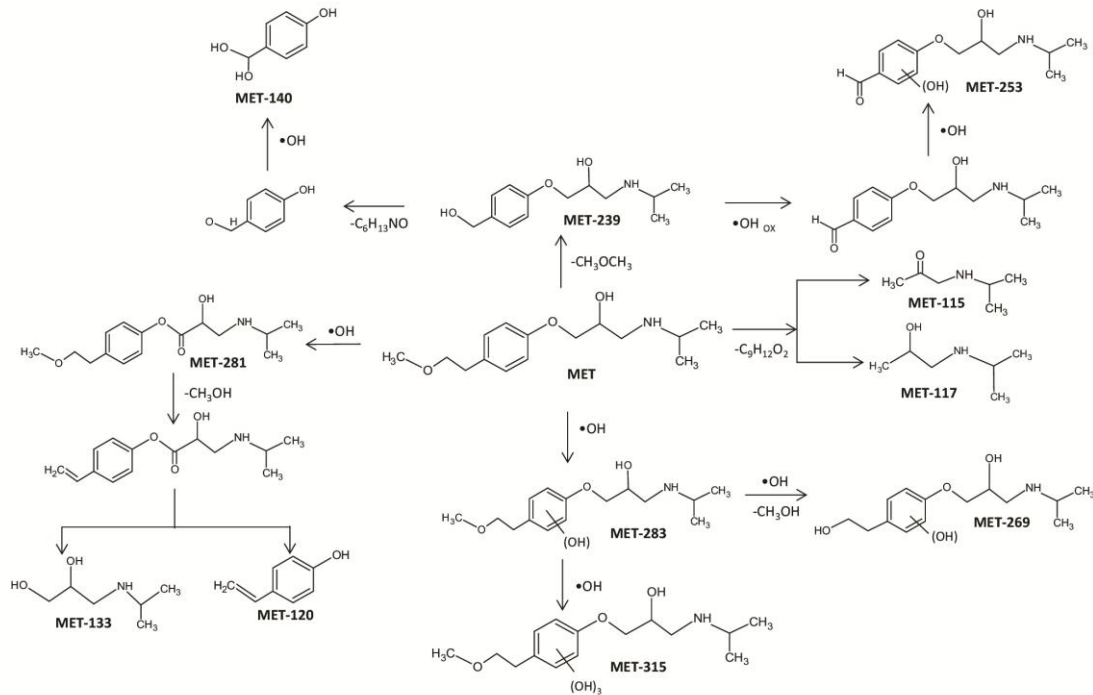
Fig. 13. MET degradation pathways for UV–Vis/H_2O_2/TiO_2 process in SB and CPC reactors.
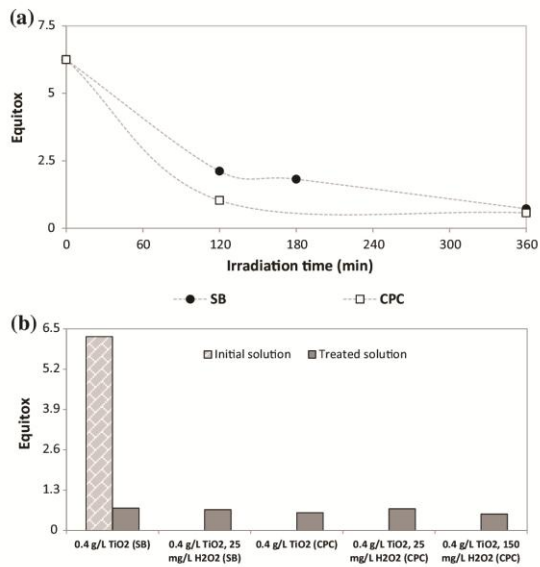

Fig. 14. Equitox for (a) MET photocatalysis/TiO_2 along of the irradiation time in SB and CPC reactors and (b) MET photocatalysis/TiO_2 and UV–Vis/H_2O_2/TiO_2, using 0.4 g TiO_2/L in SB and CPC reactor.

Comparing the by-products when UV–Vis/H_2O_2/TiO_2 process was carried out in SB and CPC reactor, it can be observed that the cleavage of MET molecule leads to smaller fragments when

SB was used. Besides, in CPC the by-products observed may be attributed to hydroxylated intermediates. This fact can be also a possible explanation of the plateau observed at the initial times when concentration is represented vs time in CPCs.

Photocatalysis/TiO_2 and UV–Vis/H_2O_2/TiO_2 processes using solarbox and a solar pilot plant reactor have produced at the end of the processes more biodegradable compounds.

Regarding to hazardousness of treated solutions (toxicity by *V. fischeri*) was assessed for photocatalysis/TiO_2 and UV–Vis/H_2O_2/TiO_2 processes in both devices, Fig. 14(a) shows that the oxidation of MET by photocatalysis/TiO_2 promoted the overall toxicity reduction of the solution since the beginning of the treatment. The results demonstrate that, for all processes, effluents toxicity decreases along of the irradiation time due to the degradation products formed, as all treatments carried out in SB and CPC reactors are sufficient to produce effluents within safe toxicity limits. Fig. 14(b) depicts the equitox of the initial and the treated solution for all different processes tested. In SB, using photocatalysis/(0.4 g/L TiO_2), after 360 min of irradiation the equitox value obtained was 0.72, and for UV–Vis/(25 mg/L H_2O_2)/(0.4 g/L), after 300 min, the equitox value reached was 0.67. In CPC, the equitox values obtained were 0.57, 0.70 and 0.53 using photocatalysis/(0.4 g/L TiO_2), UV–Vis/(25 mg/L H_2O_2)/(0.4 g/L) UV–Vis/(150 mg/L H_2O_2)/(0.4 g/L) respectively at the end of the irradiation time.

4. Conclusions

The efficiency of the heterogeneous photocatalysis with TiO_2 in suspension for Metoprolol removal has been demonstrated using natural solar light and simulated solar light. The MET degradation values obtained for both devices are clearly acceptable and TOC values can be improved by long irradiation time. For the different

processes described (photolysis, photocatalysis (TiO_2), UV–Vis/H_2O_2 and UV–Vis/H_2O_2/TiO_2) the best results in terms of MET degradation were obtained with UV–Vis/H_2O_2/TiO_2 (0.4 g/L TiO_2 and 150 mg/L H_2O_2) achieving complete MET degradation in 120 min and a TOC removal of almost 40% in solarbox. In CPCs it was obtained 95.6% of MET conversion and 38.3% of TOC removal after 180 min. When only photocatalysis was employed (TiO_2 without H_2O_2) results are rather low using real matrix water (20.8% in 300 min) due the competition of the organic matter present for light and catalyst and higher conversions are also reached in Mili Q matrix water: 100% (300 min) of MET conversion but for this process without H_2O_2 higher times of irradiation were needed in solarbox and in CPC (81.5% of MET conversion at 270 min).

A first kinetic approach assuming simple first order kinetics was calculated for both devices as 6.7×10^{-4}, 6.1×10^{-3}, 9.3×10^{-3} and 1.2×10^{-2} min^{-1} using the solarbox and 3.2×10^{-4}, 3.9×10^{-3}, 5.0×10^{-3} and 7.1×10^{-3} min^{-1} using the CPC, for 0, 0.05, 0.1 and 0.4 g TiO_2/L respectively.

For comparison, in the case of photocatalysis, the energy needed to remove 1 mg of MET was evaluated. The results obtained show that, for both devices (solarbox and CPCs), the minimum values were obtained for the maximum catalyst concentration (0.4 g/L TiO_2), being 0.275 and 0.065 kJ/mg in solarbox and CPC respectively.

Regarding to biodegradability, the study carried out showed that the treated solutions of 25 and 50 mg/L of MET, using solarbox, can be coupled to biological process after 300 and 360 min of irradiation respectively due to the BOD$_5$/COD ratio is higher than 0.4. Nevertheless, the effluent obtained in CPC is not enough for a subsequent biological treatment.

Toxicity showed that photocatalysis/TiO_2, and UV–Vis/H_2O_2/TiO_2 processes, using two different experimental devices (solarbox and a solar pilot plant), have promoted the overall toxicity reduction of MET solution, hence, toxicity assessment has demonstrated that MET is degraded by all processes tested in both devices, allowing safe disposal of the effluent. Intermediates were identified for UV–Vis/H_2O_2/TiO_2 and compared with UV–Vis/TiO_2 in both devices and a new MET degradation pathway was proposed. This proposed pathway indicates that UV–Vis/H_2O_2/TiO_2 present different photodegradation when a promoter is used. According to the intermediates identified and comparing the by-products when UV–Vis/H_2O_2/TiO_2 process was carried out in SB and CPC reactor, it can be observed that the cleavage of MET molecule leads to smaller fragments when SB was used. Besides, in CPC the by-products observed may be attributed to hydroxylated intermediates. Photocatalysis/TiO_2 and UV–Vis/H_2O_2/TiO_2 processes, using two different experimental devices (solarbox (SB) and a solar pilot plant reactor), have produced more biodegradable compounds at the end of the processes.

Acknowledgements

References

[1] D.W. Kolpin, E.T. Furlong, M.T. Meyer, E.M. Thurman, S.D. Zaugg, L.B. Barber, H.T. Buxton, Pharmaceuticals, hormones, and other organic wastewater contaminants in U.S. streams, 1999–2000: a national reconnaissance, Environ. Sci. Technol. 36 (2002) 1202–1211.
[2] C.D. Metcalfe, X.S. Miao, B.G. Koenig, J. Struger, Distribution of acidic and neutral drugs in surface waters near sewage treatment plants in the lower Great Lakes, Canada, Environ. Toxicol. Chem. 22 (2003) 2881–2889.
[3] I. Muñoz, J.C. López-Doval, M. Ricart, M. Villagrasa, R. Brix, A. Geiszinger, A. Ginebreda, H. Guasch, M.J. López, A.M. Romaní, S. Sabater, D. Barceló, Bridging levels of pharmaceuticals in river water with biological community structure in the Llobregat river basin (northeast Spain), Environ. Toxicol. Chem. 28 (2009) 2706–2714.
[4] M. Petrovic, M. Gros, D. Barceló, Multi-residue analysis of pharmaceuticals in wastewater by ultra-performance liquid chromatography–quadrupole-time-of-flight mass spectrometry, J. Chromatogr. A 1124 (2006) 68–81.
[5] M. Gros, M. Petrovic, D. Barceló, Development of a multi-residue analytical methodology based on liquid chromatography–tandem mass spectrometry (LC–MS/MS) for screening and trace level determination of pharmaceuticals in surface and wastewaters, Talanta 70 (2006) 678–690.
[6] H. Yang, T. An, G. Li, W. Song, W.J. Cooper, H. Luo, X. Guo, Photocatalytic degradation kinetics and mechanism of environmental pharmaceuticals in aqueous suspension of TiO2: a case of ß-blockers, J. Hazard. Mater. 179 (2010) 834–839.
[7] J.T. Yu, E.J. Bouwer, M. Coelhan, Occurrence and biodegradability studies of selected pharmaceuticals and personal care products in sewage effluent, Agric. Water Manage. 86 (2006) 72–80.
[8] S.F. Owen, E. Giltrow, D.B. Huggett, T.H. Hutchinson, J. Saye, M.J. Winter, J.P. Sumpter, Comparative physiology, pharmacology and toxicology of ß-blockers: mammals versus fish, Aquat. Toxicol. 82 (2007) 145–162.
[9] M. Cleuvers, Aquatic ecotoxicity of pharmaceuticals including the assessment of combination effects, Toxicol. Lett. 142 (2003) 185–194.
[10] D. Fatta, A. Achilleos, A. Nikolaou, S. Meriç, Analytical methods for tracing pharmaceutical residues in water and wastewater, TrAC, Trends Anal. Chem. 26 (2007) 515–533.
[11] F.J. Benitez, F.J. Real, J.L. Acero, G. Roldan, Removal of selected pharmaceuticals in waters by photochemical processes, J. Chem. Technol. Biotechnol. 84 (2009) 1186–1195.
[12] A.A.M. Stolker, W. Niesing, E.A. Hogendoorn, J.F.M. Versteegh, R. Fuchs, U.A.T. Brinkman, Liquid chromatography with triple-quadrupole or quadrupole-time of flight mass spectrometry for screening and confirmation of residues of pharmaceuticals in water, Anal. Bioanal. Chem. 378 (2004) 955–963.
[13] B. Kasprzyk-Hordern, R.M. Dinsdale, A.J. Guwy, The removal of pharmaceuticals, personal care products, endocrine disruptors and illicit drugs during wastewater treatment and its impact on the quality of receiving waters, Water Res. 43 (2009) 363–380.
[14] D. Bendz, N.A. Paxéus, T.R. Ginn, F.J. Loge, Occurrence and fate of pharmaceutically active compounds in the environment, a case study: Höje River in Sweden, J. Hazard. Mater. 122 (2005) 195–204.
[15] S. Wiegel, A. Aulinger, R. Brockmeyer, H. Harms, J. Löffler, H. Reincke, R. Schmidt, B. Stachel, W. von Tümpling, A. Wanke, Pharmaceuticals in the river Elbe and its tributaries, Chemosphere 57 (2004) 107–126.
[16] K.V. Thomas, C. Dye, M. Schlabach, K.H. Langford, Source to sink tracking of selected human pharmaceuticals from two Oslo city hospitals and a wastewater treatment works, J. Environ. Monit. 9 (2007) 1410–1418.
[17] J.A. Polar, The fate of pharmaceuticals after wastewater treatment, Florida Water Res. J. (2007) 26–31.
[18] K.H. Langford, K.V. Thomas, Determination of pharmaceutical compounds in hospital effluents and their contribution to wastewater treatment works, Environ. Int. 35 (2009) 766–770.
[19] F. Méndez-Arriaga, S. Esplugas, J. Giménez, Photocatalytic degradation of non-steroidal anti-inflammatory drugs with TiO2 and simulated solar irradiation, Water Res. 42 (2008) 585–594.
[20] F.J. Rivas, O. Gimeno, T. Borralho, M. Carbajo, UV-C radiation based methods for aqueous Metoprolol elimination, J. Hazard. Mater. 179 (2010) 357–362.
[21] V. Romero, N. De La Cruz, R.F. Dantas, P. Marco, J. Giménez, S. Esplugas, Photocatalytic treatment of metoprolol and propranolol, Catal. Today 161 (2011) 115–120.
[22] B. Abramovic, S. Kler, D. Sojic, M. Lausevic, T. Radovic, D. Vione, Photocatalytic degradation of metoprolol tartrate in suspensions of two TiO 2-based photocatalysts with different surface area. Identification of intermediates and proposal of degradation pathways, J. Hazard. Mater. 198 (2011) 123–132.
[23] E. Isarain-Chávez, R.M. Rodríguez, P.L. Cabot, F. Centellas, C. Arias, J.A. Garrido, E. Brillas, Degradation of pharmaceutical beta-blockers by electrochemical advanced oxidation processes using a flow plant with a solar compound parabolic collector, Water Res. 45 (2011) 4119–4130.
[24] S. Malato, P. Fernández-Ibáñez, M.I. Maldonado, I. Oller, M.I. Polo-López, Solar photocatalytic pilot plants: commercially available reactors, in: Pierre Pichat (Ed.), Photocatalysis and Water Purification, Wiley-VCH, Weinheeim-Germany, 2013, pp. 377–397.
[25] R.F.P. Nogueira, M.C. Oliveira, W.C. Paterlini, Simple and fast spectrophotometric determination of H2O2 in photo-fenton reactions using metavanadate, Talanta 66 (2005) 86–91.
[26] N. De La Cruz, V. Romero, R.F. Dantas, P. Marco, B. Bayarri, J. Giménez, S. Esplugas, O-Nitrobenzaldehyde actinometry in the presence of suspended TiO2 for photocatalytic reactors, Catal. Today 209 (2013) 209–214.
[27] M. Scepanovic, B. Abramovic, A. Golubovic, S. Kler, M. Grujic-Brojcin, Z. Dohcevic-Mitrovic, B. Babic, B. Matovic, Z.V. Popovic, Photocatalytic degradation of metoprolol in TiO2 suspension of TiO2 nanopowders prepared using sol–gel route, J. Sol-Gel Sci. Technol. 61 (2012) 390–402.
[28] L.A. Ioannou, E. Hapeshi, M.I. Vasquez, D. Mantzavinos, D. Fatta-Kassinos, Solar/TiO2 photocatalytic decomposition of β-blockers atenolol and propranolol in water and wastewater, Sol. Energy 85 (2011) 1915–1926.

[29] E.M. Rodríguez, G. Márquez, E.A. León, P.M. Álvarez, A.M. Amat, F.J. Beltrán, Mechanism considerations for photocatalytic oxidation, ozonation and photocatalytic ozonation of some pharmaceutical compounds in water, J. Environ. Manage. 127 (2013) 114–124.

[30] N. De la Cruz, R.F. Dantas, J. Giménez, S. Esplugas, Photolysis and TiO2 photocatalysis of the pharmaceutical propranolol: solar and artificial light, Appl. Catal. B Environ. 130–131 (2013) 249–256.

[31] F. Méndez-Arriaga, M.I. Maldonado, J. Gimenez, S. Esplugas, S. Malato, Abatement of ibuprofen by solar photocatalysis process: enhancement and scale up, Catal. Today 144 (2009) 112–116.

[32] B. Jenny, Pierre Pichat, Determination of the actual photocatalytic rate of H_2O_2 decomposition over suspended TiO_2, Fitting to the Langmuir-Hinshelwood Form, 7, Langmuir, 1991, pp. 947–954.

[33] D.D. Dionysiou, M.T. Suidan, E. Bekou, I. Baudin, J.M. Laîné, Effect of ionic strength and hydrogen peroxide on the photocatalytic degradation of 4-chlorobenzoic acid in water, Appl. Catal. B Environ. 26 (2000) 153–171.

[34] S. Parsons, Advanced Oxidation Processes for Water and Wastewater Treatment, IWA Publishing, London, 2004.

[35] Metcalf & Eddy, Wastewater Engineering, Treatment, Disposal and Reuse, third ed., McGraw-Hill, Inc., New York, 1991.

[36] O. González, C. Sans, S. Esplugas, S. Malato, Application of solar advanced oxidation processes to the degradation of the antibiotic sulfamethoxazole, Photochem. Photobiol. Sci. 8 (2009) 1032–1039.

[37] V. Romero, P. Marco, J. Gimenéz, S. Esplugas, Adsorption and photocatalytic decomposition of the β-blocker metoprolol in aqueous titanium dioxide suspensions: kinetics, intermediates, and degradation pathways, Int. J. Photoenergy (2013), Article ID 138918, 10 pages. http://dx.doi.org/10.1155/2013/138918.

o-Nitrobenzaldehyde actinometry in the presence of suspended TiO₂ for photocatalytic reactors

Natalia De la Cruz, Violette Romero, Renato F. Dantas, Pilar Marco, Bernardí Bayarri, Jaime Giménez*, Santiago Esplugas

Department of Chemical Engineering, University of Barcelona, C/Martí i Franquès 1, 08028 Barcelona, Spain

ARTICLE INFO

ABSTRACT

In this study the o-nitrobenzaldehyde (o-NB) actinometry is used to measure the photon flow entering a photocatalytic reactor. Two different proposed methods in bibliography are adapted and compared: by following pH or o-NB concentration. In addition, it was studied the influence of suspended TiO₂ particles, inside the photoreactor, on the o-NB actinometry. Particularly, the appearance of photocatalytic products was followed during actinometries with suspended TiO₂. It seems that these photocatalytic products do not come from the o-NB photocatalysis, but from the photocatalytic reaction of its photo-product (o-nitrosobenzoic acid), catalyzed by TiO₂. Therefore, this actinometry, following the o-NB concentration, can be used in the presence of suspended TiO₂ to determine the apparent photon flow entering a photoreactor or apply it to suitable models.

© 2012 Elsevier B.V. All rights reserved.

1. Introduction

Water pollution has received an increasing attention worldwide, because water is essential for the economic development of societies, human health and survival. Thus, wastewater treatments are an effective strategy for water conservation.

A large part of wastewater can be effectively treated by traditional methods such as biological processes or adsorption with activated carbon. Nevertheless, there are cases where these kinds of treatments are not enough to reach certain law requirements, or where persistent, toxic and/or non biodegradable organic pollutants appear in effluents from wastewater treatment plants. Therefore, complementary processes such as Advanced Oxidation Processes (AOPs) may be required.

Among AOPs, heterogeneous photocatalysis represents a promising technique for water treatment. Its efficiency has been proved in degrading a wide range of different refractory organics into readily biodegradable compounds, and mineralizing them to innocuous carbon dioxide and water [1–6]. This process is based on the presence of a semiconductor, which absorbs photonic energy higher than or equal to its bandgap energy, generating e⁻/h⁺ pairs. These pairs induce a series of reductive and oxidative reactions on the semiconductor's surface, which can lead to the degradation of different pollutants. Among semiconductors, titanium dioxide has received high interest since it is active, resistant, safe and cheap.

Furthermore, this semiconductor has special interest, since it can use natural (solar) UV of wavelength in the range of 300–390 nm [7].

The strict modeling of photocatalytic reactors is a highly complex assignment, due to the requirement of the analysis of the radiation field. In this process, the radiation can control the kinetic mechanism of contaminants degradation, which is based on the quantity of absorbed photons. Therefore, the interaction assessment between light and TiO₂ particles becomes necessary to understand the overall photochemical mechanism. In this sense, some researches have developed different photocatalytic degradation kinetics including mathematical models of the radiation inside the photoreactor. These models can provide information for both scaling-up and design of commercial photoreactors [8–11].

Thus, to study the kinetic mechanism of a photocatalytic process, radiation should be quantified. Chemical actinometries are often used to calculate the light entering into the system. Actinometries are well known processes based on the reaction of a determined compound, as a result of a photon absorption in a specified wavelengths range. The actinometric reaction rate is related to photons absorption. In the case of AOPs activated by light, actinometries are commonly applied under exactly the same experimental conditions and device, to estimate the irradiance intensity to which the solution is exposed.

Many actinometries have been developed [12]. They are based on diverse chemicals and procedures which lead to the measure of photon absorptions over different and specified wavelength ranges. In this study, o-nitrobenzaldehyde (o-NB) actinometry has been selected, primarily because of its accordance to the TiO₂ absorption

---

* Corresponding author. Tel.: +34 934021293; fax: +34 934021291.
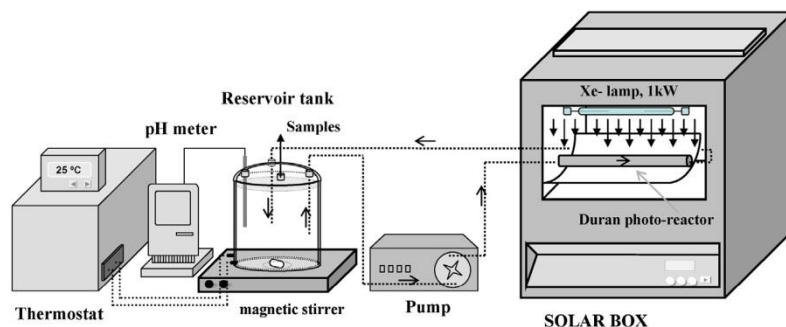 *E-mail address:* j.gimenez.fa@ub.edu (J. Giménez).

Fig. 1. Experimental device.

wavelength range, giving photon absorption data in the range from 290 to 400 nm. It also entails a safe experimental procedure and easy to perform. Another advantage is that the o-NB actinometry may be used with common UV lamps and also in solar photoreactors. This is an actinometry which has been not deep studied yet. Others, more commonly used and studied, were not selected for different reasons. For instance, the uranyl oxalate actinometry was rejected because of environmental and toxic matters. The potassium ferrioxalate actinometry, which must be developed under dark red light, was not useful in this case.

To characterize the radiation in a TiO_2/UV system, it becomes important to compute the photonic flow reaching the solution inside a photoreactor. Different light phenomena would take place in this system, such as transmission, reflection, refraction or absorption. An option to reach this purpose could be to quantify the light absorbed by an actinometric solution inside the photoreactor, when the heterogeneous catalyst is added [13]. However, when o-NB actinometry is used, it could be possible that photocatalytic reactions would take place, as the o-NB is an organic compound.

Thus, the goal of this study was to contribute to estimate the light entering into a photocatalytic heterogeneous system by using the o-NB actinometry. In order to have an actinometric system which could be used to calculate the radiation absorbed by TiO_2, the influence of adding TiO_2 to the o-NB actinometry has been approached. HPLC chromatograms were considered to detect the appearance of photocatalytic reactions during actinometric measurements. Diverse photocatalytic scavengers have also been used with the objective of deducting possible reacting pathways in these conditions. Furthermore, two different ways of developing the o-NB actinometry have been carried out and compared.

2. Materials and methods

2.1. Chemicals

Solutions of o-NB were prepared in 50% ethanol per 50% Milli Q water and stored in the dark. o-Nitrobenzaldehyde (98%) and ethanol (96%, v/v) were from Panreac Química (Spain), formic acid (85%) and tert-butyl alcohol were from Probus S.A. (Spain), ρ-benzoquinone (for synthesis) from Merck (Germany) and sodium hydroxide (98%) from Panreac (Spain). Synthetic amorphous titanium dioxide (Degussa P-25, Spain) was used as catalyst.

2.2. Analytical procedures

The o-NB concentration was monitored by using a high-performance liquid chromatograph (HPLC) from Waters with a *SEA18* 5 μm 15 × 0.46 Teknokroma column, and a Waters 996

photodiode array detector using the Empower Pro software 2002 Water Co. The mobile phase was composed by water and acetonitrile (40:60), injected with a flow-rate of 0.6 mL min^{-1} and detected at maximum UV absorbance set at wavelength of 258 nm. In order to remove the catalyst, before the HPLC analysis, samples were filtered with a polyethersulfone membrane filter of 0.45 μm. The measurement of pH was carried out by a Crison GLP 22 instrument with pH electrode from VWR international (662-1759).

2.3. Photoreactor

A magnetically stirred reservoir tank (1.0 L) was filled with o-NB solutions (Fig. 1). Reagents as formic acid, tert-butanol, benzoquinone or suspended TiO_2 were added when needed.

Solution was continuously pumped (peristaltic pump Ecoline VC-280 II, Ismatec) into a solar simulator (Solarbox Co.fo.me.gra, 220 V, 50 Hz), and recirculated back to the reservoir tank with a flow of 0.65 L min^{-1}. Inside the Solarbox, a duran tubular photoreactor (0.078 L) was irradiated by a Xe-lamp of 1 kW (Phillips XOP 15-OF 1CT). Reactor was located at the bottom of solarbox in the axis of a parabolic mirror. The solution was maintained at constant temperature of 25 °C; the jacket temperature of the stirred tank was controlled with an ultra-thermostat bath (Haake K10).

Before irradiation started, a 5 mL sample was collected from the reservoir tank representing time zero. After turning on the lamp, samples were collected every 5 min during a total period of 45 min. pH was also monitored.

All connections and pipes employed were made of Teflon and/or glass material to avoid losses by adsorption.

3. Results and discussion

3.1. o-NB actinometry

Experiments were carried out to quantify the irradiance intensity of a Xe-lamp light and to compare two different ways of performing the o-NB actinometry.

The photo-degradation of o-NB has been reported by different authors [14–16] and it is generally accepted that the phototransformation of o-NB leads to o-nitrosobenzoic acid (o-HNB). This reaction involves an intramolecular rearrangement where the first step is a hydrogen migration from the aldehyde moiety to the nitro group, leading to the formation of the nitronic acid which rapidly deprotonates to give the nitronate anion (Fig. 2).

3.1.1. o-NB actinometry based on pH
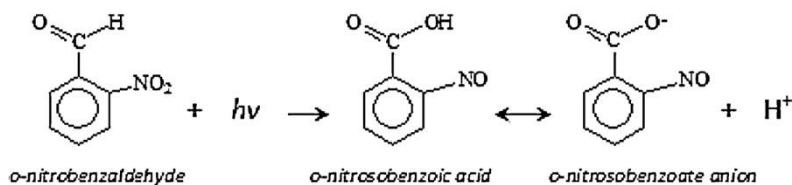o-NB actinometry was carried out by adapting the method described by Allen et al. [17]. The procedure used in our work

Fig. 2. Phototransformation of o-NB.

involved the preparation of 1 L of a 0.1 M o-NB solution in NaOH 0.0048 M water/ethanol solution 50:50. This solution was irradiated and continuously recirculated in the tubular reactor described before.

During the actinometric runs, the pH of the actinometric solution was monitored every minute or less at the reservoir tank and plotted as a function of illumination time. Time zero was established when turning the lamp on. The end point of the reaction was determined from the first derivative plot of the data; dpH$/dt$ versus t. When enough acid was formed, the added NaOH was neutralized and the pH dropped very fast. At this point, the end time was established resulting to be 57 min.

At this time, the number of moles of [H$^+$] formed was equivalent to the number of moles of o-HNB formed and to the number of moles of o-NB consumed. The o-NB actinometer has a quantum yield (ϕ) of 0.5 across the 290–400 nm range. Thus, the photon flow was calculated by Eq. (1), obtaining 2.81×10^{-6} Einstein s^{-1}.

$$\frac{\text{moles of o-NB consumed}}{\phi(\text{mol Einstein}^{-1}) \cdot \text{end point(s)}} = 2.81 \times 10^{-6} \text{ Einstein s}^{-1} \quad (1)$$

Afterwards, the photon flow in Einstein s^{-1} was converted to W m^{-2}. Firstly, the weighted-average wavelength of our Xe-lamp was calculated, resulting to be 369 nm (Eq. (2)).

$$\frac{\sum_{290\,\text{nm}}^{400\,\text{nm}}(\lambda_{\text{nm}})(\text{Irradiance}_{\text{W m}^{-2}})}{\sum_{290\,\text{nm}}^{400\,\text{nm}}\text{Irradiance}_{\text{W m}^{-2}}} \quad (2)$$

The energy computed of a 369 nm photon was calculated by Planck's equation, giving 5.37×10^{-19} J photon^{-1} (3.24×10^5 J Einstein^{-1}). With the irradiated reactor's surface (151 cm^2), the incident light flux was calculated, giving 60.2 W m^{-2} (Eq. (3)),

$$\frac{2.81 \times 10^{-6}(\text{Einstein s}^{-1}) \cdot 3.24 \times 10^5(\text{J Einstein}^{-1})}{0.0151 \text{ m}^2}$$
$$= 60.2 \text{ W m}^{-2} \quad (3)$$

3.1.2. Actinometry based on o-NB concentration

o-NB actinometry was also carried out adapting the method proposed by Willet and Hites [18]. Thus, 1 L solution of o-NB 2.5×10^{-3} M was prepared using water/ethanol (50:50) as solvent. Solvent was changed from the originally proposed in order to exactly repeat the experimental conditions in Section 3.1.1. That was possible since, in this type of actinometry, the quantum yield is independent of the organic solvent used [19].

In this set of experiments, samples were collected from the reservoir tank every 5 min after the lamp was turned on, from time zero (before irradiating). Samples were analyzed by HPLC to follow the o-NB concentration during the procedure. Then, o-NB concentration was plotted as a function of irradiation time. The curve was

fitted to zero-order kinetics in the first 10 min (~25% o-NB degradation). The incident photon flow (I_o) was calculated through Eq. (4).

$$I_o = \frac{d[\text{o-NB}]}{dt}\left(\frac{1}{\phi}\right)\left(\frac{1}{1 - 10^{-\varepsilon b[\text{o-NB}]o}}\right) \quad (4)$$

$d[\text{o-NB}]/dt$ was approximated to the average zero-order kinetics constant (6.358×10^{-5} mol L^{-1} s^{-1}), ϕ is the quantum yield (0.5 mol Einstein^{-1} (290–400 nm)), ε the molar absorptivity (128.6 L mol^{-1} cm^{-1}) and b the path length of the light (2.11 cm). ε was evaluated for the average wavelength of the lamp (369 nm).

Thus, the incident photon flow obtained was 2.68×10^{-6} Einstein s^{-1}. The incident light flux in W m^{-2} was also calculated, following the steps stated in Section 3.1.1, resulting 57.7 W m^{-2}.

It was observed a slight variation on the two actinometric methods, with final values difference of 5%.

3.2. Effect of TiO₂ on o-NB actinometry

Experiments were carried out in order to identify the influence of TiO₂ on the o-NB actinometry. Two purposes were chased during this type of actinometric experiment. (i) To assess the effect of having TiO₂ particles related to absorption and scattering phenomena. (ii) To test possible photocatalytic transformations of the o-NB. Therefore, the possibility of using this actinometric system with TiO₂ for modeling purposes could be established [13].

Due to the possibility that o-NB and its photoproducts can suffer photocatalysis when TiO₂ is present, the actinometries were always based on the o-NB concentration, and not on the pH.

3.2.1. TiO₂ effect on the photon flow

To carry out the runs, 0.4 g L^{-1} of TiO₂ were added to the actinometric solution. Then, it was irradiated for 45 min and samples were collected periodically to follow the o-NB concentration and observe the chromatographic peaks formed during reactions.

Representing o-NB concentration versus irradiation time (Fig. 3), the function was fitted to zero-order kinetics in the first 15 min (~25% o-NB degradation). Following steps stated in Section 3.1.2, the apparent photon flow obtained was 1.68×10^{-6} Einstein s^{-1} (36.1 W m^{-2}).

Fig. 3 shows that the o-NB reacts slower when TiO₂ is present in the media. It could be assumed that titania absorbs part of the incident light and besides scattering losses are taking place. The same could be proposed from the photon flows data, this value went down from 2.68×10^{-6} to 1.68×10^{-6} Einstein s^{-1} when TiO₂ was added. The presence of the suspended catalyst seemed to produce a decrease of 38% in the apparent radiation absorbed by the o-NB. Radiation was called "apparent", because it is not strictly calculated since TiO₂ absorbs part of the radiation, and that changes the wavelength distribution available for o-NB.

Next work presented was developed in order to assure that the observed difference on the photon flows was due to only TiO₂ absorption and lost scattering phenomena. Thus, possible parallel o-NB photocatalytic reactions were evaluated.
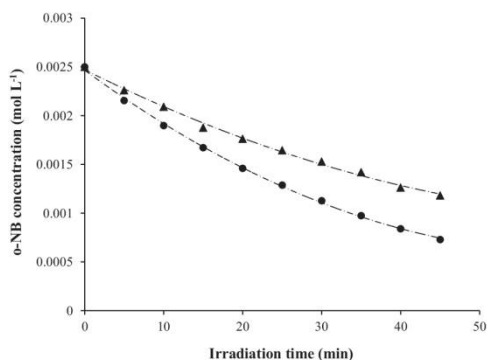
Fig. 3. Variation of o-NB concentration during time, ▲ with TiO$_2$ and ● without TiO$_2$.

3.2.2. Evaluation of possible o-NB photocatalytic reactions – chromatograms

To evaluate if o-NB was undergoing photocatalysis, HPLC chromatograms along the o-NB actinometry were studied, with and without TiO$_2$. Evaluating the HPLC chromatograms from the actinometry without TiO$_2$ (Section 3.1.2), it could be observed that o-NB (absorption bands centered around 220 and 260 nm) decreased when irradiation time increased (Fig. 4).

To date, it has been generally accepted that the photo-transformation of o-NB gives o-HNB [14–16,20]. Thus, as o-NB concentration decreased, new peaks appeared with absorption bands centered around 280 and 310 nm, which correspond to formation of the o-HNB photoproduct [21]. In addition, these peaks

increased with time, confirming the formation of o-HNB due to o-NB photoexcitation.

Observing the chromatograms of the actinometry employing 0.4 g L^{-1} of TiO$_2$ (Fig. 5), while o-NB was decreasing during irradiation, peaks corresponding to o-HNB became stronger with time; nevertheless this increase was much less noticeable than before. In this case, two new peaks came into view related to photocatalytic processes, with equal absorption bands centered around 217 and 326 nm, and became higher during irradiation competing with the formation of o-HNB peaks.

It could be assumed that photocatalytic reactions were taking place. Next step in the research was to evaluate if this unknown photocatalytic product was related to the photocatalytic transformation of the actinometer.

3.2.3. Evaluation of possible o-NB photocatalytic reactions – scavengers

To evaluate if o-NB was suffering photocatalysis when there was TiO$_2$ in the actinometric media, experiments employing different photocatalytic scavengers were carried out. The aim was to block likely pathways of the o-NB reacting with TiO$_2$ and consequently discern which reactions could be implicated. All the experiments were performed monitoring the o-NB concentration.

It is well known that reactions in photocatalysis are attributed to the presence of both dissolved oxygen and water molecules. The presence of water molecules allows the formation of the highly reactive hydroxyl radical ($^{\bullet}$OH). On the other hand, the presence of oxygen allows the formation of superoxide radical ($O_2^{\bullet-}$) and prevents the recombination of the electron-hole pair.

Furthermore, h$^+$ are powerful oxidants, while e$^-$ are good reducers, depending on the type of catalysts and oxidation conditions, so they could react directly with organic species.
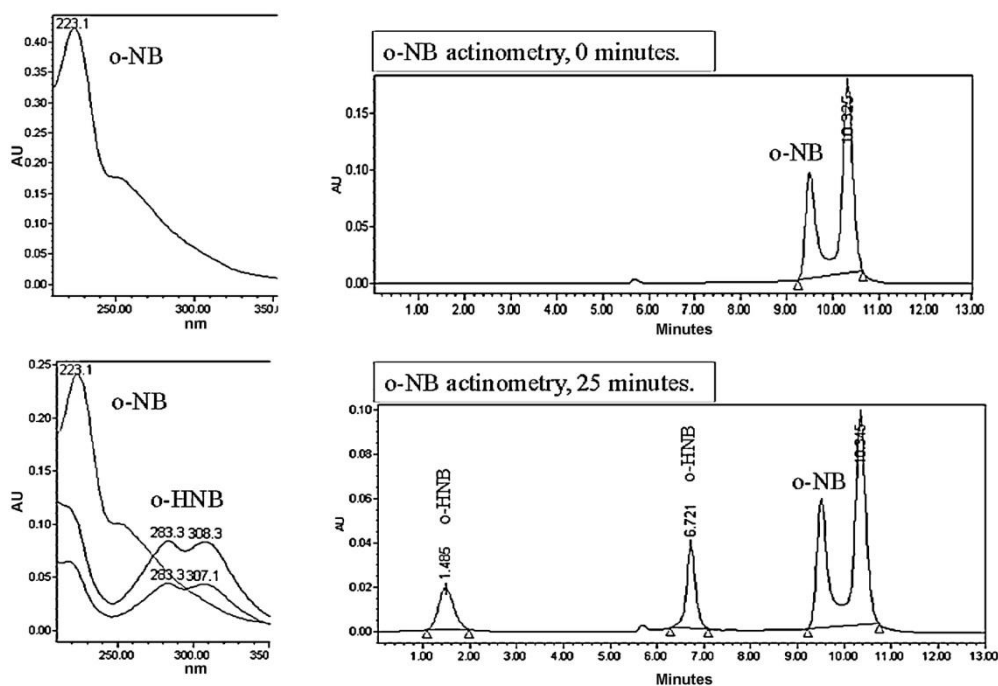

Fig. 4. o-NB actinometry without TiO$_2$. Chromatograms at times 0 and 25 min. Peaks corresponding o-NB and o-HNB. On the right side: chromatographic peaks, on the left: UV absorbances for each peak.
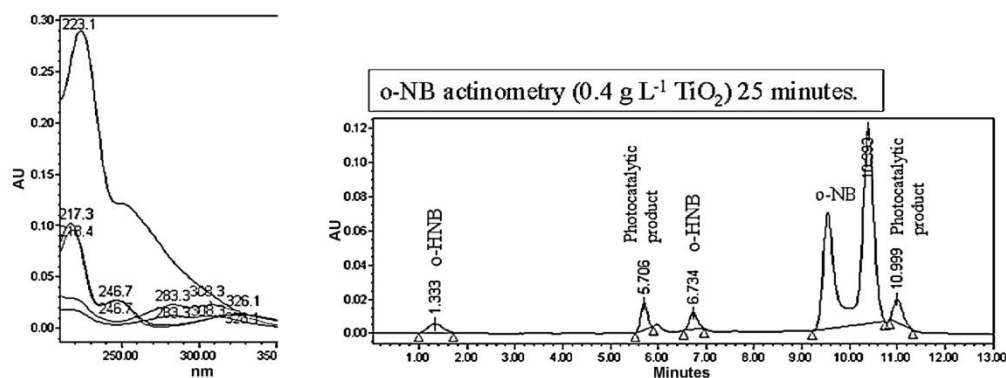
232

Fig. 5. o-NB actinometry with 0.4 g L^{-1} of TiO$_2$. Chromatogram at 25 min. Peaks of o-NB, o-HNB and a photocatalytic product. On the right side: chromatographic peaks, on the left: UV absorbances for each peak.

Thus, the reactive species (i.e., h$_{VB}^+$, e$_{CB}^-$, OH$^\bullet$, O$_2^{\bullet-}$, HOO$^\bullet$, H$_2$O$_2$, etc.) generated during TiO$_2$ photocatalysis can lead to the degradation of several compounds [2,3,22]. To recognize possible roles of the different reactive species involved in the o-NB reaction with TiO$_2$, diverse scavengers were employed.

Experiments were carried out adding 0.4 g L^{-1} of TiO$_2$, to the 0.0025 M o-NB solution and a suitable scavenger dose. The studied scavengers and its corresponding doses were: oxygen (saturation with air), p-benzoquinone (BQ) (0.027 g L^{-1} corresponding to a molar relation of 1:10 for BQ:o-NB), tert-butyl alcohol (60 and 150 mL L^{-1}) and formic acid (1 and 2 g L^{-1}, and 1 g L^{-1} combined with 150 mL L^{-1} of tert-butyl alcohol).

Oxygen is an electron scavenger used to inhibit recombination of the e$^-$/h$^+$ pair, promoting oxidative processes such as the formation of hydroxyl radicals [23]. In addition, as a result of this process, superoxide radical O$_2^{\bullet-}$ is produced, which can react directly by oxidative pathways. O$_2^{\bullet-}$ is produced by the reduction of oxygen molecules adsorbed on the catalyst surface by the photogenerated electrons [22].

To determine the O$_2^{\bullet-}$ participation in a photocatalytic reaction, benzoquinone (BQ) was used as a scavenger. BQ has the ability to trap superoxide anions by a simple electron transfer mechanism (Eq. (5)) [24,25].

$$BQ + O_2^{\bullet-} \rightarrow BQ^{\bullet-} + O_2 \tag{5}$$
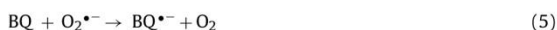
Hydroxyl radical is generally believed to play the primary role in promoting oxidation, as it has the second higher oxidation potential known. Thus, OH$^\bullet$ has very high reactivity, non-selectivity for functional groups, electrophilic behavior, and short lifetime.

tert-Butyl alcohol (t-BuOH) is a OH$^\bullet$ scavenger, reacting as illustrated by Eq. (6) [26].

$$OH^\bullet + t\text{-BuOH} \rightarrow H_2O + {}^\bullet CH_2C(CH_3)OH \tag{6}$$
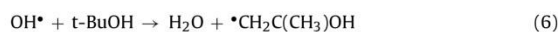
Formic acid (FA) can be used as hole (h$^+$) scavenger during TiO$_2$ photocatalysis [26–28]. This scavenger consumes the hole by HCO^{2-} (Eq. (7)), which in addition can eliminate or intercept the generation of hydroxyl radicals on TiO$_2$. Formic acid under neutral and acidic conditions is strongly adsorbed onto the surface of TiO$_2$.
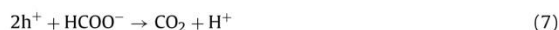
$$2h^+ + HCOO^- \rightarrow CO_2 + H^+ \tag{7}$$

Fig. 6 represents the o-NB degradation with irradiation time during actinometries employing different scavenger doses. Experiments with scavengers involved showed very similar trends. Slopes resulted to be close to the degradation profile of employing TiO$_2$ alone and even slightly higher degradation rates were observed. Somehow, scavengers contribute to o-NB consumption. Perhaps, scavengers adsorption, onto TiO$_2$ surface, modified catalyst's light absorption properties and more photons were available for the o-NB. The aim of this set of experiments was to discern if o-NB was undergoing photocatalysis besides photolysis. If o-NB had reacted by photocatalysis, the block of this reaction by any scavenger would have given a lower degradation rate, however this did not occur. Thus, from the results, we can assume that o-NB was not being consumed by photocatalytic reactions.

To discern the appearance of unknown photocatalytic products at the o-NB actinometry with suspended TiO$_2$, further experiments were carried out.

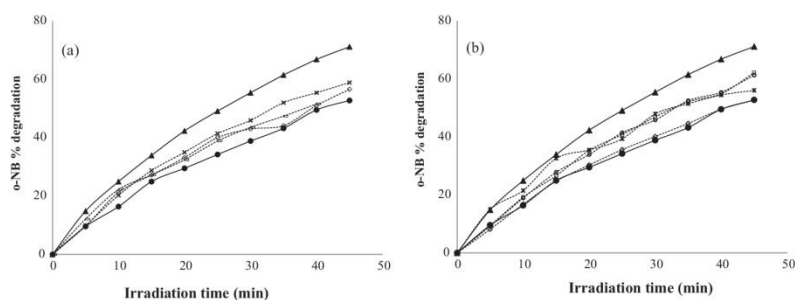**Fig. 6.** o-NB actinometries employing different scavengers. Percentage of o-NB degradation versus time ▲ without TiO$_2$ ● 0.4 g L^{-1} TiO2, (a) TiO$_2$ + 60 mL L^{-1} t-BuOH; ◇, TiO$_2$ + 150 mL L^{-1} t-BuOH; ×, TiO$_2$ + 150 mL L^{-1} t-BuOH + 1 g L^{-1} FA. (b) ×, TiO$_2$ + air; ○, TiO$_2$ + 1 g L^{-1} FA; □, TiO$_2$ + 2 g L^{-1} FA; ◇, TiO$_2$ + 0.027 g L^{-1} BQ.
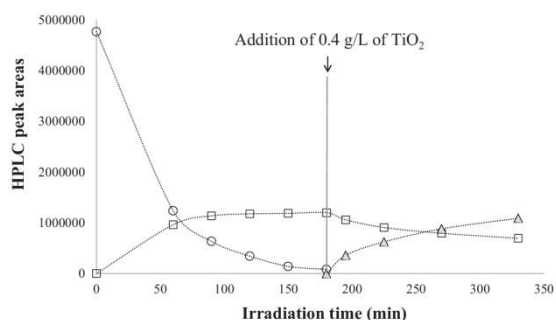
Fig. 7. Three hours of basic o-NB actinometry, followed of 1 h of photocatalysis of o-HNB with $0.4\,g\,L^{-1}$ of TiO_2. HPLC peak areas versus time. ○, o-NB; □, o-HNB; △, photocatalytic product.

3.2.4. Parallel photocatalytic reactions in o-NB actinometry

Chromatograms of the o-NB actinometry, with suspended TiO_2, showed the appearance of photocatalytic reactions. By employing scavengers, it resulted unlikely that the o-NB was undergoing photocatalysis. Thus, experiments were carried out to explain the appearance of photocatalytic products (peaks centered in 217 and 326 nm), which turned up only when there was TiO_2 involved. Following this purpose, 1 L of 0.025 M o-NB solution, without catalyst, was irradiated during 3 h to convert all the o-NB into o-HNB. Afterwards, $0.4\,g\,L^{-1}$ of TiO_2 was added to the o-HNB solution and irradiated for one additional hour.

As Fig. 7 shows, in the first 3 h of irradiation o-NB was converted into o-HNB. At this point, when catalyst was added, the o-HNB concentration decreased with irradiation time. Meanwhile, the peaks related to the photocatalytic product constantly increased. Consequently, it could be assumed that the actinometric photoproduct, o-HNB, is the compound which underwent photocatalytic reactions when TiO_2 was added, and not the o-NB.

Thus, the appearance of photocatalytic products in the o-NB actinometry, when there was TiO_2 present, was related with reactions of the photoproduct o-HNB, but not the actinometer. This means that o-NB can be used as actinometer in the presence of TiO_2, since its decomposition is only due to the radiation absorption and not to photocatalysis.

4. Conclusions

This work has given some more light to the o-NB actinometry used for photocatalytic reactors. This actinometry has not been deeply studied, as the most common ones are those based on uranyl oxalate or potassium ferrioxalate. With this purpose, o-NB actinometry was carried out in two different ways, based on pH or o-NB concentration, giving photon flows of 2.81×10^{-6} Einsteins s^{-1} and 2.68×10^{-6} Einstein s^{-1}, respectively.

In addition, this work has demonstrated that the o-NB actinometry, followed by o-NB concentration consumption, could be used in the presence of the catalyst TiO_2. HPLC analysis pointed out the apparition of photocatalytic products during the actinometry with suspended TiO_2. However, in this study we state that o-NB

suffers only photolysis and not photocatalysis, and it can be used to estimate the radiation entering the photoreactor when titania is present. It is the photolytic product (o-HNB) the compound which undergoes photocatalytic reactions when there is TiO_2 present. Thus, this actinometry may be interesting for further studies about TiO_2 radiation absorption and modeling.

References

[1] V. Romero, N. De la Cruz, R.F. Dantas, P. Marco, J. Gimenez, S. Esplugas, Catalysis Today 161 (2011) 115–120.
[2] M.N. Chong, B. Jin, C.W.K. Chow, C. Saint, Water Research 44 (2010) 2997–3027.
[3] S. Ahmed, M.G. Rasul, R. Brown, M.A. Hashib, Journal of Environment Management 92 (2011) 311–330.
[4] A. Bernabeu, R.F. Vercher, L. Santos-Juanes, P.J. Simón, C. Lardín, M.A. Martínez, J.A. Vicente, R. González, C. Llosá, A. Arques, A.M. Amat, Catalysis Today 161 (2011) 235–240.
[5] A.R. Khataee, M.B. Kasiri, Journal of Molecular Catalysis A: Chemical 328 (2010) 8–26.
[6] F. Mazille, T. Schoettl, N. Klamerth, S. Malato, C. Pulgarin, Water Research 44 (2010) 3029–3038.
[7] S. Malato, P. Fernández-Ibáñez, M.I. Maldonado, J. Blanco, W. Gernjak, Catalysis Today 147 (2009) 1–59.
[8] M.L. Satuf, M.J. Pierrestegui, L. Rossini, R.J. Brandi, O.M. Alfano, Catalysis Today 161 (2011) 121–126.
[9] O.M. Alfano, A.E. Cassano, Advances in Chemical Engineering 36 (2009) 229–287.
[10] Ballari, R. Brandi, O. Alfano, A. Cassano, Chemical Engineering Journal 136 (2008) 50–65.
[11] Marugan, R. van Grieken, A.E. Cassano, O.M. Alfano, Applied Catalysis B: Environmental 85 (2008) 48–60.
[12] H.J. Kuhn, S.E. Braslavsky, R. Schmidt, Pure and Applied Chemistry 76 (2004) 2105–2146.
[13] B. Bayarri, J. Giménez, D. Curcó, S. Esplugas, Chemical Engineering Journal 200–202 (2012) 158–167.
[14] J. Choi, M. Terazima, Journal of Physical Chemistry B 107 (2003) 9552–9557.
[15] G. Bonetti, A. Vecli, C. Viappiani, Chemical Physics Letters 269 (1997) 268–273.
[16] M.V. George, J.C. Scaiano, Journal of Physical Chemistry 84 (1980) 492–495.
[17] J.M. Allen, S.K. Allen, S.W. Baertschi, Journal of Pharmaceutical and Biomedical 24 (2000) 167–178.
[18] K.L. Willett, R.A. Hites, Journal of Chemical Education 77 (2000) 900–902.
[19] E.S. Galbavy, K. Ram, C. Anastasio, Journal of Photochemistry and Photobiology A 209 (2010) 186–192.
[20] B. Heinz, T. Schmierer, S. Laimgruber, P. Gilch, Journal of Photochemistry and Photobiology A 199 (2008) 274–281.
[21] S. Cheng, P. Song, S. Yang, H. Yin, K. Hana, Physical Chemistry Chemical Physics 12 (2010) 9067–9074.
[22] U.I. Gaya, A.H. Abdullah, Journal of Photochemistry and Photobiology C 9 (2008) 1–12.
[23] J. Ryu, W. Choi, Environmental Science and Technology 38 (2004) 2928–2933.
[24] R. Palominos, J. Freer, M.A. Mondaca, H.D. Mansilla, Journal of Photochemistry and Photobiology A 193 (2008) 139–145.
[25] P. Raja, A. Bozzi, H. Mansilla, J. Kiwi, Journal of Photochemistry and Photobiology A 169 (2005) 271–278.
[26] S. Zheng, Y. Cai, K.E. O'Shea, Journal of Photochemistry and Photobiology A 210 (2010) 61–68.
[27] V.N. Hoai Nguyen, D. Beydoun, R. Amal, Journal of Photochemistry and Photobiology A 171 (2005) 113–120.
[28] T.Y. Timothy Tan, D. Beydoun, R. Amal, Journal of Molecular Catalysis A: Chemical 202 (2003) 73–85.

Photocatalytic treatment of metoprolol and propranolol

V. Romero, N. De la Cruz, Renato F. Dantas, P. Marco, J. Giménez*, S. Esplugas

Department of Chemical Engineering, Faculty of Chemistry, University of Barcelona, C/Martí i Franquès, 1, 08028 Barcelona, Spain

A B S T R A C T

The aim of this study was to investigate and compare the effect of an advanced oxidation process, the photocatalysis, on the removal of two emerging contaminants in water; the pharmaceuticals metoprolol tartrate salt (MET) and propranolol hydrochloride (PRO). The analyzed parameters were pharmaceutical removal, total organic carbon (TOC), specific UV absorbance (SUVA), chemical oxygen demand (COD), biochemical oxygen demand (BOD_5), toxicity and formed intermediates. Besides, the optimal photocatalyst concentration was determined. Afterwards, photocatalytic experiments were carried out with $0.4 \, g \, L^{-1}$ of TiO_2 as suspended catalyst and a Xenon lamp (Philips XOP 15-OF, 1000 W) as irradiation source. According to the results, after 240 min of irradiation, a removal near to 94% was obtained for both compounds. After 360 min of treatment, a mineralization degree in the vicinity of 55% was observed. Biodegradability index (BOD_5/COD) improved from values close to zero (raw solution) up to 0.4 and 0.6 for MET and PRO. The acute toxicity measured by the inhibition percentage of bioluminescence from *Vibro fischeri* indicates that the photocatalytic treatment of this kind of compounds promotes toxicity reduction. According to the experimental results, photocatalysis appears as a useful technique for the degradation of both β-blockers.

© 2010 Elsevier B.V. All rights reserved.

1. Introduction

Environmental problems represent an increasing concern in our society and the treatment of different pollutants receives more and more attention. In this way, the emerging pollutants imply a new challenge. Among them, pharmaceuticals are an increasing problem, because, nowadays, they appear at low concentrations in surface waters. However, their increasing consumption [1] due to the increase of the world population and its age means that they can appear at high concentrations in a few years, if measures are not taken. Drugs in waters come from hospitals, pharmaceutical industry or from domestic waters, by rejected drugs not used or by human excretions, because they are partially metabolized by the body and excreted [2].

Once in the sewage treatment plants, the complete removal of these pharmaceuticals cannot be assured by conventional water treatment methods because of the recalcitrant nature of many of these compounds. In addition, the amount of these compounds is continuously increasing and they can arrive to be ecotoxicological important [2], because of their biological activity, causing potential environmental impact. Ecotoxicological studies show that aquatic organisms are sensitive to these substances.

Metoprolol tartrate salt (MET) and propranolol hydrochloride (PRO) are two β-blockers which may be considered as emerging contaminants, which have not been deeply studied yet. Both are used for several diseases such as hypertension, angina pectoris, cardiovascular system and lately chronic heart failure [3–6]. Propranolol has the highest acute and chronic toxicity within the class of the β-blockers, followed by metoprolol [7–9]. These two β-blockers have been detected in surface waters [10–12] and, in addition, this kind of compounds appear in sewage treatment plants, and they cannot be totally eliminated [7,12–17]. Due to the potential environmental effects of the target compounds, alternative treatments should be tested. Advanced oxidation processes (AOPs) appear as a good alternative. Some references report the treatment of these drugs by different oxidation processes. Metoprolol can be degraded by UV/H_2O_2 [18,19], photo-Fenton [5,18], ozonation [20], UV/O_3, O_3/H_2O_2 [19] and photocatalysis [5,6]. On the other hand, the AOPs used to treat propranolol which have been studied are: ozonation [21,22], photodegradation [23,24], UV/H_2O_2 [22,25], UV/O_3 [25], O_3/H_2O_2 [25], photocatalysis [6,22].

Previous reports, which have studied the effect of photocatalysis on metoprolol and propranolol, provided data of degradation, kinetics, effect of the pH, intermediates and degradation pathways [6]. Besides, toxicity tests (*Synechococcus leopoliensis* and *Brachyonus calyciflorus*) have also been studied [22]. Although previous works attempted to investigate the degradation of MET and PRO by photocatalysis, this work contributes with experiments carried

---

a MET molecular structure   b PRO molecular structure
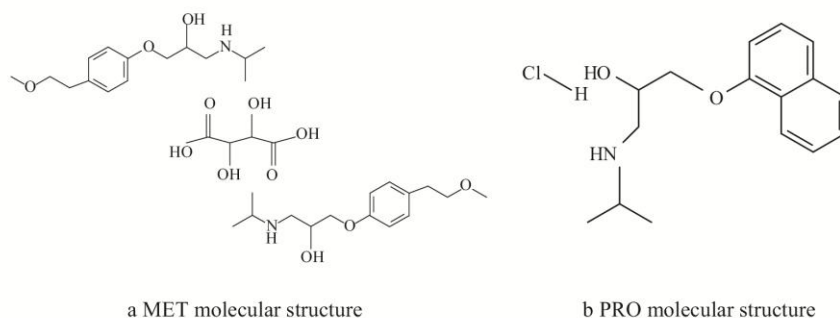
Fig. 1. β-Blockers molecular structures.

out with simulated solar light (Xe lamp) as well as investigates the biodegradability, organic matter oxidation and acute ecotoxicity (*Vibro fischeri*) of the formed intermediates along the reaction time.

The aim of this work is to test the possibilities of a photocatalytic treatment of MET and PRO by using TiO_2 in suspension as catalyst for their removal. In addition, the effect of the TiO_2 loading, the evolution of some lumped parameters as TOC, COD, BOD, SUVA and the toxicity will give important information about the degradation of the main pollutants and their reaction.

2. Materials and methods

2.1. Chemicals

Aqueous pharmaceutical solutions were prepared in Milli Q water with MET [56392–17–7] and PRO [318–98–9], which were purchased from Sigma–Aldrich Chemical Co. (Spain). Synthetic amorphous titanium dioxide (Degussa P-25, Spain) was used as received. Fig. 1 shows the structure of the target pharmaceuticals, in order to facilitate the understanding of the reaction between •OH radicals and the pharmaceuticals.

2.2. Analytical procedures

The target compounds concentrations were monitored by a high-performance liquid chromatograph (HPLC) from Waters using a *SEA18* 5 μm 15 × 0.46 Teknokroma column, and a Waters 996 photodiode array detector using the Empower Pro software 2002 Water Co. The mobile phases were composed by water and acetonitrile (MET 20:80 and PRO 50:50), injected with a flow-rate of 0.85 and 0.80 mL min^{-1} and detected at maximum UV absorbance set at wavelengths of 221.9 and 213.7 for MET and PRO, respectively. In order to remove the catalyst, before the HPLC analysis, samples were filtered with a polyethersulfone membrane filter of 0.45 μm.

Total organic carbon (TOC) was measured in a Shimadzu TOC-V CNS instrument. Spectrophotometric measurements to obtain MET and PRO absorption spectrum were carried out in a PerkinElmer UV/vis Lambda 20 (220–700 nm range) spectrophotometer. Biochemical oxygen demand (BOD$_5$) determinations were carried out according to the Standard Methods (5120) by the OxiTop® procedure. To analyze the chemical oxygen demand (COD), the Standard Methods (5220D) procedures were followed. The specific UV absorbance (SUVA$_{254\,nm}$) values were calculated dividing the UV$_{254\,nm}$ absorbances by COD (SUVA = (UV$_{254}$/COD) × 100). pH was measured by a Crison GLP 22 instrument. The ecotoxicity of the samples were measured by the acute toxicity using Microtox tests, where the inhibition of *Vibrio fischeri* bioluminescence at 15 min

of incubation was determined. For the intermediates identification, samples were analyzed by the electrospray ionization/mass spectrometry using an electrospray (ion spray) ESI-MS, and a LC-MSD-TOF (2006) mass spectrometer [26,27].

2.3. Photoreactor

A stirred reservoir tank (1.0 L) was filled with the pharmaceutical-TiO_2 (suspended) aqueous solution. The aqueous suspension was continuously pumped (peristaltic pump Ecoline VC-280 II, Ismatec) into the Solarbox (Co.fo.me.gra 220 V 50 Hz) and recirculated to the reservoir tank with a flow of 0.65 L min^{-1}. In the Solarbox, the Duran tubular photoreactor (0.078 L) was irradiated by a Xe-OP lamp (Phillips 1 kW) with a photon flux equal to 3.34×10^{-5} Einstein s^{-1} (290–400 nm), determined by uranyl oxalate actinometry [28]. In order to keep the solution at 25 °C, the jacket temperature of the stirred tank was controlled with an ultra-thermostat bath (Haake K10). All connections and pipes employed were made of Teflon and/or glass material to avoid losses by adsorption.

3. Results and discussion

As shown in Fig. 1, pharmaceutical solutions were not prepared with the pure compound. The salt present in the MET commercial form has influence on analytical measurements, and this fact has to be taken into account in the assessment of MET photocatalytic degradation.

As a first step, blank experiments were carried out to verify the influence of secondary source of errors in the results. Blank experiments of photolysis, adsorption and stripping were performed, accomplishing a maximum error of 4.7% for MET, and 9.0% for PRO.

Reproducibility experiments were carried out as well, obtaining a standard deviation average of 0.33 on the pharmaceutical removal for MET, and 2.24 for PRO.

3.1. MET and PRO removal

The initial pharmaceutical concentration solution chosen was 50 mg L^{-1}. Experiments with pharmaceuticals concentration close to the range detected in real water samples were not possible due to analytical limitations. Before carrying out the assessment of the pharmaceuticals removal, the determination of the best catalyst concentration for our system was attempted.

3.1.1. Influence of TiO_2 concentration

A scanning of TiO_2-catalyst concentration was performed for both compounds. Fig. 2 shows the pharmaceuticals removal after
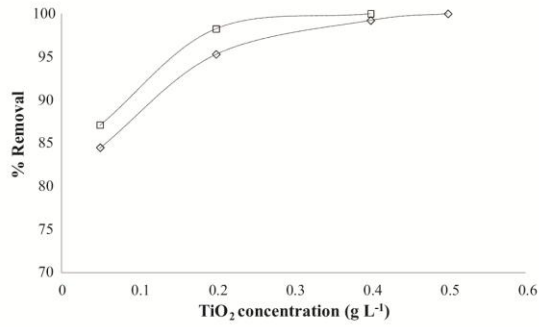
Fig. 2. MET and PRO scan TiO$_2$–catalyst concentration at 6 h of experiment. ◊: PRO; □: MET.

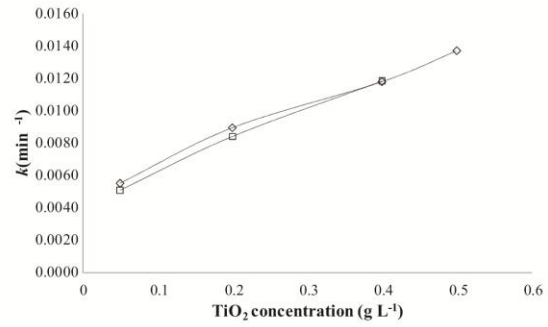**Fig. 4.** MET and PRO kinetic constants (300 min). □: MET; ◊: PRO.

360 min of treatment vs. TiO$_2$ concentration. The experiment lasted about 360 min to ensure the total pharmaceutical removal from the solution. TiO$_2$ ranged from 0.05 and 0.5 g L^{-1}, which were chosen as the most used concentrations find on the literature surveillance. For both compounds, the final removal increased when the catalyst concentration also increased. Although the highest catalyst concentration (0.5 g L^{-1}) achieved the best result, the concentration of 0.4 g L^{-1} appeared to be the best condition investigated, because catalyst deposition in the reactor can appear when working at higher concentrations.

3.1.2. Compounds removal and kinetics

Working with 0.4 g TiO$_2$ L^{-1}, the two compounds removal was followed during the photocatalytic process (Fig. 3). The treatment was able to completely remove MET and PRO after 300 and 360 min of irradiation, respectively.

In order to quantify the β-blockers removal rate, the pseudo-first order kinetic constant (k) was calculated for each TiO$_2$ concentration (see Fig. 4). k values could be obtained from the regression curves slopes representing $-\ln(C/Co)$ vs. time, within the period of 300 min, for each TiO$_2$ concentration. Constant values for 0.4 g TiO$_2$ L^{-1} obtained were 0.0113 ± 5 × 10^{-4} min^{-1} for MET and 0.0118 ± 3 × 10^{-4} min^{-1} for PRO. Thus, it can be assumed that the studied compounds have similar degradation behavior when treated by photocatalysis. The pH of the treated samples decreased slowly during the reaction time, standing at acidic condition during all the reaction. Although the main structural difference between

the studied compounds is in the aromatic rings, the results indicate that their removal rates are similar. On the other hand, the organic salt present in MET commercial formulation should be taken into account since it would compete with MET molecules for the reaction with •OH radicals.

Fig. 5. TOC/TOCo, COD/CODo and SUVA for MET and PRO photocatalysis, using 0.4 g TiO$_2$ L^{-1}. *: TOC/TOCo$_{MET}$; o: COD/CODo$_{MET}$; +: SUVA$_{MET}$; ◊: TOC/TOCo$_{PRO}$; △: COD/CODo$_{PRO}$; □: SUVA$_{PRO}$.
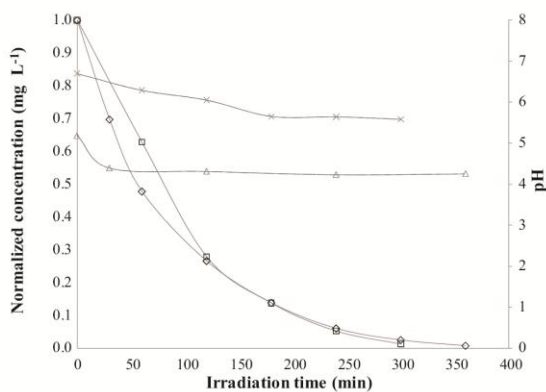
Fig. 3. MET and PRO photocatalysis removal, using 0.4 g TiO$_2$ L^{-1}. □: MET; ◊: PRO; x: pH$_{MET}$; △: pH$_{PRO}$.

237

Table 1
Intermediates proposed structures for the photocatalytic degradation of MET and PRO.

Compound	m/z (+)	Molecular formula	Proposed Structure
Metoprolol	268	C15H25NO3	
A	300	C15H25NO5	
B	318	C15H27NO6	
C	134	C6H15NO2	
Propranolol	260	C16H21NO2	
A′	266	C14H19NO4	
B′	282	C14H19NO5	
C′	292	C16H21NO4	
D′	308	C16H21NO5	

3.2. Intermediates oxidation and identification

3.2.1. Mineralization, oxidation and aromaticity

Fig. 5 represents the normalized TOC and COD concentration during the photocatalytic process. The mineralization and oxidation profile, represented as the TOC and COD removal, decreased significantly during the irradiation time, achieving values near to 55% after 360 min. It is remarkable that TOC and COD removal reached high values, indicating that the oxidation of intermediates promoted a continuous cleavage of the initial organic structures. Aromaticity, represented by SUVA, which is a measure that indicates the DOC aromatic content, was determined. SUVA is calculated by measuring the DOC and the UV absorbance at 254 nm of a 0.45 μm filtered water sample. Unexpectedly, a global increase of aromaticity appeared. While scanning it during the experiment, it could be seen how it increased in the first hours (Fig. 5). Finally, there is a decrease of it at six hours of irradiation, where the value goes down, but still being higher than the initial one.
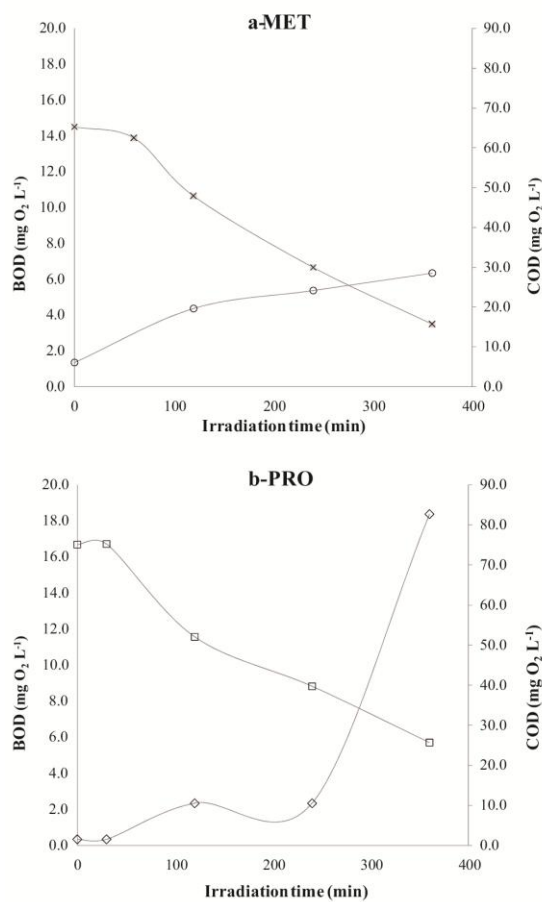
Fig. 6. BOD and COD for MET and PRO photocatalysis, using $0.4\,g\,TiO_2\,L^{-1}$. o: BOD_{MET}; x: COD_{MET}; $\Diamond$: BOD_{PRO}; $\square$: COD_{PRO}.

3.2.2. Intermediates identification

Intermediates identification was carried out in samples collected in the range of 180-360 min of treatment, where intermediates' chromatographic picks had high intensity. Several ions masses were identified during the β-blockers photocatalytic degradation. The *m/z* (mass-to-charge ratio) is shown in Table 1.

According to the proposed structures, the oxidation of PRO takes place mainly by the cleavage of the naphthalene ring. However, before this step of oxidation, the continuous hydroxylation of the aromatic ring should occur. Although, the intermediate B′ and D′ would be formed due to an additional •OH attack on the amino group, this pathway of oxidation is not favored in the experimental conditions used. The intermediate D′ was already found in a great extent by the ozonation of PRO at pH 8, where the presence of •OH radical is noticeable [21]. As the pKa of PRO is about 9.42 [23], the reactivity of the amino group is very weak. The step of oxidation on the amino group could be considered as a secondary reaction pathway, occurring only when the oxidized naphthalene ring became less reactive. Concerning the MET oxidation, a similar degradation pathway is proposed. Hydroxyl radical supposed to attack the aromatic ring in first place. Afterwards an additional hydroxylation would happen. As already commented, some inter-

mediates would come from the •OH attack on the amino group as a secondary reaction center, which was the case of the proposed intermediate B. Intermediate C, would be in a more advanced oxidation state, when the aromatic ring is completely oxidized. The formation of intermediate C is in agreement with a degradation pathway proposed in a previous work [6].

3.3. Biodegradability and toxicity assessment

In order to evaluate the suitability of the photocatalytic treatment in waters containing β-blockers, the biodegradability and toxicity tests were performed along the reaction time. For both compounds, the biodegradability (BOD_5/COD) of the un-treated solution was near zero, indicating that the target compounds solutions are not biodegradable. Nevertheless, the continuous compounds oxidation promoted by the reaction with hydroxyl radicals favored the formation of more biodegradable compounds.

Fig. 6 performances BOD and the COD for both compounds during the treatment, showing an increase on the BOD while the COD decreases during the irradiation time.

With the aim of illustrating the biodegradability profile of the formed intermediates during the photocatalytic process, Fig. 7
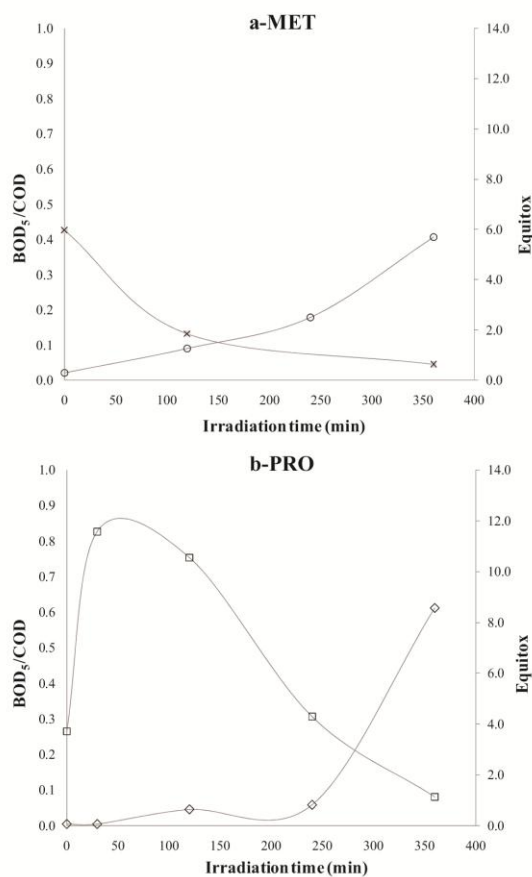

Fig. 7. BOD_5/COD and equitox for MET and PRO photocatalysis, using $0.4\,g\,TiO_2\,L^{-1}$. o: BOD_5/COD_{MET}; x: $Equitox_{MET}$ $\Diamond$: BOD_5/COD_{PRO}; $\square$: $Equitox_{PRO}$.

depicts the biodegradability indicator value (BOD_5/COD) during the reaction time. MET oxidation leaded to a gradual formation of more biodegradable compounds since the first minutes of reaction, achieving at the end of irradiation time a biodegradability indicator value higher than 0.4. In the case of PRO, the biodegradability improvement was not observed until 250 min of treatment. At the end of the experiment (360 min), the formation of high biodegradability products was observed. Therefore, treatment time is an important factor to improve the biodegradability of the effluent in waters polluted with PRO. To complement the information about the hazardousness of a treated effluent to the environment, the toxicity assessment was also carried out. The toxicity of the treated samples presented different trends. Fig. 7a shows that the oxidation of MET promoted the overall toxicity reduction of the sample since the beginning of the treatment. On the other hand, PRO photocatalytic treatment (Fig. 7b) induced a first step of oxidation where the formed intermediates are more toxic than the primary compound. Then, after 30 min of irradiation, the toxicity decreases constantly, achieving a lower toxicity value after 360 min. Consequently, this behavior confirms the importance of the reaction time in the case of the treatment of waters containing PRO. The overall toxicity reduction caused by the oxidation of the target compounds shown in this work is in agreement with previous investigation carried out with other toxicity methods [22].

4. Conclusions

- At the used experimental conditions, photocatalytic treatment was proved to be an effective method to achieve mineralization degrees in the vicinity of 55% for waters containing β-blockers MET and PRO.
- The tested compounds presented similar removal rate by photocatalysis. After 360 min of treatment, with $0.4\,g\,L^{-1}$ of catalyst, both compounds were totally removed.
- The oxidation of MET and PRO is accomplished mainly due to the •OH attack on the aromatic rings with the posterior cleavage of the naphthalene group in the case of PRO and formation of aliphatic compounds after MET oxidation.
- Biodegradability of the samples increased with time. However, in the case of PRO, biodegradability starts to increase only after 4 h of treatment, implying that the irradiation time is an important factor.
- 360 min of irradiation promoted the decrease of the overall toxicity of the samples. Nevertheless, a toxicity peak is observed in the first minutes of reaction of the PRO solution.

Acknowledgements

References

[1] M. Grung, T. Kallqvist, S. Sakshaug, S. Skurtveit, K. Thomas, Environmental assessment of Norwegian priority pharmaceuticals based on the EMEA guideline, Ecotoxicology and Environmental Safety 71 (2008) 328.

[2] L. Santos, A. Araújo, A. Fachini, A. Pena, C. Deleure-Matos, M. Montenegro, Ecotoxicological aspects related to the presence of pharmaceuticals in the aquatic environment, Journal of Hazardous Materials 175 (2010) 45.

[3] J. Franciosa, β-Adrenergic blocking agents: past, present, and future perspectives, Coronary Artery Disease 10 (1999) 369.

[4] The merck Index, 12th ed., Entry # 6235.

[5] F. Rivas, O. Gimeno, T. Borralho, M. Carbajo, UV-C radiation based methods for aqueous metoprolol elimination, Journal of Hazardous Materials 179 (2010) 357.

[6] H. Yang, G. Taicheng An, W. Li, W. Song, H. Cooper, X. Luo, Guo, Photocatalytic degradation kinetics and mechanism of environmental pharmaceuticals in aqueous suspension of TiO_2: a case of β-blockers, Journal of Hazardous Materials 179 (2010) 834.

[7] M. Maurer, B. Richle, C. Schaffner, A. Alder, Elimination of β-blockers in sewage treatment plants, Water Research 41 (2007) 1614.

[8] A. Munch Christensen, B. Markussen, A. Baun, B. Halling-Sörensen, Probabilistic environmental risk characterization of pharmaceuticals in sewage treatment plant discharges, Chemosphere 77 (2009) 351.

[9] K. Fent, A. Weston, D. Caminada, Ecotoxicology of human pharmaceuticals, Aquatic Toxicology 76 (2006) 122.

[10] M. Gros, M. Petrovic, A. Ginebreda, D. Barceló, Removal of pharmaceuticals during wastewater treatment and environmental risk assessment using hazard indexes, Environment International 36 (2010) 15.

[11] M. Gros, M. Petrovic, D. Barceló, Wastewater treatment plants as a pathway for aquatic contamination by pharmaceuticals in the Ebro river basin (Northeast Spain), Environmental Toxicology and Chemistry 26 (2007) 1553.

[12] C.M. Coetsier, S. Spinelli, L. Lin, Discharge of pharmaceutical products (PPs) through a conventional biological sewage treatment plant: MECs vs PECs? Environment International 35 (2009) 787.

[13] J.L. Zhou, Z.L. Zhang, E. Banks, Pharmaceutical residues in wastewater treatment works effluents and their impact on receiving river water, Journal of Hazardous Materials 166 (2009) 655.

[14] T.A. Ternes, Analytical methods for the determination of pharmaceuticals in aqueous environmental samples, Trac-Trends in Analytical Chemistry 20 (2001) 419.

[15] D.L. Sedlak, K. Pinkston, C.H. Huang, Occurrence Survey of Pharmaceutically Active Compounds, AWWA Research Foundation, Denver, CO, USA, 2005.

[16] R. Andreozzi, M. Raffaele, P. Nicklas, Pharmaceuticals in STP effluents and their solar photodegradation in aquatic environment, Chemosphere 50 (2003) 1319.

[17] M. Gros, M. Petrovic, D. Barceló, Development of a multi-residue analytical methodology based on liquid chromatography–tandem mass spectrometry (LC–MS/MS) for screening and trace level determination of pharmaceuticals in surface and wastewaters, Talanta 70 (2006) 678.

[18] F. Benitez, F. Real, J. Acero, Removal of selected pharmaceuticals in waters by photochemical processes, Chemical Technology Biotechnology 84 (2009) 1186.

[19] I.H. Kim, H. Tanaka, T. Iwasaki, Classification of the degradability of 30 pharmaceuticals in water with ozone and H_2O_2, Water Science Technology 57 (2008) 195.

[20] N. Vieno, H. Harkki, T. Tuhkanen, L. Kronberg, Ocurrence of pharmaceuticals in river water and their elimination in a pilot-scale drinking water treatment plant, Environmental Science and Technology 41 (2007) 5077.

[21] J. Benner, T. Ternes, Ozonation of propranolol: formation of oxidation products, Environmental Science and Technology 43 (2009) 5086.

[22] R. Andreozzi, L. Campanella, B. Fraysse, Effects of advanced oxidation processes (AOPs) on the toxicity of a mixture of pharmaceuticals, Water Science and Technology 50 (2004) 23.

[23] I. Kim, H. Tanaka, Photodegradation characteristics of PPCPs in water with UV treatment, Environment International 35 (2009) 793.

[24] A. Piram, A. Salvador, C. Verne, Photolysis of β-blockers in environmental waters, Chemosphere 73 (2008) 1265.

[25] I.H. Kim, N. Yamashita, Y. Kato, Discussion on the application of UV/H2O2, O3 and O3/UV processes as technologies for sewage reuse considering the removal of pharmaceuticals and personal care products, Water Science and Technology 59 (2009) 945.

[26] Z. Spáčil, L. Nováková, P. Solich, Comparison of positive and negative ion detection of tea catechins using tandem mass spectrometry and ultra high performance liquid chromatography, Food Chemistry 123 (2010) 535.

[27] B. Avula, Y.-H. Wang, R.S. Pawar, Y.J. Shukla, B. Schaneberg, I.A. Khan, Determination of the appetite suppressant P57 in Hoodia gordonii plant extracts and dietary supplements by liquid chromatography/electrospray ionization mass spectrometry (LC-MSD-TOF) and LC-UV methods, Journal of AOAC International 89 (2006) 606.

[28] A. Braun, M.T. Maurette, E. Oliveros, Photochemical Technology, Wiley, 1991.

Research Article

Adsorption and Photocatalytic Decomposition of the β-Blocker Metoprolol in Aqueous Titanium Dioxide Suspensions: Kinetics, Intermediates, and Degradation Pathways

Violette Romero, Pilar Marco, Jaime Giménez, and Santiago Esplugas

Department of Chemical Engineering, University of Barcelona, C/Martí i Franquès 1, 08028 Barcelona, Spain

Correspondence should be addressed to Pilar Marco; pmarco@ub.edu

This study reports the photocatalytic degradation of the β-blocker metoprolol (MET) using TiO_2 suspended as catalyst. A series of photoexperiments were carried out by a UV lamp, emitting in the 250–400 nm range, providing information about the absorption of radiation in the photoreactor wall. The influence of the radiation wavelength on the MET photooxidation rate was investigated using a filter cutting out wavelengths shorter than 280 nm. Effects of photolysis and adsorption at different initial pH were studied to evaluate noncatalytic degradation for this pharmaceutical. MET adsorption onto titania was fitted to two-parameter Langmuir isotherm. From adsorption results it appears that the photocatalytic degradation can occur mainly on the surface of TiO_2. MET removed by photocatalysis was 100% conditions within 300 min, while only 26% was achieved by photolysis at the same time. TiO_2 photocatalysis degradation of MET in the first stage of the reaction followed approximately a pseudo-first-order model. The major reaction intermediates were identified by LC/MS analysis such as 3-(propan-2-ylamino)propane-1,2-diol or 3-aminoprop-1-en-2-ol. Based on the identified intermediates, a photocatalytic degradation pathway was proposed, including the cleavage of side chain and the hydroxylation addition to the parent compounds.

1. Introduction

The presence of pharmaceutical drugs and endocrine disruptors in surface, ground, and drinking waters is a growing environmental concern [1–9]. This pollution is caused by emission from production sites, direct disposal of surplus drugs in households, excretion after drug administration to humans and animals, wastewater from fish and other animal farms, and industry [3, 10, 11]. Some of these drugs, as β-blockers, have been detected in the order of $ng\,L^{-1}$ to $\mu g\,L^{-1}$ in the water [3–9, 12]. As an example, metoprolol tartrate salt (MET), which is usually prescribed as antihypertensive or antiarrhythmic, has been quantified up to $2\,\mu g\,L^{-1}$ in sewage treatment plant (STP) effluents and to $240\,ng\,L^{-1}$ in rivers [13]. Metoprolol and atenolol together account for more than 80% of total β-blockers consumption in Europe [6]. During the last years, metoprolol usage increased by a factor of 4, probably due to a change in human behavior [6]. Although full ecotoxicity data are not available [13, 14], it has been

shown that they can adversely affect aquatic organisms, even at low concentration [2]. Due to its widespread occurrence and potential impact, MET must be removed from treated water before discharge or reuse.

Several treatments for the removal of these compounds have been reported in the literature, including membrane filtration [15], activated carbon adsorption [16], and reverse osmosis [17, 18]. However, the conventional water treatment processes are relatively inefficient in treating these compounds [4, 19]. These pharmaceuticals can undergo abiotic degradation (hydrolysis, photolysis) [13] and most of them are photoactive because their structural compositions consist of aromatic rings, heteroatoms, and other functional groups that can absorb solar radiation [20]. Thus, sunlight induced photochemical treatments should be considered as an alternative to traditional treatment. Several researches have demonstrated that MET shows slow direct phototransformation and/or hydrolysis [13, 21, 22]. In this context, advanced oxidation processes (AOPs) appear as a good
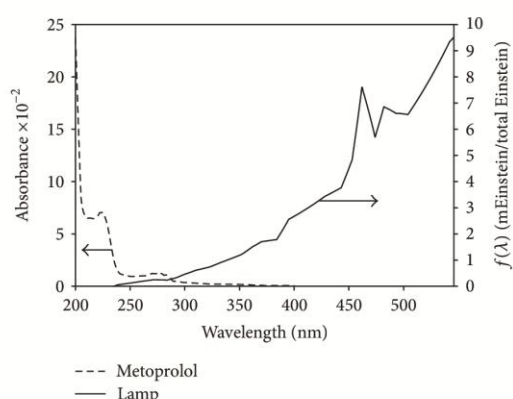
FIGURE 1: Absorbance spectrum of MET for aqueous concentration of $10 \, \text{mg L}^{-1}$ (left axis) and lamp spectrum (right axis), where $f(\lambda)$ represents the spectral distribution of the lamp.

and they were used without further purification. Titanium dioxide (TiO_2) Degussa P-25 (commercial catalyst ~70% anatase, ~30% rutile, surface area $50 \pm 5.0 \, \text{m}^2 \, \text{g}^{-1}$, and $300 \, \mu\text{m}$ particle size [25]) was used as received. This TiO_2 is a photochemical stable material [6, 26, 27].

2.2. Analytical Instruments. The target compounds concentrations were monitored by a high-performance liquid chromatograph (HPLC) from Waters using a *SEA18* $5 \, \mu\text{m}$ 15×0.46 Teknokroma column and Waters 996 photodiode array detector using Empower Pro software 2002 Water Co. The mobile phase was composed by water and acetonitrile ($20 : 80$), injected with a flow-rate of $0.85 \, \text{mL min}^{-1}$, and detected at maximum metoprolol (221.9 nm). Total organic carbon (TOC) was measured in a Shimadzu TOC-V CNS. pH was measured by a Crison GLP 22 instrument. UV-VIS spectra of MET (Figure 1) were obtained for $10 \, \text{mg L}^{-1}$ aqueous solution on a PerkinElmer UV/vis Lambda 20 (200–400 nm range) spectrophotometer.

alternative for its degradation due to their versatility and ability to increase biodegradability [23, 24]. Among the different advanced oxidation processes, heterogenous photocatalysis has been a potential alternative for the degradation of hazardous pollutants. Oxidation of organic compounds by means of TiO_2 was achieved by hydroxyl radical generation through the e^-/h^+ pair generated when the semiconductor is exposed to UV radiation [11, 14].

The main objective of this investigation is to undertake a study on the heterogeneous photocatalytic degradation and mineralization of MET in aqueous suspensions with TiO_2. In addition, the contribution of the degradation of MET by direct photolysis and the adsorption of the metoprolol onto TiO_2 were studied. In this way, the effect of different initial pH values on the photodegradation rate and the adsorption isotherms of metoprolol in TiO_2 suspensions were determined. The contribution of direct photolysis in photocatalysis was also examined in detail by using different wavelengths and glass type photoreactors. Additionally, an attempt has been completed to estimate the kinetic parameters and to identify the main intermediates formed during the photocatalytic degradation of MET.

2. Materials and Methods

2.1. Chemicals and Reagents. Metoprolol tartrate (MET) salt was purchased from Sigma Aldrich Chemical Co. (Spain) and used as received (1-[4-(2 methoxyethyl)phenoxy]-3-(propan-2-ylamino)propan-2-ol tartrate (2:1), CAS no 56392-17-7, $(C_{15}H_{25}NO_3)_2 \, C_4H_6O_6$, MW 684.81). Solutions of $50 \, \text{mg L}^{-1}$ of MET were prepared using deionized water to assure accurate measurements of concentrations, to follow the TOC, to secure identification of intermediates, and to make predictions about possible mechanisms of photocatalysis. For pH adjustment, $0.1 \, \text{mol L}^{-1}$ sulphuric acid or $0.1 \, \text{mol L}^{-1}$ sodium hydroxide was used. All chemicals were HPLC grade,

2.3. Experimental Procedure. Photodegradation experiments were conducted in a Solarbox (CO.FO.MEGRA, Milan, Italy) and equipped with a Xenon lamp (Phillips XOP, 1000W) and a tubular-horizontal photoreactor (0.084L illuminated volume) located at the axis of a parabolic mirror in the bottom of the Solarbox. The photon flux inside the photoreactor was evaluated by o-nitrobenzaldehyde actinometry [28, 29], being $2.68 \, \mu\text{Einstein s}^{-1}$. A stirred reservoir tank (1.0 L) was filled with the pharmaceutical-TiO_2 (suspended) aqueous solution. The solution was continuously pumped (peristaltic pump Ecoline VC-280 II, Ismatec) to the equipment and recirculated to the reservoir tank with a flow of $0.65 \, \text{L min}^{-1}$. In order to keep the solution at $25°C$, the jacket temperature of the stirred tank was controlled with an ultrathermostat bath (Haake K10). Samples were taken every 30 minutes during 300 minutes and quickly analyzed. Before HPLC analysis, samples were filtered through $0.20 \, \mu\text{m}$ PVDF membrane to separate TiO_2. All the experiments were duplicated and the results presented were the mean values.

According to the literature [13], metoprolol stability in aqueous solution was previously verified, by storing $50 \, \text{mg L}^{-1}$ during 3 days in the dark at room temperature, and no degradation was observed.

MET adsorption of TiO_2 was also measured. Thus, MET solution (0 to $50 \, \text{mg L}^{-1}$) was prepared with TiO_2 in suspension ($0.4 \, \text{g L}^{-1}$) and placed into 25 mL hermetic closed flasks, adjusting the pH with NaOH solution ($0.1 \, \text{mol L}^{-1}$). The conical flasks were shaken at a constant speed of 100 rpm and at room temperature ($25 \pm 0.5°C$). Samples were taken every 24 h, assuming that adsorption equilibrium was reached.

For the identification of byproducts, the final sample mixture, at 300 minutes, was analyzed by electrospray ionization/mass spectrometry using a PerSeptive, TOF Mariner Jascoo AS-2050 plus IS mass spectrometer into the m/z range of 50–1000. The experiments were carried out in replicate.
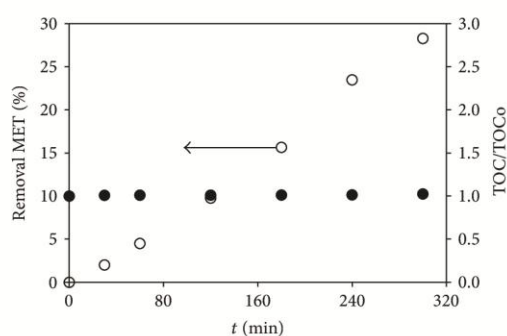
3

FIGURE 2: MET photodegradation removal (○) and TOC/TOCo (●) under simulated UV.

3. Results and Discussion

3.1. Effect of UV Radiation Photolysis on Metoprolol Degradation. When studying photocatalysis, it is very important to be able to separate the influence of photolysis, since it is expected to tackle the degradation of the substances mainly induced by the action of the catalyst. For this purpose, a series of experiments was done with UV illumination, and without catalyst to highlight the metoprolol ability to absorb the radiation reaching the system.

Figure 2 shows the results obtained after applying simulated sunlight. As observed, MET is not fast enough to be photodegraded in water by direct photolysis [30]; only 26% of MET in 300 minutes was degraded under simulated UV. Moreover, it shows that direct photolysis was not able to produce MET mineralization at the experimental conditions tested. This behavior can be explained because the MET absorption spectrum overlaps only slightly the spectrum of the incoming radiation (Figure 1).

The UV-VIS absorbance was used to calculate the molar absorption coefficient (ε) of the metoprolol at a wavelength of 221.9 nm (Figure 1), assuming that Beer-Lambert's law is followed:

$$A = -\log(T) = \varepsilon \times l \times C, \qquad (1)$$

where A is the absorbance (measured directly by the spectrophotometer), T is the transmittance, ε is the molar absorption coefficient, l is the distance that the light travels through the material, and C is the concentration of pollutant. The molar absorption coefficient (ε) was 281 L mol^{-1} cm^{-1}; this value is very similar to other reported values [12, 13]. This low value explains the MET stability in direct photolysis conditions. Nevertheless, different studies [12, 13, 31] show a high photoability of some β-blockers, for example, propranolol, nadolol, and alprenolol. The rapid photodegradation of these compounds was supported by a high molecular absorption coefficient ($\varepsilon > 800$ L mol^{-1} cm^{-1}). This confirmed the hypothesis that photoinitiated reactions contribute to the degradation of naphthalene backbone (i.e., propranolol) [32], whereas the metoprolol, having a benzoic skeleton, is not sensitive to direct photolysis when dissolved in deionized water [33].
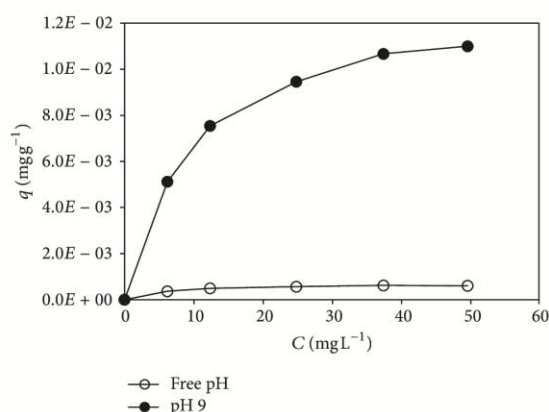

FIGURE 3: Effect of pH on adsorption of MET over TiO$_2$ at 25°C, pH 9 (●), and free pH (○).

The efficiency of the photochemical transformation process depends on many factors such as the irradiation setups, the characteristics of the light source, the water matrix used, the initial concentration, and the pH of the solutions [31]. Tests were carried out using different photoreactors, a borosilicate Duran, and quartz glass reactor, cutting out wavelengths shorter than 290 and 320 nm, respectively. Other experiments have been done with and without glass filter for restricting transmissions of light below 280 nm.

In this study, the effect of borosilicate Duran and quartz glass material reactor has been investigated under UV radiation. It was observed that MET removal was 25% and 28% and the TOC reduction was 3.60% and 1.62%, for reactors made with borosilicate Duran and quartz, respectively. Thus, although the mineralization was not significant, there is a small photodegradation of MET for the two tested reactors, after 300 minutes of reaction. Moreover, the effect of a filter glass cutting out wavelengths shorter than 280 nm has been investigated. As a result, only 19% of MET in 300 minutes has been removed with the glass filter; however, MET removal of 25% can be achieved without filter glass. TOC conversion was 6.37% and 3.60% with and without filter, correspondingly after 300 minutes, thus confirming that the mineralization is very low in both cases.

Summarizing, UV irradiation in the absence of TiO$_2$ achieved an MET degradation lower than 30% after 300 minutes of irradiation, confirming that the direct photolysis is not fast enough to be considered as an adequate technology.

3.2. The Role of the Adsorption on the Photocatalytic Degradation. Since the adsorption can play an important role in the evolution of the photodegradation, adsorption experiments at constant temperature (25 ± 0.5°C) were carried out. The adsorption capacity of MET, q_e (mg g^{-1}), was calculated from the difference in MET concentration in the aqueous phase before and after adsorption at different initial MET concentrations (0, 6.2, 12.5, 25, 37.5, and 50 mg L^{-1}). The variation in adsorption of MET onto TiO$_2$ was studied at two pHs: 9 and free pH (pH ≈ 5.8). Figure 3 presents the obtained

TABLE 1: Isotherm parameters for MET adsorption onto TiO_2 obtained by linear method at 25°C.

Two-parameter model	Parameters	pH	
		Free	9
Langmuir	q_m (mol g^{-1})	0.0014	0.0250
$q_e = \dfrac{q_m K_a C_e}{1 + K_a C_e}$	K_L (L mol^{-1})	0.0930	0.0817
	R^2	0.987	0.998
Freundlich	$1/n$	0.244	0.670
$q_e = K_F C_e^{1/n}$	K_F (L mol^{-1})	0.00042	0.00129
	R^2	0.105	0.147
Temkin	RT/b	0.00024	0.00508
$q_e = \dfrac{RT}{b} \ln (K_T + C_e)$	K_T (L mol^{-1})	2.718	0.962
	R^2	0.604	0.982
Dubinin-Radushkevich	q_D (mol g^{-1})	0.0013	0.0233
$q_e = q_D \exp\left(-B_d \left[RT \ln\left(1 + \dfrac{1}{C_e}\right)\right]\right)$	$B_D \times 10^{-3}$ (mol^2 kJ^{-2})	1.533	1.532
	R^2	0.835	0.778
Three-parameter model			
Redlich-Peterson	K_{RP} (L mol^{-1})	0.00011	0.10
	a_R (L mol^{-1})	0.051	18.040
$q_e = \dfrac{K_{RP} C_e}{1 + a_R C_e^{\beta}}$	β	0.999	0.679
	R^2	0.826	0.789
Langmuir-Freundlich	K_{LF} (L mol^{-1})	0.000205	0.00809
	a_{LF} (L mol^{-1})	0.134	0.310
$q_e = \dfrac{K_{LF} C_e^{n_{LF}}}{1 + \left(a_{LF} C_e\right)^{n_{LF}}}$	n_{LF}	0.779	0.92
	R^2	0.211	0.734

results and indicates that the amount adsorbed increases when pH does it.

The increase in the adsorption of metoprolol with increasing pH can be elucidated by considering the surface charge of the adsorbent material (pH$_{pzc}$ ~ 6.5) [13, 34]. That is, titanium dioxide surface is positively charged in acid media pH (pH ≤ 7) whereas it is negatively charged under alkaline conditions (pH ≥ 7) [29, 35]. Also, metoprolol can be transformed to MET anion in the basic pH (pH ~ 10) since the pK$_a$ value of metoprolol is 9.7 [36]. Under free pH conditions, close to the point zero charge of TiO_2 (6.5) [30], MET is positively charged. A low adsorption was observed due to no electrostatic attraction between the surface charge and MET. A highest adsorption between MET and TiO_2 would be observed at pH 9, because the negative charges of the surface of the catalyst attract the protonated MET form. In addition the photocatalytic degradation would be expected on the surface of the catalysis.

Two-parameter isotherm models (Langmuir, Freundlich, Temkin, and Dubinin-Radushkevich) and three-parameter isotherm models (Redlich-Peterson and Langmuir-Freundlich) were tested in the fitting of the adsorption data of MET onto titanium dioxide [37, 38].

K_a, K_F, K_T, K_{RP}, and K_L are the Langmuir, Freundlich, Temkin, Redlich-Peterson and Langmuir-Freundlich adsorption equilibrium constants (L mol^{-1}), respectively; a_R and a_{LF} are also the Redlich-Peterson and Langmuir-Freundlcih

constants (L mol^{-1}), respectively; C_e and q_e are the equilibrium concentration (mol L^{-1}) and the adsorption capacity (mol g^{-1}), respectively; q_D is the Dubinin-Radushkevich saturation capacity (mol g^{-1}). The parameter q_m represents the maximum monolayer adsorption capacity (mol g^{-1}) and $1/n$ the adsorption intensity, which provides an indication of favorability and capacity of the adsorbent/adsorbate system. The parameter b is related to the adsorption heat; B_D gives the mean adsorption free energy E_D (kJ mol^{-1}). The parameters β and n_{LF} are the Redlich-Peterson and Langmuir-Freundlich exponents which lie between 0 and 1 [39]. And R^2 is the corresponding sum of squares error obtained in the fitting experimental data of each model.

From Table 1, it was observed that the best fitting were obtained for Langmuir isotherm ($R^2 = 0.987$ and 0.998 for free pH and pH 9, respectively). Thus, these models represent the equilibrium adsorption of MET on TiO_2 particles in the range of concentration studied. Accordingly, the adsorption mechanism may be interpreted as a monolayer coverage of the catalyst surface.

For free pH MET adsorption (q_m) was lower than for pH 9, 0.0014 mol g^{-1}, and 0.0250 mol g^{-1}, respectively. In these cases, the adsorption does not play an important role in the photocatalytic process. The MET percentage removal in dark conditions was 0.1% and 11% for free pH and pH 9. These low adsorption values and MET percentage removals suggest that

TABLE 2: Kinetics of metoprolol UV-C photodegradation under different conditions.

|	Glass material reactor	Glass filter $\lambda \geq 280$ nm	pH	$t_{1/2}$ (h)
Photolysis	Borosilicate	with	5.8 ± 1	16.5 ± 0.5
		without	5.8 ± 1	11.6 ± 0.6
	Quartz	without	5.8 ± 1	10.5 ± 0.5
Photocatalysis	Borosilicate	without	5.8 ± 1	0.81 ± 0.4
		without	9.0 ± 1	0.58 ± 0.3

the most possible way of degradation could be reached by migration of •OH radicals to the bulk of the suspension.

3.3. Degradation of MET by Photocatalytic Process.

The photocatalytic degradation of MET solution ($50 \, \mathrm{mg \, L^{-1}}$) was carried out during 300 minutes, in the presence of $0.4 \, \mathrm{g \, L^{-1}}$ of TiO_2 under UV-VIS light at room temperature. It is know that, in heterogeneous photocatalysis, the rate of degradation is not always proportional to the catalyst load [40]. An optimal point exists where TiO_2 loaded shows a maximum degradation rate. Previous studies carried out in our research group reported that the optimum catalyst concentration was $0.4 \, \mathrm{g \, L^{-1}}$ [41]. Over this value, scattering can appear, and therefore increase in degradation rate does not occur.

Firstly, the solution mixture was stirred for 24 hours without irradiation in order to get the equilibrium of MET adsorption.

Figure 4 depicts the photocatalytic degradation of MET at free pH and pH 9. Maximum conversions are achieved at 240 and 300 minutes for pH 9 and free pH, respectively. An important remark is that the initial removal rate for free pH and pH 9 experiments is different, being higher at pH 9. The effect of pH on the conversion is a complex issue related to the ionization states of the catalyst surface and the substrate, as well as the rate of formation of radicals and other reactive species in the reaction mixture [42]. These effects can be assessed since the action of the holes is favored at acidic conditions, while hydroxyl radicals become the dominant species at neutral and alkaline conditions [42].

As known, photocatalysis occurs through the energy adsorption by the catalyst (light between 200 and 400 nm for TiO_2). Under excited condition, the valance band-electron is transferred to the conduction band forming the hole-electron pair (h^+/e^-) (2). The hydroxyl radicals are formed by cleavage of adsorbed molecules of water [43]:

$$TiO_2 + h\gamma \longrightarrow TiO_2^* \left(\frac{h^+}{e^-} \right) \qquad (2)$$

$$h^+ + H_2O \longrightarrow \bullet OH + H^+ \qquad (3)$$
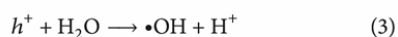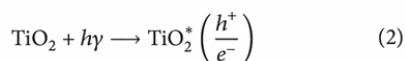
If organic compounds are absorbed on the surface of the catalyst, the •OH nonselective attack promotes the cleavage of compounds bounds. The higher MET degradation and the low MET adsorption on catalyst at a pH 9 suggest that the •OH attack in the bulk of solution can be responsible for the MET degradation [40, 44].

The values of TOC during the photocatalytic degradation of MET, at two different pHs, are given in Figure 4. The TOC
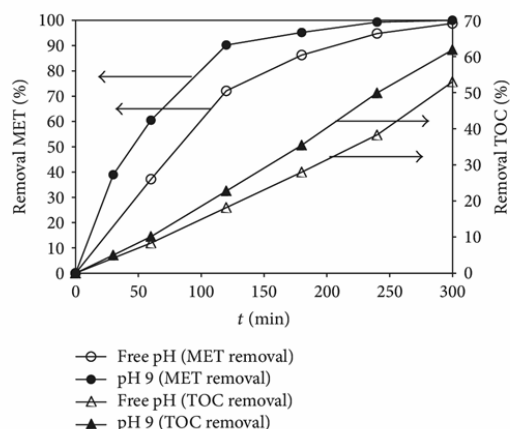

FIGURE 4: MET and TOC removal (%) versus time (min) at free pH and pH 9 in photocatalytic experiments.

- ○ Free pH (MET removal)
- ● pH 9 (MET removal)
- △ Free pH (TOC removal)
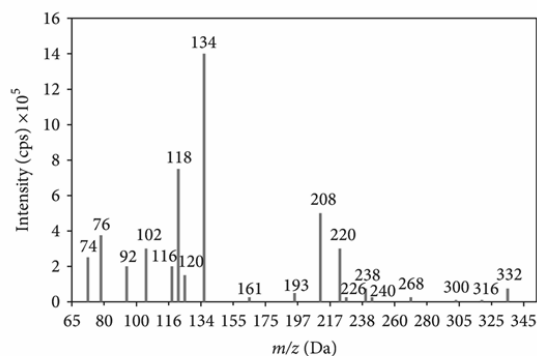- ▲ pH 9 (TOC removal)

FIGURE 5: MS spectrum of major oxidation products of metoprolol.

increases with time, indicating the increasing mineralization of the initial organic structures.
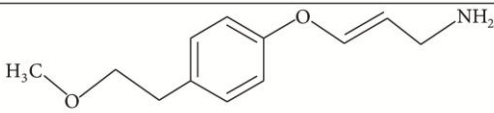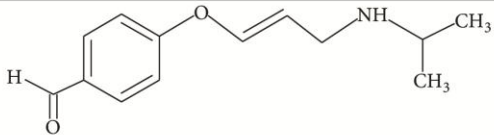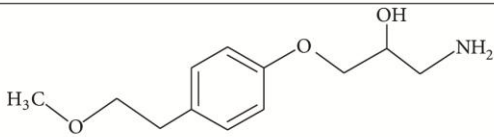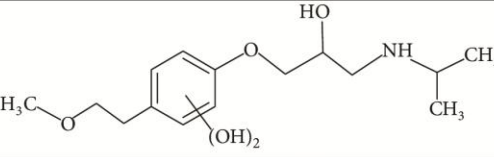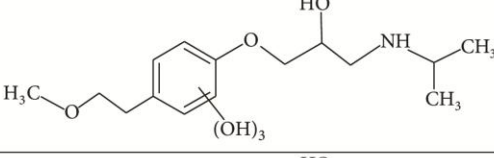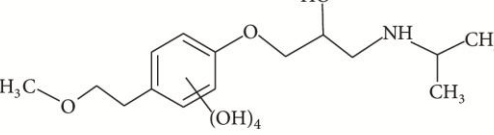
3.4. Kinetics of MET Degradation.

The Langmuir-Hinshelwood (L-H) model is usually used to describe the kinetics of photocatalytic degradation of organic pollutants [12, 13, 30, 31, 41, 45], being the kinetic equation expressed as

$$r = -\frac{dC}{dt} = \frac{K_{ads} \cdot k_{H-L} \cdot C}{1 + K_{ads} \cdot C}, \qquad (4)$$

TABLE 3: Intermediates proposed for the photocatalytic degradation of MET.

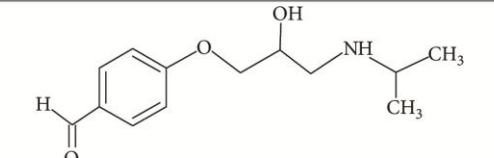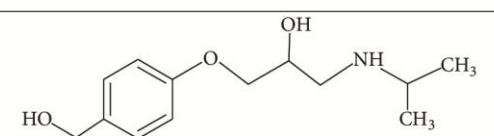| Detected compound (DP)	Ret. time (min)	m/z (Da)	Molecular formula	Proposed structure
Metoprolol	3.24	268	$C_{15}H_{25}NO_3$	
1	2.59	74	$C_4H_{11}N$	
2	3.24	76	C_3H_9NO	
3	2.59	92	$C_3H_9NO_2$	
4	2.59	102	$C_5H_{11}NO$	
5	2.59	116	$C_6H_{13}NO$	
6	3.24	118	$C_6H_{15}NO$	
7	2.59	120	$C_5H_{125}NO_2$	
8	2.59	134	$C_6H_{15}NO_2$	
9	3.23	161	$C_{11}H_{12}O$	
10	3.23	193	$C_{12}H_{16}O_2$	

TABLE 3: Continued.

Detected compound (DP)	Ret. time (min)	m/z (Da)	Molecular formula	Proposed structure
11	3.24	208	$C_{12}H_{17}NO_2$	
12	3.03	220	$C_{13}H_{17}NO_2$	
13	3.03	226	$C_{12}H_{19}NO_3$	
14	4.71	238	$C_{13}H_{19}NO_3$	
15	3.23	240	$C_{13}H_{21}NO_3$	
16	3.98	300	$C_{15}H_{25}NO_5$	
17	3.98	316	$C_{13}H_{25}NO_6$	
18	3.23	332	$C_{13}H_{19}NO_7$	

where r is the degradation rate, C is the reactant concentration, t is the time, k_{H-L} is the rate constant, and K_{ad} is the adsorption equilibrium constant.

This model assumes that adsorption is a rapid equilibrium process and that the rate-determining step of the reaction involves the species present in a monolayer at the solid–liquid interface. Furthermore if the adsorption of MET onto the surface of the photocatalysts is very low, $K_{ads} \cdot C$ can be neglected in the denominator simplifying the equation to a pseudo-first-order equation as given by [46]

$$r = -\frac{dC}{dt} = K_{ads} \cdot k_{H-L} \cdot C = k \cdot C. \qquad (5)$$
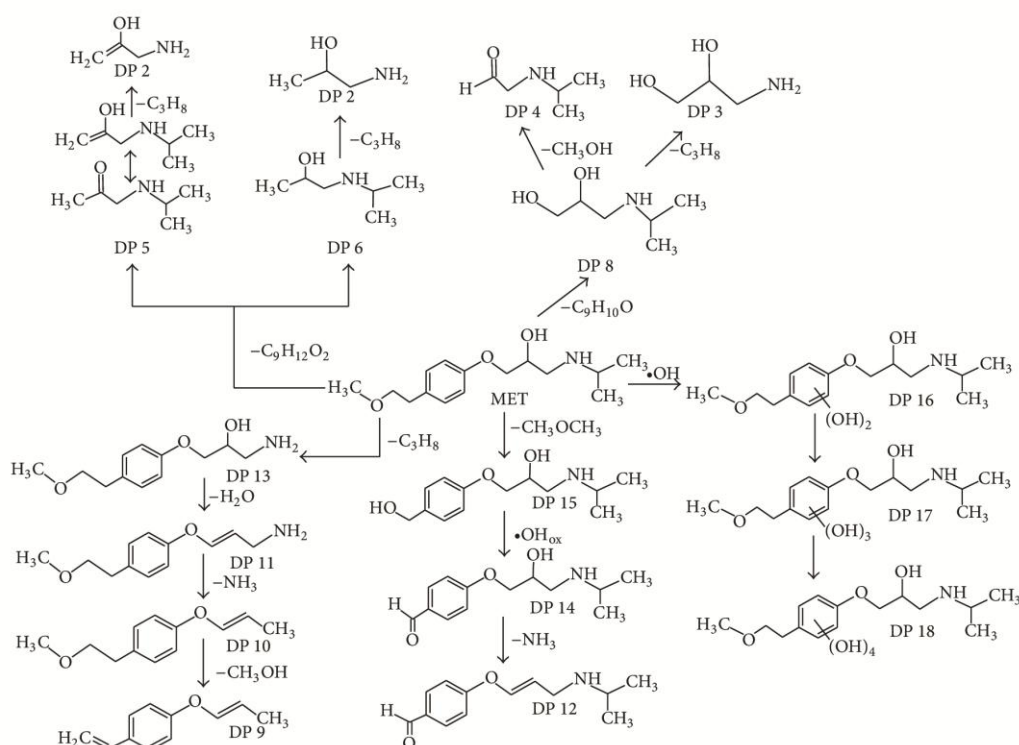
FIGURE 6: Proposed pathways for the degradation of MET.

The integrated form of the above equation is represented by

$$\ln\left(\frac{C_o}{C}\right) = k_{app} \cdot t, \tag{6}$$

where C_0 is the initial pollutant concentration and k_{app} is the apparent pseudo-first-order reaction rate constant.

The half-life was calculated with the following expression:

$$t_{1/2} = \frac{\ln 2}{k}. \tag{7}$$

The values of $t_{1/2}$ in Table 2 verify that the direct photolysis under simulated light was very low. The low photodegradation of MET was also supported by a low molar absorption coefficient ($281\,L\,mol^{-1}\,cm^{-1}$) measured at $221.9\,nm$ wavelength. However, an important increasing difference is observed in the MET degradation when TiO_2 is present. Also, when photocatalytic process is applied, results in TOC conversion (63%) are notoriously improved, for initial concentration of $50\,mg\,L^{-1}$ of MET and $0.4\,g\,L^{-1}$ of catalyst.

If both processes are compared, photocatalytic process is always much faster than the photolytic degradation of MET. Therefore, the interest of using photocatalysis in the treatment of this type of pollutant is obvious.

3.5. Intermediates during Reaction. The major by-products formed during 6 hours of photocatalytic treatment of MET

were identified (Figure 5). The study was carried out using HPLC/MS in positive electrospray model. The degradation intermediates for MET are shown in Table 3.

The metoprolol has a molecular weight [M + H+] = 268. Three intermediates corresponding to the binding of •OH radicals in the aromatic ring were detected at m/z 300, 316, and 332, di-(DP (Detected Compound) 16), tri-(DP 17), and tetrahydroxy (DP 18) DPs, respectively. After breaking the C–C bond in the aliphatic part of the MET molecule, amino-diol (DP 8) was identified as one of the dominant intermediates with m/z of 134. Different fragments of the ethanolamine side were also identified (DP 1, DP 2, DP 3, DP 4, DP 5, DP 6, and DP 7), probably due to the loss of the hydroxyl group and the loss of isopropyl moiety.

PD 15 can be formed probably by reactions which involve attack on the ether side chain followed by elimination. On the other hand, the oxidation of alcohols to aldehydes can be explained by the formation of DP 14 with $m/z = 238$ [47]. The hydrogen abstraction and the water elimination of DP 14 probably generate a carbonyl, followed by an intermolecular electron transfer; it generates a double bond and the consequent formation of DP 12.

Oxidative attack on the dimethylamine moiety results in a DP 13 with $m/z = 226$. Following this, the hydrogen abstraction and elimination of water of DP 13 generate a carbonyl which followed by intermolecular electron transference, generates a double bond and forming DP 11. The DP

11 can generate DP 10 corresponding to a loss of ammonia after the hydrogen abstraction. The intermediate 9 could be formed by the loss of methanol combined with the attack of •OH on the C atom next to the ether oxygen in the aliphatic part of DP 10.

A simplified fragmentation pathway of metoprolol degradation is shown in Figure 6.

4. Conclusions

Langmuir isotherm fits very well the experimental data, which indicates that the adsorption of the MET onto TiO_2 is by monolayer coverage of the catalyst surface. The results confirmed that the degradation of MET is not able to undergo by direct photolysis due to its lower absorption coefficient. In contrast, the addition of TiO_2 photocatalyst significantly increases its degradation rate and, after 240 min of irradiation, MET was totally eliminated for pH 9. The experimental data indicates that TiO_2 photocatalysis allows a fast and efficient removal of metoprolol, transforming substrate into by-products that are more difficult to be degraded by photocatalysis, as evidenced by the level of mineralization achieved (63%). Disappearance of MET by photocatalysis follows Langmuir-Hinshelwood model that can be simplified as a pseudo-first-order equation, as usually found in heterogenous photocatalysis at low concentration. Photocatalytic degradation rate of MET depends on pH, occurring the faster degradation at pH 9. At last, based on the identified degradation intermediates at 6-hour reaction time, a photocatalytic degradation pathway of metoprolol was proposed. The main pathways involved in the photocatalytic degradation process include hydroxilation of the aromatic ring, shortening of methoxyl contained in the lateral chain, and cleavage of or addition of •OH to the amine lateral chain.

Acknowledgments

References

[1] A. Pal, K. Y.-H. Gin, A. Y.-C. Lin, and M. Reinhard, "Impacts of emerging organic contaminants on freshwater resources: review of recent occurrences, sources, fate and effects," *Science of the Total Environment*, vol. 408, no. 24, pp. 6062–6069, 2010.

[2] Y. Xu, T. V. Nguyen, M. Reinhard, and K. Y.-H. Gin, "Photodegradation kinetics of p-tert-octylphenol, 4-tert-octylphenoxy-acetic acid and ibuprofen under simulated solar conditions in surface water," *Chemosphere*, vol. 85, no. 5, pp. 790–796, 2011.

[3] A. Jurado, E. Vàzquez-Suñé, J. Carrera, M. López de Alda, E. Pujades, and D. Barceló, "Emerging organic contaminants in groundwater in Spain: a review of sources, recent occurrence and fate in a European context," *Science of the Total Environment*, vol. 440, pp. 82–94, 2012.

[4] M. Huerta-Fontela, M. T. Galceran, and F. Ventura, "Occurrence and removal of pharmaceuticals and hormones through drinking water treatment," *Water Research*, vol. 45, no. 3, pp. 1432–1442, 2011.

[5] M. Pedrouzo, F. Borrull, E. Pocurull, and R. M. Marcé, "Presence of pharmaceuticals and hormones in waters from sewage treatment plants," *Water, Air, and Soil Pollution*, vol. 217, no. 1–4, pp. 267–281, 2011.

[6] A. C. Alder, C. Schaffner, M. Majewsky, J. Klasmeier, and K. Fenner, "Fate of β-blocker human pharmaceuticals in surface water: comparison of measured and simulated concentrations in the Glatt Valley Watershed, Switzerland," *Water Research*, vol. 44, no. 3, pp. 936–948, 2010.

[7] M. Maurer, B. I. Escher, P. Richle, C. Schaffner, and A. C. Alder, "Elimination of β-blockers in sewage treatment plants," *Water Research*, vol. 41, no. 7, pp. 1614–1622, 2007.

[8] B. Abramović, S. Kler, D. Šojić, M. Laušević, T. Radović, and D. Vione, "Photocatalytic degradation of metoprolol tartrate in suspensions of two TiO_2-based photocatalysts with different surface area. Identification of intermediates and proposal of degradation pathways," *Journal of Hazardous Materials*, vol. 198, pp. 123–132, 2011.

[9] M. Maurer, B. I. Escher, P. Richle, C. Schaffner, and A. C. Alder, "Elimination of β-blockers in sewage treatment plants," *Water Research*, vol. 41, no. 7, pp. 1614–1622, 2007.

[10] E. Isarain-Chávez, J. A. Garrido, R. M. Rodríguez et al., "Mineralization of metoprolol by electro-fenton and photoelectro-fenton processes," *Journal of Physical Chemistry A*, vol. 115, no. 7, pp. 1234–1242, 2011.

[11] L. Prieto-Rodríguez, I. Oller, N. Klamerth, A. Agüera, E. M. Rodríguez, and S. Malato, "Application of solar AOPs and ozonation for elimination of micropollutants in municipal wastewater treatment plant effluents," *Water Research*, vol. 47, pp. 1521–1528, 2013.

[12] I. Kim and H. Tanaka, "Photodegradation characteristics of PPCPs in water with UV treatment," *Environment International*, vol. 35, no. 5, pp. 793–802, 2009.

[13] A. Piram, A. Salvador, C. Verne, B. Herbreteau, and R. Faure, "Photolysis of β-blockers in environmental waters," *Chemosphere*, vol. 73, no. 8, pp. 1265–1271, 2008.

[14] H. Fang, Y. Gao, G. Li et al., "Advanced oxidation kinetics and mechanism of preservative propylparaben degradation in aqueous suspension of TiO_2 and risk assessment of its degradation products," *Environmental Science and Technology*, vol. 47, pp. 2704–2712, 2013.

[15] L. D. Nghiem, A. I. Schäfer, and M. Elimelech, "Pharmaceutical retention mechanisms by nanofiltration membranes," *Environmental Science and Technology*, vol. 39, no. 19, pp. 7698–7705, 2005.

[16] T. Heberer, "Occurrence, fate, and removal of pharmaceutical residues in the aquatic environment: a review of recent research data," *Toxicology Letters*, vol. 131, no. 1-2, pp. 5–17, 2002.

[17] C. Hartig, M. Ernst, and M. Jekel, "Membrane filtration of two sulphonamides in tertiary effluents and subsequent adsorption on activated carbon," *Water Research*, vol. 35, no. 16, pp. 3998–4003, 2001.

[18] J. Radjenović, M. Petrović, F. Ventura, and D. Barceló, "Rejection of pharmaceuticals in nanofiltration and reverse osmosis membrane drinking water treatment," *Water Research*, vol. 42, no. 14, pp. 3601–3610, 2008.

[19] P. Westerhoff, Y. Yoon, S. Snyder, and E. Wert, "Fate of endocrine-disruptor, pharmaceutical, and personal care product chemicals during simulated drinking water treatment processes," *Environmental Science and Technology*, vol. 39, no. 17, pp. 6649–6663, 2005.

[20] J. Peuravuori and K. Pihlaja, "Phototransformations of selected pharmaceuticals under low-energy UVA-vis and powerful UVB-UVA irradiations in aqueous solutions-the role of natural dissolved organic chromophoric material," *Analytical and Bioanalytical Chemistry*, vol. 394, no. 6, pp. 1621–1636, 2009.

[21] Q.-T. Liu, R. I. Cumming, and A. D. Sharpe, "Photo-induced environmental depletion processes of β-blockers in river waters," *Photochemical and Photobiological Sciences*, vol. 8, no. 6, pp. 768–777, 2009.

[22] Q.-T. Liu, R. I. Cumming, and A. D. Sharpe, "Photo-induced environmental depletion processes of β-blockers in river waters," *Photochemical and Photobiological Sciences*, vol. 8, no. 6, pp. 768–777, 2009.

[23] R. Molinari, F. Pirillo, V. Loddo, and L. Palmisano, "Heterogeneous photocatalytic degradation of pharmaceuticals in water by using polycrystalline TiO_2 and a nanofiltration membrane reactor," *Catalysis Today*, vol. 118, no. 1-2, pp. 205–213, 2006.

[24] W. Song, W. J. Cooper, S. P. Mezyk, J. Greaves, and B. M. Peake, "Free radical destruction of β-blockers in aqueous solution," *Environmental Science and Technology*, vol. 42, no. 4, pp. 1256–1261, 2008.

[25] M. Janus, J. Choina, and A. W. Morawski, "Azo dyes decomposition on new nitrogen-modified anatase TiO_2 with high adsorptivity," *Journal of Hazardous Materials*, vol. 166, no. 1, pp. 1–5, 2009.

[26] T. E. Doll and F. H. Frimmel, "Fate of pharmaceuticals—photodegradation by simulated solar UV-light," *Chemosphere*, vol. 52, no. 10, pp. 1757–1769, 2003.

[27] M. Šcepanovic, B. Abramovic, A. Golubovic et al., "Photocatalytic degradation of metoprolol in water suspension of TiO_2 nanopowders prepared using sol-gel route," *Journal of Sol-Gel Science and Technology*, vol. 61, pp. 390–402, 2012.

[28] K. L. Willett and R. A. Hites, "Chemical actinometry: using o-Nitrobenzaldehyde to measure light intensity in photochemical experiments," *Journal of Chemical Education*, vol. 77, no. 7, pp. 900–902, 2000.

[29] N. De la Cruz, V. Romero, R. F. Dantas et al., "o-Nitrobenzaldehyde actinometry in the presence of suspended TiO_2 for photocatalytic reactors," *Catalysis Today*, vol. 209, pp. 209–214, 2013.

[30] F. J. Rivas, O. Gimeno, T. Borralho, and M. Carbajo, "UV-C radiation based methods for aqueous metoprolol elimination," *Journal of Hazardous Materials*, vol. 179, no. 1–3, pp. 357–362, 2010.

[31] D. Fatta-Kassinos, M. I. Vasquez, and K. Kümmerer, "Transformation products of pharmaceuticals in surface waters and wastewater formed during photolysis and advanced oxidation processes - Degradation, elucidation of byproducts and assessment of their biological potency," *Chemosphere*, vol. 85, no. 5, pp. 693–709, 2011.

[32] S. Sortino, S. Petralia, F. Boscà, and M. A. Miranda, "Irreversible photo-oxidation of propranolol triggered by self-photogenerated singlet molecular oxygen," *Photochemical and Photobiological Sciences*, vol. 1, no. 2, pp. 136–140, 2002.

[33] Q.-T. Liu and H. E. Williams, "Kinetics and degradation products for direct photolysis of β-blockers in water," *Environmental Science and Technology*, vol. 41, no. 3, pp. 803–810, 2007.

[34] P. Fernández-Ibáñez, F. J. De Las Nieves, and S. Malato, "Titanium dioxide/electrolyte solution interface: electron transfer phenomena," *Journal of Colloid and Interface Science*, vol. 227, no. 2, pp. 510–516, 2000.

[35] A. Mills and S. Le Hunte, "An overview of semiconductor photocatalysis," *Journal of Photochemistry and Photobiology A*, vol. 108, no. 1, pp. 1–35, 1997.

[36] F. J. Benitez, J. L. Acero, F. J. Real, G. Roldan, and F. Casas, "Bromination of selected pharmaceuticals in water matrices," *Chemosphere*, vol. 85, no. 9, pp. 1430–1437, 2011.

[37] K. Y. Foo and B. H. Hameed, "Insights into the modeling of adsorption isotherm systems," *Chemical Engineering Journal*, vol. 156, no. 1, pp. 2–10, 2010.

[38] K. V. Kumar and K. Porkodi, "Relation between some two- and three-parameter isotherm models for the sorption of methylene blue onto lemon peel," *Journal of Hazardous Materials*, vol. 138, no. 3, pp. 633–635, 2006.

[39] J. S. Piccin, G. L. Dotto, and L. A. A. Pinto, "Adsorption isotherms and thermochemical data of FDandC RED Nº 40 Binding by chitosan," *Brazilian Journal of Chemical Engineering*, vol. 28, no. 2, pp. 295–304, 2011.

[40] F. Méndez-Arriaga, J. Gimenez, and S. Esplugas, "Photolysis and TiO_2 photocatalytic treatment of naproxen: degradation, mineralization, intermediates and toxicity," *Journal of Advanced Oxidation Technologies*, vol. 11, no. 3, pp. 435–444, 2008.

[41] V. Romero, N. de La Cruz, R. F. Dantas, P. Marco, J. Giménez, and S. Esplugas, "Photocatalytic treatment of metoprolol and propranolol," *Catalysis Today*, vol. 161, no. 1, pp. 115–120, 2011.

[42] L. A. Ioannou, E. Hapeshi, M. I. Vasquez, D. Mantzavinos, and D. Fatta-Kassinos, "Solar/TiO_2 photocatalytic decomposition of β-blockers atenolol and propranolol in water and wastewater," *Solar Energy*, vol. 85, no. 9, pp. 1915–1926, 2011.

[43] F. Méndez-Arriaga, S. Esplugas, and J. Giménez, "Photocatalytic degradation of non-steroidal anti-inflammatory drugs with TiO_2 and simulated solar irradiation," *Water Research*, vol. 42, no. 3, pp. 585–594, 2008.

[44] H. Yang, T. An, G. Li et al., "Photocatalytic degradation kinetics and mechanism of environmental pharmaceuticals in aqueous suspension of TiO_2: a case of β-blockers," *Journal of Hazardous Materials*, vol. 179, no. 1–3, pp. 834–839, 2010.

[45] R. F. Dantas, O. Rossiter, A. K. R. Teixeira, A. S. M. Simões, and V. L. da Silva, "Direct UV photolysis of propranolol and metronidazole in aqueous solution," *Chemical Engineering Journal*, vol. 158, no. 2, pp. 143–147, 2010.

[46] C. Sahoo, A. K. Gupta, and I. M. S. Pillai, "Heterogeneous photocatalysis of real textile wastewater: evaluation of reaction kinetics and characterization," *Journal of environmental science and health A*, vol. 47, pp. 2109–2119, 2012.

[47] M. L. Wilde, W. M. M. Mahmoud, K. Kümmerer, and A. F. Martins, "Oxidation-coagulation of β-blockers by K2FeVIO4 in hospital wastewater: assessment of degradation products and biodegradability," *Science of the Total Environment*, vol. 452-453, pp. 137–147, 2013.

Chapter X

Abbreviations

10 ABBREVIATIONS

(AOS)   Average Oxidation State

(AOPs)   Advanced Oxidation Processes

(BAP)   Bicarbonate-activated hydrogen peroxide

(BLB)   Black light blue lamps

(β-blockers)   Beta blockers

(BOD$_5$)   Biochemical Oxygen Demand at 5 days (mg/L)

(BQ)   Benzoquinone

(COD)   Chemical Oxygen Demand (mg/L)

(CPC)   Compound Parabolic Concentrators

(DOC)   Dissolved organic carbon (mg/L)

(DW)   Drinking water

(DWTP)   Drinking water treatment plant

(e^-/h^+)   Electron-hole

(E)   Energy

(E$_g$)   Band-gap energy (electron volts)

(E^0)   Standard redox potential

(EC$_{50}$)   The median effective concentration

(FA)   Formic acid

(hv)   Radiation

(HA)   Humic acid

(HP)   Heterogeneous photocatalysis

(HPLC)   High Performance Liquid Chromatograph

(I$_o$)   Incident photon flow (kJ/s)

(IR)	Infrared
(m/z)	mass-charge relation
(MET)	Metoprolol (mg/L)
(o-HNB)	o-nitrosobenzoic acid
(o-NB)	o- Nitrobenzaldehyde
(P)	Photolysis
(PF)	Photo-Fenton
(pKa)	Dissociation constant
(POPs)	Persistent organic pollutants
(PTCs)	Parabolic-trough concentrators
(PPCPs)	Pharmaceuticals and personal care products
(Q)	Accumulated energy (kJ/L)
(ROS)	Reactive oxygen species
(r)	Rate constants (min^{-1})
(SB)	solarbox
(SUVA)	Specific Ultraviolet Absorbance (L/mg-M)
(TBA)	Tert-butyl alcohol
(TOC)	Total Organic Carbon (mg/L)
(UPLC)	Ultra Performance Liquid Chromatography
(UV)	Ultraviolet light
(UVA)	Ultraviolet absorbance
(UV-A)	Ultraviolet light range 315-400 nm
(UV-B)	Ultraviolet light range 280-315 nm
(UV-C)	Ultraviolet light range 200-280 nm

(UV-Vis)   Ultraviolet-visible

(VUV)   Vacuum ultraviolet

(WW)   Waste water

(WWTP)   Wastewater treatment plant

(X-ray)   X-radiation

(ZVI)   Zerovalent iron

Greek letters

(Φ)   Quantum yield

(λ)   Irradiation Wavelength (nm)

(ε)   Absorption coefficient ($M^{-1}\ cm^{-1}$)

Subscript

0   Initial concentration

Acronyms

(ASTM)   American Society for Testing and Materials

(BBC)   British Broadcasting Corporation

(CAS)   Chemicals Abstracts Service

(ECOS-CMC)   Emerging Contaminants Environmental Council of the States - Cross Media Committee

(EPA)   Environmental Protection agency

(EU)   Europe Union

(U.S.)   United States

(WFD)   Water Framework Directive

(EFPIA)	European Federation of Pharmaceutical Industry and Associations
(UNDESA)	United Nations Department of Economic and Social Affairs
(UNICEF)	United Nations International Children's Emergency Fund
(USGS)	U.S. Geological Survey

Chapter XI

RESUMEN

11 RESUMEN

11.1 Introducción

El agua es vida y es esencial para el planeta, para la vida humana, animal y vegetal. El agua es un recurso indispensable que juega un papel muy importante en la regulación del ciclo climático y por lo tanto es necesario preservarla y asegurar su protección. El agua es finita y no puede ser remplazada por otros recursos.

Sólo el 2% del agua del planeta es agua dulce y se estima que, debido al uso inapropiado de este recurso, puede que se produzca un déficit mundial de suministro de agua en un futuro no muy lejano (United Nations of Population Fund, 2011; Water Resources Group, 2014).

Dentro de este marco, hoy en día existe la preocupación a nivel mundial con respecto a problemas medioambientales tales como escasez, sequía y calidad del agua. Por ello, se ha intentado, y se intenta, mantener un equilibrio con respecto a la cantidad y a la calidad. Por lo tanto la gestión del ciclo del agua de forma sostenible ha sido la clave para proteger y preservar tanto los recursos humanos como la salud humana (ver figura 11.1).

Figura 11.1- Ciclo integral del agua.

Con respecto a la contaminación del agua, el problema se ha ido incrementando con el tiempo hasta el punto de llegar a ser una amenaza para el medio ambiente. El control de la contaminación ha llegado, por lo tanto, a ser de prioritaria importancia. Un elemento primordial ha sido la prevención, control y reducción de la descarga de sustancias contaminantes en los sistemas acuáticos.

Existe un amplio número de contaminantes que se encuentran presentes en los sistemas acuáticos entre ellos los fármacos, considerados contaminantes emergentes ya que previamente no habían sido detectados (Polar, 2007) o detectados en pequeñas cantidades. Estos contaminantes se consideran como un riesgo, aunque todavía no están sujetos a ninguna regulación, dado que se han empezado a detectar en las aguas residuales (Dougherty et al., 2010; Vulliet et al., 2009) hace no muchos años y, en muchos casos, se desconocían, y se desconocen, sus posibles efectos. No obstante, es muy posible que sean considerados en futuras regulaciones dependiendo de los posibles efectos en la salud humana, en la vida acuática y el medioambiente (Malato et al., 2014; Petrovic et al., 2003). Muchos de estos contaminantes emergentes se caracterizan por ser omnipresentes, persistentes, y tener una actividad biológica alta asociada a su persistente carácter toxico (Muñoz, Lopez-Doval, et al., 2009; Suárez et al., 2008).

Entre estos contaminantes emergentes, cabe citar el beta bloqueante Metoprolol (MET), que es un fármaco prescrito a nivel mundial para tratar enfermedades tales como la hipertensión, la taquicardia y ataques al corazón (Benitez et al., 2009; Owen et al., 2007; Rivas et al., 2010; Scepanovic et al., 2012; Yang et al., 2010). Varios estudios (Cleuvers, 2005; Dzialowski et al., 2006; Escher et al., 2006; Fraysse & Garric, 2005; Hernando et al., 2006; Owen et al., 2007) indican que este compuesto es de potencial relevancia medioambiental debido al efecto adverso en los organismos acuáticos y a que presenta una persistencia en contra la degradación biológica, presentando un impacto potencial.

Estos fármacos entran en el medioambiente a través de emisiones directas desde los centros de producción (industria farmacéutica), por la eliminación directa de medicamentos sobrantes en hogares y hospitales, y por la excreción a través de los sistemas de alcantarillado (Carballa et al., 2005; Gros et al., 2007; Heberer, 2002; Joss et al., 2005; Kolpin et al., 2004; Petrovic et al., 2009; J. L. Santos et al., 2007; Suárez et al., 2008) después de la administración de fármacos en humanos y animales.

Una vez en las plantas de tratamiento de aguas residuales (EDAR) no se puede asegurar la eliminación completa de estos fármacos por medio de los tratamientos de agua convencionales, debido fundamentalmente a la naturaleza recalcitrante de los mismos. Por lo tanto, es necesario utilizar tratamientos alternativos tales como los Procesos de Oxidación Avanzada (POAs) los cuales se basan en la producción de especies muy reactivas como los radicales hidroxilo (OH·).

Dependiendo del proceso físico-químico que conduce a la formación de radicales, los POAs se pueden dividir en fotoquímicos y no fotoquímicos. Las técnicas más comunes se presentan en la tabla 11.1.

Tabla 11.1- Procesos de Oxidación Avanzada. Adaptada de (Litter & Quici, 2010).

Procesos no fotoquímicos	Procesos Fotoquímicos	
	Tipo de Proceso	Rango de longitudes de onda de radiación (nm)
Ozonización en medio alcalino (O_3/HO^-)	Fotólisis del agua con ultravioleta de vacío (UVV)	<190
Ozonización con peróxido de hidrógeno (O_3/H_2O_2)	UV/peróxido de hidrógeno (UV/H_2O_2)	<280
Fenton y procesos relacionados (Fe^{2+}/H_2O_2)	UV/ozono (UV/O_3)	280-315
Oxidación electroquímica	Foto-Fenton y procesos relacionados	UV-Visible hasta 450
Radiólisis γ y tratamiento con haces de electrones	Fotocatálisis heterogénea con TiO_2	UV hasta 380-400
Plasma no térmico (superficie de corona de descarga)	Fotocatálisis heterogénea con peróxido de hidrógeno (TiO_2/H_2O_2)	UV hasta 380-400
Ultrasonido, descarga electrohidráulica	Hierro cero-valente y UV	UV
Oxidación con aire húmedo	-	-
Oxidación supercrítica		
Hierro cero-valente		
Ferrato		

Los procesos fotoquímicos se describen a continuación:

Fotólisis

Es el proceso mediante el cual la luz puede producir la transformación de los compuestos. Existen dos tipos de fotólisis: la directa y la indirecta. En la fotólisis directa el contaminante que debe ser eliminado absorbe directamente la radiación y se degrada a partir de su estado excitado. En la fotólisis indirecta se puede producir en primer lugar la fotosensibilización o la fotólisis de alguno de los compuestos presentes en el medio (agua, materia orgánica, foto-sensibilizadores, etc.) y los compuestos formados son los que reaccionan con los compuestos a degradar.

UVC/H$_2$O$_2$

Los procesos UV/H$_2$O$_2$ generalmente implican la generación de radicales OH· a través de la fotólisis UV de H$_2$O$_2$ (ecuación 11.1), dado que la absorbancia máxima de H$_2$O$_2$ se produce cerca de 220 nm.

$$H_2O_2 + h\nu \rightarrow OH\cdot + OH\cdot \tag{11.1}$$

Por lo tanto, el compuesto orgánico se degrada por medio del ataque de fotones (fotólisis UV directa) y/o de las reacciones con radicales hidroxilo.

Fotocatálisis

Como es sabido, la fotocatálisis heterogénea se basa en la utilización de semiconductores (TiO$_2$, ZnO, etc.) que al recibir luz de longitud de onda con energía igual o superior a la del bandgap (Eg), registran la generación de pares "electrón/hueco" (e$^-$/h$^+$) (ver ecuación 11.2). Estos pares pueden dar lugar a reacciones redox, dado que los huecos de la capa de valencia son poderosos oxidantes, mientras que los electrones de la capa de conducción son buenos reductores.

$$TiO_2 + h\nu \rightarrow e^- + h^+ \tag{11.2}$$

El TiO$_2$ es hasta el momento el semiconductor más útil para los propósitos fotocatalíticos, debido a sus propiedades ópticas y electrónicas excepcionales, a su estabilidad química y su bajo coste. La energía de bandgap de las formas fotocatalítica de TiO$_2$, anatasa y rutilo, es de 3,23 eV (correspondiente a 384 nm) y 3,02 eV (correspondiente a 411 nm), respectivamente.

Fenton

El proceso de Fenton (Fe (II)/H$_2$O$_2$) implica la reacción entre Fe (II) disuelto y H$_2$O$_2$ en una solución acuosa ácida (pH=2.8) conduciendo a la oxidación de Fe (II) a Fe (III) y la producción de radicales hidroxilo (OH·).

$$Fe\,(II) + H_2O_2 \rightarrow Fe\,(III) + OH\cdot + OH^- \tag{11.3}$$
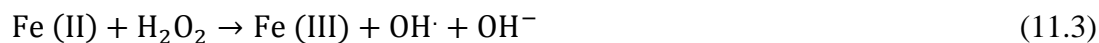
La reacción es espontánea y se produce sin la presencia de la luz.

Foto-Fenton

El proceso de foto-Fenton o foto-Fenton asistido (Fe (II)/H_2O_2/luz) involucra la irradiación con luz, lo que aumenta la velocidad de degradación del contaminante mediante la estimulación de la reducción de Fe (III) a Fe (II) de manera cíclica y que se promueve de forma paralela con la generación adicional de OH·.

$$Fe\ (III) +\ H_2O_2 + h\nu \rightarrow Fe(II) + HO\cdot + H^+ \tag{11.4}$$

Método de Bicarbonato- peróxido de hidrógeno activado (BPA)

En este método el anión bicarbonato (HCO_3^-) activa el H_2O_2 para producir especies oxidantes activas tales como el peroximonocarbonato (HCO_4^-) formado por una reacción de pre-equilibrio.

$$HCO_3^- + H_2O_2 \leftrightarrow HCO_4^- + H_2O \tag{11.5}$$
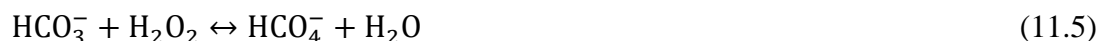
Sistema de Cobalto (II)/bicarbonato- peróxido de hidrógeno

La adición de un catalizador tal como el cobalto al sistema bicarbonato/H_2O_2 produce la formación de radicales OH· en el medio, los cuales aceleran el proceso de degradación de los contaminantes.

11.2 Objetivos

El objetivo general de este trabajo ha sido estudiar la eficacia de varios Procesos de Oxidación avanzada (UVC/H_2O_2, fotocatálisis, Fenton, foto-Fenton, bicarbonato/H_2O_2 con y sin catalizador) para degradar el contaminante Metoprolol presente en aguas, en diferentes condiciones experimentales.

Además se ha comparado la eficiencia energética de diferentes procesos y diferentes instalaciones con respecto a la eliminación de Metoprolol.

Finalmente se realizó un estudio de un método actinométrico para poder realizar mediciones de radiación en un reactor fotocatalítico en presencia de un catalizador en suspensión.

11.3 Materiales y métodos

Los principales reactivos utilizados y su aplicación en este estudio se resumen en la tabla 11.2.

Tabla 11.2– Reactivos utilizados y su aplicación.

Nombre	CAS No.	Formula	Suministrado por	Pureza (%)	Usado para/en
Metoprolol	56392-17-7	$C_{15}H_{25}NO_3$	Sigma-Aldrich	99	Todos los procesos
Dióxido de Titanio Degussa P-25	13463-67-7	TiO_2	Sigma-Aldrich	anastase~70 and rutile ~30	Fotocatálisis
Peróxido de hidrógeno	7722-84-1	H_2O_2	Merck and Sinopharm Chemical Reagent Co. Ltd	30	Todos los procesos
Sulfato de hierro (II) hepta-hidratado	7782-63-0	$FeSO_4.7H_2O$	Panreac and Sinopharm Chemical Reagent Co. Ltd.	99	Fenton y foto-Fenton y Fe/bicarbonato/H_2O_2
Acetato de Cobalto (II) tetra-hidratado	6147-53-1	$(CH_3COO)_2Co \cdot 4H_2O$	Sinopharm Chemical Reagent Co. Ltd.	98	Cobalto-bicarbonato- H_2O_2
Carbonato hidrogeno de Sodio	144-55-8	$NaHCO_3$	Sinopharm Chemical Reagent Co. Ltd.	99.7	Cobalto-bicarbonato- H_2O_2 y bicarbonato- H_2O_2
Acetonitrilo	75-05-8	C_2H_3N	Fischer Chemical	98	Fase móvil para HPLC
Acido ortofosfórico	7664-38-2	H_3PO_4	Panreac	85	Ajustar pH de agua para HPLC
Bisulfito de Sodio	7631-90-5	$NaHSO_3$	Panreac	40	Para detener reacciones de H_2O_2, para análisis de TOC
Metanol	67-56-1	CH_3OH	Panreac	98	Para detener reacciones de H_2O_2, para análisis de HPLC
Catalasa	9001-05-2	$H_2O_2:H_2O_2$ oxidoreductasa	Sigma-Aldrich	-	Para detener reacciones de H_2O_2, para análisis de DQO
Acido sulfúrico	7664-93-998	H_2SO_4	Panreac	98	Ajuste de pH (~2.8) en Fenton, foto-Fenton y Fe/bicarbonato/H_2O_2.
o-Nitrobenzaldehído	552-89-6.	$C_7N_5NO_3$	Panreac	98	Actinometrías
Etanol	64-17-5	C_2H_6O	Panreac	96	Actinometrías
Acido formico	64-18-6	CH_2O_2	Probus S.A	85	Secuestrante en actinometrías
Tert-butyl alcohol	75-65-0	$C_4H_{10}O$	Probus S.A	99	Actinometrías y hierro/bicarbonato/H_2O_2 como secuestrante
Benzoquinona	106-51-4	$C_6H_4O_2$	Merck	98	Secuestrante en actinometrías
hidróxido de sodio	1310-73-2	$NaOH$	Panreac	98	Actinometrías

Entre las técnicas utilizadas tenemos:

- Cromatografía líquida de alto rendimiento (HPLC), Cromatografía líquida de ultra rendimiento (UPLC) y Cromatografía líquida de alto rendimiento HPLC-DAD-ESI-TOF (+) 175V Isocrático: utilizadas para el seguimiento de las concentraciones del Metoprolol, del o-nitrobenzaldehído y la identificación de intermedios.

- Carbono Orgánico Total (TOC): medido mediante el equipo Shimadzu TOC-V-CNS, con auto-sampler ASI-V.

- Demanda Química de Oxígeno (DQO): ha sido medida por el método analítico colorimétrico 5220D.

- Demanda Biológica de Oxígeno (DBO_5): ha sido determinada de acuerdo al método estándar 5210, por medio del proceso respirométrico, utilizando el equipo de Oxitop.

- Aromaticidad: se determinó por espectrofotómetro a 254 nm.

- Consumo de peróxido de hidrógeno: este análisis se determinó por el procedimiento espectrofotométrico del metavanadato.

- Medida de hierro disuelto: este seguimiento se llevó a cabo por el método colorimétrico de o-fenontraleina.

- Las medidas de radiación solar se realizaron con espectroradiómetro.

- Toxicidad: El test de toxicidad se realizó mediante la medición, del efecto inhibitorio de la emisión de luz de la bacteria Vibrio fischeri.

- Biodegradabilidad: la biodegradabilidad de las muestras se estableció como la relación entre la DBO_5 y la DQO, considerándose biodegradable o adecuado para acoplarse a un tratamiento bilógico cuando la relación es mayor a 0,25.

Las instalaciones utilizadas se describen a continuación:

- Solarbox (SB): Este equipo utiliza una lámpara de xenón (1000 W) como fuente de radiación con un flujo fotónico de 2,68 µE/s. La disolución a tratar se prepara en un tanque agitado de 1 L, desde donde se bombea continuamente al reactor tubular (0,084L) que se encuentra en la base de la solarbox en el foco de un espejo de aluminio.

- Planta piloto solar basada en concentradores parabólicos compuestos (CPC): Esta instalación está formada por un módulo inclinado 41º (latitud de Barcelona), con seis fotoreactores de cuarzo de tipo CPC (0,95 L). Los fotoreactores tienen un área

de captación de 0,228 m^2. La disolución se prepara en un tanque agitado de 10 L y desde allí, se bombea continuamente a los fotoreactores y se recircula nuevamente.

- Reactor UVC: Esta instalación consta de un fotorreactor cilíndrico de 2 L, dotado de una camisa externa para la refrigeración mediante un baño termostático. Sumergidas dentro del reactor hay tres lámparas fluorescentes de mercurio de baja presión de 8W de poder nominal cada una, emitiendo en total 1,7 μE/s a 254 nm.

- Reactor Black light blue lamps (BLB): Esta instalación consta de un fotorreactor cilíndrico de 2 L, con una camisa externa para refrigeración, idéntico al descrito para el reactor UVC. En este caso, dentro del reactor hay tres lámparas fluorescentes UVA (Philips 8W) que emiten un total de 6,0 μE/s.

- Reactor para Fenton: esta instalación consta de un fotoreactor cilíndrico de 2 L, recubierto de papel aluminio para evitar la entrada de luz ambiental, dotado también de camisa externa para la refrigeración mediante un baño termostático.

- Reactor para bicarbonato/H_2O_2 con y sin catalizador: Esta instalación consta de un fotoreactor cilíndrico de 0,5 L, recubierto de papel aluminio para evitar la entrada de luz ambiental.

11.4 Resultados y discusión

Fotólisis

Los experimentos de fotólisis se realizaron con 50 mg/L iniciales de MET en agua Mili-Q, pH libre y 25ºC en las diferentes instalaciones (SB, CPC, BLB y UVC). Los resultados muestran que, después de 240 minutos de irradiación, la degradación del MET era muy baja excepto con el reactor UVC con el cual se alcanzó un 93,5% de conversión (ver figura 11.2). Posiblemente la alta absorbancia del MET, centrada en 221 y 273 nm, puede ser la responsable del buen rendimiento del UVC. Sin embargo, la fotólisis no produjo resultados relevantes de mineralización en ninguna de las instalaciones utilizadas.
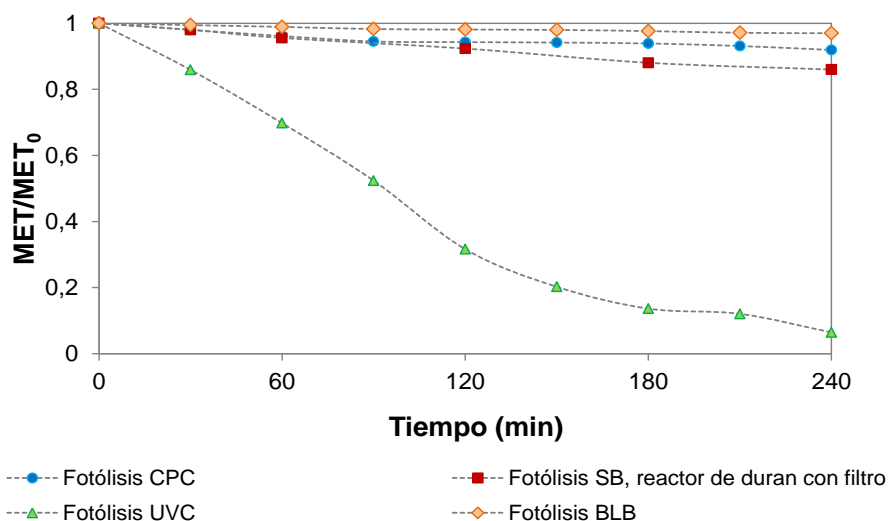
Figura 11.2- Degradación del MET por fotolisis utilizando las instalaciones de SB, CPC, BLB y UVC, 50 mg MET/L, pH libre y 25 ºC

UVC/H_2O_2

Los experimentos en el reactor UVC se realizaron con 50 mg/L iniciales de MET en agua Mili-Q, a diferentes pH y concentraciones de peróxido de hidrógeno y 25ºC. El mejor rendimiento en la degradación del MET (98% en 7,5 min) y en mineralización (7,07 en 230 minutos) se obtuvo para una concentración de 125 mg/L de H_2O_2 (ver figura 11.3), debido al incremento en la producción de OH·.
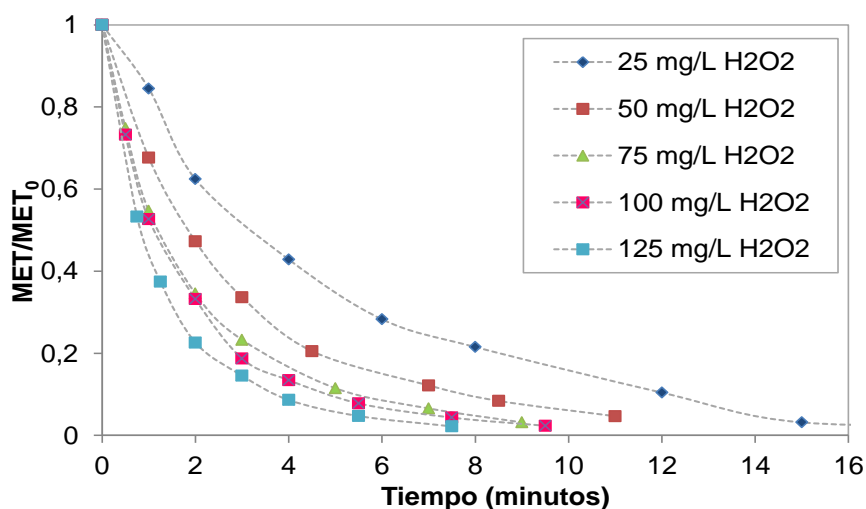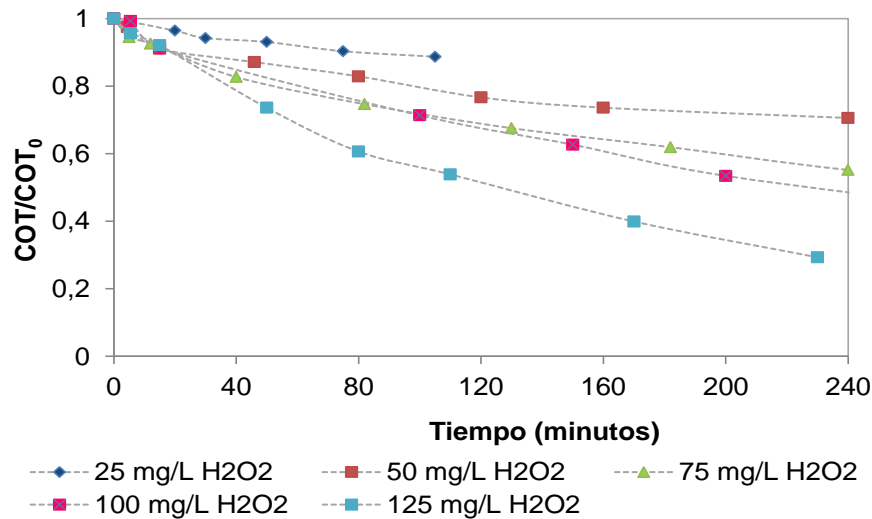
a-

b-

Figura 11.3- a-MET y b- COT degradaciones a diferentes concentraciones de peróxido de hidrógeno en el reactor UVC. $[MET]_0$=50 mg/L, pH libre y 25 ºC.

Fotocatálisis

Los experimentos de fotocatálisis se realizaron con 50 mg/L iniciales de MET en agua Mili-Q, pH libre y 25ºC en las instalaciones de SB y CPC. Se estudió la influencia de la concentración de TiO_2 (0,05, 0,10 y 0,40 g/L) en ambas instalaciones, encontrándose que la concentración óptima para la degradación de MET y la mineralización, era de 0,4 g/L de TiO_2. Después de 300 minutos de tratamiento en la SB, se llegó a la eliminación completa del MET y a una mineralización de 45,7% (ver figura 11.4).
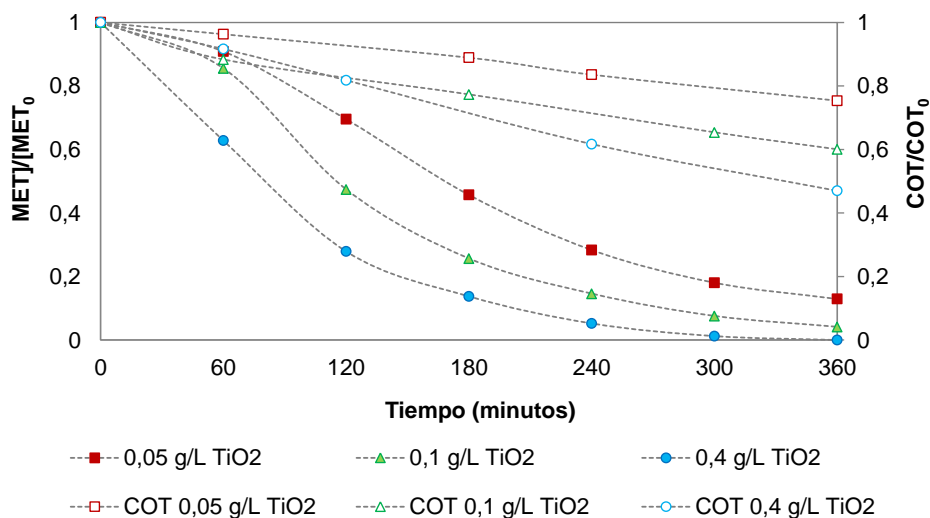
Figura 11.4- MET y COT degradaciones utilizando diferentes concentraciones iniciales de TiO_2 en SB.

268

También se realizaron experimentos de fotocatálisis, con 0,4 g/L TiO_2 pero variando la concentración inicial del MET (25, 50 y 100 mg/L), el pH y la matriz acuosa. Se observó que, al disminuir la concentración inicial de MET, se alcanzaron valores más altos de degradación y de mineralización debido a que, para una misma cantidad de catalizador dada, se produce una determinada cantidad de OH· que se utiliza para degradar una cantidad mayor o menor de Metoprolol (25 mg/L o 100 mg/L). Por otra parte, cuando se cambió el pH a 9, se observó que el MET se degradaba completamente en 240 minutos. El efecto del pH sobre la degradación es una cuestión compleja que se relaciona con los estados de ionización de la superficie del catalizador y del sustrato, así como la velocidad de formación de radicales y otras especies reactivas en la mezcla de reacción. Estos efectos pueden ser evaluados a partir de que la acción de los huecos se ve favorecida a condiciones de pH ácido, mientras que el radical hidroxilo se convierten en la especie dominante en condiciones neutras y alcalinas. Cuando se varió la matriz de agua Mili-Q por una matriz proveniente del efluente de una planta de tratamiento de agua residual, se obtuvo solo un 20,8% de degradación de Metoprolol, debido a que las especies reactivas producidas por la fotocatálisis pueden ser parcialmente consumidas para degradar la materia orgánica presente en la matriz de agua residual. Al adicionar 25 y 150 mg/L de H_2O_2 a la solución de 50 mg/L de MET, con catalizador se observó la eliminación completa de MET en 180 y 120 minutos, respectivamente.

El proceso de fotocatálisis en CPC también ha demostrado ser una buena alternativa para la degradación del MET. Con 0,4 g/L de TiO_2 se llegó a una degradación del 81,5% y a una mineralización del 29,2% para un tiempo de 270 minutos, para el cual la cantidad total de radiación recibida era de 2,6 kJ/L (ver figura 11.5).
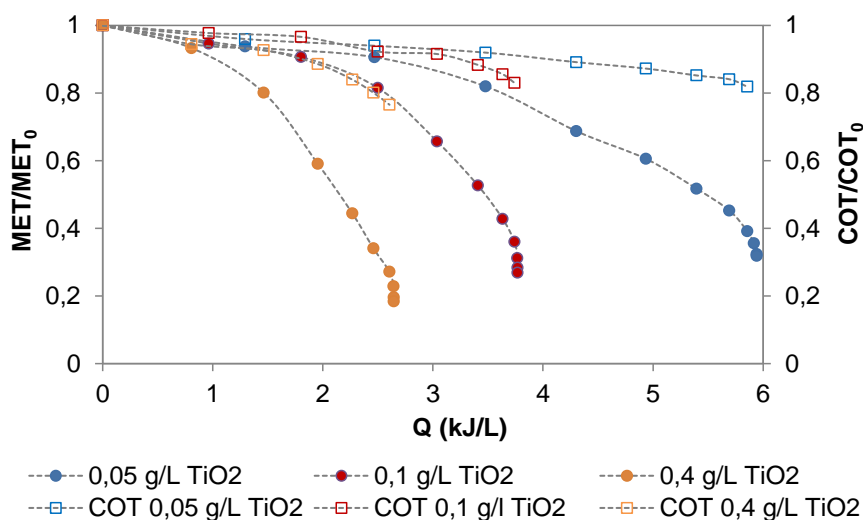
Figura 11.5- MET y COT degradaciones utilizando diferentes concentraciones iniciales de TiO_2 en CPC.

Los experimentos de fotocatálisis también se llevaron a cabo con 0,4 g/L TiO_2 y adicionando 25 y 150 mg/L de H_2O_2 a la solución de 50 mg/L de MET. Se observó una degradación de MET de 70% (Q= 3,1 kJ/L) y 96% (Q= 6,0 kJ/L) utilizando 25 y 150 mg/L de H_2O_2, respectivamente. Obviamente, la adición de peróxido de hidrógeno como agente oxidante es una fuente extra de radicales OH· para el proceso de fotocatálisis, tanto en SB como en CPC, y de ahí que el porcentaje de eliminación de MET y de mineralización aumente.

Por otra parte, se realizaron los diferentes análisis de biodegradabilidad y se determinó que los experimentos de fotocatálisis que se realizaron con 50 mg/L iniciales de MET después de 360 minutos de tratamiento en la SB podrían ser acoplados posteriormente a un tratamiento biológico (BOD_5/COD= 0,41), mientras que los tratados en el CPC después de 270 minutos de irradiación no alcanzaron el grado suficiente de biodegradabilidad (BOD_5/COD= 0,12). Con respecto a la toxicidad, se encontró que al final de los tratamientos tanto en SB como en CPC los efluentes disminuyeron su toxicidad considerablemente, alcanzándose valores de 0,72 Equitox/m^3 en la SB y de 0.57 Equitox/m^3 en el CPC.

Adicionalmente, se realizó la identificación de los diferentes intermedios producidos en los procesos de fotocatálisis/TiO_2 y UV-Vis/H_2O_2/TiO_2 y se han establecido los posibles caminos de degradación del MET, en donde se detectan principalmente ataques oxidativos y adiciones de radicales OH· en el anillo aromático.

Fenton

Los experimentos de Fenton se realizaron con 50 mg/L iniciales de MET in agua Mili-Q, pH 3,0 y 25ºC en un reactor de 2 L. Se han usado dos concentraciones diferentes de Fe (II) (2,5 mg/L y 10 mg/L) y de peróxido de hidrógeno (25 mg/L y 150 mg/L). Las mejores conversiones del proceso (degradación de MET de 67%, mineralización 8%, 7,6% de DQO) se han alcanzado para las concentraciones más altas tanto de catalizador como de H_2O_2, ya que con estas concentraciones se ha alcanzado la producción más alta de radicales OH·. Para mejorar el proceso, la adición del Fe (II) se dividió en 5 adiciones realizadas a intervalos constantes de tiempo durante 60 minutos. Con ello se obtuvo un 87% de conversión de MET y una mineralización de 15.6% (ver figura 11.6), para las concentraciones más altas de Fe (II) y H_2O_2. Por tanto, al adicionar el hierro por etapas la eficacia del proceso mejora.
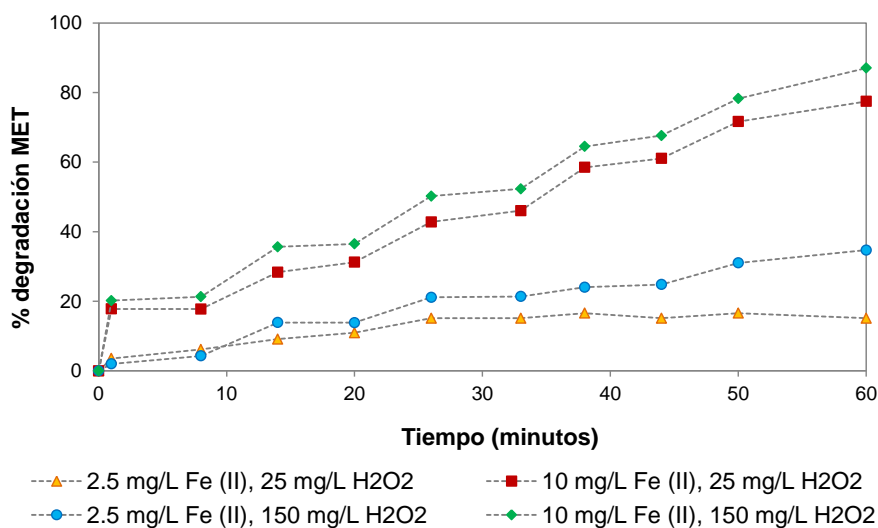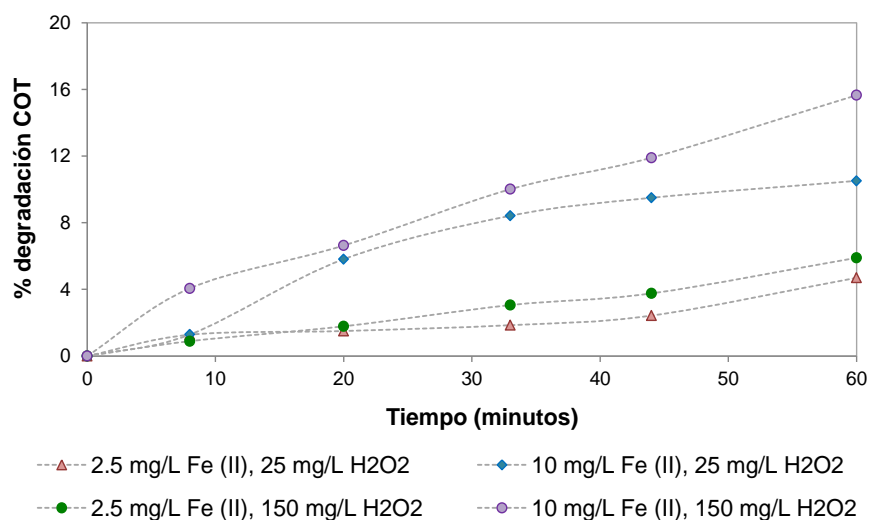
a-

b-

Figura 11.6– Degradación de 50 mg/L de MET por medio del proceso de Fenton, adicionando el Fe (II) por etapas. a- Degradación de MET. b- Degradación de COT.

Con respecto a la toxicidad, se encontró que al final de los tratamientos, tanto adicionando el hierro en su totalidad al principio (0,93 Equitox/m^3) como adicionándolo por etapas (0,90 Equitox/m^3), la toxicidad había disminuido considerablemente.

También como en el proceso de fotocatálisis se identificaron los intermedios para Fenton y de igual manera se propusieron los posibles caminos de degradación del MET.

Foto-Fenton

Los experimentos de foto-Fenton se realizaron con 50 mg/L iniciales de MET en agua Mili-Q, pH 3,0 y temperaturas de 14ºC y 25ºC en las instalaciones de BLB, SB, CPC y UVC. Se han ensayado también dos concentraciones diferentes de Fe (II) (2,5 mg/L y 10 mg/L) y de peróxido de hidrógeno (25 mg/L y 150 mg/L) excepto en UVC en donde únicamente se realizó el experimento con 2,5 mg de Fe (II) y 25 mg/L de H_2O_2. Las mejores conversiones del proceso en todas las instalaciones (BLB: 100% en 7 min; SB: 97,3%, en 7 min; CPC: 98,3%, en 3 min) se han alcanzado para las concentraciones más altas de Fe (II) y H_2O_2 debido a la alta producción de radicales OH·. En UVC se ha alcanzado 97% de conversión de MET en 20 min. Por lo que respecta a la temperatura, los experimentos realizados a 25ºC mostraron una mayor velocidad de degradación y de mineralización que los desarrollados a 14ºC (ver figura 11.7), debido a que un incremento en la temperatura conlleva cinéticas más rápidas del proceso.
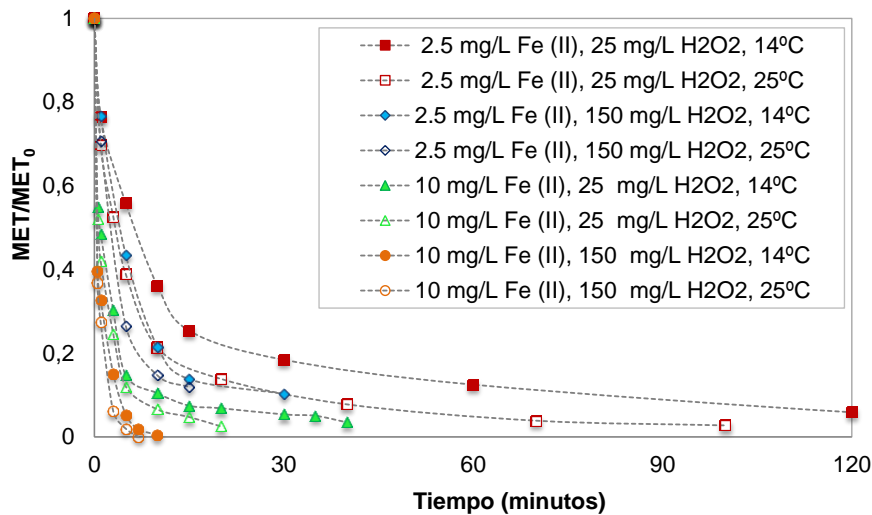
Figura 11.7– Degradación de MET para las diferentes condiciones de operación utilizadas en el reactor BLB. [MET]$_0$=50 mg/L.

Por otra parte, se determinó que los experimentos de foto-Fenton llevados a cabo en el reactor BLB, que alcanzaron el grado suficiente de biodegradabilidad al final del proceso y que podrían ser acoplados posteriormente a un tratamiento biológico son (2.5 mg/L Fe con 150 mg/L H$_2$O$_2$) y (10 mg/L Fe con 150 mg/L H$_2$O$_2$) tanto a 14ºC como a 25ºC (ver tabla 11.3).

Tabla 11.3- Biodegradabilidad para foto-Fenton en el reactor BLB.

	Experimento	Tiempo (min)	Biodegradabilidad
25 ºC	2,5 mg Fe/L, 150 mg H$_2$O$_2$/L	285	0,68
	10 mg Fe/L, 150 mg H$_2$O$_2$/L	90	0,53
14 ºC	2,.5 mg Fe/L, 150 mg H$_2$O$_2$/L	510	0,70
	10 mg Fe/L, 150 mg H$_2$O$_2$/L	185	0,54

Con respecto a la toxicidad, se encontró que al final de los tratamientos llevados a cabo en todas las instalaciones los efluentes disminuyeron su toxicidad considerablemente (ver tabla 11.4).

Tabla 11.4- Toxicidad para el proceso de foto-Fenton en diferentes instalaciones

Instalación	MET (mg/L)	Fe (II) (mg/L)	H_2O_2 (mg/L)	T (ºC)	Toxicidad inicial (Equitox/m^3)	Toxicidad final (Equitox/m^3)	Otro
BLB	50	2,5	25	25		0,56	Fe una adición
BLB	50	10	150	25		0,50	Fe por etapas
SB	50	2,5	25	25	6,25	0,51	Fe una adición
CPC	50	2,5	25	30 ± 5		0,59	Fe una adición
UVC	50	2,5	25	25		0,43	Fe una adición

Se realizó establecieron los posibles caminos de degradación del MET en donde se detectan principalmente ataques oxidativos por parte del radical OH·.

Bicarbonato/peróxido de hidrogeno activado

Los experimentos correspondientes a este proceso se realizaron con 5 mg/L iniciales de MET en agua potable, pH libre y temperatura ambiental en un reactor de 0,5 L. Este proceso ha mostrado una conversión de MET baja (19,5%) utilizando 600 mg/L de $NaHCO_3$ y 600 mg/L de H_2O_2 (ver figura 11.8), esta degradación se debe a la generación de iones HCO_4^- para degradar el MET.
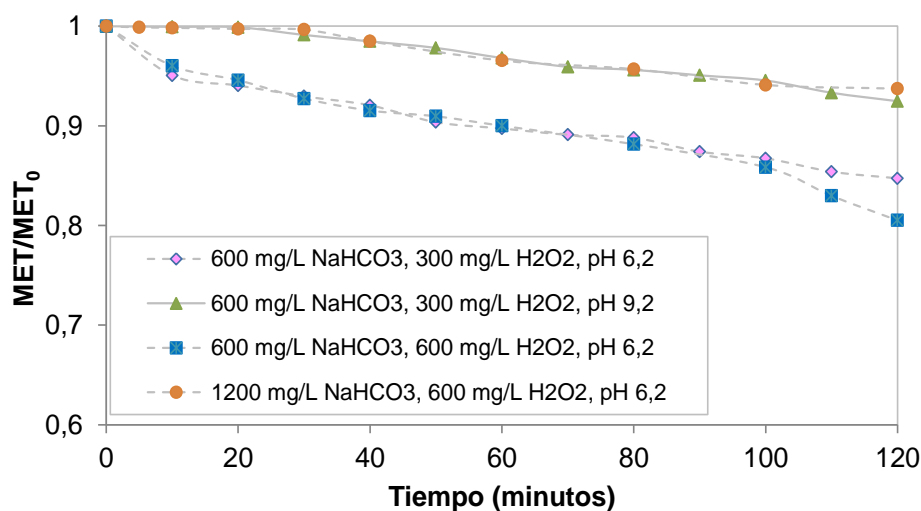
Figura 11.8- Degradación de MET por medio del proceso de bicarbonato/peróxido de hidrogeno activado.

Catalizador/bicarbonato/peróxido de hidrogeno

Con el fin de mejorar el proceso de bicarbonato/peróxido de hidrógeno, se ha adicionado un catalizador (Cobalto (II)) en la disolución inicial de MET y se ha observado que utilizando 1 mg/L de Co (II) la degradación del MET se incrementa 1,6 veces, ya que la presencia de un catalizador como el cobalto (II) reacciona con el peróxido de hidrógeno generando radicales OH·. La conversión más alta de MET alcanzada mediante este proceso ha sido de 47,2% utilizando 1 mg/L de Co (II), 600 mg/L de $NaHCO_3$ y 2400 mg/L de H_2O_2 (ver figura 11.9).
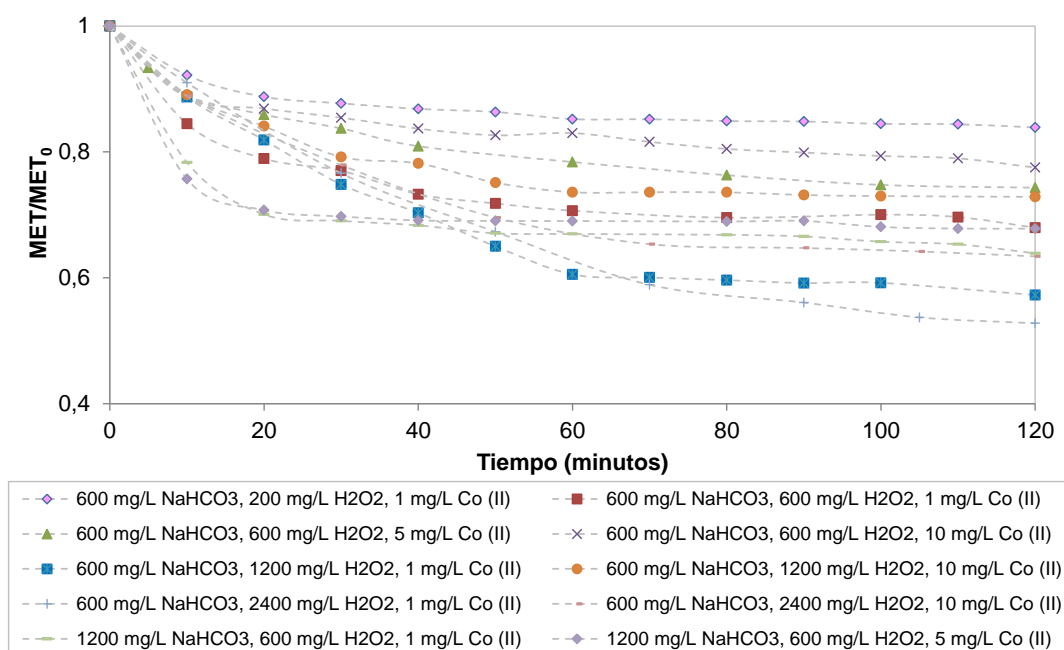
Figura 11.9- Degradación de MET por medio del proceso de Cobalto/bicarbonato/peróxido de hidrogeno.

En otra tanda de experimentos, el cobalto (II) fue sustituido por Fe (II) como catalizador, la concentración inicial de MET fue de 25 mg/L y el pH 3,0. Se ensayaron tres concentraciones diferentes de Fe (II) 2,5 mg/L, 5,0 mg/L, y 10 mg/L y la concentración de peróxido de hidrógeno se mantuvo constante en 25 mg/L. Cuando el proceso se llevó a cabo sin bicarbonato, se obtuvo la conversión de MET más baja (25,5%). Cuando se adicionó el bicarbonato, se obtuvo una conversión de MET 1,3 veces mayor.

Con el fin de mejorar la eficiencia de eliminación del MET, en lugar de adicionar todo el hierro al principio del experimento, se fue añadiendo en dosis iguales en cinco veces y a intervalos de 12 minutos. De esta forma, para la concentración más alta de

hierro (10 mg/L), se alcanzó la eliminación completa del MET en 40 minutos. Al adicionar un secuestrante de radicales OH·, la eliminación de MET decreció 6,7 veces, lo cual indica que parte de eliminación del MET se debe a especies diferentes a radicales OH·.

11.5 Comparativa de diferentes POAs e instalaciones

Comparativa de los procesos UV/H_2O_2, foto-Fenton y fotocatálisis

Se ha comparado el rendimiento de tres procesos diferentes (UVC/H_2O_2, foto-Fenton en SB y fotocatálisis en SB) en la eliminación de MET y COT.

En todos los experimentos la concentración inicial de MET ha sido de 50 mg/L y la temperatura de 25ºC. Por lo que respecta a las condiciones de operación, han sido las siguientes: para UVC/H_2O_2 (25 mg/L de H_2O_2), para foto-Fenton (2,5 mg/L de Fe (II), 25 mg/L H_2O_2), y para fotocatálisis (0,4 g/L de TiO_2). El parámetro utilizado para comparar los tres procesos ha sido la relación entre la energía acumulada y la cantidad de MET eliminado. Para homogeneizar los cálculos, se ha calculado la energía para un 90% de degradación de MET. Por otra parte, se ha calculado la relación entre la energía suministrada a la lámpara (potencia nominal) y cantidad de MET eliminado. En la siguiente tabla (tabla 11.5) se muestran los diferentes procesos comparados con los respectivos tiempos de irradiación correspondientes a una eliminación de MET del 90%.

Tabla 11.5- Energía por MET eliminado.

Proceso	Dispositivo experimental	Tiempo para degradar 90% de MET (min)	Q (kJ/L) (300-500 nm) para 90% de MET degradado	Energía/MET degradado (kJ/mg)	Energía suministrada a la lámpara/MET degradado (kJ/mg)
UVC/H_2O_2	UVC	13	3	0,07	0,2
Fotocatálisis	SB	220	11,5	0,25	293,3
Foto-Fenton	SB	62	13,4	0,30	82,7

La ratio energía suministrada a la lámpara/MET eliminado se ha evaluado por medio de ecuación 11.6:

$$\frac{P*t}{(C_0-C_f)*V_T}$$

(11.6)

Donde, P es la potencia nominal de la lámpara, t es el tiempo de irradiación (s), C_0 es la concentración inicial de MET (mg/L), C_f es la concentración final de MET (mg/L) y V_T es el volumen total de la solución.

Se observa que, mediante UVC/H_2O_2, se alcanza más rápidamente el 90% de eliminación de MET (13 minutos).

Con respecto a la relación energía/MET eliminado, la mayor eficiencia se ha obtenido en el proceso UVC/H_2O_2, posiblemente debido a la alta absorbancia del MET en la zona UVC (221 y 273 nm).

Por otro lado, comparando la relación entre la energía suministrada a las lámparas y el MET eliminado, se observa que la eficiencia para la SB es muy baja comparada con la del sistema UVC. Ello es debido a que la lámpara de Xenón de la SB requiere una gran cantidad de energía (1000 W), gran parte de la cual no se utiliza en el proceso de fotocatálisis, mientras que las lámparas de UVC requieren mucha menos energía (24 W) y la mayor parte de ella se aprovecha en el proceso.

Comparativa del proceso de fotocatálisis en SB y en CPC

Se compara el rendimiento en la eliminación de MET, por medio de fotocatálisis, en dos instalaciones SB y CPC.

La concentración inicial de MET ha sido siempre 50 mg/L y se han ensayado las tres concentraciones de catalizador: 0,05 g/L, 0,1 g/L y 0,4 g/L de TiO_2. Los resultados se resumen en la tabla 11.6 para 240 minutos de tratamiento.

Tabla 11.6-Tabla resumen de la energía en función del MET eliminado y el TiO_2 inicial para 240 minutos de irradiación.

Instalación	TiO_2 inicial (g/L)	MET eliminado (%) para 240 min	Q (kJ/L) (290-400 nm) para 240 min	Energía por mg de MET eliminado (kJ/mg MET) a 240 min	Cantidad de TiO_2 y energía utilizada para eliminar 1 mg MET (g TiO_2 kJ/mg MET) a 240 min	g TiO_2/mg MET
SB	0,05	71,7	12,6	0,358	0,018	0,001
	0,1	85,4	12,6	0,307	0,030	0,002
	0,4	94,8	12,6	0,275	0,110	0,009
CPC	0,05	60,8	5,9	0,205	0,010	0,002
	0,1	68,8	3,8	0,109	0,011	0,003
	0,4	80,4	2,6	0,065	0,026	0,010

En términos de tiempo, la degradación de MET parece ser más eficiente en SB que en CPC. Sin embargo, en términos de la energía utilizada el CPC es más eficiente que la SB. Es posible que en la SB, parte de la radiación pueda escapar del reactor y no ser absorbida, sin embargo, el CPC debido a la geometría de la instalación es capaz de concentrar prácticamente toda la radiación que llega a los colectores.

Se ha observado, además, que la energía utilizada por mg de MET eliminado decrece cuando la concentración de TiO_2 aumenta, en ambas instalaciones. Por tanto, al aumentar la concentración de catalizador, aumenta también la velocidad de reacción, dentro del rango de concentraciones estudiado.

El COT no se eliminó en su totalidad en ninguna de las dos instalaciones. Después de 240 minutos de irradiación y con 0,4 g/L de TiO_2 la mineralización obtenida fue 38,3% en SB y 28,1% en CPC.

Comparación del proceso de foto-Fenton

En este apartado, se compara el rendimiento en la eliminación de MET, por medio del proceso de foto-Fenton, en cuatro instalaciones diferentes: CPC, SB, BLB y UVC.

Las condiciones de operación han sido: 25 mg/L de H_2O_2, 2,5 mg/L de Fe (II) y 25ºC. En todos los experimentos la concentración inicial de MET ha sido de 50 mg/L.

La eficiencia energética, expresada como la ratio energía acumulada por MET eliminado, se ha calculado para el 90% de degradación de MET (ver tabla 11.7). Por otra parte, se ha evaluado también la ratio entre la energía suministrada a las lámparas y la cantidad de MET eliminado. Sólo se ha tenido en cuenta la radiación con longitud de onda inferior a 500 nm, debido a que es la parte útil del espectro para el proceso de foto-Fenton.

Tabla 11.7. Energía para eliminar MET.

Proceso	Instalación	Tiempo para degradar 90% de MET (min)	Q (kJ/L) (300-500 nm) para 90% de MET eliminado	Energía /MET degradado (kJ/mg)	Energía suministrada a la lámpara/MET degradado (kJ/mg)
Foto-Fenton	BLB	34	1,85	0,04	0,5
Foto-Fenton	UVC	9	2,20	0,05	0,1
Foto-Fenton	SB	62	13,5	0,30	82,0
Foto-Fenton	CPC	50	9,7	0,26	-

Puede apreciarse que los reactores UVC y BLB muestran una mayor eficiencia en cuanto a energía/MET eliminado que los reactores de SB y CPC. Cuando se utiliza radiación UVC en el proceso foto-Fenton, puede formarse el complejo Fe $(HO)^{2+}$, predominante en condiciones ácidas, que actúa como una fuente suplementaria de radicales OH· (ver ecuaciones 11.7 y 11.8). Además, al utilizar radiación UVC cabe considerar la influencia de la fotólisis, dado el rango de absorción del MET, como se ha comentado anteriormente.

$$Fe^{2+} + H_2O_2 \rightarrow Fe\,(OH)^{2+} + OH^{\cdot} \tag{11.7}$$

$$Fe\,(HO)^{2+} + h\nu \rightarrow Fe^{2+} + OH^{\cdot} \tag{11.8}$$

Por otra parte, si sólo se comparan los reactores UVC y BLB, que tienen el mismo volumen y el mismo diseño de reactor, se observa que existe un 18% de diferencia entre los resultados. Esto podría atribuirse al distinto tipo de radiación que emplean, ya que el proceso foto-Fenton, en principio, funciona mejor con longitudes de onda de 365 nm que con longitudes de onda de 254 nm. Finalmente, si se compara la energía que se suministra a las lámparas, se observa que la eficiencia en SB es muy bajo en comparación con UVC y BLB, dada la alta potencia nominal (1000 W) de la lámpara Xe utilizada en SB, tal y como se ha comentado en apartados anteriores.

Comparativa general de los diferentes procesos utilizados

En este apartado, se han comparado los diferentes procesos utilizados a lo largo del trabajo, indicando las condiciones de operación utilizadas para obtener la mayor eliminación de MET, el tiempo requerido, la mineralización correspondiente a dicha eliminación y la ratio entre la energía y el MET eliminado (tabla 11.8).

Tabla 11.8- Datos generales de degradaciones de MET y COT y condiciones de operación para las mejores eliminaciones de MET obtenidas en los diferentes procesos.

Proceso	MET inicial (mg/L)	Condiciones de operación	Tiempo (min)	Radiación (kJ/L)	MET Conv. (%)	COT Conv. (%)	Energía/MET degradado (kJ/mg)
UVC	50	125 mg/L H$_2$O$_2$	7.5	1,8	97,8	4,5	0,038
Fotocatálisis SB	50	0.4 g/L TiO$_2$	300	15,8	100	45,2	0,330
Fotocatálisis CPC	50	0.4 g/L TiO$_2$	270	2,6	81,5	29,2	0,065
Fenton	50	10 mg/L Fe, 150 mg/L H$_2$O$_2$, 1 adición	60	-	67,0	8,0	-
Fenton	50	10 mg/L Fe, 150 mg/L H$_2$O$_2$, Por etapas	60	-	87,0	15,6	-
Foto-Fenton BLB	50	10 mg/L Fe, 150 mg/L H$_2$O$_2$, 1 adición, 25 ºC	7	0,4	100	22,3	0,008
Foto-Fenton SB	50	10 mg/L Fe, 150 mg/L H$_2$O$_2$	7	1,5	97,3	14,3	0,030
Foto-Fenton CPC	50	10 mg/L Fe, 150 mg/L H$_2$O$_2$	3	0,7	98,3	15,3	0,014
Foto-Fenton UVC	50	2,5 mg/L Fe, 25 mg/L H$_2$O$_2$	20	4,8	97,0	10,7	0,097
HCO$_3^-$/H$_2$O$_2$	5	600 mg/L NaHCO$_3$, 600 mg/L H$_2$O$_2$, pH 6,2	120	-	19,5	-	-
Co/HCO$_3^-$/H$_2$O$_2$	5	600 mg/L NaHCO$_3$, 2400 mg/L H$_2$O$_2$, 1 mg/L Co, pH 6,2	120	-	47,2	-	-
Fe/HCO$_3^-$/H$_2$O$_2$	25	100 mg/L NaHCO$_3$, 25 mg/L H$_2$O$_2$, 10 mg/L Fe, pH 3,0, por etapas	40	-	100	-	-

Se observa que, en la mayoría de procesos, se alcanza la casi completa degradación del MET. Sin embargo, el tiempo necesario para ello cambia mucho de unos a otros.

Dependiendo de las condiciones utilizadas en cada proceso se ha obtenido la relación entre la energía acumulada y el MET eliminado. En cuanto al proceso de fotocatálisis se puede apreciar que bajo las mismas condiciones de operación (0,4 g/L TiO_2), el CPC presenta una mayor eficiencia energética. En cuanto al proceso de foto-Fenton, se observa que utilizando las concentraciones más altas de catalizador y de promotor (10 mg Fe (II)/L y 150 mg H_2O_2/L), se alcanza una alta eficiencia energética en BLB.

Por otra parte, en cuanto a Fenton, se puede apreciar que adicionar el Fe (II) por etapas mejora la degradación de MET y de COT.

Intermedios y caminos de degradación para los diferentes procesos

En esta parte se han propuesto el MET y sus principales subproductos detectados en los diferentes procesos (tabla 11.9) y también se propone un esquema general de los mecanismos de degradación del MET por medio de los POAs utilizados (figura 11.10).

Tabla 11.9 MET y sus principales intermedios detectados por medio de análisis de LC/MS en los procesos de UVC, fotocatálisis, Fenton y foto-Fenton.
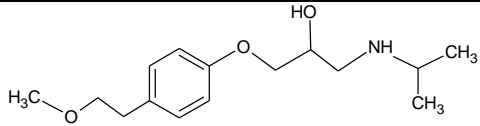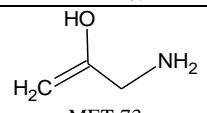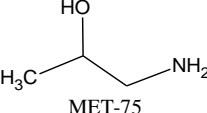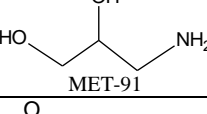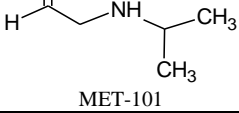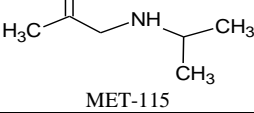
m /z	Composición elemental	Estructura propuesta (Label)	UVC	fotocatálisis	Fenton	Foto-Fenton
267	$C_{15}H_{25}NO_3$	MET-267	X	X	X	X
73	$C_4H_{11}N$	MET-73	-	X	-	X
75	C_3H_9NO	MET-75	-	X	-	-
91	$C_3H_9NO_2$	MET-91	X	X	-	-
101	$C_5H_{11}NO$	MET-101	-	X	-	-
115	$C_6H_{13}NO$	MET-115	X	X	X	X
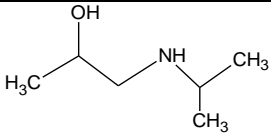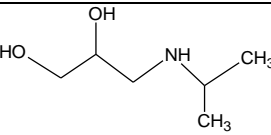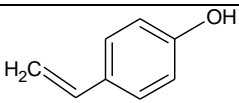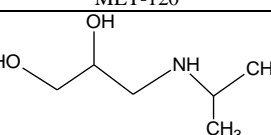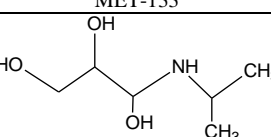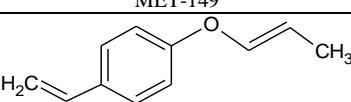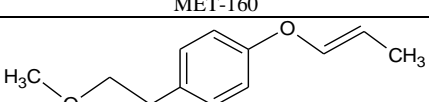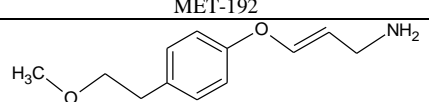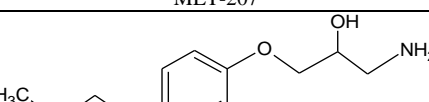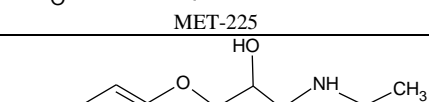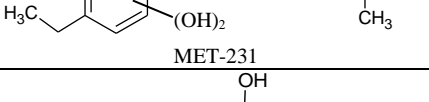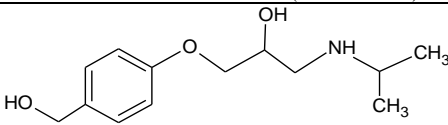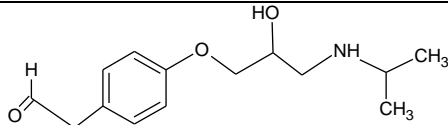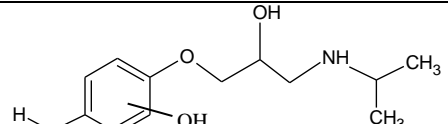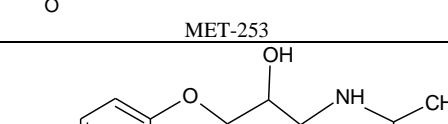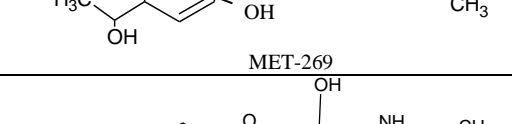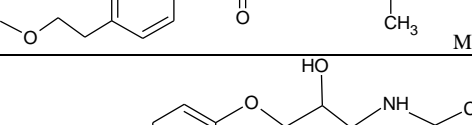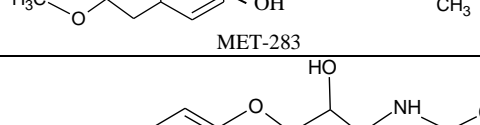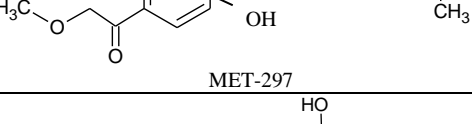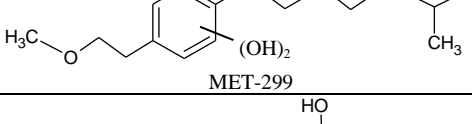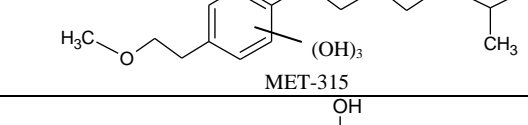
Tabla 11.9 (Continuación)						
117	$C_6H_{15}NO$	MET-117	-	X	-	X
119	$C_5H_{13}NO_2$	MET-119	-	X	-	-
120	C_8H_8O	MET-120	-	-	X	X
133	$C_6H_{15}NO_2$	MET-133	X	X	X	X
49	$C_6H_{15}NO_3$	MET-149	X	-	-	X
160	$C_{11}H_{12}O$	MET-160	-	X	-	-
192	$C_{12}H_{16}O_2$	MET-192	-	X	-	-
207	$C_{12}H_{17}NO_2$	MET-207	-	X	X	X
225	$C_{12}H_{19}NO_3$	MET-225	-	X	-	X
231	$C_{10}H_{17}NO_5$	MET-231	-	-	-	X
237	$C_{13}H_{19}NO_3$	MET-237	-	X	X	X

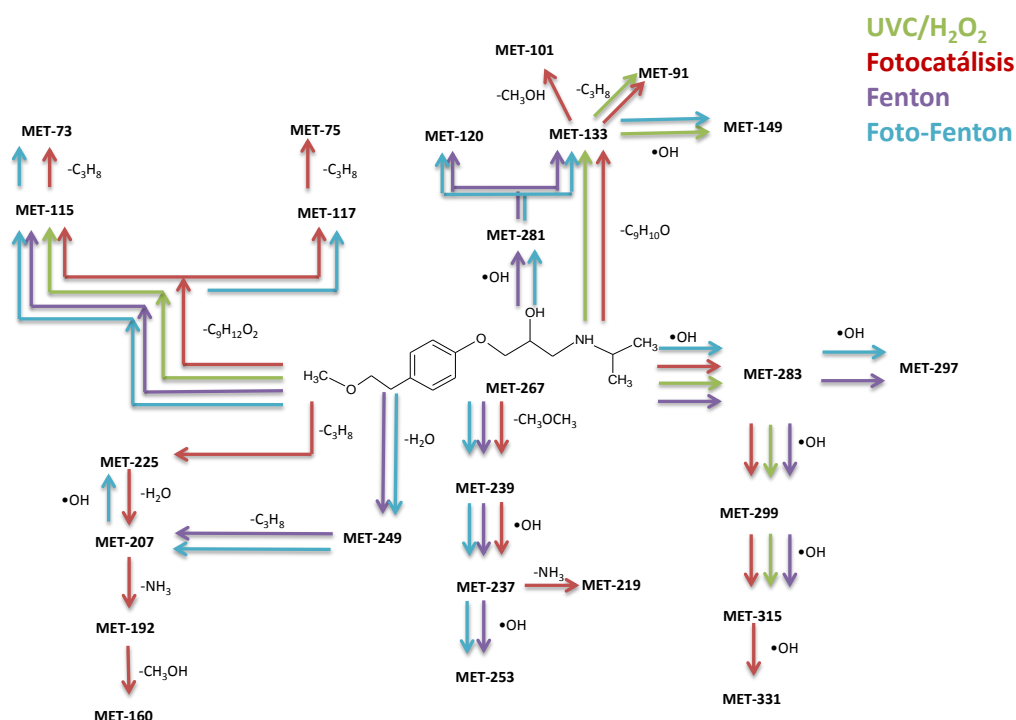|		Tabla 11.9 (Continuación)				
239	C$_{13}$H$_{21}$NO$_3$	MET-239	-	X	X	X
251	C$_{14}$H$_{21}$NO$_3$	MET-251	-	-	X	X
253	C$_{13}$H$_{19}$NO$_4$	MET-253	X	-	X	X
269	C$_{14}$H$_{23}$NO$_4$	MET-269	X	-	X	X
281	C$_{15}$H$_{23}$NO$_4$	MET-281	-	-	X	X
283	C$_{15}$H$_{25}$NO$_4$	MET-283	X	X	X	X
297	C$_{15}$H$_{23}$NO$_5$	MET-297	-	-	X	X
299	C$_{15}$H$_{25}$NO$_5$	MET-299	X	X	X	-
315	C$_{15}$H$_{25}$NO$_6$	MET-315	X	X	X	-
331	C$_{15}$H$_{25}$NO$_7$	MET-331	-	X	-	-

Figura 11.10- Propuesta de caminos de degradación del MET por medio de los procesos de UVC, Fotocatálisis, Fenton y foto-Fenton.

El Metoprolol ha sido identificado como MET-267. Entre los diferentes intermedios identificados cabe resaltar los intermedios MET-283, MET-299, MET-315 y MET-331correspondientes a la adición del radical OH· en el anillo aromático formando mono, di, tri y tetra-hidroxilados, respectivamente. El MET-133 ha sido reconocido como amino-diol. Diferentes fragmentos del lado de la etanolamina han sido también identificados (MET-73, MET-75, MET-115, MET-117). En general, como se puede apreciar en la figura 11.10, principalmente se detectaron ataques oxidativos.

11.6 Estudio de radiación para reactores fotocatalíticos

Se determinó la radiación que entra en el reactor utilizando la actinometría basada en la degradación del o-nitrobenzaldehído (o-NB), siguiendo dos métodos: el pH y la concentración de o-NB. Los flujos fotónicos obtenidos han sido de 2,81 µE/s y 2,68 µE/s, respectivamente.

Por otra parte, se analizó el efecto de la presencia de TiO_2 en suspensión en la actinometría de o-NB, siguiendo el método de medición de concentración de o-NB. Por

medio de la utilización de distintos atrapadores (scavengers), se ha demostrado que él o-NB no se degradaba fotocatalíticamente por el TiO_2 sino sólo por el proceso normal de la actinometría. Por lo tanto, esta actinometría se puede utilizar en reactores con presencia de TiO_2 para determinar el flujo fotónico entrante.

11.7 Conclusiones

- Todas las técnicas utilizadas (Fotólisis, UVC/H_2O_2, fotocatálisis, Fenton, foto-Fenton, Bicarbonato/H_2O_2, Co/bicarbonato/H_2O_2 y Fe/bicarbonato/H_2O_2) pueden ser utilizadas para degradar Metoprolol. Obviamente, la velocidad de eliminación del MET es diferente para cada técnica.

- Utilizando UVC/H_2O_2, fotocatálisis y foto- Fenton, se han alcanzado altos niveles de mineralización. Sin embargo, la fotólisis y el Fenton han mostrado bajas eliminaciones de COT.

- Los procesos de UVC/H_2O_2 (DBO_5/DQO: 0,38), fotocatálisis (SB) (DBO_5/DQO: 0,41) y Foto-Fenton (BLB) (DBO_5/DQO: 0,53) permiten aumentar la biodegradabilidad, de manera que las soluciones tratadas se pueden considerar como biodegradables.

- UVC/H_2O_2 (0,42 Equitox/m^3), fotocatálisis (0,72 Equitox/m^3 con SB y 0,57 Equitox/m^3 con CPC), Fenton (0,93 Equitox/m^3) y foto- Fenton (0,50 Equitox/m^3 con BLB, 0,51 Equitox/m^3 con SB, 0,59 Equitox/m^3 con CPC y 0,43 Equitox/m^3 con el reactor UVC) permiten reducir la toxicidad de las soluciones iniciales hasta valores muy bajos.

- Las diferentes comparativas realizadas entre procesos e instalaciones indican que el proceso UVC/H_2O_2, ha mostrado mayor eficiencia energética que fotocatálisis y foto-Fenton. Por otra parte, fotocatálisis en SB ha mostrado menor eficiencia energética que en CPC. Foto-Fenton ha mostrado mejor eficiencia en los reactores BLB y UVC que en los reactores SB y CPC.

- Se determinó la radiación que entra en el reactor SB basándose en la degradación del o-NB, siguiendo el pH y la concentración del o-NB. Se ha demostrado que esta actinometría se puede llevar a cabo en presencia de TiO_2 en suspensión para hacer medidas de radiación dentro del reactor, puesto que el o-NB no se degrada por fotocatálisis.

11.8 Recomendaciones

- Basándose en la experiencia actual, sería recomendable estudiar la degradación del Metoprolol en aguas reales y a más bajas concentraciones.

- Para complementar el trabajo de fotocatálisis, resultaría interesante investigar con nuevos catalizadores para poder comparar y buscar mejorar el proceso.

- Sería interesante continuar trabajando con los procesos de Fenton y foto-Fenton a pH neutro.

- Sería recomendable realizar un estudio económico exhaustivo de los diferentes Procesos de oxidación Avanzada utilizados. De esta manera, también sería interesante realizar un estudio de impacto medioambiental, en donde se pueda establecer una comparativa tanto económica como medioambiental referida a la eficiencia de los Procesos de oxidación Avanzada.

11.9 Publicaciones

A continuación se detallan las publicaciones científicas que han derivado del trabajo realizado durante esta tesis:

Artículos publicados

- Romero, V., González, O., Bayarri, B., Marco, P., Giménez, J., & Esplugas, S. Performance of different advanced oxidation technologies for the abatement of the beta-blocker Metoprolol. Catalysis Today, 240, 86-92 (2015).

- Romero, V., Méndez-Arriaga, F., Marco, P., Giménez, J., & Esplugas, S. Comparing the photocatalytic oxidation of Metoprolol in a solarbox and a solar pilot plant reactor. Chemical Engineering Journal, 254, 17-29 (2014).

- De la Cruz, N., Romero, V., Dantas, R. F., Marco, P., Bayarri, B., Giménez, J., & Esplugas, S. o-Nitrobenzaldehyde actinometry in the presence of suspended TiO_2 for photocatalytic reactors. Catalysis Today, 209, 209-214 (2013).

- Romero, V., Marco, P., Giménez, J., & Esplugas, S. (2013). Adsorption and Photocatalytic Decomposition of the-Blocker Metoprolol in Aqueous Titanium Dioxide Suspensions: Kinetics, Intermediates, and Degradation Pathways. International Journal of Photoenergy, (2013). http://dx.doi.org/10.1155/2013/138918.

- Romero, V., De la Cruz, N., Dantas, R. F., Marco, P., Giménez, J., & Esplugas, S. Photocatalytic treatment of Metoprolol and Propranolol. Catalysis Today, 161, 115-120 (2011).

Publicaciones en proceso:

- Romero, V., González, O., Bayarri, B., Marco, P., Giménez, J., & Esplugas, S. Photo-Fenton process comparison using different set-ups for the degradation of the emergent contaminant Metoprolol.
- Romero, V., Acevedo, S., Marco, P., Giménez, J., & Esplugas, S. Enhancement of Fenton and photo-Fenton processes at initial circumneutral pH for the degradation of Metoprolol.